Centre for Drug Research
Division of Pharmaceutical Biosciences
Faculty of Pharmacy
University of Helsinki
Finland

Liposomal Drug Delivery: Light Triggered Drug Release and Targeting to the Posterior Segment of the Eye

Tatu Lajunen

ACADEMIC DISSERTATION

To be publicly discussed, with the permission of the Faculty of Pharmacy of the University of Helsinki, in lecture hall 1, Infocenter Korona, Viikinkaari 11, on October 14th, 2016 at 12 noon.

Helsinki 2016

Supervisors: Professor Arto Urtti, Ph.D.
Division of Pharmaceutical Biosciences
Faculty of Pharmacy
University of Helsinki
Finland

Professor Marjo Yliperttula, Ph.D.
Division of Pharmaceutical Biosciences
Faculty of Pharmacy
University of Helsinki
Finland

Reviewers: Professor Jessica Rosenholm, Ph.D.
Pharmaceutical Sciences Laboratory
Åbo Akademi University
Finland

Professor Stefaan De Smedt, Ph.D.
Laboratory of General Biochemistry and Physical Pharmacy
Faculty of Pharmaceutical Sciences
Ghent University
Belgium

Opponent: Professor Paolo Caliceti, Ph.D.
Department of Pharmaceutical and Pharmacological Sciences
University of Padova
Italy

ISBN 978-951-51-2469-2 (Paperback)
ISBN 978-951-51-2470-8 (PDF)
ISSN 2342-3161 (Paperback)
ISSN 2342-317X (PDF)
http://ethesis.helsinki.fi

Unigrafia Oy
Helsinki Finland 2016

Abstract

Biomolecules are emerging as the most important source of new therapeutic compounds. Commonly these molecules are fairly large and unstable in biological environment. Furthermore, the target sites are often located inside cells and specialized tissues. Another drug group of increasing importance are cancer medicines. Serious adverse effects are common with these drugs, because they target and destroy tumors that in many ways resemble healthy tissue. All of these challenges may be solved by sophisticated drug delivery systems that protect the active ingredient, reduce the adverse effects, distribute the drug preferentially to the target tissue, and enable efficient drug release inside the diseased cells. Nanoparticle based systems, including liposomes, have become the most studied method of biologics delivery. They increase drug stability in blood circulation and facilitates drug accumulation at the target site. However, often the amount of drug released remains insufficient. Lately, several stimuli-responsive nanoparticles have been developed for better control of the drug release. Among these are light triggered liposomes, which are the focus of this work.

The main aim during this thesis work was to develop liposomes as a robust and highly controllable platform for delivery and release of various drug compounds for specific target sites. New manufacturing methods for liposomal size control were explored and several light triggered liposomal formulations were designed. Detailed characterization was carried out in order to understand the mechanisms behind the observed drug release. The final goal was to achieve safe and efficient stimuli-responsive liposomes that have several benefits over currently commonly used nanoparticle based drug carriers.

Liposomes consist of spherical bilayer forming lipids, phospholipids and sometimes additional stabilizers, such as cholesterol. The liposomes in this thesis were made with different manufacturing processes, among which the most common was the thin film hydration method. The size of the formed liposomes was reduced by extrusion, sonication or high pressure microfluidization. Light triggered release of cargo from the liposomes was achieved by encapsulating gold nanoparticles (AuNP) or indocyanine green (ICG), that convert light energy into heat. The produced heat affects the thermosensitive bilayer of the liposomes, making it more permeable for the drug molecules. The fluidity of the bilayer was analyzed to determine the optimal phospholipid composition. The size of the liposomes was measured by dynamic light scattering to evaluate the size reduction and uniformity. The stability of the different formulations was evaluated and compared with each other. Fluorescent molecules were used as model drug compounds to study the release properties of the liposomes in controlled *in vitro* and cell experiments.

The microfluidizer was capable of producing small (around 50 nm) liposomes that distributed to retinal pigment epithelium after topical administration on rat eyes. Larger liposomes remained in the choroidal vessels and did not reach the target site. Liposomes with gold nanoparticles were developed for light triggered drug release. The liposomal formulation utilized pH- and thermosensitivity to pinpoint the release of cargo within the target cells upon visual or near infrared (NIR) light activation. The light absorbance of the AuNPs depend on their size. Hence, the total diameter of these liposomes was rather large (> 150 nm). ICG was used as an alternative triggering material for the AuNPs to reduce the total size of the drug carrier down to less than 40 nm. These ICG-liposomes were shown to be highly efficient in completely releasing small compounds as well as macromolecules within 15 seconds upon NIR light irradiation, while still remaining stable during storage. The light-to-heat conversion of AuNPs and ICG was evaluated by two nanothermoprobes, i.e. laurdan and cadmium selenide quantum dots (CdSe

QD). The light signals used for triggering the drug release and the liposomes encapsulating either AuNPs or ICG were found to be very well tolerated by cells in viability experiments.

In this work, a large portfolio of methods and formulations was developed. By combining these properties into a single drug delivery system, efficient protection of the cargo and the healthy tissue, distribution to challenging target sites, controlled spatial and temporal drug release can be achieved. The next steps in this work involve evaluation of the optimized carrier with applicable disease models, analysis of the *in vivo* pharmacokinetics and more profound toxicological experiments. Even though many challenges remains to be solved, the beneficial qualities of the light triggered liposomes show great potential for treatment of posterior eye conditions, cancer and other diseases lacking in therapeutic efficacy.

Acknowledgements

The work for this thesis was carried out at the Centre for Drug Research, Division of Pharmaceutical Biosciences, Faculty of Pharmacy, University of Helsinki. Also, significant portion of the work was done at the Laboratory of Pharmaceutics & Drug Delivery, Tokyo University of Pharmacy & Life Sciences. The research and the completion of this dissertation was only possible with the help of numerous people during my doctoral studies. It is my great pleasure to offer my sincerest thanks to them.

I am very grateful to the supervisors, Prof. Arto Urtti and Prof. Marjo Yliperttula, for their support and guidance during the studies and research work. When I was deciding on my Master of pharmacy specialization, Prof. Urtti gave an inspiring lecture on the possibilities of advanced drug delivery systems. Even though I did my specialization in pharmacognosy, Prof. Urtti allowed me to do the experimental portion of the Master's thesis in his group. After graduating, Prof. Urtti's connections enabled me to have a fruitful yearlong research period in Japan at Santen Pharmaceuticals Research Centre, Nara. Likewise, Prof. Urtti had a vital role in arranging my doctoral student position and then exchange student periods in Tokyo University of Pharmacy & Life Sciences and Kyoto University. I want to thank Prof. Urtti for all of his valuable teaching, research planning guidance, comments on the manuscripts and providing the means to conduct my research. Prof. Yliperttula is thanked for her energetic teaching during the doctoral studies. Her passion for science never ceases to amaze and inspire me. Furthermore, I would like to thank Prof. Yliperttula for insightful comments and valuable guidance during the preparation and submission of the manuscripts. Prof. Yuuki Takashima of Tokyo University of Pharmacy & Life Sciences is thanked for her great support during my early steps in the doctoral studies. I feel that, with her help, I grew immensely as an independent scientist during the time working in her lab.

Prof. Jessica Rosenholm from Åbo Akademi University and Prof. Stefaan De Smedt from Ghent University are acknowledged for their review and wise comments of the doctoral dissertation manuscript. It is my honor that Prof. Paolo Caliceti was interested in being the opponent of my dissertation and making time in his busy schedule to attend my thesis defense.

I wish to thank all co-authors for their indispensable contributions to this research. Prof. Lasse Murtomäki is thanked for his management of the LITRE project that formed the bulk of this thesis work. Dr. Leena Kontturi is gratefully thanked for her help in the lab as one half of "duo sterile". I want to thank Lauri Viitala for providing numerous formulae about the detailed phenomena behind the functions of our drug delivery system. Dr. Tapani Viitala and Dr. Timo Laaksonen gave valuable guidance and offered their expertise during the work. Dr. Alex Bunker is acknowledged for the molecular dynamics simulations that elucidated the fine structure of our formulation.

I want to show my warmest thanks to my colleagues in the Centre for Drug Research and the Division of Pharmaceutical Biosciences. All of you make the great working environment and offer support in the time of need. Special thanks to Leena Pietilä, Erja Piitulainen and Timo Oksanen for keeping the wheels of our group rolling. Without them, the research group would crash and burn within a couple of days. The besterestest (sic!) thanks to all members of the epic Whisky Friday club; Jakko/Jaako Itkonen, Patrick Laurén, Andreas "Danny" Helfenstein, Aniket Magarkar, Teemu Suutari, Fumitaka Tasaka and the supporting non-whisky-drinking members; Heli Paukkonen, Anna-Kaisa Rimpelä, Mecki Schmitt, Dominique Richardson, Annukka Hiltunen, Edouard Mobarak and Feng Deng. Thank you all for the uplifting "scientific" discussions. May the whisky and spam flow forever!

I want to thank all my friends, family and relatives for supporting me throughout the years. Special thanks goes to my parents, Markku and Päivi, for fostering an interest in new things and supporting my studies. I would like to thank my brothers; Topi, Atte and Iivo, for being a source of encouragement and entertainment during the years. Especially I want to thank my lovely wife, Kanako, for being a great support and motivator during the busy time in my life.

Lastly, I wish to acknowledge the Academy of Finland for supporting my research in Finland (LITRE-project) and Japan (Researcher mobility grant). Evald and Hilda Nissin foundation, Mary and Georg Ehrnrooth foundation, Sokeain Ystavät Ry, Retina Ry, Sasakawa foundation and Silmä- ja kudospankki foundation are acknowledged for their financial support. The funding was vital for the successful completion of this work.

Helsinki, 2016

Tatu Lajunen

Contents

List of original publications

This thesis is based on the following publications:

I Lajunen T., Hisazumi K., Kanazawa T., Okada H., Seta Y., Yliperttula M., Urtti A., Takashima Y. (2014). Topical drug delivery to retinal pigment epithelium with microfluidizer produced small liposomes. European Journal of Pharmaceutical Sciences, 62, 23-32.

II Lajunen T., Viitala L., Kontturi L. S., Laaksonen T., Liang H., Vuorimaa-Laukkanen E., Viitala T, Le Guével X, Yliperttula M, Murtomäki L Urtti A. (2015). Light induced cytosolic drug delivery from liposomes with gold nanoparticles. Journal of Controlled Release, 203, 85-98.

III Viitala L., Pajari S., Lajunen T., Kontturi L., Laaksonen T., Viitala T., Urtti A., Murtomäki L. (2016). Photothermally Triggered Lipid Bilayer Phase Transition and Drug Release from Gold Nanorod and Indocyanine Green Encapsulated Liposomes. Langmuir, 32, 4554–4563.

IV Lajunen T., Kontturi L., Viitala L., Róg T., Bunker A., Laaksonen T., Viitala T., Murtomäki L., Urtti A. (2016). Indocyanine Green-Loaded Liposomes for Light-Triggered Drug Release. Molecular Pharmaceutics, 13, 2095–2107.

Publications are referred to in the text by their roman numerals.

Author's contributions

Publication I: Topical drug delivery to retinal pigment epithelium with microfluidizer produced small liposomes.

The author designed the experiments together with the supervisors. The author performed and analyzed all the experiments in the publication. The author wrote the first draft of the manuscript and revised it later according to the recommendations and comments of supervisors, co-authors and referees.

Publication II: Light induced cytosolic drug delivery from liposomes with gold nanoparticles.

The author designed the experiments together with the supervisors, project leaders and co-authors. The author performed and analyzed all the experiments in the publication except the Langmuir-BAM measurements, which were designed, performed and analyzed by Dr. Huamin Liang. Leena-Stiina Kontturi contributed significantly to conducting the experiments. The author wrote the first draft of the manuscript and revised it later according to the recommendations and comments of supervisors, co-authors and referees.

Publication III: Photothermally Triggered Lipid Bilayer Phase Transition and Drug Release from Gold Nanorod and Indocyanine Green Encapsulated Liposomes.

The author contributed in experimental design. The author designed, performed and analyzed the calcein release studies of the publication. All other experiments were performed and analyzed by Lauri Viitala and Saija Pajari. Lauri Viitala wrote the first draft of the manuscript. The author wrote the draft of materials & methods and results portions for the calcein release studies and actively advised on refining the manuscript to the final form.

Publication IV: Indocyanine Green-Loaded Liposomes for Light-Triggered Drug Release.

The author designed the experiments together with the supervisors, project leaders and co-authors. The author performed and analyzed all the experiments in the publication except the molecular dynamics simulations, which were performed and analyzed by Moutusi Manna, Oana Cramariuc, Tomasz Róg and Alex Bunker. Leena-Stiina Kontturi contributed significantly to conducting the experiments. The author wrote the first draft of the manuscript and revised it later according to the recommendations and comments of supervisors, co-authors and referees. The first draft of molecular dynamics simulations portions was written by Tomasz Róg.

Abbreviations

AMD	Age-related macular degeneration
ARM	Age-related maculopathy
ARPE-19	Spontaneously arising retinal pigment epithelial cell line
AuNP	Gold nanoparticle
BAM	Brewster angle microscopy
CdSe QD	Cadmium selenide quantum dot
CHEMS	Cholesteryl hemisuccinate
CMV	Cytomegalovirus
COPD	Chronic obstructive pulmonary disease
CTAB	Cetyl trimethylammonium bromide
DDS	Drug delivery system
DiI	1,1´-dioctadecyl-3,3,3´,3´-tetramethylindocarbocyanine perchlorate
DME	Diabetic macular edema
DMPC	1,2-dimyristoyl-sn-glycero-3-phosphocholine
DMTAP	1,2-dimyristoyl-3-trimethylammonium-propane
DNA	Deoxyribonucleic acid
DOPE	1,2-dioleoyl-sn-glycero-3-phosphoethanolamine
DPPC	1,2-dipalmitoyl-sn-glycero-3-phosphocholine
DR	Diabetic retinopathy
DSPC	1,2-distearoyl-sn-glycero-3-phosphocholine
DSPE-PEG	1,2-distearoyl-sn-glycero-3-phosphoethanolamine-N-polyethylene glycol
EPR	Enhanced permeability and retention
FDA	Food and drug administration
FITC	Fluorescein isothiocyanate
HUVEC	Human umbilical vein endothelial cell
ICG	Indocyanine green
IR	Infrared

LUV	Large unilamellar vesicle
Lyso PC	1-stearoyl-2-hydroxy-sn-glycero-3-phosphocholine
MLV	Multilamellar vesicle
MPS	Mononuclear phagocyte system
miRNA	Micro ribonucleic acid
mRNA	Messenger ribonucleic acid
MRP	Multidrug resistant protein
NIR	Near infrared
PC	Phosphatidylcholine
PE	Phosphatidylethanoamine
PEG	Polyethylene glycol
PG	Phosphatidylglycerol
P-gp	P-glycoprotein
PLGA	Poly lactic-co-glycolic acid
PVA	Polyvinyl alcohol
PVR	Proliferative vitreoretinopathy
QD	Quantum dot
RES	Reticulo-endothelial system
RNA	Ribonucleic acid
RPE	Retinal pigment epithelium
siRNA	Small interfering ribonucleic acid
SUV	Small unilamellar vesicle
TAP	Trimethylammonium-propane
TAT	Trans-activator of transcription
T_m	Transition temperature
UV	Ultraviolet
WHO	World health organization

1. Introduction

As the expected life span of populations continues to increase, cancer has become one of the most prevalent causes of death (Figure 1) in affluent countries (WHO 2014). Many active molecules for cancer treatment are large biopharmaceutics or have severe adverse effects in case of small molecular compounds. The elderly population has also increased incidence of ocular diseases (Figure 1). Extensive surveys estimated in 2010 that there were almost 300 million visually impaired and 40 million blind people in the world (Pascolini and Mariotti 2012). More than 50% of the ophthalmic patients are older than 50 years and among elderly Finnish people (> 65 years) the incidences of cataract (34%), glaucoma (13%), age-related maculopathy (12%) and diabetic retinopathy (2%) are relatively high (Laitinen, et al. 2010).

Development of new efficient and safe drugs has become difficult and expensive. Typical cost to develop new drug is about 1 billion euros. Currently, about 1/3 of the new accepted medicines are proteins and the importance of other biologicals is also increasing. Even though the pharmacologic efficacy of the compounds may be excellent, they permeate only poorly to the sites of action. Also, many small molecules that are developed in the screening projects have poor solubility, limited tissue penetration or short half-life *in vivo*. Thus, drug delivery is one of the most critical challenges of current drug research.

Carefully designed drug delivery systems (DDS) are needed to improve drug access to the tumors in cancer treatment. Successful targeted delivery of drugs to the tumors should lead to effective treatment at reduced drug doses thereby improving the drug safety. Ocular drug delivery is also challenging. Especially the retinal diseases cause severe visual impairment and blindness, but the retinal drug delivery methods are sub-optimal in terms of efficacy, safety and patient comfort (Urtti 2006). Development of more sophisticated drug delivery systems may lead to more effective and safer drug treatment and improved quality of patients' lives.

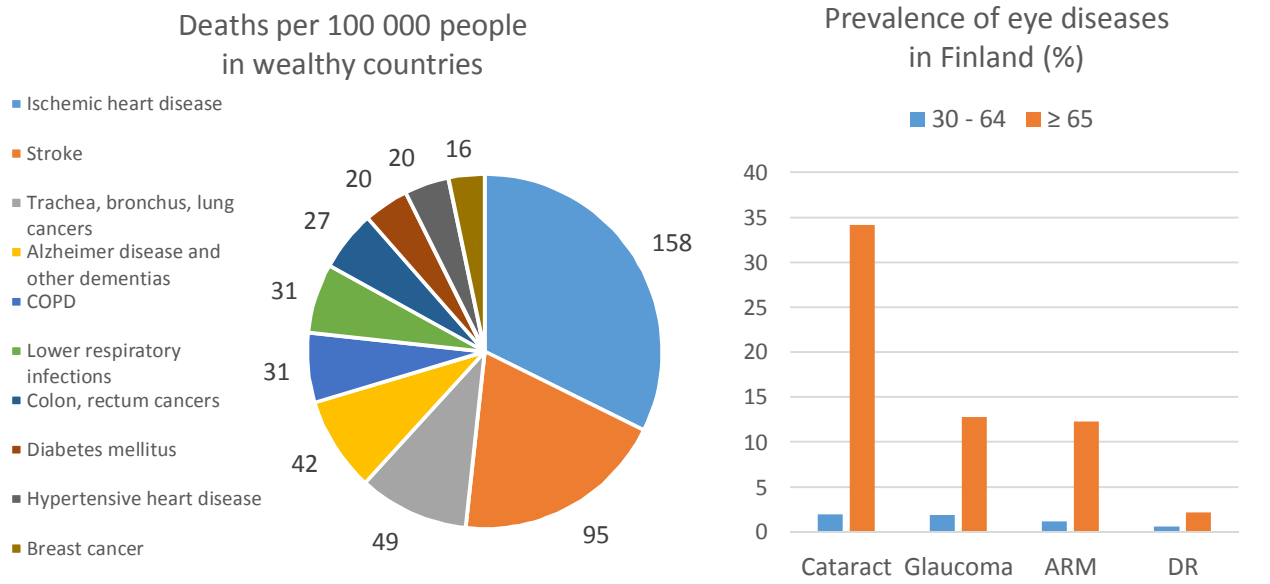

Figure 1. Left: The top 10 causes of deaths in wealthy countries in 2012 (WHO 2014). Right: The percentage of population with various eye diseases in Finland (Laitinen, et al. 2010). The groups were divided by age to 30 – 64 years old people (blue bars) and people of 65 years and older (orange bars). COPD = chronic obstructive pulmonary disease, ARM = age-related maculopathy, DR = diabetic retinopathy.

Nanoparticles have shown promise as drug delivery systems. Their ability to encapsulate and stabilize various therapeutic compounds and highly modifiable surface chemistry for active targeting makes them a robust

delivery method. Nanoparticles have sizes ranging from a few nanometers to hundreds of nanometers. They can be produced from various materials, such as polymers, lipids, peptides, metals, oligonucleotides, and their combinations. Liposomes are nanoparticles formed from lipid bilayers. They were originally introduced already in the 1960's (Bangham, et al. 1965) and since then various modifications have been published. The liposomes are efficient, safe and versatile drug carriers (Torchilin 2005; Torchilin 2012). Both, hydrophilic and lipophilic cargoes can be packed into liposomes. Furthermore, the liposomal surface can be modified with targeting ligands for selective accumulation to the target cells. Drug release from the liposomes has been controlled in many ways, also using different triggering signals for induction of the release. The stimulus for drug release can be endogenous (e.g. intracellular local pH) or external factor (e.g. ultrasound, light) (Mura, et al. 2013). The external signal offers possibility to control both time and location of drug release from the liposomes. Light as a triggering signal would allow localized drug release with high precision laser technologies.

This study aimed to generate technologies for light triggered drug release from the liposomes. Such liposomes might be useful tools for drug delivery in ophthalmology, oncology and possibly other fields of medicine. We also explored the retinal drug delivery from liposome eye drops. Overall, these studies included both physicochemical and biological studies on liposomal drug delivery.

2. Review of literature

2.1. Liposomes as a drug delivery system

Liposomes have been widely studied for the delivery of various drugs. A brief overview of liposomal structure and its modifications is given in this chapter. Additionally, the general pharmacokinetics and drug release, including triggering options, are covered. Liposomes in ocular drug delivery and light triggered drug release are discussed in separate chapters.

2.1.1. Structure and preparation

Liposomes are small round particles consisting of lipid bilayers surrounding an aqueous internal space (Bangham, et al. 1965). The main component of liposomes is the phospholipid bilayer that separates the aqueous core from the external solvent (Figure 2). The phospholipid structure includes a hydrophilic group, typically phosphatidylcholine (PC) or phosphatidylethanoamine (PE), and one or two hydrophobic alkyl chains. Depending on the preparation method the liposomes self-assemble and form spherical vesicles with diameters ranging from 40 nm to a few micrometers. Only the polar hydrophilic groups are in contact with the external and internal aqueous solutions forming a bilayer with thickness of about 4-7 nm (Balgavý, et al. 2001). Liposomes are roughly categorized by their size and lamellarity. Small unilamellar vesicles (SUV) have one bilayer and diameter less than 200 nm, large unilamellar vesicles (LUV) also have one bilayer, but their diameter is in the range of 200 to 1000 nm. Multilamellar vesicles (MLV) have several bilayers contained in larger liposomes with a diameter ranging from 500 nm to several µm and often have high polydispersity.

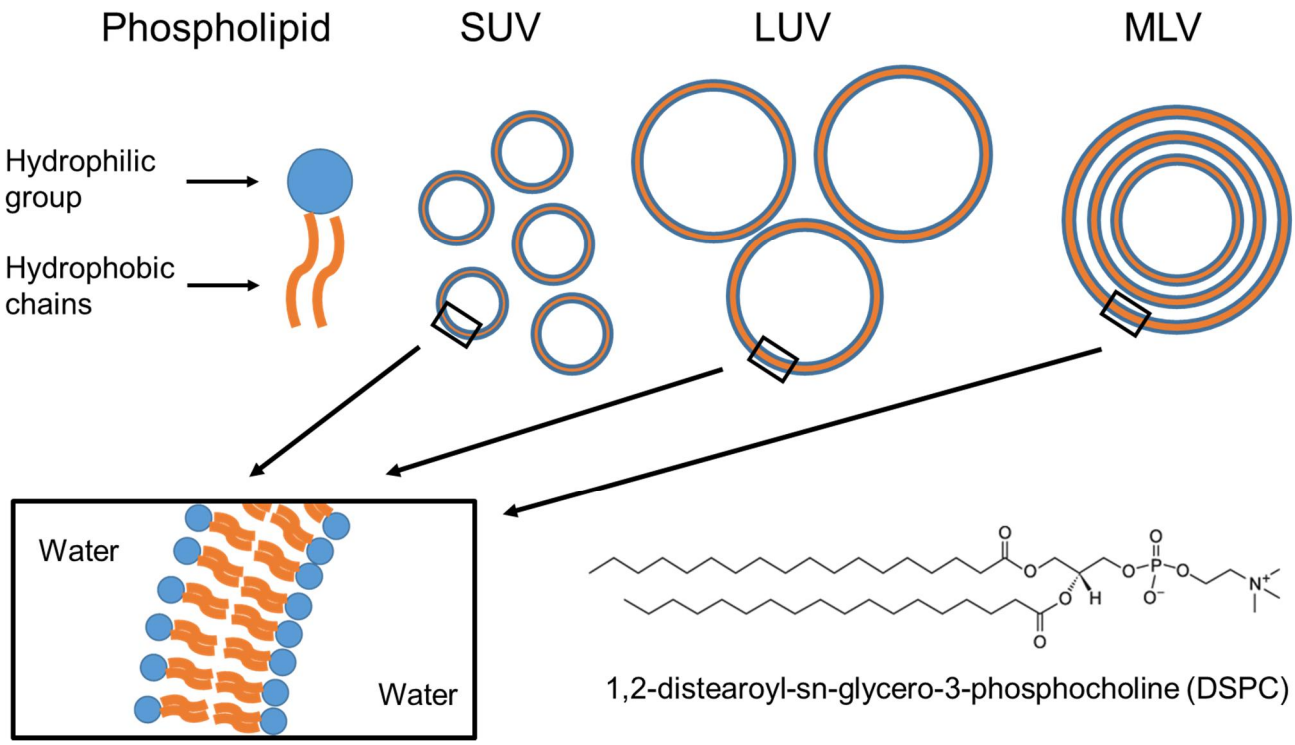

Figure 2. Schematics of liposomes, the phospholipid bilayer and the molecular structure of a DSPC phospholipid.

The properties of liposomes are defined by the phospholipids in the bilayer. Firstly, the hydrophilic head group of phospholipids is usually neutral in net charge, but actually zwitter ionic (e.g. PC and PE). Some liposomes may contain lipids with charged head groups, like anionic phosphatidylglycerol (PG) and cationic trimethylammonium propane (TAP). Secondly, the length and saturation of the hydrophobic alkyl chains

affect the rigidity and the permeability of the bilayer (Clejan, et al. 1979). Most liposomes have a specific phase transition temperature (T_m) for a change from a more rigid gel phase to a more permeable liquid crystalline phase. With longer hydrocarbon chain length, van der Waals interactions become stronger requiring more energy to disrupt the phospholipid, leading to higher T_m. On the other hand, unsaturation of the hydrocarbon chain causes a bend that disrupts the phospholipid packing and lowers the phase transition temperature. The hydrophilic head groups also have a small effect on T_m as PE lipids have higher T_m values than PC lipids with identical hydrocarbon chains. Cholesterol is commonly added to the bilayer to increase the stability of liposomes (Kirby, et al. 1980; Ulrich 2002). Cholesterol is located in the free space between the alkyl chains and it increases bilayer rigidity and decreases lateral diffusion in the lipid bilayer.

Ever since their discovery in the 1960's (Bangham, et al. 1965), the liposomes have been studied intensively as a drug carrier (Sharma and Sharma 1997; Torchilin 2012). Liposomes can protect the drug from the degrading factors in the body and they may also protect the body from the adverse drug effects. Liposomes are biocompatible, because their structure mimics the lipid bilayers found in the body. This enables drug delivery with relatively low immune response and toxicity. Furthermore, liposomes are a robust nanocarrier with high loading capacity (Ulrich 2002). Hydrophilic drugs are encapsulated in the aqueous core of the liposomes, whereas the lipophilic drugs may be embedded into the lipid bilayer. Additionally, the large aqueous core offers possibilities to encapsulate small nanoparticles or other agents in the liposomes. The charge of the anionic or cationic liposomes can be used to actively encapsulate drug compounds with opposite electric charge (Ulrich 2002). Liposomes may extend the half-life of the drug in blood circulation and improve their delivery to target tissues and cells. The liposomes accumulate especially in the liver and the spleen (Litzinger, et al. 1994), which may be undesirable in some cases. The size and surface properties of liposomes can be easily modified by careful selection of components and preparation methods. Due to their versatility, liposomes became the first nanocarriers that were approved for clinical use by the Food and Drug Administration (FDA) in 1995. The products include, for example doxorubicin (Doxil) and amphotericin B liposomes (Barenholz 2012).

Liposomes are commonly prepared by mixing the phospholipids in organic solvent (e.g. chloroform) followed by solvent evaporation and the formation of a thin lipid film in a vial (Figure 3 A) (Szoka Jr and Papahadjopoulos 1980; Ulrich 2002). The lipid film is subsequently hydrated by a buffer solution that is heated above the T_m of the lipids consequently forming a polydisperse mixture of MLVs. The MLVs can be further processed by sonication, membrane extrusion, homogenization or other methods, to form unilamellar vesicles of desired size. Other preparation methods include reverse phase evaporation and microfluidic processes (Barnadas-Rodríguez and Sabés 2001; Paasonen, et al. 2010; Talsma, et al. 1989).

Sonication and membrane extrusion are the most common methods of liposomal size control. In sonication, the liposome sample vial is placed in a bath sonicator or a probe sonicator is inserted into the sample. Ultrasonic sound energy causes size reduction of the liposomes (De Kruijff, et al. 1975), but the sonicated liposomes are polydisperse. The extrusion method, on the other hand, allows preparation of liposomes with defined size. MLVs are pushed through a polycarbonate membrane with a precise pore size at temperature above the T_m of the liposome formulation to ensure fluidity of the bilayer (Olson, et al. 1979). After extrusion, the sample is cooled below the T_m to stabilize the structure. High-pressure homogenization, or microfluidization, reduces the liposomal size by pushing the sample liquid through narrow micro channels at very high pressure (Barnadas-Rodríguez and Sabés 2001; Talsma, et al. 1989). The shear forces of the liquid flow as well as particle collisions to the chamber walls and to each other break the larger particles to smaller size. By controlling the pressure, temperature and passage times, large volumes of a monodisperse liposomes can be produced.

In reverse phase evaporation (Szoka and Papahadjopoulos 1978), the lipids are first dissolved in an organic solvent and an aqueous solution is mixed with the organic phase to form a water-in-oil emulsion. The organic solvent is gradually and completely evaporated to form the liposomes in an aqueous solvent. The method can increase the loading efficiency compared to the thin film hydration method, particularly for hydrophilic drugs. Microfluidic methods, not to be confused with microfluidization or high-pressure homogenization, offers a straightforward way to produce liposomes without additional size control steps (Jahn, et al. 2007; Jahn, et al. 2008). In this method, a continuous flow of two aqueous streams and a separating organic solvent including the phospholipids are mixed in narrow channels (Figure 3 B). The liposomes are formed by evaporation of the organic solvent, thus bringing the two lipid monolayers of the water-oil interfaces together. The benefits of the microfluidic process are high encapsulation efficiency by isolation of the inner phase and the possibility for continuous preparation of large sample volumes.

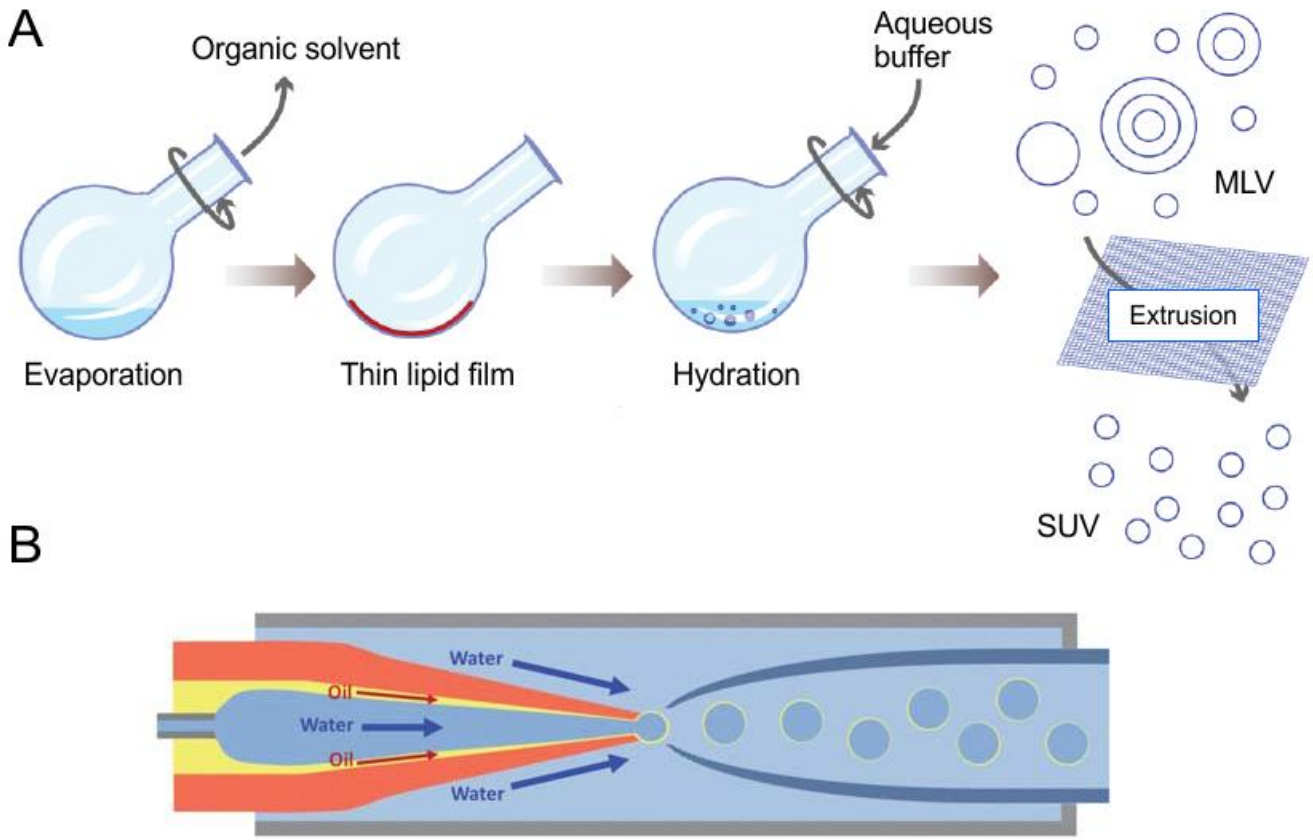

Figure 3. A: Liposome preparation by thin film hydration method. B: Schematic of microfluidic liposome manufacturing. Modified from (Calle, et al. 2015; Kim, et al. 2011).

2.1.2. Administration routes and distribution

Intestinal lipases render per oral delivery impossible for most types of liposomes. Some success have been achieved with polymer coated liposomes (Takeuchi, et al. 2005a; Takeuchi, et al. 2005b), but the oral delivery of liposomes is a marginal field. Liposomes can be administrated via other routes, for instance topically to the skin or eyes, as injections into the blood circulation or vitreous cavity, and inhalation to the respiratory tract. These application routes have distinct advantages and challenges. Delivery of liposomes to the skin is very simple and non-invasive, and thus pleasant for the patients, but the tightly layered stratum corneum prevents the permeation of intact liposomes through the skin. Stratum corneum barrier can be circumvented to some extent by trafficking liposomes through the hair follicles and sweat glands (du Plessis, et al. 1994).

The surface area of these routes is only < 0.01% of the total surface area of the skin and thus this approach is suitable only for localized delivery in some dermal conditions. Drug permeation across the skin can be enhanced with liposomes if they are highly flexible and fuse with the stratum corneum (Kirjavainen, et al. 1996). Alternatively, the liposomes can be applied through the skin with iontophoresis (Essa, et al. 2002).

Tissue barriers of the cornea and conjunctiva limit drug delivery to the eye after topical instillation as eye drops (Urtti 2006). Also, the short residence time of the drug on the ocular surface limits bioavailability to less than 5% (Urtti 2006). Nevertheless, some progress have lately been made in topical liposome delivery to the eyes and targets in the anterior and posterior segment of the eye have been reached. This is discussed in more detail in chapter 2.2.

Administration to the nasal cavity or the lungs may offer interesting opportunities for the use of liposome technology. The liposomes can be prepared for inhalation products using spray drying (Mansour, et al. 2009). The liposomal diameter must be carefully controlled, since the deposition of inhaled particles in the respiratory tract depends on the size of the inhaled particles (Gill, et al. 2007). Particles larger than 15 µm will be retained in the throat and swallowed. For example, localized immune system treatment and insulin delivery can be achieved with liposomal delivery to the respiratory tract (Huang and Wang, 2006;Khatri et al., 2008).

In most studies, the liposomes are given as injections (e.g. intravenous, subcutaneous). In these cases, the tissue barriers are by-passed and the delivery to the site of injection is controlled (Torchilin 2005). However, liposomes must get across the tissue barriers to reach the extravascular sites. In some cases (e.g. intravitreal injection), the invasive drug delivery sets limits to the acceptable duration of drug action (Del Amo and Urtti 2008). Intravenous injections enable rapid dosage to the systemic blood circulation and fast distribution to easily accessible tissues (Moghimi and Szebeni 2003; Torchilin 2005). Subcutaneous injections on the other hand can be used for prolonged local effect or preferable targeting of the lymphatic system (Oussoren, et al. 1997). Liposomes larger than 100 nm are mostly retained at the injection site whereas small liposomes (40-70 nm) are distributed to the lymphatic system and blood circulation.

2.1.3. Elimination, surface modifications and targeting

Despite the advantages of liposomes (e.g. safety and biocompatibility), their main drawbacks as nanocarriers are plasma interactions that modify their elimination (Koo, et al. 2005). When liposomes reach the blood circulation, selective serum opsonins (e.g. the complement system) bind to their surface (Harashima, et al. 1994; Moghimi and Patel 1989). The binding depends on the size and the lipid composition of the liposomes. Mononuclear phagocyte system (MPS) recognizes the opsonized liposomes and removes them from the bloodstream. It is generally thought that large liposomes are eliminated from the blood circulation more quickly than smaller liposomes (Senior and Gregoriadis 1982) and negatively charged liposomes have a shorter half-life in the bloodstream than neutral liposomes (Chonn, et al. 1992), but this view has been contested by some reports (Immordino, et al. 2006). In any case, the reticulo-endothelial system (RES), primarily in the liver and spleen, removes the uncoated liposomes efficiently from the systemic circulation within a few hours.

The current state-of-the-art for liposomes with longer circulation times consist of polyethylene glycol (PEG) or other polymer coating that, sterically protects the liposomes from opsonisation (Allen, et al. 2002). The detailed mechanism of the enhanced stability of PEG liposomes is not fully understood. Flexible and hydrophilic PEG covers the liposomal surface even at relatively low molar amounts. The sterically stabilized liposomes show improved accumulation in the tumors by enhanced permeability and retention (EPR) effect (Chonn and Cullis 1998). The tumor tissue stimulates a rapid angiogenesis leading to abnormally leaky blood vessels. Furthermore, the tumor tissue often lacks the normal lymphatic drainage. This causes the

nanoparticle accumulation and the EPR effect. Even though PEG coating has obvious benefits, it does not render the liposomes completely 'invisible' to the MPS (Moghimi and Szebeni 2003). The PEGylated liposomes have also been shown to activate the defense mechanisms through the complement system. Eventually PEG liposomes are eliminated by the liver and spleen (Allen, et al. 1995). Their retention time in the systemic blood circulation is approximately 24-48 hours.

The liposome surface can be further modified with ligands, such as antibodies, peptides and other molecules that recognize and bind to the target cells (Park 2002). The active targeting enables preferential accumulation in pathological tissues in comparison to the healthy tissues thereby protecting the patient from adverse drug reactions and enhancing bioavailability. The targeting ligands can be bound covalently to the liposome surface or tethered at the end of the PEG chain (Maruyama, et al. 1997). Cancer cell targeting with antibodies, transferrin, folate and other ligands has especially been widely studied (Lee and Huang 1996; Noble, et al. 2014; Torchilin 2005). In principle, the PEG tethered ligand should be readily available for binding at the target cell surface, but in practice the ligand may be masked within the PEG layer (Lehtinen, et al. 2012; Noble, et al. 2014).

Cationic lipids and polymers have been used to efficiently encapsulate DNA, mRNA, siRNA, miRNA and various oligonucleotides into liposomes (Behr, et al. 1989; Felgner, et al. 1987). These can be used to deliver genes or alter the cellular functions. Viral methods of transfection are more effective than the non-viral systems, but cationic liposomes are easy to prepare, they have low immunogenicity and they are relative inexpensive to produce. Anionic liposomes are less commonly used, but they have also been tested for gene delivery (Lee and Huang 1996; Patil, et al. 2004).

Versatile liposomes allow sophisticated formulation design (Figure 4) to tackle difficult therapeutic challenges. Some restraint should be used to avoid design of too complicated drug delivery systems, as it may reduce the biological robustness, be impossible to scale-up, or lead to economic constraints for an actual commercial drug use.

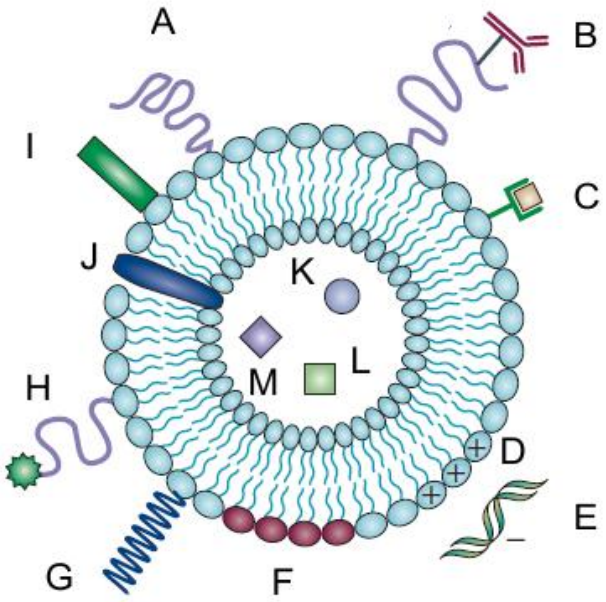

Figure 4. Schematic of a super multifunctional liposome with protective polymer (A), polymer tethered targeting ligand (B), diagnostic label compound (C), charged lipids (D), complexed DNA (E), stimuli-responsive lipids (F), stimuli sensitive polymer (G), cell penetrating peptide (H), viral structure (I), hydrophobic drug (J), hydrophilic drug (K), magnetic compound for targeting (L) and metal nanoparticle for triggered release (M). Modified from (Torchilin 2005).

2.1.4. Cellular uptake

Like most nanoparticles, liposomes are most commonly internalized into the cells through endocytosis pathways, although several other uptake paths have been suggested (Figure 5). The capacity and speed of cellular uptake varies greatly depending on the cell type. Phagocytosing cells are the most efficient in the cellular uptake of liposomes. Targeting to binding sites on the cellular plasma membrane can increase the uptake and make the liposomes more selective (Torchilin 2005). Endocytosis mechanisms are complex phenomena that are energy dependent and consist of several pathways. Uptake of 100 – 200 nm sized liposomes is subjected to clathin-dependent mechanisms, whereas small 40 nm liposomes are endocytosed via a dynamin-dependent pathway and 70 nm liposomes are taken up by both mechanisms (Andar, et al. 2014). Large particles (> 1 µm) are taken up by micropinocytosis or phagocytosis. Often the endocytosis leads the cargo into lysosomes that may break down the liposomes and release the drug cargo by enzymatic activity and acidic environment (Ulrich 2002). Some drugs may tolerate the lysosomal conditions, but more sensitive compounds should escape from the endosomes before trafficking to the lysosomes and degradation.

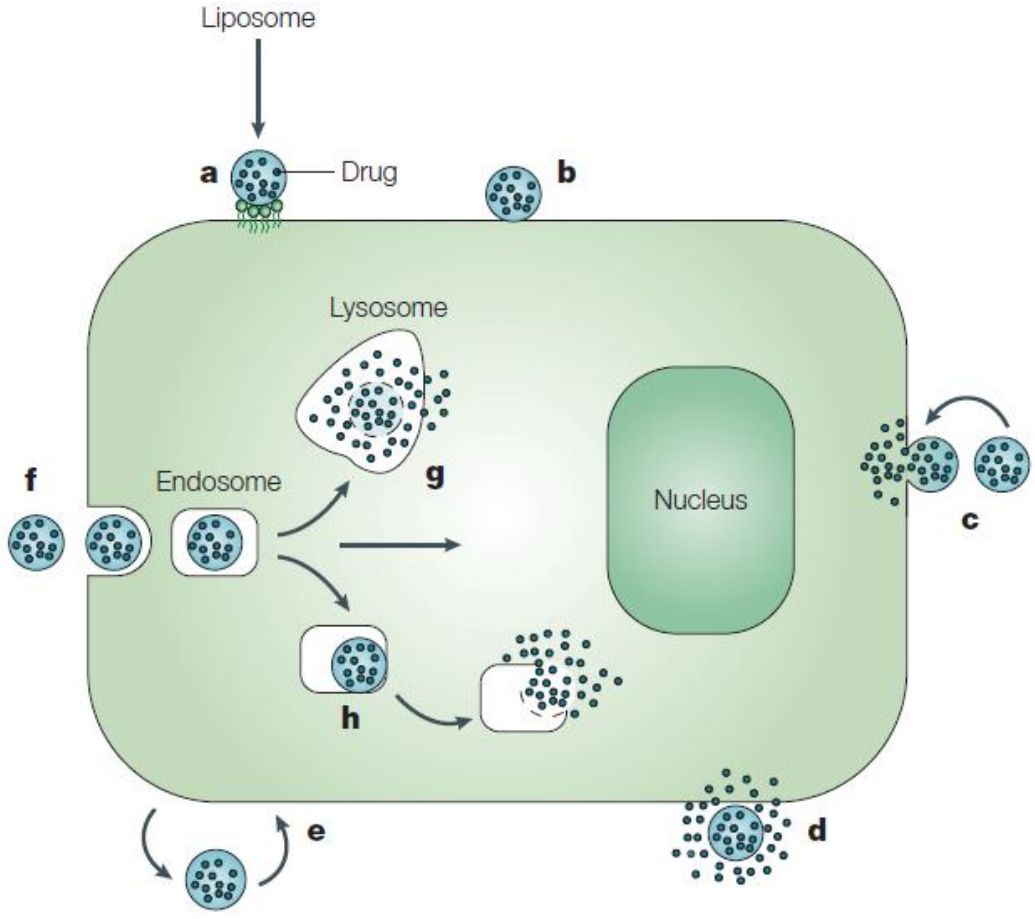

Figure 5. Interactions of liposomes with cells: specific (a) or non-specific (b) attachment to the cell surface, fusion with the cell membrane (c), drug release near the target cell (d), transfer of lipids with the cell membrane (e), endocytosis (f), delivery into the lysosome (g) and destabilization of the endosomal wall and cytosolic drug release (h). Modified from (Torchilin 2005).

2.1.5. Drug release from liposomes

Passive diffusion is the simplest form of drug release from liposomes. This process is driven by the concentration gradient between the liposome core and outside medium. The lipid bilayer properties (i.e. rigidity, charge) control the rate of passive drug release (Szoka Jr and Papahadjopoulos 1980). Reduction in the alkyl chain length and increased unsaturation render the bilayer more permeable. Likewise, the

properties of the drug affect the passive permeation through the bilayer. Generally, relatively small and lipophilic compounds can pass through the liposomal bilayers faster than larger molecules that need disruption in the ordered bilayer for their escape from the liposome (Szoka Jr and Papahadjopoulos 1980). Charged compounds have notably reduced permeation from the liposomes compared to neutral molecules of the same size with permeability of 0.054 and 0.227 (10^{-6} cm/s) for carboxy-fluorescein and fluorescein sodium, respectively (Flaten, et al. 2006).

Internal triggers of drug release. Even though the correct liposomal size and active targeting may increase the uptake of the liposomes to the target cells, the therapeutic effect might remain unsatisfactory due to the inefficient endosomal escape and drug release from the liposomes (Shum, et al. 2001). Endogenous stimuli can be used to enhance the drug release. These mechanisms are based on the specific changes in the cellular environment. One of the first applications of triggered release from liposomes was reported in the 1970's. The liposomes were formulated with a thermosensitive combination of phospholipids that released the contents upon hyperthermia (Yatvin, et al. 1978). This is based on specific T_m of the phospholipids at which point bilayer changes to permeable state and releases the encapsulated drug. Phospholipid bilayer should remain in the gel state at + 37 °C and converted to fluid state at hyperthermia, for instance in the tumors (Yatvin, et al. 1978). Cancerous tissue has approximately 2 °C higher temperature than the surrounding healthy tissue (Goldson 2012). Alternatively, a thermosensitive component, like a leucine zipper, can be included in the liposome formulation to render it thermosensitive at required temperature range (Al-Ahmady, et al. 2012). The release may also be triggered by heating the target tissue, but this is obviously limited to the surface tissues. Hyperthermia affects extracellular and intracellular liposomes in the tissue similarly. This is a problem in intracellular drug targeting (e.g. DNA and RNA delivery). Also, the operative temperature range in these approaches is limited and this restricts the selection of suitable lipids.

One of the most common methods for increased contents release within the cells, is to formulate pH-sensitive liposomes. After being endocytosed in the stable form, these liposomes break down as a results of the lower pH inside the endosomes (Chu, et al. 1990; Yatvin, et al. 1980). The increased endosomal release has been commonly achieved by the incorporation of a pH-sensitive combination of lipids, co-polymers or orthoesters (Chu, et al. 1990; Sawant, et al. 2012; Zhu, et al. 2000). In addition to pH-sensitive formulations, enzymatic degradation has been utilized as a release mechanism. Higher concentrations of proteases in cancer tissue has been used to enhance drug release from liposomes (Banerjee, et al. 2009). A recent approach for enhanced cellular uptake and contents release to the cytosol uses viral component modified liposomes (Bungener, et al. 2002). These cell-penetrating peptides and proteins, such as the transactivating transcriptional activator (TAT), are reported to enable delivery through micropinocytosis and enhanced endosomal escape (Koren, et al. 2012). The underlying mechanism is poorly known and other report has indicated that the enhanced uptake is not due to the specific structure of the TAT, but rather the cationic charge of the molecule (Subrizi, et al. 2012).

External triggers of drug release. Exogenous triggering of drug release is an attractive option, because it allows precise and time dependent control of drug release. As mentioned earlier, thermosensitive liposomes can be triggered with external heating of the target. The method has been used in cancer research: target tissue has been heated with hot water pouches, radio oscillators or small microwave devices (Huang, et al. 1994; Kono, et al. 2010). The most sophisticated thermosensitive liposome formulations are stable at body temperature, but release the contents rapidly after an increase in the temperature over 40 °C (Tagami, et al. 2011). In addition to the temperature, pH and enzymes discussed above, external triggers, such as ultrasound, magnetic field and light have been explored. Light as an external trigger is discussed in a dedicated chapter below.

Ultrasound has been extensively investigated as an approach for triggered drug release from the liposomes. The method is attractive due to its non-invasive nature and adjustment of tissue penetration by frequency (Huang 2008). In liposomes, ultrasound causes cavitation in the bilayer enabling the drug release (Schroeder, et al. 2009). Small air pockets or encapsulated perfluorocarbon nanoemulsion can enhance the cavity formation and achieve increased sensitivity to ultrasound without causing damage to cellular bilayers. This method has been used in the treatment of cerebral ischemia, gene delivery and cancer vaccination (Britton, et al. 2010; Negishi, et al. 2012; Un, et al. 2011). It has been found that ultrasonic signal also causes pore formation in the endosomes of the target cells improving endosomal escape (Omata, et al. 2011). Cavity formation requires high ultrasound frequencies (> 1 MHz) that should be used with care, because it can heat the tissues to damaging temperatures within seconds (ter Haar 2007). On the other hand, milder localized heating and drug release from thermosensitive liposomes can be achieved with low frequency ultrasound (20 – 100 kHz) (Huang 2008), but in this case the triggering is more difficult to pinpoint to a small target area.

Magnetic field can be used to guide the liposomes to their targets. This method concentrates the liposomes in the target tissue. For example, magnetic Fe_3O_4 and Fe_2O_3 nanocrystals have been encapsulated into liposomes for this purpose (Plassat, et al. 2011). Magnetism can be used to trigger drug release, because the magnetic nanoparticles produce heat via hysteresis and Néel relaxation when they are within a rapidly oscillating magnetic field. The heat will trigger the contents release when the bilayer permeability is increased in the thermosensitive liposomes (Katagiri, et al. 2011; Tai, et al. 2009).

2.2. Drug delivery to eyes

Ocular drug delivery, particularly to the retina, is a difficult challenge (Del Amo and Urtti 2008; Urtti 2006). The eye is well protected from the surroundings by various barriers and defense mechanisms. The eye is also at least partially an immune privileged organ. Development of efficient drug delivery systems is vital for effective therapy to the retina. Several ocular diseases (i.e. age-related macular degeneration (AMD), diabetic macular edema (DME), proliferative vitreoretinopathy (PVR), posterior uveitis, cytomegalovirus (CMV) infection and glaucoma) are affecting the posterior parts of the eye, particularly the retina. Therefore, development of efficient drug delivery to the posterior eye segment is important (Del Amo and Urtti 2008; Thrimawithana, et al. 2011).

2.2.1. Structure of the eye

In the context of drug delivery, the eye can be divided into two main parts: anterior and posterior segments. The anterior segment includes roughly one-third of the eye consisting of cornea, conjunctiva, pupil, aqueous humor, iris, lens and ciliary body (Figure 6). The posterior segment consists of vitreous humor, retina, choroid, sclera and optic nerve making up the remaining two-thirds in the back of the eye.

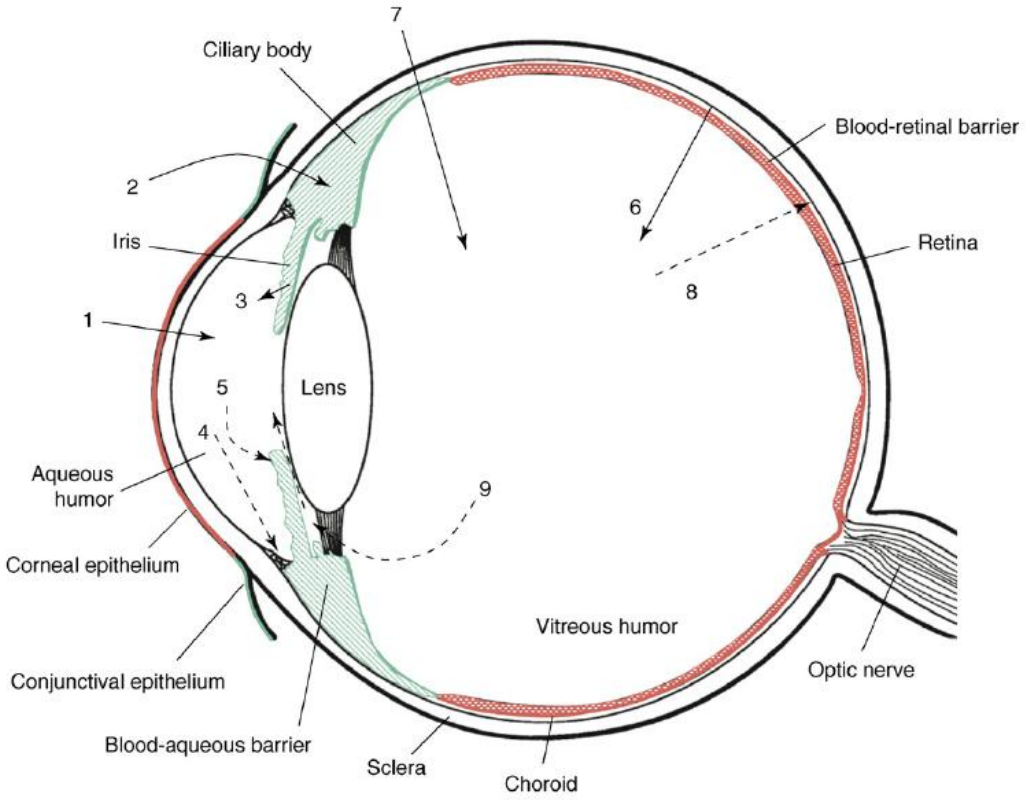

Figure 6. Schematic presentation of the ocular tissues. Routes of drug administration and distribution (solid arrows), and elimination (dashed arrows) are shown. Topical permeation route through the cornea (1). Topical permeation route via conjunctiva and sclera to anterior uvea (2). Drug distribution from ciliary body into the anterior chamber (3). Elimination of drug from the anterior chamber to Schlemm's canal (4) and the blood circulation in the anterior uvea (5). Drug distribution from the choroidal blood into the posterior eye (6). Intravitreal drug delivery (7). Elimination of drug from vitreous to choroidal blood flow via blood-retina barrier (8). Drug distribution and elimination from the vitreous to the posterior and anterior chamber (9). Image from (Del Amo and Urtti 2008).

2.2.2. Barriers of drug delivery

The anterior segment of the eye, consisting of cornea, conjunctiva, anterior chamber and uvea, is most commonly treated with topical eye drops. Although the anterior parts might seem to be easily accessible for topical drug delivery, several barriers in the eye limit the ocular bioavailability of drugs. Firstly, the lacrimal fluid flow (induced and normal baseline) on the ocular surface removes the instilled eye drop to the nasolacrimal duct and nasal cavity, where the drug may absorb into the systemic circulation (Urtti, et al. 1985; Urtti and Salminen 1993). Secondly, the corneal epithelium limits drug absorption to the anterior chamber (Maurice and Mishima 1984). The epithelium consists of matured corneal epithelial cells with tight junctions on the apical surface. Therefore, the drug should have some lipophilicity for adequate permeability across the cornea (Prausnitz and Noonan 1998). The corneal drug permeability was correlated with the chemical structure recently (Kidron, et al. 2010). Drug permeability was predicted well with hydrogen bonding capacity and $\log D_{7.4}$. Conjunctiva has a leakier epithelium compared to the cornea, and its surface area is almost 20 times larger than the cornea (Prausnitz and Noonan 1998). The permeation of hydrophilic and large drug compounds is therefore significantly better in the conjunctiva than in the cornea suggesting that such compounds are absorbed into the eye preferably through the conjunctiva and sclera instead of cornea (Ahmed and Patton 1985). On the other hand, the palpebral conjunctival is a route for direct systemic drug absorption from the lacrimal fluid, and this factor also limits the ocular bioavailability (Urtti, et al. 1985; Urtti, et al. 1990). Overall, less than 5% of the initial dose, often less than 1%, is absorbed into the eye after topical eye drop administration (Maurice and Mishima 1984; Urtti, et al. 1990)

In analogy with the blood-brain barrier, the blood-ocular barrier protects the eye from the xenobiotics in the systemic blood circulation. The blood-ocular barrier consists of blood-aqueous barrier in the anterior uvea and a blood-retina barrier in the posterior segment of the eye (Maurice and Mishima 1984). Drugs may distribute through these barriers from the systemic circulation to the inner eye. The blood-retina barrier is further divided to two parts: the retinal capillaries in the neural retina and the retinal pigment epithelium (RPE). The walls of the retinal capillaries are tight and form a strong barrier against drug permeation. On the other hand, in the choroid the blood flow is high and the vessels have fenestrated leaky walls (pore size of about 80 nm) (Guymer, et al. 2004). Thus drugs and small nanoparticles can pass through the choroidal endothelia to the extravascular space, but further distribution to the retina is limited by the RPE. Tight junctions and efflux transporters of the RPE cells form a specific barrier against further drug permeation into the eye (Mannermaa, et al. 2006). Generally, lipophilic molecules permeate the blood-retina barrier more readily than hydrophilic compounds (Pitkänen, et al. 2005).

2.2.3. Ocular routes of drug delivery

Topical eye drop instillation on the ocular surface is the most common way of drug administration in ocular drug treatment. This is due to the relative ease of administration, usually high patient acceptance, and low cost. The drugs are absorbed from the lacrimal fluid to the eye via corneal or conjunctival routes. The challenges of topical drug delivery include short contact time and tissue barriers that reduce the drug access the target sites. This can be improved with formulations that have prolonged residence time on the ocular surface and improved bioavailability (e.g. gels, ointments, inserts). The disease targets for eye drops are in the anterior part of the eye, because drug distribution to the posterior segment is too low to be therapeutically effective (Urtti 2006). Common topically treated diseases include glaucoma, cataract and infections of the anterior part (e.g. conjunctivitis).

After systemic administration, the blood-retina barrier limits the drug access to the retina (Maurice and Mishima 1984; Vellonen, et al. 2015). Only a small portion of total blood circulation goes through the choroidal vessels and thus large doses may be needed for satisfactory therapeutic effect in the retina. This can lead to adverse effects in other parts of the body.

Direct intravitreal injections and implants bypass most ocular barriers and this route of administration is the golden standard in the treatment of the ocular posterior segment. The drug is delivered efficiently with a small needle through the conjunctiva, the sclera and the uvea to the vitreous at pars plana region. Higher initial drug concentration near the diseased tissue enables smaller drug dose reducing systemic side effects. On the other hand, the invasive nature of intravitreal injections may reduce patient comfort and it can be costly because the drug must be applied by medical professionals (Jonas, et al. 2008; Wu, et al. 2008b). Overall the injection complications are rare during the intravitreal drug treatment (e.g. antibody treatments for age related macular degeneration). The dosing interval may be prolonged with controlled release systems (gels, implants).

Subconjunctival and periocular routes are used to treat anterior conditions (e.g. local anesthesia), but these routes are also interesting options for the treatment of the uvea and the posterior segment of the eye. A simple injection or drug insert is placed between the conjunctiva and the sclera. Thereafter, drug should permeate through sclera towards the inner part of the eye. Even though most of the drug absorbs systemically from the injection site (Ranta, et al. 2010), drug delivery to the posterior segment can be effective due the high permeability of the sclera, even for macromolecules (Prausnitz and Noonan 1998). Furthermore, subconjunctival and periocular injections have shown better safety when compared to more invasive intravitreal injections (Raghava, et al. 2004), although some complications, including intraocular pressure rise, strabismus and cataract, have been reported during periocular treatments (Castellarin and

Pieramici 2004). In addition to scleral penetration, the drug should pass through the choroid and the RPE for retinal treatment. Drug removal to the choroidal blood flow an RPE barrier limit the retinal drug bioavailability (Ranta, et al. 2010).

2.2.4. Pharmacokinetics of the eye

After topical drug administration, the peak concentration in the aqueous humor is commonly reached in about 30 minutes. Usually, the drug distributes to the anterior chamber by passive permeation, but the distribution of some compounds (e.g. acyclovir prodrug) may be enhanced by peptide transporters located in the cornea (Anand and Mitra 2002). Other potential transporters in the cornea are various amino acid transporters (Anand, et al. 2004; Ganapathy and Ganapathy 2005). The drug may distribute from the aqueous humor to the surrounding tissues, for example ciliary body and the iris, where melanin binding may take place (Salminen, et al. 1984). This binding can act as a prolonged release mechanism that extends the therapeutic drug effect (e.g. atropine) (Menon, et al. 1989). The drug elimination from the anterior chamber takes place through aqueous humor flow to the Sclemm's canal and via drug distribution to the blood circulation in the anterior uvea. The elimination via aqueous flow has a relatively constant rate and it is independent of drug properties. On the other hand, elimination through the blood flow depends on the ability of the drug to permeate through the endothelial vessel walls to the systemic blood circulation. As lipophilic drugs permeate the cellular barriers more readily, they have faster clearance from the anterior chamber compared to hydrophilic compounds (Urtti 2006). Frequent dosing is often required in topical ocular drug treatment.

The pharmacokinetics of drug delivery from the systemic blood flow are not completely understood (Vellonen, et al. 2015). Hydrophilic compounds have lower permeation through the cellular RPE than lipophilic drugs (Vellonen, et al. 2015). It is known that the choroidal blood flow plays a major role in drug clearance from the posterior segment. The flow rate of blood through a choroidal vessel is 6 µL/min (Miura, et al. 2012) and it is important for the drugs to escape to the extracellular space before being carried away by the choroidal circulation. The retina has the highest metabolic rate per tissue weight, even higher than the brain, and thus needs a lot of energy (Winkler 1981). For meeting this energy need, the blood-retina barrier has many glucose transporters that might be utilized for drug permeation, if the drug can fit the high specificity of the transporters. The RPE has several efflux transporters, including P-glycoprotein (P-gp) and multidrug resistant protein (MRP), which limit the permeation of several drugs to the retina (Aukunuru, et al. 2001; Constable, et al. 2006). These efflux transporters have also been found in the cornea (Dey, et al. 2003; Zhang, et al. 2008).

Distribution of the drug within the vitreous after intravitreal injection is relatively free due to the lack of major barriers. Drugs distribute rapidly in the vitreous and move towards the retina, but the elimination though the blood-retina barrier is strongly dependent on compound properties (del Amo, et al. 2015; Maurice and Mishima 1984) Small lipophilic molecules escape from the vitreous rapidly, half-lives are typically a few hours (del Amo, et al. 2015). However, compounds with high molecular weights exceeding 40 kDa retain longer in the vitreous humor due to their lower permeability in the blood ocular barriers (Marmor, et al. 1985). Thus, their half-lives are many days in the vitreous (Maurice and Mishima 1984). Vitreous does not limit molecular movement significantly so that even particles up to the size 500 nm can move freely in the vitreous (Xu, et al. 2013). Vitreous can represent significant barrier for the distribution and elimination of positively charged compounds (Figure 7). Small molecules are eliminated from the vitreous via blood ocular barriers and via diffusion from the vitreous to the aqueous humor thereafter to the Schlemm's canal (del Amo, et al. 2015). Macromolecules utilize only the anterior elimination route via aqueous humour, since their permeability in the blood retina barrier is very low (del Amo, et al. 2015; Pitkänen, et al. 2005).

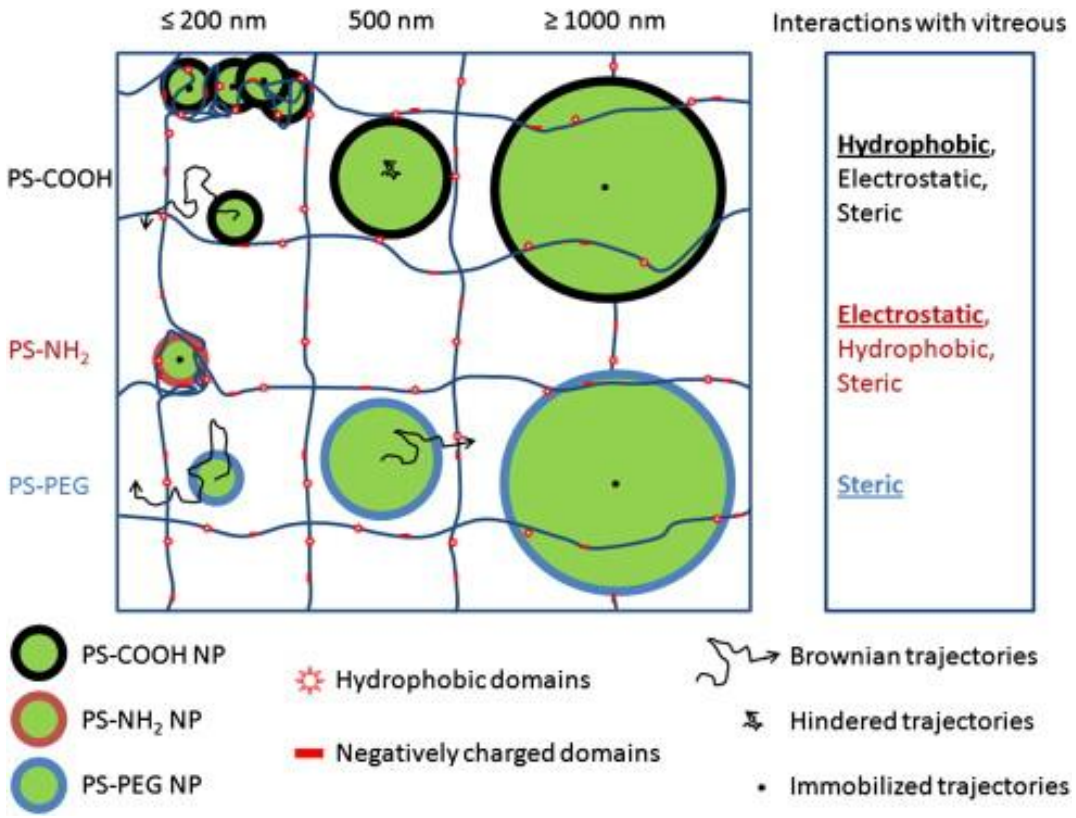

Figure 7. Freedom of movement of nano- and microparticles in bovine vitreous. PS = polystyrene. NP = nanoparticle. PEG = polyethylene glycol. Image from (Xu, et al. 2013).

Conjunctival blood circulation and lymphatic flow reduces the bioavailability after subconjunctival drug administration (Ranta and Urtti 2006). On the other hand, the high permeability of the sclera enables efficient drug distribution (Prausnitz and Noonan 1998), but choroidal blood flow may limit the further permeation to retina (Ranta, et al. 2010). It has been shown that direct penetration through the sclera is the predominant pathway for the drug to enter the vitreous after subconjunctival injection and distribution via blood circulation or diffusion from aqueous chamber to vitreous are minimal (Lee and Robinson 2001). Even though the drug is distributing through highly vascularized tissues after subconjunctival injection, the systemic plasma concentrations have reported to be similar with intravitreal injections (Nomoto, et al. 2009).

2.2.5. Ocular drug delivery systems

As discussed earlier, eye drops are frequently administered and their use results in low ocular bioavailability. Some enhancement of ocular permeation can be achieved with prodrug approach (Shirasaki 2008), since prodrugs can improve the solubility, stability, and permeability of the instilled drugs. In addition to simple eye drops, several other approaches have been used for topical drug delivery to the eye (Table 1).

Table 1. Examples of ocular drug delivery systems.

DRUG DELIVERY SYSTEM	*ACTIVE SUBSTANCE*	*EFFECT*	*REFERENCES*
OCUSERT CONJUNTIVAL SAC INSERT	Pilocarpine	Greater hypotensive effect than an ophthalmic solution for 2-4 days with a single insert. Problems with insert slip outs from the sac.	(Abrahamson 1975; Armaly and Rao 1973)
GEL FORMING EYE DROPS	Timolol	Reduction of dosage frequency. Gel forming eye drops once a day had the same hypotensive effect as an ophthalmic solution applied twice a day.	(Shedden, et al. 2001)
MICROEMULSION	Pilocarpine	Reduction of dosage frequency. Similar hypotensive effect with the microemulsion once or twice a day and an ophthalmic solution four times a day.	(Garty, et al. 1994; Naveh, et al. 1994)
NANOSUSPENSION	Piroxicam, cloricromene	Enhanced anti-inflammatory effect compared to a microsuspension. Improved stability compared to a simple solution.	(Adibkia, et al. 2007; Pignatello, et al. 2006)
DRUG INFUSED CONTACT LENSES	Lidocaine	Therapeutic levels of drug release for 3-5 days.	(Gulsen and Chauhan 2004)

Simple intravitreal injections have widely been used for treatment of the posterior segment diseases, for example age-related macular degeneration. The drug access to the posterior segment is significantly improved, but the need of repeated and unpleasant injections remains as a problem. Depending on the drug, half-lives of one hour to many days have been reported (del Amo, et al. 2015). Simple injection of drug solution is applicable only for large molecules with long half-life, wide therapeutic index and high potency. Otherwise, frequent injections (interval of days) would be needed and this is unacceptable. Therefore, prolonged action intravitreal delivery systems have been investigated and developed.

Two decades ago, the first intravitreal implant was launched to the clinical use to prolong the drug exposure and enable stable concentration in the vitreous (Vitrasert) (Dhillon, et al. 1998). Since then, several intravitreal implants have been developed (Table 2). Non-biodegradable (e.g. polyvinyl alcohol, PVA) controlled release implants may have duration of action of several years, while biodegradable implants have shorter duration of months, but they do not need to be removed from the eye (Bourges, et al. 2006). Polymeric biodegradable implants often have three phases of drug release: an initial burst, a middle phase and a final burst release. Newer implants have achieved prolonged and more stable release profiles with near zero-order drug release kinetics (Kunou, et al. 2000; Yasukawa, et al. 2005). In addition to the prolonged release, the implants have other benefits, such as reduction of adverse effects, because of lower drug concentrations without initial peak are maintained throughout the treatment period and less drug is needed for therapeutic effect. Some implants (for example Medidur) have been formulated into the shape of long cylinder, which enables injection of the implant instead of surgery which reduces the invasiveness of the treatment (Lee, et al. 2010). Implants can also be located outside the vitreous in the sclera or subconjunctival space thus eliminating the need to perforate the sclera or uvea (Lee, et al. 2010). Another option is to inject a gelifying formulation that is in a liquid state prior the injection, but forms a more rigid gel via a change in temperature, ionic concentration or pH (Bochot, et al. 1998; Del Amo and Urtti 2008). With this approach, invasiveness is reduced, but the typical drug release period is shorter than with implants.

Table 2. List of intravitreal implants. Modified from (Del Amo and Urtti 2008).

IMPLANT FORMULATION	*ACTIVE SUBSTANCE*	*ADMINISTRATION METHOD*	*PHYSICAL SIZE*	*REFERENCES*
VITRASERT (NON-BIODEGRADABLE)	Ganciclovir	Implantation at the pars plana	Few millimeters	(Bourges, et al. 2006; Dhillon, et al. 1998)
RETISERT (NON-BIODEGRADABLE)	Fluocinolone acetonide	Implantation at the pars plana	3 x 2 x 5 mm	(Jaffe, et al. 2006)
MEDIDUR (BIODEGRADABLE)	Fluocinolone acetonide	Intravitreal injection	3.5 x 0.37 mm cylinder	(Lee, et al. 2010)
POSURDEX (BIODEGRADABLE)	Dexamethasone	Intravitreal injection or through small incision at the pars plana	Microsized	(Kuppermann, et al. 2007)

Drugs can be formulated into micro- or nanoparticles for topical administration or intravitreal injection. Biodegradable and FDA approved polymers (poly lactic-co-glycolic acid (PLGA), polyethylene glycol, polylactide) can release drugs up to several months (Moshfeghi and Peyman 2005). The large microparticles sediment slowly to the bottom of the vitreous while the smaller particles float freely and may cause clouding of the vitreous. A less invasive method is to inject the particles to the subconjunctival space, but then the compound must permeate several barriers in order to reach the retinal tissues. Nanoparticles have lately been of great interest in ocular drug delivery. Their small size enables efficient distribution and their properties can easily be adjusted by the selection of formulation and surface modification. Furthermore, nanoparticles can significantly increase the solubility of some poorly soluble drug compounds (Kayser, et al. 2005). Nanoparticles can be built from polymers or lipids forming uniform beads, dendrimers, liposomes or micelles (Gaudana, et al. 2009). These delivery systems are taken up by phagocytosing cells, such as the RPE and can be found at the target for as long periods as 4 months (Bourges, et al. 2003). Even more specific targeting can be achieved by attaching ligands of specific receptors on the surface of the nanoparticles, especially in the case of dendrimers (Sahoo, et al. 2008). The most sophisticated nanoparticle based drug carriers can be remotely monitored and the drug release triggered at desired location and time point. Nanoparticles may function as a controlled release devices for topical drug delivery offering a prolonged duration (Cavalli, et al. 2002) and enhanced corneal permeation (De Campos, et al. 2003) compared to simple eye drops. In the case of liposomes, the surface charge plays an important role in the distribution in the eye. Cationic positively charged liposomes are bound by the negatively charged corneal surface after topical delivery. This increases the residence time and corneal uptake (Felt, et al. 1999). On the other hand, cationic particles do not move freely in the vitreous, as discussed earlier. With optimized liposome formulation, increased permeation into the eye and higher concentration at the target site can be achieved (Lajavardi, et al. 2007; Nagarsenker, et al. 1999; Shen and Tu 2007).

One interesting avenue for prolonged drug effect is localized production of the therapeutic compound by encapsulated cells. The cells can be suspended in microcapsules or a gel (Kontturi, et al. 2011; Kontturi, et al. 2015; Wikström, et al. 2008). Optionally, larger implants can also be used to house the drug producing cells (Sieving, et al. 2006; Thanos, et al. 2004; Uteza, et al. 1999). The encapsulated cells are genetically modified to produce the protein drug and polymer isolates the cells from the body components. Nutrients and oxygen diffuse into the device keeping the cells alive and the produced drug and waste compounds are released outside the device. Treatment periods of several months or even years are possible with such devices.

Iontophoresis offers a non-invasive alternative for increasing the drug permeation into the eye (Parkinson, et al. 2003; Vollmer, et al. 2002). The method consists of electrical current that drives ionized drug

compounds through the cellular membranes. Iontophoresis can be applied for corneal and scleral drug trafficking. Trans-scleral route is more preferable, because of less tight barriers and a more direct path to the posterior segment of the eye. The benefits of iontophoresis are reduced invasiveness compared to injections and implants, but the drug effect is shorter, and the range of applicable drug compounds is more limited. Also practical use may be difficult, and there is no targeting of specific cell types.

Microneedles are another alternative for delivering a wider range of drug compounds with very low invasiveness. The needle is inserted into the sclera and drug substance is injected into a suprachoroidal space (Jiang, et al. 2007). Different needle lengths and injection pressures affect the distribution in the suprachoroidal space (Patel, et al. 2011). Microneedle delivery is suitable many drug compounds and formulations, but it is more invasive as a method than iontophoresis.

2.3. Light triggered drug delivery systems

External triggering of drug release is feasible in the light-accessible organs, such as eye and skin. Light is an attractive remote triggering method for drug release, because it can be used with great spatial and temporal control. Furthermore, the parameters (i.e. beam diameter, exposure duration, wavelength and light intensity) can be adjusted in versatile manner for the specific drug delivery system and target tissue (Alvarez‐Lorenzo, et al. 2009). This high level of control may allow therapy adjustments according to the progression of the disease and cyclic changes in the body. Nanocarriers can release their cargos via several mechanisms upon light triggering, such as surface plasmon absorption and photothermal reaction, light driven isomerization and oxidation, hydrophobicity changes due to light exposure, photo fragmentation of polymer backbone and photo driven de-crosslinking (Alvarez‐Lorenzo, et al. 2009; Timko, et al. 2010). The used materials vary greatly depending on the particular light triggering method. Light triggered DDS can be roughly divided into single use (i.e. all of the cargo is released upon triggering) or switchable systems (i.e. drug release can be controlled by turning the triggering light on and off for pulsed release) (Timko, et al. 2010). It should be noted that light triggered DDS is a distinct method from photodynamic therapy, where light signal causes cell death through localized heating and singlet oxygen release from a photosensitizer compound (Wilson and Patterson 2008). These systems represent different mechanisms and purpose, not controlled drug release and delivery.

2.3.1. Triggering materials

General requirements for light triggered materials are an adequate stability during shelf-life storage and *in vivo*, and selective drug release after exposure to irradiation by the ultraviolet (UV), visible or infrared (IR) range. The light must induce some structural changes in the system that leads to the drug release (Fomina, et al. 2012). UV and visible light can be used to trigger only superficial tissues, because the wavelengths under 700 nm do not reach tissues deeper than 1 cm (Weissleder and Ntziachristos 2003). On the other hand, near-infrared (NIR) light (700 – 900 nm) has minimal absorbance to hemoglobin (abs. < 650 nm), water (abs. > 900 nm) and lipids, and it can penetrate to the tissues several centimeters depending on the light intensity (Weissleder 2001). In addition to the efficient release mechanisms, the materials should be able to carry drugs. For cellular targeting, the nanosized systems should be amenable for targeting ligand conjugation to the nanoparticles.

Gold and other metal nanoparticles. NIR wavelengths are preferred for light triggered drug release, due to deep tissue penetration. Metal nanoparticles can be activated with NIR light as these particles absorb light and release the light energy as heat energy, and in some cases fluorescence, that arises from the oscillation of electrons on the nanoparticle surface, i.e. surface plasmon resonance (Jain, et al. 2006). One of the benefits

of metal nanoparticles is the tunable absorbance wavelength that depends on the size and shape of the particle. Gold is the most commonly used material due to its inertness and availability of various sizes (from 2 nm to over 100 nm) and shapes of nanoparticles (spheres, rods, shells, stars, cages) with distinct reactions upon light induction (Timko, et al. 2010) (Figure 8).

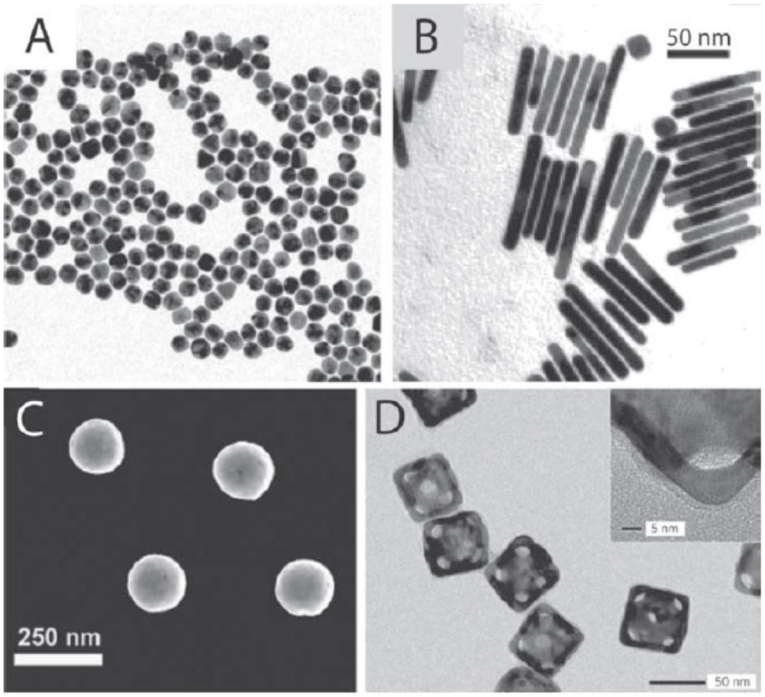

Figure 8. Transmission electron microscopy (TEM) images of gold nanospheres (A), nanorods (B), nanoshells (C) and nanocubes (D). Image from (Timko, et al. 2010).

The most common way to produce gold nanorods is by anisotropic lengthening in the presence of the cetyltrimethylammonium bromide (CTAB) surfactant (Jana, et al. 2001; Nikoobakht and El-Sayed 2003). The nanorod is built from a small spherical gold seed and the process is stopped once the desired length is reached. Nanorods have two light absorption wavelength maximums, a shorter wavelength for the short axis of the particle and the more useful longer wavelength for the long axis (Huang, et al. 2006). In one example, a cancer drug, doxorubicin, was bound by thermosensitive DNA helices tethered on the surface of gold nanorods (Xiao, et al. 2012). Localized heat produced by the nanorods upon light triggering released the drug from the DDS. In another release method, short laser pulses can break down the nanorods into nanospheres and simultaneously releasing the contents (Chen, et al. 2006).

Hollow gold nanospheres or nanoshells can be induced with variable absorbance wavelengths (from mid visual to infrared range) (Timko, et al. 2010). The frequency of surface plasmon resonance is dependent on the diameters of the inner and outer surfaces of the nanoshells. One study showed encapsulation of doxorubicin into gold nanospheres and release of the contents upon NIR light triggering, which increased the anticancer efficacy compared to free doxorubicin (You, et al. 2012). Also triggered macromolecule release, e.g. DNA and siRNA release, have been achieved with gold nanoshells (Barhoumi, et al. 2009; Braun, et al. 2009). The cargoes were bound to the surface of the nanoshells by linkers that react to the surface plasmon resonance upon light triggering.

Gold nanocages are among the most complex metal particles. They are porous and hollow cubes with sizes ranging from 30 nm to 200 nm (Skrabalak, et al. 2008). Gold nanocages can encapsulate the drug in the

hollow internal space if the cage is coated with hydrophobic thermosensitive polymer (Yavuz, et al. 2009). When the DDS is irradiated with NIR light, the heat produced by the cage breaks down the polymer layer and the contents are released. Large compounds, such as enzymes, can be encapsulated and released with the nanocages.

Polymers. A tight polymer structure can be made more porous by breaking the light sensitive crosslinks (e.g. o-nitro benzyl) between the polymer backbones (Fomina, et al. 2012; Mura, et al. 2013). For example, dendrimers can be built around a light sensitive core that breaks the whole structure upon light triggering, enabling fast release of the contents (Amir, et al. 2003). Most de-couplings of the crosslinks require UV or short wavelength visible light thereby limiting usefulness of this approach *in vivo*. Alternatively, photo-crosslinking or photo-polymerization can be used as a drug release scheme, even though it may seem counter-intuitive. The crosslinking can be used to shrink parts of the liposome surface, which in turn produces pores and enables contents release (Regen, et al. 1981). Initial studies utilized UV light, but later visible light methods with specific sensitizers have been reported (Fomina, et al. 2012). Crosslinking and photo-polymerization can also be used with polymeric particles where light causes shrinkage of the particle that in turn forces the drug out of the particle as the internal volume is reduced (Shi, et al. 2008). Light triggering can also control the fluidity of some gels. This opens up one possibility of injectable solutions that form a gel *in situ* (introduced in the chapter 2.2.5). The fluidity of the gel is increased with UV light and a more viscous gel is formed under visible light (Suzuki, et al. 2006). The method is based on azobenzene crosslinkers that in *trans* form make a ladder structure between the polymer chains under visible light. UV light on the other hand changes the azobenzenes to *cis* form breaking the ladder structure and reducing viscosity.

Another light induced controlled release method is based on micellar amphiphilic polymers that undergo light triggered structural changes. Photosensitivity of block copolymers is often achieved by incorporating a chromophore to the hydrophobic block. In this case, light activation causes a conformational or structural change in the hydrophilicity balance causing disruption of the micellar form (Zhao 2007). The triggering wavelength depends on the chromophore and this allows flexibility in design of the DDS (El Halabieh, et al. 2004). Later variations of this method enabled reversible change between amphiphilicity and hydrophilicity, where UV light produces hydrophilic block copolymers and visible light reverted them back to an amphiphilic state. This effect can be achieved with specific azobenzenes that change between amphiphilic *trans* form and hydrophilic *cis* form upon visible and UV light exposure, respectively (Lu, et al. 2008; Pouliquen and Tribet 2006). In some formulations, both UV and NIR can be used, where single UV photon per polymer is absorbed in the former case and two NIR photons in the latter case, thus offering flexibility in regards of triggering equipment and light penetration depth (Jiang, et al. 2006).

Another option is to formulate temperature sensitive polymer structures and incorporate a light to heat transforming element to the polymeric DDS. The most commonly used material is gold nanoparticle (Gorelikov, et al. 2004; Sershen, et al. 2000) that was discussed in the previous chapter. The heat produced by light triggering can also be used as such for photo-thermal destruction of cancer cells without more invasive surgical procedures (Hirsch, et al. 2003).

***Lipid micelles and liposomes*.** Liposomes constructed from photosensitive lipids can release the contents upon light triggering overcoming the problem of inefficient drug release from traditional liposomes (Shum, et al. 2001). Light triggered liposomes use several different mechanisms, including photo-polymerization, photochemical triggering, photo-isomerization and photo-thermal release (Alvarez‐Lorenzo, et al. 2009).

In photo-polymerized liposomes, light of a suitable wavelength causes reactive dienoyl, sorbyl or steryl groups in the bilayer to form large clusters disrupting the liposomal structure and allowing the contents to leak out (Bondurant, et al. 2001; Spratt, et al. 2003). Basically, parts of the lipid bilayer form tight raft

structures with irreversible covalent bonds and pores are formed on the surface of the liposomes. Additionally, photo-polymerizing polymers can also be incorporated into the liposomal bilayer to create light triggered liposomes (Kostarelos, et al. 2005). The use of UV light for photo-polymerization and formation of reactive molecules limit the applicability for therapy.

Light can also cause degradation of some lipids. Thompson et al. reported a method where liposomes were formed by semi-synthetic lipids and photosensitizer (Thompson, et al. 1996). Visible light caused oxidation in the alkyl chain linker and the formation of a single chain phospholipid, which in turn induces a phase transition in the lipid bilayer. Photo-oxidation has also been used to facilitate more efficient delivery to the cytosol by singlet oxygen mediated disruption of endosomal membranes (Gerasimov, et al. 1999). Light induced cleavage has been used in several other liposome formulations (Chandra, et al. 2006; Zhang and Smith 1999). Light triggered liposomes can also be used to control viscosity of injectable gels, much like the stimuli-responsive polymers. In one study, $CaCl_2$ was released from liposomes upon NIR light triggering, which caused the surrounding hydrogel to cross-link consequently increasing the viscosity significantly (Zhang, et al. 2002), which may be used to reduce the drug release rate. Photochemical triggering methods usually induce an irreversible change in the liposome structure, which means that the mechanisms are useful for single burst release applications, not for gradual and repeated pulses of drug release.

Photo-isomerization in liposomes can be used for light induced drug release in analogy with light switchable polymers. Azobenzene groups can be incorporated to the phospholipids for light triggering (Bisby, et al. 2000; Yagai, et al. 2005). Light triggering of azobenzenes alter the polarity of the lipids and subsequently the bilayer structure is altered and the contents are released from the liposomes. Another creative application is to use photo-isomerization in spiropyran conjugated lipid nanoparticles, where UV exposure causes a reversible shrinkage of the particles enabling a better tissue penetration (Tong, et al. 2012).

Light induced pulsed drug release has been achieved also with thermosensitive liposomes and photo-thermal triggering material, such as gold nanoparticles (Paasonen, et al. 2007; Paasonen, et al. 2010). In this case, the drug release is controlled by the phase state of the lipid bilayer that will change from stable gel state to leaky rippled and fluid state when the temperature is locally increased within the bilayer. After the light trigger is switched off, the bilayer returns to its earlier conformation with the decrease in temperature. Drug release can be controlled with the properties of the bilayer (particularly phase transition temperature), size and shape of gold nanoparticles, and power and wavelength of the triggering light. In another method, coated liposomes with a gold shell have absorption wavelengths in the visual-NIR range. Powerful laser excitation has shown to deform the shell and the liposomal structure allowing contents release (Jin and Gao 2009). The structural change was shown to be irreversible, therefore repeated pulsatile drug release is not possible with this DDS.

***Light triggering molecules*.** Some of the earliest small molecules for light triggering agent were reported in 1980 (Kano, et al. 1980). The method consisted of the previously mentioned azobenzene that undergoes photo-isomerization when irradiated with UV light. The molecule changes from a straight *trans*-form into a more curved *cis*-form upon exposure to light at 366 nm. Azobenzene was incorporated into a 1,2-dipalmitoyl-sn-glycero-3-phosphocholine (DPPC) liposomal bilayer where the change in the conformation of azobenzene increased the permeation of the contents. Interestingly, the conformational change of azobenzene can be reversed by visible light irradiation (> 420 nm), thereby allowing reversible molecular switching (Lednev, et al. 1998; Tsuda, et al. 2000; Willner, et al. 2001). Likewise, as with polymers and liposomes, azobenzenes can be used with porous silica structures (Angelos, et al. 2007; Liu, et al. 2004). In those drug delivery systems, the structure of the pores is changed and the material flow is increased upon visible light triggering. Nevertheless, the clinical usefulness of these methods *in vivo* are lacking due to the low tissue penetration and poor safety of visible and UV lights. Furthermore, the safety of azobenzenes is questionable.

Photosensitive o-nitrobenzyl bromide has been covalently attached to a surface of silica and gold nanoparticles for light triggered release (Agasti, et al. 2009; Wu, et al. 2008a). Various drugs were attached to the bromide compounds. Irradiation with light (310 nm) caused cleavage of drug molecules from the surface of the nanoparticles. Another small molecular trigger, 1,1´-dioctadecyl-3,3,3´,3´-tetramethylindocarbocyanine perchlorate (Dil), has been included in liposomes causing drug release upon light triggering (550 nm) (Miller, et al. 2000). In one approach, onium salts form acidic compounds via photo-induced electron transfer bond cleavage (Saeva 1990). This can be combined with pH-sensitive nanostructures, for example liposomes, to form light triggered DDS (Gerasimov, et al. 1997). Some molecules produce heat upon light irradiation. One of the most interesting options is indocyanine green (ICG), which converts IR light into heat (Chen, et al. 1995; Ma, et al. 2013; Sawa, et al. 2004). The heat might be used to trigger drug release from thermosensitive formulations.

2.3.2. Safety

The DDS should be safe; otherwise it will not be accepted for the clinical use in the patients. Gold nanoparticles are generally well tolerated in short term (Alkilany and Murphy 2010), but their long-term toxicology is poorly understood. The cells have limited means to deal with metal nanoparticles, therefore accumulation of these non-biodegradable materials may pose problems in long term treatment. Although azobenzenes have been widely studied as photo-triggering agents, they are regarded to be toxic by the FDA, and this limits their applicability in the clinical medicine. Likewise, the o-nitrobenzyl groups and several polymers have not been proven to be safe enough for clinical therapy (Mura, et al. 2013; Timko, et al. 2010).

In addition to the actual DDS, the safety of the triggering light should also be considered. Even though many chemical triggering methods, like isomerization and fragmentation have good technical qualities, their usefulness is limited by safety problems of UV light. Initial studies on light triggered liposomal DDS also utilized UV light (Paasonen, et al. 2007; Paasonen, et al. 2010). The shorter wavelength light is more damaging to the cells than the NIR radiation, and additionally it has poorer tissue penetration (Standard 1993). Light in the NIR region does not cause significant heating in the application area and has been shown to be better tolerated in ocular and other tissues (Delori, et al. 2007; Mochizuki-Oda, et al. 2002; Nagasaki and Shinkai 2007). NIR light can also penetrate several centimeters into tissues, widening the target profile. Thus, NIR light is seen as the most promising triggering signal for light activated drug delivery systems.

3. Aims of the study

The general objective of this thesis was to develop new liposomal formulations as potential delivery systems for drug treatment of the posterior segment of the eye. The focus was on the liposomes that could be used for topical and/or light triggered drug delivery to the posterior eye segment.

The specific aims of the thesis were:

1) To investigate the microfluidizing process parameters for the production of small sized liposomes with good encapsulation efficiency of a model compound.

2) To determine the distribution of different sized liposomes in the retinal pigment epithelium and choroid after the liposome application topically on the surface of the eye.

3) To develop and investigate visual and near-IR light triggered liposomes based on gold nanoparticles and pH- and/or thermosensitive liposomes for triggered release.

4) To investigate the cytosolic delivery of those liposomes.

5) To develop small sized near-IR light triggered liposomes based on indocyanine green (ICG) as release inducer for small and large molecules.

6) To understand the light-to-heat conversion of gold nanoparticles and ICG in liposomal carriers.

4. Overview of the materials and methods

The materials and methods of this thesis are listed in table 3. The roman numerals refer to the corresponding articles in the list of original publications. UR refers to unpublished results.

Table 3. Summary of materials and methods used in the publications and unpublished results.

THEME	*STUDY OBJECTIVE*	*MATERIALS AND METHODS*	*PUBLICATION*
LIPOSOME MANUFACTURING	Production of liposomes with specific lipid composition	Thin film hydration	I, III, IV, UR
	Production of small sized uniform liposomes	Microfluidizer, ultrasonication, small pore extrusion	I, IV, UR
	Enhanced cargo encapsulation	Double emulsion preparation with the microfluidizer	I
	Liposomes with encapsulated gold nanoparticles	Reverse evaporation	II
LIPOSOME CHARACTERIZATION	Particle size analysis	Dynamic light scattering	I, II, IV, UR
	Liposome surface charge	Electro-kinetic analysis	I
	DNA encapsulation efficiency	SYBR Green assay	I
	Light absorbance	Spectroscopy	II, III, IV
	Lipid phase transition	Differential scanning calorimetry	II, IV
	Lipid layer structure	Langmuir films – Brewster angle microscopy (BAM)	II
	Bilayer localization of ICG	Molecular dynamics simulations	IV
	Light-to-heat conversion in liposomes upon light activation	Laurdan and PEGylated CdSe QD measured with spectroscopy	III
STABILITY	Size stability of the liposomes	Dynamic light scattering	I, IV, UR
	Contents leakage stability	Spectroscopic detection of fluorescent molecule	IV
	Indocyanine green stability	Spectroscopy	IV
***IN VITRO* DRUG RELEASE**	Temperature induced contents release	Controlled heating and spectroscopic detection of the fluorescent molecule (calcein, FITC-dextran)	II, IV, UR
	Light induced contents release	Laser exposure at 37 °C and spectroscopic detection of the fluorescent molecule (calcein, FITC-dextran)	II, III, IV, UR
CELL STUDIES	Cellular uptake of liposomes	Flow cytometry - fluorescence assisted cell sorting (ARPE-19, HUVEC)	II, UR
	Cellular drug release	Confocal microscopy, flow cytometry - fluorescence assisted cell sorting (ARPE-19, HUVEC)	II, UR
	Cell toxicity	Alamar blue assay (ARPE-19, HUVEC) Annexin V assay (ARPE-19)	II, UR UR
***IN VIVO* STUDIES**	Liposome distribution after topical instillation on the eye	*In vivo* experiment on rats; recovery, freezing, slicing and confocal microscopy of the eyes	I

5. Study I: Topical drug delivery to retinal pigment epithelium with microfluidizer produced small liposomes

European Journal of Pharmaceutical Sciences 62 (2014) 23–32

Contents lists available at ScienceDirect

European Journal of Pharmaceutical Sciences

journal homepage: www.elsevier.com/locate/ejps

Topical drug delivery to retinal pigment epithelium with microfluidizer produced small liposomes

T. Lajunen [a,b], K. Hisazumi [c], T. Kanazawa [a], H. Okada [a], Y. Seta [a], M. Yliperttula [b], A. Urtti [b,d], Y. Takashima [a,*]

[a] Tokyo University of Pharmacy & Life Sciences, Japan
[b] Centre for Drug Research, Division of Pharmaceutical Biosciences, University of Helsinki, Finland
[c] Powrex Corporation, Itami, Japan
[d] School of Pharmacy, University of Eastern Finland, Finland

ARTICLE INFO

Article history:
Received 21 February 2014
Received in revised form 24 April 2014
Accepted 26 April 2014
Available online 5 May 2014

Keywords:
Liposome
Targeting
Microfluidizer
Retinal pigment epithelium
Delivery vehicle
Eye drop delivery

PubChem:
hydrogenated soy L-α-phosphatidylcholine (PubChem CID: 94190)
1,2-dioleoyl-3-trimethylammonium-propane (PubChem CID: 6437371)
1,2-dimyristoyl-3-trimethylammonium-propane (PubChem CID: not available)
1,2-dimyristoyl-sn-glycero-3-phosphocholine (PubChem CID: 5459377)
egg L-α-phosphatidylcholine (PubChem CID: 24778933)
1,2-distearoyl-sn-glycero-3-phosphoethanolamine-N-[amino(polyethylene glycol)-2000] (PubChem CID: 406952)
1,2-distearoyl-sn-glycero-3-phosphoethanolamine-N-[maleimide(polyethylene glycol)-2000] (PubChem CID: 406952)
1,2-dioleoyl-sn-glycero-3-phosphoethanolamine-Atto 647N (PubChem CID: 9546744)
cholesterol (PubChem CID: 5997)
Holo-transferrin (PubChem CID: not available)

ABSTRACT

Drug delivery from topically instilled eye drops to the posterior segment of the eye has long been one of the greatest challenges of ocular drug development. We developed methods of liposome preparation utilizing a microfluidizer to achieve adjustable nanoparticle size (even less than 80 nm) and high loading capacity of plasmid DNA. The microfluidizing process parameters were shown to affect the size of the liposomes. Higher operating pressures and passage for at least 10 times through the microfluidizer produced small liposomes with narrow size distribution. The liposomes were physically stable for several months at +4 °C. *In vivo* distribution of the optimized liposome formulations in the rat eyes was investigated with confocal microscopy of the histological specimens. Transferrin was used as a targeting ligand directed to retinal pigment epithelium. Size dependent distribution of liposomes to different posterior segment tissues was seen. Liposomes with the diameter less than 80 nm permeated to the retinal pigment epithelium whereas liposomes with the diameter of 100 nm or more were distributed to the choroidal endothelium. Active targeting was shown to be necessary for liposome retention to the target tissue. In conclusion, these microfluidizer produced small liposomes in eye drops are an attractive option for drug delivery to the posterior segment tissues of the eye.

* Corresponding author. Address: 1432-1 Horinouchi, Hachioji, Tokyo 192-0392, Japan. Tel./fax: +81 42 676 4492.
E-mail address: takasima@toyaku.ac.jp (Y. Takashima).

http://dx.doi.org/10.1016/j.ejps.2014.04.018
0928-0987/

1. Introduction

The posterior segment of the eye remains as a difficult target for drug delivery (Urtti, 2006). Only the anterior part of the eye can be treated with relative ease by using topical instilled eye drops. So far, the most common delivery approach to the ocular posterior segment has been the direct injections into the vitreal cavity (Del Amo and Urtti, 2008). Intravitreal injections must be applied by medical professionals, frequent dosing is required and such drug administrations are burdensome to the patients and health care system. For example, exudative form of age-related macular degeneration (AMD) is treated monthly by bilateral intravitreal antibody injections for the rest of the patients' lives. Because the use of repeated invasive injections involves a risk of infections and other ocular complications, broad spectrum antibiotic treatment follows every injection in large patient populations, a procedure that might give rise to evolution of resistant bacterial strains. The monthly dosing regimen is feasible with the antibodies (Prager et al., 2009) that usually have half-life about one week in the vitreous (Bakri et al., 2007; Kim et al., 2006; Mordenti et al., 1999), but still the convenience and the non-dependence on medical professionals of topical drug delivery cannot be achieved. Furthermore this approach is not suitable for small molecular weight drugs with typical half-lives of 1–10 h in the vitreous (Kidron et al., 2012). For small molecules, slowly dissolving suspensions or sophisticated controlled release implants can be used (Nagai et al., 2014), but the invasive nature and many associated problems of drug delivery are not avoided. Therefore, the controlled release implants are not used widely in the clinics. Non-invasive drug delivery methods, amenable to out-patient use, would constitute major improvement in the management of the retinal diseases, such as age related macular degeneration, diabetic retinopathy, macular edema and retinal apoptosis in glaucoma.

At the ocular surface eye drops are rapidly cleared and corneal epithelium hinders drug absorption into the inner eye (Maurice and Mishima, 1984; Urtti, 2006). The classical trans-corneal route of drug entry into the eye is only suitable for lipophilic small molecules, because it consists of one lipophilic layer with tightly packed cells and two hydrophilic layers (Beuerman and Pedroza, 1996; Huang et al., 1983). Compared to the cornea the permeability of conjunctiva is higher and more amenable also to large molecules (Horibe et al., 1997; Hämäläinen et al., 1997). Also, non-corneal route is more favorable in the delivery of macromolecules than small molecules, because their loss to the systemic blood circulation is less (Ranta et al., 2010). Nevertheless, the drug delivery via the non-corneal route into the posterior eye segment is a complicated process that involves tissue barriers (conjunctiva, sclera, retinal pigment epithelium) and fluid flow factors, such as conjunctival and choroidal elimination to the blood flow (Ranta et al., 2010). This reduces the posterior segment bioavailability small molecular weight drugs, like timolol, to the range of 0.01% (Maurice, 2002; Urtti et al., 1990). Conjunctival capillaries are fenestrated and transfer from epithelium to the blood vessels has few barriers for macromolecules and nanoparticles (Krachmer et al., 2011). Blood circulation distributes the drug around the eye, thereby helping the delivery process. Conjunctival artery and ciliary arteries orient to the posterior segment of the eye further distributing to choriocapillaris (Forrester, 2008). The capillaries below the retinal pigment epithelium are densely fenestrated with small pores (Cavallotti et al., 2005; Guymer et al., 2004; Sugita et al., 1982). The diameter of the pores is only 75–85 nm that may limit the size of the particles passing through (Guymer et al., 2004).

Since the pivotal studies of Bangham (Bangham et al., 1965), liposomes have been investigated in drug delivery. They have been investigated also for topical ocular and intravitreal drug delivery (Kawakami et al., 2001; Law et al., 2000; Wang et al., 2012). Topical administration for posterior segment delivery is the greatest challenge and opportunity of ocular liposomal drug delivery. It has been shown that liposomal drug can reach the choroid, RPE and retinal ganglion cells after intravitreal injections and neural retina and ganglion cells after topical eye drop administration, respectively (Davis et al., 2014; Masuda et al., 1996). Lately, also nanosized lipid emulsions have been utilized a topical drug delivery system to the retina (Ying et al., 2013). However, delivery to the RPE and the route of transport from the surface of the eye to the back remains to be studied. Also large differences in delivery were noted between liposome types. Liposome formulation variables might be used to tune the delivery properties to the ocular tissues. It is very unlikely that liposomes could permeate in the tight corneal barrier. Conjunctiva and would be more probable route of penetration. Paracellular transport through the conjunctiva is possible for particles up to diameter of 5.5 nm and any particles larger than that would be carried via endocytosis pathways (Horibe et al., 1997). Conjunctiva can take up nanoparticles with diameter of 300 nm (Enriquez de Salamanca et al., 2006) and permeation of liposomes through the conjunctiva has been shown *in vitro* (Kompella et al., 1998). After passing through the conjunctiva, the drugs can reach the back of the eye via diffusion through sclera and vitreous or more directly via blood circulation to the choroid (Forrester, 2008; Hughes et al., 2005). Blood vessel mediated liposomal delivery to the posterior segment can be achieved only if the liposomes are able to distribute to the ocular tissues. For this purpose, the size of the liposomes is critically important due to the limited size of choroidal and conjunctival fenestrations (Guymer et al., 2004; Krachmer et al., 2011).

To achieve small liposomal size, we developed methods utilizing microfluidizers. The device drives liquid with high pressure (even 30,000 psi) through an interaction chamber. Thereafter, the liquid is collected or re-cycled through the microfluidizer. Particle size reduction is due to the shear forces at the chamber walls (Z-type chamber) or shear forces and the particle collisions (Y-type chamber) when high speed fluid streams with opposite directions merge. Microfluidizers have been used to process emulsions (Mahdi Jafari et al., 2006), polymer particles (Bodmeier and Huagang, 1990; Sani et al., 2009), crystalloid solids (Siqueira et al., 2009) and liposomes (Takahashi et al., 2009; Thompson and Singh, 2006). As a method of producing liposomes, microfluidizing has benefits of low polydispersity (Mahdi Jafari et al., 2006), continuous flow of solvent without a danger of clogging, suitability to heat sensitive drugs, and ease of scale up to larger volumes (Sorgi and Huang, 1996). The final particle size depends on the main process parameters, such as the pressure, temperature, and passage times through the microfluidizer (Mayhew et al., 1984; Saheki et al., 2012; Thompson and Singh, 2006; Washington and Davis, 1988).

Microfluidizer methods were optimized to produce small sized (<85 nm) liposomes. In order to elucidate the importance of liposomal diameter, we determined the effect of the liposomal size on their *in vivo* distribution in rat eyes after topical administration as eye drops. We demonstrate liposomal targeting to the retinal pigment epithelium with small transferrin conjugated liposomes.

2. Materials and methods

2.1. Materials

Hydrogenated soy L-α-phosphatidylcholine (HSPC) was a gift from NOF CORPORATION (Tokyo, Japan). 1,2-dioleoyl-3-trimethylammonium-propane (DOTAP), 1,2-dimyristoyl-3-trimethylammonium-propane (DMTAP), 1,2-dimyristoyl-sn-glycero-3-phosphocholine (DMPC), egg L-α-phosphatidylcholine (Egg PC), 1,2-distearoyl-sn-

glycero-3-phosphoethanolamine-N-[amino(polyethylene glycol)-2000] (DSPE-PEG), 1,2-distearoyl-sn-glycero-3-phosphoethanolamine-N-[maleimide(polyethylene glycol)-2000] (DSPE-PEG-Mal) and cholesterol (Chol) were purchased from Avanti Polar Lipids (Alabaster, AL, U.S.A.). 1,2-dioleoyl-sn-glycero-3-phosphoethanolamine-Atto 647N (ATTO-DOPE) was from ATTO-TEC (Siegen, Germany). Holo-Transferrin (Trf) and 2-iminothiolane hydrochloride (2-IT) were bought from Sigma–Aldrich (St. Louis, MO, U.S.A.). Luciferase plasmid DNA (pDNA) was produced in Tokyo University of Pharmacy & Life Sciences laboratory as described previously (Takashima et al., 2007). Sybr Green was from Lonza (Basel, Switzerland). Chloroform and other chemicals of analytical grade were bought from Wako Pure Chemical Industries (Osaka, Japan). Ultra pure water was made by Aquarius RFD24ONA water distillation apparatus and CPW-100 ultra pure water system (Advantec, Tokyo, Japan). Throughout the article, the ultra pure water is referred as water.

2.2. Microfluidizer process parameter study

HSPC and cholesterol powders were dissolved in chloroform to make 10 mg/ml and 5 mg/ml stock solutions respectively. 2780 µl of HSPC and 1410 µl of cholesterol stock solutions were added to a round bottomed 100 ml glass bottle and mixed gently. Total lipid content was 54.7 µmol with molar ratio of 2:1 (HSPC/Chol). The solution was evaporated to form a thin phospholipid film with a rotary evaporator system consisting of CCA-1111 Recirculating Chiller, DPE-1120 Solvent recovery unit, NVC-2100 Vacuum Controller, N-1100 Rotary Evaporator, OSB-2100 water bath (Eyela, Tokyo, Japan) and DIVAC 1.2 L vacuum pump (Oerlikon, Pfäffikon, Switzerland). Briefly, the glass bottle was attached to the evaporator system with a nitrogen gas flow, set to a slow rotation speed and lowered to a surface of water bath set at 65 °C. Pressure was slowly reduced to about 300–400 mmHg and the solution was evaporated. After no solution could be seen in the bottle pressure was lowered to controlled minimum of 20 mmHg for 30 min in order to evaporate the chloroform completely and to form the thin lipid film. Pressure was slowly returned to atmospheric pressure and the bottle was detached from the evaporator. Lipid film was hydrated with 15 ml of ultra pure water, heated over transition temperature of the lipid by immersing into the 65 °C water bath for 30 min and after that sonicated for 5 min with UC-1331 ultrasonicator (Tocho, Tokyo, Japan) to form large liposomes.

The samples with large liposomes were processed with M-110P (Y-type chamber) or LV-1 (Z-type chamber) microfluidizers (Fig. 1) (Microfluidics, Newton, MA, U.S.A.) with various processing parameters. LV-1 is a low volume version of the microfluidizer that uses a syringe type inlet, instead of a reservoir of M-110P model. This allows more precise loading of the sample into the microfluidizer in order to guarantee that the entire sample will be properly processed. Other main difference was that M-110P was equipped with a Y-type interaction chamber, whereas LV-1 had a Z-type interaction chamber. In Y-type chamber the size reduction of the particles is due to the shear forces to the walls of the chamber and the high speed collision of particles to each other when separated liquid streams merge. In Z-type chamber the size reduction is only due to the shear forces to the walls and has a somewhat weaker energy transfer level.

Water with a temperature above the transition temperature of the phospholipids (at 65 °C) was circulated in the heat exchanger (M-110P) to achieve the necessary fluidity of the liposomal bilayer for particle size reduction. The microfluidizer was primed with water and the samples were processed at pressures of 5000 psi (345 bar), 10,000 psi (689 bar) and 20,000 psi (1379 bar) and passage times ranging from 1 to 20. Contents of the product inlet reservoir were mixed with a product outflow stream exiting the microfluidizer in case of the model M-110P microfluidizer. With the model LV-1 microfluidizer, the samples were circulated by detaching the filled outflow syringe including the processed product and attaching the syringe to the inlet valve for next process cycle. A new sterile syringe was attached to outflow valve for the sample exiting the microfluidizer at next passage time.

2.3. Double emulsion method for liposome manufacturing by microfluidizer

The basic principle of the double emulsion method for liposome preparation is shown in Fig. 1. In detail, HSPC/DOTAP/Chol, DMPC/DMTAP/Chol or EggPC/DMTAP/Chol in molar ratios of 1:2:0.5 were dissolved in 13 ml of chloroform and vortexed for a few seconds to form a solution with free lipids (Fig. 1A). Total amount of lipids per sample was 30 µmol. 2 ml of water, with or without pDNA (16.3 µg/ml), was added to the solution, vortexed shortly and sonicated for 5 min to form a water–chloroform emulsion. The microfluidizer was primed with chloroform. Heat exchanger was filled with water and ice to prevent the evaporation of the organic solvent.

Emulsion was microfluidized at a pressure of 20,000 psi with 10 passage times to form small reverse micelles in organic solvent (Fig. 1B). Sample was retrieved from the microfluidizer after which

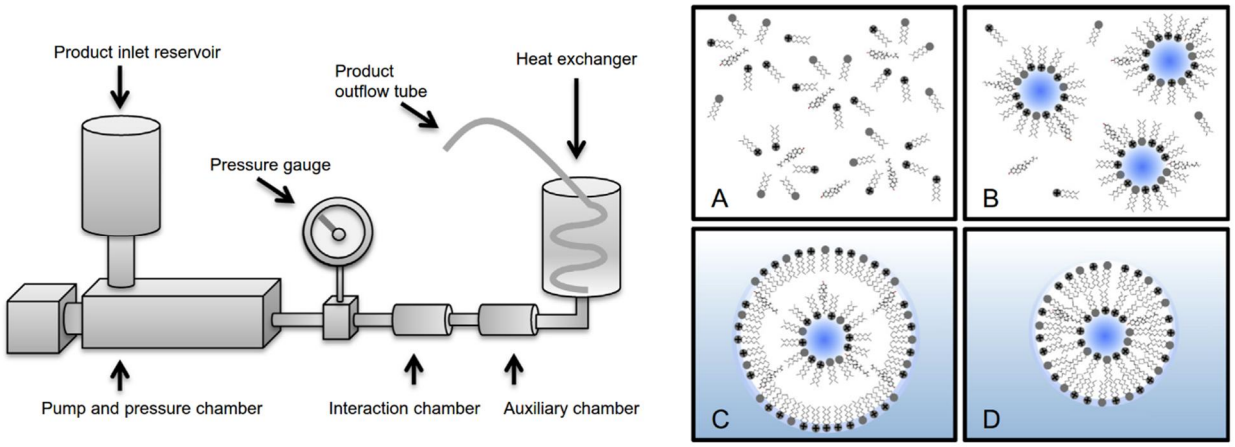

Fig. 1. The structural components of typical microfluidizer (M-110P) and steps of double emulsion liposome production. (A) Free lipids in organic solvent, (B) reverse micelles with aqueous core in organic solvent, (C) double emulsion with aqueous core, organic solvent between the lipid layers and aqueous outer phase, and (D) finished liposomes in aqueous phase.

water of 2 times the volume of the sample was added and mixture was vortexed. Microfluidizer was primed with water. Sample mixture was microfluidized at a pressure of 8000 psi (552 bar) with 5 passage times. After the microfluidizing process, a homogenous white opaque W/O/W – double emulsion was formed with organic phase filling a small space between the lipid layers (Fig. 1C).

Samples were placed in glass bottles with magnetic stirring bars, and the chloroform was evaporated by stirring at room temperature for 24 h. When the evaporation was complete, phospholipids formed a typical liposomal bi-layer (Fig. 1D) and the solution was colorless and transparent.

2.4. Liposome characterization

2.4.1. Particle size measurement

The particle size was measured with Photal DLS-7000 dynamic light scattering particle sizer (Otsuka Electronics Inc., Osaka, Japan) by argon gas laser with wave length of 488 nm, scattering angle of 90° and controlled temperature of 25 °C. Size was determined by Marquadt analysis and presented as mean particle diameter of weight histogram.

2.4.2. Zeta potential measurement

The zeta potential of the liposomes was measured with Nicomp 380 ZLS zeta sizer (PSS NICOMP, Santa Barbara, CA, U.S.) using automatic scattering intensity and measurement time of 2 min.

2.4.3. Measurement of plasmid DNA release from liposomes

Release of pDNA from the liposomes was determined with a SYBR Green assay suitable for pDNA analysis (Even-Chen and Barenholz, 2000). 50 µl of double emulsion liposome samples including pDNA was added to a 96-well plate. 50 µl of Sybr Green dilution (1:1000) was added to the wells. Sybr Green forms a fluorescent complex with the free pDNA outside the liposomes. Fluorescence was measured with Safire F129013 microplate reader (Tecan Group Ltd., Männedorf, Switzerland) with excitation and emission wavelengths of 494 nm and 521 nm, respectively. 50 µl of 0.5 mM dextran sulfate solution was added to the wells and fluorescence was measured again. Dextran sulfate binds to cationic phospholipids more strongly than pDNA, thus replacing the liposomal surface bound pDNA for fluorescent detection. Then 50 µl of 1% Triton-X solution was added to the wells and fluorescence was measured for the final time. Triton-X breaks the lipid bilayer and frees the pDNA from inside the liposomes. Fluorescence intensity caused by pDNA was calculated by reducing the intensity of empty liposomes (same formulation without pDNA) from the intensity of the pDNA liposomes. The percentage of pDNA inside the liposomes is calculated by subtracting the fluorescence intensity of free and surface bound pDNA from the total fluorescence intensity.

2.5. In vivo distribution study

2.5.1. Sample preparation

Stock solutions of HSPC (10 mg/ml), Chol (5 mg/ml), DSPE-PEG (10 mg/ml) and fluorescent ATTO-DOPE (0.1 mg/ml) in chloroform were prepared. Large HSPC/Chol/DSPE-PEG/ATTO-DOPE liposomes with molar ratios of 2:1:0.02:0.005 and total lipid amount of 15.1 µmol in 15 ml of water was prepared by thin film hydration method as described earlier in process parameter study. These liposomes were processed with microfluidizer (20,000 psi, 10 passage times) to form the small PEG-liposomes.

For active targeting to RPE, transferrin modified liposomes were produced. First DSPE-PEG-Trf micelles were produced with a following method. 2-IT was weighed to Eppendorf tube and dissolved with Hepes (pH 8) to form a 1 µg/µl solution. 5 mg of Trf was put into a test tube and dissolved with 500 µl of Hepes (pH 8) while stirring with a magnetic stirrer. 88 µl of 2-IT solution and 412 µl of Hepes (pH 8) were added to the Trf solution. Mixture was stirred for 1 h in dark and room temperature. 100 µl of DSPE-PEG-Mal in chloroform (2.5 mg/ml) was put into a test tube. Chloroform was evaporated by N_2-stream to form a lipid film. 850 µl of Mes-buffer (pH 6.5) was added into the tube to hydrate the film. 837 µl of DSPE-PEG-Mal solution and 403 µl of Mes-buffer (pH 6.5) were put into a larger test tube. 40 µl of Hepes (pH 8) was added to the Trf/2-IT solution and the whole volume (1040 µl) was added to the large test tube drop by drop while stirring the contents by magnetic stirrer. The mixture was left in room temperature and stirred gently in dark overnight.

After 24 h sucrose was added to the solution up to concentration of 0.09 g/ml, after which the solution was frozen to −80 °C and freeze dried over night with Freezvac 3C freeze-drier (Tozai Tsusho, Tokyo, Japan). A mixture of 100 µl water and 500 µl chloroform was added to the test tube to dissolve the phospholipids. HSPC, Chol and ATTO-DOPE stock solutions were added to a tube to achieve same molar ratios and lipid amounts as with the small PEG-liposomes described earlier, but including the transferrin modified PEG. Large Trf-PEG-liposomes were prepared by thin film hydration method and the liposome solutions were processed in microfluidizer at pressure of 20,000 psi with 10 passage times to from a sample of small Trf-PEG-liposomes, or at pressure of 5000 psi with 2 passage times to form a sample of large Trf-PEG-liposomes.

2.5.2. Topical instillation of liposomes and tissue imaging

200 µl of PEG-liposomes, small Trf-PEG-liposomes with diameter of about 60 nm, large Trf-PEG-liposomes with diameter of about 100 nm or isotonic water as control were dropped into right eyes of 12 week old male SD-rats. The prepared liposomes were used immediately after preparation in order to ensure the correct size of the liposomes. 5 min or 15 min after the treatment by the eye drops, the rats were killed and both eyes were removed. The eye samples were washed with phosphate buffered saline, stored in concentrated sucrose solution in a cold room (4 °C). The sucrose concentration was increased with 6 h intervals up to 20%. The eyes were moved into small containers that were filled with tissue mount solution and frozen tissue cubes were formed by cooling with liquid nitrogen. The eye tissue cubes were cut to 10 µm thick slices, which were then mounted on glass slides and photographed with Fluoview FV1000 confocal microscope (Olympus, Tokyo, Japan). All experiments with animals were carried out in accordance with a protocol approved by the Animal Care and Ethics Committee of Tokyo University of Pharmacy and Life Sciences (Test permission number P12-26).

2.6. Statistical analysis

Tests were performed in replicates to retrieve standard deviation. Student's *t*-test was used to evaluate the difference between the groups. The differences between the results were deemed to be significant with *p*-values less than 0.05.

3. Results and discussion

3.1. Effects of microfluidizer process parameters on particle size

The batches of the large liposomes were produced by thin film hydration method. The diameters of the liposomes varied from 2290 nm to 3523 nm with the standard deviations of (sd) of 434–1212 nm. The large liposomes were processed with microfluidizer at the pressures of 5000 psi, 10,000 psi and 20,000 psi.

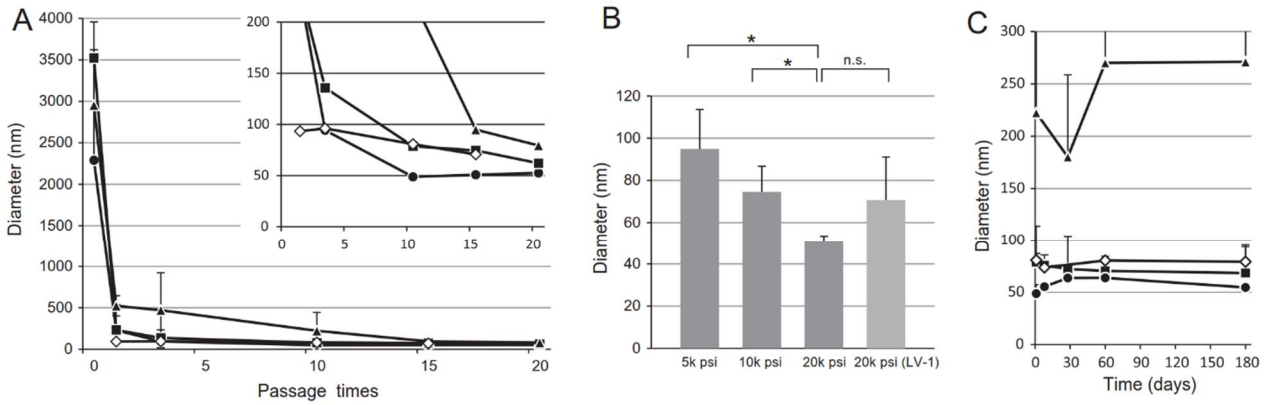

Fig. 2. (A) Liposome size of samples made by pressure of 5000 **psi** (black triangles), 10,000 **psi** (black squares), 20,000 **psi** (black circles) with M-110P and pressure of 20,000 **psi** with LV-1 (open diamonds). Insert graph is a zoomed in view of 0–200 nm diameter range. (B) The sizes of liposome samples obtained at different pressures and with 15 passage times. Samples without (LV-1) label were produced with M-110P microfluidizer. (C) Stability of 15 passage time liposomes with operating pressures 5000 **psi** (black triangles), 10,000 **psi** (black squares) and 20,000 **psi** (black circles) using M-110P and pressure of 20,000 **psi** with LV-1 (open diamonds). Error bars represent the standard deviations ($n = 3$). $^{*}p < 0.05$, n.s. = not significant.

Samples were collected after the liposome solutions had passed through the microfluidizer 1, 3, 10, 15 and 20 time(s) and liposome diameter was analyzed with dynamic light scattering (Fig. 2A).

The first passage through the microfluidizer had the most pronounced effect on the size of the liposomes. With all pressures used the diameter was reduced to sub-micron sizes. After 3 passages through the microfluidizer, diameter of the 20,000 psi sample was already at 94 ± 64 nm while 10,000 psi and 5000 psi samples had diameters of 136 ± 98 nm and 470 ± 452 nm, respectively. As can be seen, the standard deviations were still quite large. Continuing the microfluidizing further to 10 passage times still had significant effect on the size of the 5000 psi produced liposomes and it also reduced the polydispersity of the particles as indicated by smaller standard deviations. For example the average sizes of 20,000 psi liposomes were 2290 ± 1212 nm without microfluidizing, at 1 passage time 229 ± 295 nm, at 3 passages 94 ± 64 nm, at 10 passages 49 ± 9 nm, at 15 passages 51 ± 3 nm and at 20 passages 53 ± 3 nm. No changes in the size of the liposomes were observed after about 10 passages through the microfluidizer at high operating pressures. With 5000 psi the size decreased at a steady pace throughout the passage number range. The results indicate clearly that the decrease in size of the liposomes is proportional to increase of the pressure and passages. It should be noted that this might not be the case for all nanoparticles. For example, using several passages through microfluidizer for polyethylene glycol polylactide-co-glycolide (PEG-PLGA) polymer micelles causes increase in diameter (Sani et al., 2009).

With LV-1, the passage through the microfluidizer is more complete and better controlled compared with that of M-110P model, and thus the maximal decrease of diameter of the liposomes was reached very quickly. Already with only one pass through, the size is reduced to 93 ± 11 nm. Subsequent passages through the microfluidizer had smaller effect on the particle size when compared to the M-110P model. After 15 passage times, the particle size had been reduced to about 70 ± 20 nm.

To better compare the effect of the pressure, the samples with same 15 passage times were processed at different pressures and machines (Fig. 2B). Increasing the pressure produced significantly smaller liposomes. We calculated a logarithmic regression line ($R^2 = 0.998$) for the effect of increased pressure with M-110P on the particle diameter. The equation of the regression line is

$$D = -31.81 \ln(P) + 366.44$$

where D is the diameter of the liposome and P is the operating pressure of the microfluidizer in psi. It can be used to predict the size range of the liposomes produced with specific pressure. The equation predicts that increase of pressure beyond 20,000 psi has only limited effect on the reduction of liposome size. The physical properties of phospholipid bilayers that cause tension in the structure will prevent limitless reduction in size. Also because typical maximum pressure for laboratory scale microfluidizer instruments is 30,000 psi, further increase in operating pressure is not often possible. Our results also showed that the polydispersity was reduced with higher pressures when comparing M-110P samples. Same level of decrease in size and low polydispersity could not be achieved with LV-1 microfluidizer (Z-type chamber) due to weaker shear forces in the Z-type interaction chamber compared to the Y-type.

The instability of liposomes can be seen as merging of one or more particles and thus formation of larger liposomes. This is seen as shift in particle size to larger diameter throughout the testing period. In order to see if the microfluidizing parameters affect the long term stability of the liposomes, samples were stored in the refrigerator in aqueous solution for 6 months. Diameter of the particles was measured at set time points during the storage. Results of the stability study are shown in Fig. 2C.

The size of 5000 psi liposomes remained large and polydisperse during the storage. The size of the other samples also stayed quite unchanged below the diameter of 100 nm. The final diameters for below 100 nm liposomes were 55 ± 2 nm for 20,000 psi liposomes, 68 ± 25 nm for 10,000 psi liposomes and 79 ± 16 nm for LV-1 liposomes, at the 6 month time point. Microfluidizing process does not have a negative impact on the chemical stability of the phospholipids, since the temperature increase in the interaction chamber is well below the chemical degradation temperature of the phospholipids in this study.

Liposomes of different sizes can be produced by varying the process parameters. Thus this method offers a useful tool for studies that consider the diameter of the particles to be a key element. The liposomes produced with M-110P microfluidizer at the pressure of 20,000 psi and 10 passage times had a suitable diameter to meet our requirements for retinal targeting. Therefore these process parameters were chosen for further studies.

3.2. Inner phase isolation methods

Microfluidizing uses high energy shear forces to reduce the particle size and could affect negatively to the percentage of encapsulated drug in the liposomes by temporarily breaking up the bi-layer allowing the drug to escape into solution. In order to prevent leak-

age and achieve high loading capacity of the drug during the extreme conditions of microfluidizing, methods to isolate the inner phase were studied. We theorized that two immiscible solutions that are separated by a phospholipid layer would prevent this. First we elucidated the possibility to use oil, which has high viscosity and different density than water, as a second phase. Squalene was chosen as a candidate based on previous literature (Pautot et al., 2003; Whittenton et al., 2008). This method consisted of producing pre-vesicles (reverse type) with microfluidizer followed by particle transfer through W/O-interphase. The experiment did not show promising results (see Appendix A).

In the second method we wanted to simplify the process and developed a new microfluidizer double emulsion method with inner and outer aqueous phases and an organic phase between them. This method was planned so that mainly only microfluidizer would be used to make the liposomes from the beginning to the end, and thus significantly reducing the number of necessary steps and equipment. Chloroform was chosen as an isolating immiscible organic solvent for double emulsion.

3.2.1. Microfluidizer double emulsion liposomes

As described in Section 2, the double emulsion method utilizes two immiscible phases, water and organic solvent. Through optimization, chloroform was found to be suitable solvent for our needs. Among other organic solvents, for example cyclohexane had a limited pressure range with the microfluidizer and did not dissolve all the phospholipids used in this study. Chloroform is suitable solvent for most phospholipids in liposome preparation. During the manufacturing process the chloroform is removed from the double emulsion by evaporation. Stirring the emulsion in room temperature over night was found to produce better results than simple incubation in room temperature, heating with a water bath, centrifugation or evaporation in vacuum conditions (data not shown).

3.2.1.1. pDNA release from microfluidizer double emulsion liposomes. Because delivery of pDNA and other large molecule drugs is one of the major reasons to use of liposomes as a drug delivery system, we studied the suitability of double emulsion method in pDNA encapsulation. In order to entrap negatively charged pDNA into the liposomes, cationic lipid formulations were chosen for the double emulsion experiments. Cationic liposomes can bind negatively charged nucleotides, protect pDNA from the nucleases in the body, and enhance pDNA delivery into the cells. In the double emulsion method, pDNA is isolated in the inner water phase of small volume, because of the immiscible organic solvent and the phospholipid layers. This should enable efficient encapsulation of the pDNA. First we studied combination of HSPC and DOTAP as neutral and cationic phospholipids. We also wanted to examine the effect of phospholipid carbon chain length on the pDNA encapsulation to see if method is usable for different kinds of formulations. We chose a combination of DMPC and DMTAP with shorter acyl chain length.

The release of pDNA from the liposomes was studied with a Sybr Green assay. First Sybr Green solution was added to the samples and fluorescence was measured. The possible fluorescence detected was from binding to the free pDNA molecules outside the liposomes. Next sufficient amount of dextran sulfate was added to release pDNA that was electrostatically bound to the liposomal surface. Again, this was detected with Sybr Green. Lastly Triton-X was added to break the liposomes and free all pDNA.

Both HSPC/DOTAP and DMPC/DMTAP had a quite similar profile in terms release percentage of encapsulated pDNA (Table 1). In the release of encapsulated pDNA from inside the liposomes, the difference between the two formulations was not statistically significant ($p = 0.057$ with Student's t-test). About 80% of released pDNA in both samples was from inside the liposomes indicating good isolation efficiency to inner phase. Similar percentages can be achieved also with other manufacturing methods, but they often involve more production steps and necessary production machinery (Bailey and Sullivan, 2000). Good encapsulation percentage, controllable diameter and relatively simple process with only a little necessary equipment indicate that double emulsion method is very recommendable for production of small sized pDNA liposomes.

Table 1
Detected amounts (%) of pDNA from different sites in the liposome samples with two lipid formulations ($n = 3$).

	HSPC/DOTAP	DMPC/DMTAP
Free pDNA in solution	**0.7** ± 0.3	−**3.7** ± 3.8
Bound pDNA on outer lipid surface	**13.7** ± 0.8	**26.7** ± 1.9
Encapsulated pDNA inside liposomes	**85.6** ± 1.1	**77.0** ± 1.9

3.2.1.2. Size and zeta potential analysis of microfluidizer double emulsion liposomes. Naturally with different production method, the diameter of the liposomes had to be investigated. HSPC/DOTAP formulation produced liposomes with diameter of 105 ± 8 nm with zeta potential of 37.9 ± 0.7 mV. The particle size results are shown in Fig. 3. The liposomes have a narrow polydispersity, but the particle size was outside of the target range (<85 nm) for passing through the fenestrations in the choroid (Guymer et al., 2004). On the other hand, the double emulsion method resulted in suitably small DMPC/DMTAP – liposomes with diameter of 62 ± 6 nm and zeta potential of 35.8 ± 0.8 mV.

HSPC and DOTAP have 18 carbon acyl chains: HSPC saturated and DOTAP unsaturated with single double bonds. DMPC is a zwitter-ionic phospholipid with 14 carbon acyl chains, DMTAP is a cationic phospholipid with 14 carbon chains, and the acyl chains are saturated in both cases. To further study the effect of different acyl chains on the liposome size, we changed the neutral phospholipid and produced Egg PC/DMTAP – liposomes with the double emulsion method. Egg PC is a neutral phospholipid in which predominant species have saturated 16 carbon acyl chains and unsaturated 18-C acyl chains with a single double bond. The Egg PC/DMTAP – liposomes had a diameter of 83 ± 7 nm and zeta potential of 35.5 ± 1.0 mV. All the formulations had significantly different sizes.

As the zeta potentials of these liposomes were similar and the difference between the formulations was the acyl chains of the phospholipids, we could postulate that the chain length is one of the significant key qualities for the diameter of the liposomes during the double emulsion method. It has been shown that transition temperature of the phospholipid affects the final size of the liposomes water/organic phase microfluidic conditions (Zook and Vreeland, 2010). The lower the processing temperature is compared to the transition temperature, the larger formed phospholipids will be. Longer acyl chained HSPC has higher transition temperature (appr. 50 °C) than DMPC (24 °C) and thus the temperature difference to the operating conditions is greater, which may in part result as larger liposome diameters. We think that also the different packing properties of the acyl chains may have effect on the final liposome size in double emulsion method. It is known that the spontaneous curvature of the bilayer depends largely on hydrocarbon chains (Bergström, 2006), so in addition to the operating conditions, also phospholipid composition may affect the final liposome size.

The storage stability of the formulations was investigated (Fig. 3B). DMPC liposomes produced with the double emulsion method were found to be stable for at least one month when stored

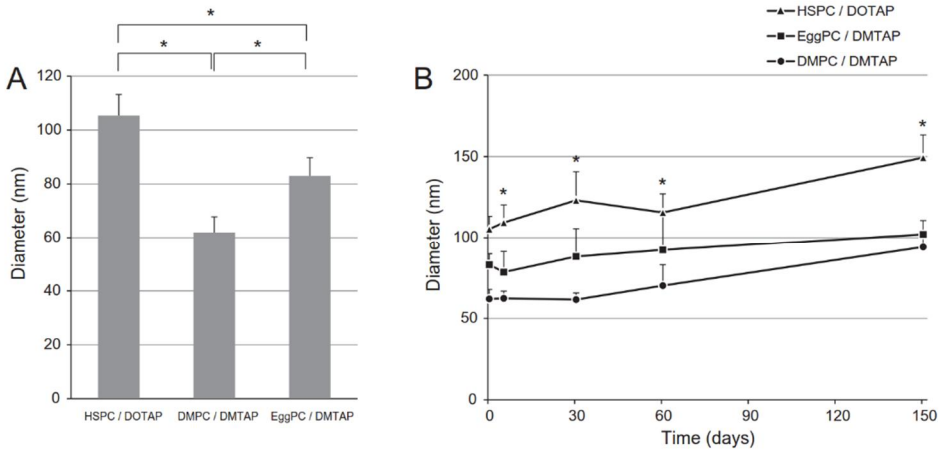

Fig. 3. Initial sizes after preparation (A) and 5 month stability study (B) of cationic double emulsion liposomes. Error bars represent the standard deviations ($n = 9$). Statistical significance between formulations $^{*}p < 0.05$.

in a refrigerator in an aqueous solution. Increase in diameter was noticed with the other formulations during this time. The DMPC/DMTAP samples also had a slight increase in diameter during the 1 month to 2 months storage period. At 2 month time point sizes of samples were 116 ± 11 nm, 92 ± 24 nm and 70 ± 13 nm for HSPC/DOTAP, EggPC/DMTAP and DMPC/DMTAP – liposomes, respectively. The diameter of the DMPC/DMTAP samples was still well within our target range up to 2 months. The steady increase is liposomal size continued throughout the storage period and at final time point of 5 months the sizes were 149 ± 14 nm, 102 ± 9 nm and 94 ± 9 nm for HSPC/DOTAP, EggPC/DMTAP and DMPC/DMTAP -liposomes, respectively. Thus the formulations were all larger than the limit of 85 nm. Differences between all of the groups during the whole storage period were statistically significant. According to the stability study, the DMPC/DMTAP liposomes should be used as soon as possible after manufacturing or at least after maximum of 1–2 months of storage in refrigerator. The stability of these liposomes is not suitable for commercial purposes in this from, but could be improved by stabilizers in buffer solution or by storing the product in a freeze dried form.

3.3. In vivo distribution of small liposomes in eye

In order to show a proof of concept, a preliminary delivery experiment was conducted. This *in vivo* study was performed in order to see qualitatively if the very small size achieved with the microfluidizing process has influence on ocular liposome delivery after administration as topical eye drops. If these small liposomes could reach the posterior segment, in particular the RPE via choroidal blood flow, it would open possibilities towards the liposomal drug delivery to the RPE in outpatient setting.

PEG in the formulation is used for masking the liposomes from defense mechanisms of the body and for improving the liposomal stability (Allen et al., 1991) and transferrin was selected as the targeting ligand, because it has been shown to improve the tissue uptake of the liposomes (Hatakeyama et al., 2004) and the RPE is rich with transferrin receptors (Yefimova et al., 2000). Furthermore, transferrin has been proven to be up-regulated in age related macular degeneration (Chowers et al., 2006). Transferrin mRNA and protein levels were higher in both neovascular and non-neovascular form of the disease compared to normal retinal tissue. This should improve the liposomal targeting to diseased parts of the posterior segment of the eye. Binding of transferrin modified liposomes to transferrin receptor expressing cells has been shown to be more efficient compared to liposomes without transferrin ligand and the transferrin modified liposomes were taken up by the cells (Voinea et al., 2002). Due to these qualities, transferrin is expected to be actively targeted to the RPE.

HSPC/Chol/DSPE-PEG and HSPC/Chol/DSPE-PEG-Trf liposomes were produced and particle size was determined immediately after manufacturing. Diameters and zeta potentials of small Trf liposomes (68 ± 5 nm), large Trf liposomes (100 ± 13 nm) and liposomes without Trf (73 ± 11 nm) are included in left side legend of Fig. 4. Based on our hypothesis, the small liposomes should be able to reach to the RPE target, but large Trf liposomes should not be able to pass through the pores of the choroid and reach RPE, because their diameter is more than 85 nm. On the other hand small Trf liposomes should show a stronger signal in RPE compared to PEG liposomes, because of active targeting to transferrin receptor rich RPE surface (Yefimova et al., 2000). In the RPE, the transferrin receptors are only located on the basolateral side (Sugasawa et al., 1994). Thus in order to utilize the receptors, the liposomes should reach to the RPE from choroidal side, not from the vitreous.

According to our hypothesis, the liposomes would distribute to the posterior segment of the eye via passage through the conjunctiva and the long posterior ciliary arteries. Movement of the particles to the target tissues should be quite fast, so relatively early time points of 5 and 15 min were chosen. This way the distribution should be visible before the liposomes are eliminated from the target area.

Tissue slices of the rat eyes were photographed by confocal microscope (Fig. 4). As expected we could not detect any fluorescence signal from control samples without liposomes. Also no signal was detected in PEG liposome samples. Small Trf liposomes showed a clear fluorescence signal from the thin RPE layer of eye drop instilled right eye at 5 min time point. This supports the idea of liposome distribution to the RPE via blood circulation. In comparison the studies targeting the neural retina via the vitreous show delivery times of two hours (Davis et al., 2014). This is expected as the vitreous is known to significantly slow down the liposome distribution to the posterior segment (Mains and Wilson, 2013). Large Trf liposomes showed a weaker signal in right eye at 5 min time point and the fluorescence was located in a thicker layer next to RPE more to the posterior, namely the choroid. A very weak signal could be detected with the small Trf liposomes in the RPE layer of untreated left eye at 5 min time point. At 15 min time point the small Trf liposomes still showed some fluorescent signal at RPE cells. Merged images of bright view photographs

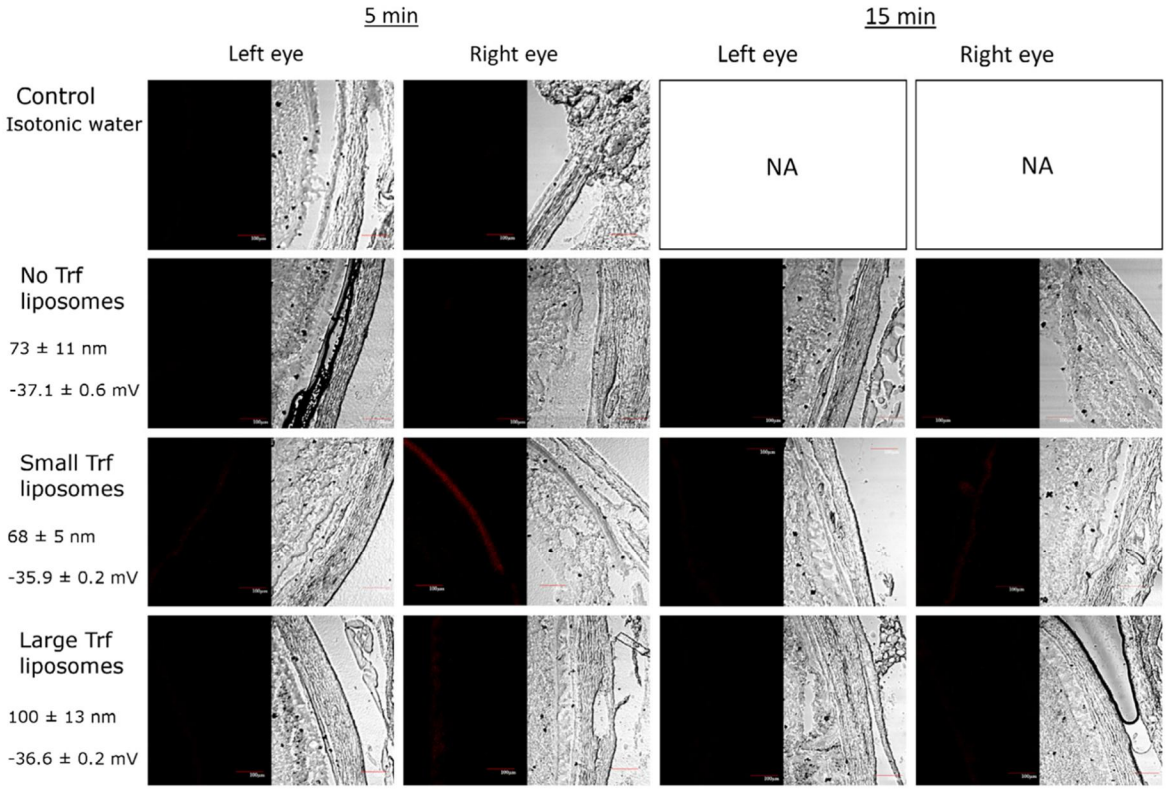

Fig. 4. Confocal microscope pictures of posterior segments of the eyes removed at 5 min and 15 min time points after eye drops to the right eyes with control sample without liposomes, small liposomes without active targeting to RPE, and small and large liposomes with active targeting. Left eyes were untreated. Liposome size and zeta potentials of samples are included in the left side legend ($n = 6$). Difference in size between small and large liposomes is statistically significant ($p < 0.05$).

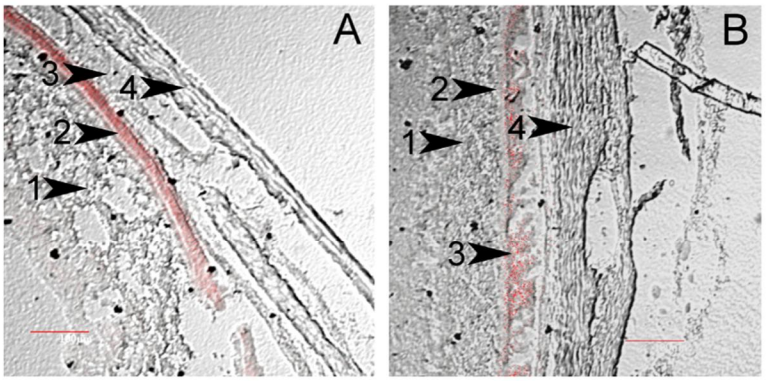

Fig. 5. Merged bright view and fluorescent channels of confocal pictures. (A) Small Trf liposomes 5 min right eye sample. (B) Large Trf liposomes 5 min right eye sample. Numbered arrowheads point the different layers of the eye: neural retina (1), retinal pigment epithelium (2), choroid (3) and sclera (4). Scale bar is 100 μm.

and fluorescent signal for small and large Trf liposomes from right eyes at 5 min time point are shown in a Fig. 5.

These results showed that the size was an important factor in liposomal delivery to the RPE. Presumably, the larger liposomes could not pass through the choroidal pores and thus remained in the choroidal side. The cells lining the choroidal capillaries also have a few transferrin receptors (Yefimova et al., 2000), so the liposomes retained in small degree to the choroidal layer. By adjusting the liposomes to suitable size range with microfluidizing technique, it is possible to target the different layers in the posterior segment of the eye. With liposomes smaller than 80 nm delivery can be achieved to the RPE, whereas liposomes at around 100 nm in diameter can be targeted to choroidal endothelial cells. The signal in the RPE at 15 min time point with the small Trf liposomes could be barely detected. If concentration of the drug formulation and retention to the RPE could be increased, the exposure time to the target tissue could be longer.

Active targeting with modified liposomes was needed for effective delivery into the target tissue, as small enough liposomes without transferrin did not show fluorescent signal in the RPE. It seems that systemic circulation also carries a small portion of the dose to the non-treated eye, as indicated by the weak signal in the left eye with small Trf liposomes. This supports the notion that the liposomes are entering the RPE from the choroidal side (i.e. blood circulation side), where the transferrin receptors are located (Voinea et al., 2002).

This study demonstrates new proof-of-principle that small liposomes with active targeting ligands can be delivered to the RPE after eye drop administration. Confocal microscopy study showed that liposomes were delivered to the RPE and choroid, but this is not quantitative analysis. Further studies are needed to elucidate the quantity of liposomes in different ocular layers and release of model drug, for example siRNA or pDNA. The pathways of liposomal permeation to the RPE are difficult to assess, but the rapid liposome distribution to the posterior segment in 5 min after topical instillation suggests that the liposomes were transferred in the blood flow of ciliary arteries. Permeation of the liposomes without blood flow in the ocular tissues would take much longer time. The alternative delivery route (permeation across the conjunctiva, sclera and choroid) should show more intense fluorescence signal in the sclera, iris and ciliary body. Because such fluorescence distribution was not detected, the results support the theory of liposome distribution via blood circulation (thereby bypassing sclera, iris and ciliary body). Distribution pattern of the liposomes also rules out the delivery across the cornea, anterior chamber and vitreous.

The principle for topical drug delivery with liposomes to specific tissues in the back of the eye was shown in this article. More specific studies should be carried out to determine the exact route and quantity of the liposome delivery from the surface of the eye to the RPE in the posterior segment.

4. Conclusions

In this study we investigated the liposomal delivery from eye drops to the posterior eye segment and preparation methods for controlled liposomal diameter. Small stable liposomes were produced using new microfluidizing procedures. After tagging the small liposomes with transferrin, they reached the RPE after topical eye drop instillation. This proof-of-principle study forms a basis to optimization of drug delivery systems that will enable treatment of retinal diseases with topical eye drops instead of intraocular injections.

Acknowledgments

We would like to thank POWREX Corporation for providing us the Microfluidizers and for technical support during this study. This research was supported by grants from Academy of Finland.

Appendix A. Supplementary material

Supplementary data associated with this article can be found, in the online version, at http://dx.doi.org/10.1016/j.ejps.2014.04.018.

References

Allen, T., Hansen, C., Martin, F., Redemann, C., Yau-Young, A., 1991. Liposomes containing synthetic lipid derivatives of poly (ethylene glycol) show prolonged circulation half-lives in vivo. Biochim. Biophys. Acta (BBA)-Biomembr. 1066, 29–36.

Bailey, A.L., Sullivan, S.M., 2000. Efficient encapsulation of DNA plasmids in small neutral liposomes induced by ethanol and calcium. Biochim. Biophys. Acta (BBA)-Biomembr. 1468, 239–252.

Bakri, S.J., Snyder, M.R., Reid, J.M., Pulido, J.S., Singh, R.J., 2007. Pharmacokinetics of intravitreal bevacizumab (Avastin). Ophthalmology 114, 855–859.

Bangham, A., Standish, M.M., Watkins, J., 1965. Diffusion of univalent ions across the lamellae of swollen phospholipids. J. Mol. Biol. 13, 238–252.

Bergström, L.M., 2006. Model calculations of the spontaneous curvature, mean and Gaussian bending constants for a thermodynamically open surfactant film. J. Colloid Interface Sci. 293, 181–193.

Beuerman, R.W., Pedroza, L., 1996. Ultrastructure of the human cornea. Microsc. Res. Tech. 33, 320–335.

Bodmeier, R., Huagang, C., 1990. Indomethacin polymeric nanosuspensions prepared by microfujidization. J. Controlled Release 12, 223–233.

Cavallotti, C., Corrado, B.G., Feher, J., 2005. The human choriocapillaris: evidence for an intrinsic regulation of the endothelium? J. Anat. 206, 243–247.

Chowers, I., Wong, R., Dentchev, T., Farkas, R.H., Iacovelli, J., Gunatilaka, T.L., Medeiros, N.E., Presley, J.B., Campochiaro, P.A., Curcio, C.A., Dunaief, J.L., Zack, D.J., 2006. The iron carrier transferrin is upregulated in retinas from patients with age-related macular degeneration. Invest. Ophthalmol. Vis. Sci. 47, 2135–2140.

Davis, B.M., Normando, E.M., Guo, L., O'Shea, P., Moss, S.E., Somavarapu, S., Cordeiro, M.F., 2014. Topical delivery of avastin to the posterior segment of the eye in vivo using annexin A5-associated liposomes. Small 10, 1575–1584.

Del Amo, E.M., Urtti, A., 2008. Current and future ophthalmic drug delivery systems: a shift to the posterior segment. Drug Discov. Today 13, 135–143.

Enriquez de Salamanca, A., Diebold, Y., Calonge, M., Garcia-Vazquez, C., Callejo, S., Vila, A., Alonso, M.J., 2006. Chitosan nanoparticles as a potential drug delivery system for the ocular surface: toxicity, uptake mechanism and in vivo tolerance. Invest. Ophthalmol. Vis. Sci. 47, 1416–1425.

Even-Chen, S., Barenholz, Y., 2000. DOTAP cationic liposomes prefer relaxed over supercoiled plasmids. Biochim. Biophys. Acta (BBA)-Biomembr. 1509, 176–188.

Forrester, J.V., 2008. The Eye: Basic Sciences in Practice. Saunders/Elsevier, Edinburgh, New York.

Guymer, R.H., Bird, A.C., Hageman, G.S., 2004. Cytoarchitecture of choroidal capillary endothelial cells. Invest. Ophthalmol. Vis. Sci. 45, 1660–1666.

Hatakeyama, H., Akita, H., Maruyama, K., Suhara, T., Harashima, H., 2004. Factors governing the in vivo tissue uptake of transferrin-coupled polyethylene glycol liposomes in vivo. Int. J. Pharm. 281, 25–33.

Horibe, Y., Hosoya, K., Kim, K., Ogiso, T., Lee, V.H., 1997. Polar solute transport across the pigmented rabbit conjunctiva: size dependence and the influence of 8-bromo cyclic adenosine monophosphate. Pharm. Res. 14, 1246–1251.

Huang, H.S., Schoenwald, R.D., Lach, J.L., 1983. Corneal penetration behavior of beta-blocking agents II: assessment of barrier contributions. J. Pharm. Sci. 72, 1272–1279.

Hughes, P.M., Olejnik, O., Chang-Lin, J., Wilson, C.G., 2005. Topical and systemic drug delivery to the posterior segments. Adv. Drug Deliv. Rev. 57, 2010–2032.

Hämäläinen, K.M., Kananen, K., Auriola, S., Kontturi, K., Urtti, A., 1997. Characterization of paracellular and aqueous penetration routes in cornea, conjunctiva, and sclera. Invest. Ophthalmol. Vis. Sci. 38, 627–634.

Kawakami, S., Yamamura, K., Mukai, T., Nishida, K., Nakamura, J., Sakaeda, T., Nakashima, M., Sasaki, H., 2001. Sustained ocular delivery of tilisolol to rabbits after topical administration or intravitreal injection of lipophilic prodrug incorporated in liposomes. J. Pharm. Pharmacol. 53, 1157–1161.

Kidron, H., del Amo, E.M., Vellonen, K., Urtti, A., 2012. Prediction of the vitreal half-life of small molecular drug-like compounds. Pharm. Res. 29, 3302–3311.

Kim, H., Csaky, K.G., Chan, C., Bungay, P.M., Lutz, R.J., Dedrick, R.L., Yuan, P., Rosenberg, J., Grillo-Lopez, A.J., Wilson, W.H., 2006. The pharmacokinetics of rituximab following an intravitreal injection. Exp. Eye Res. 82, 760–766.

Kompella, U.B., Katragadda, A.K., Aukunuru, J.V., Betageri, G.V., 1998. Effect of liposomal charge on stavudine transport across rabbit cornea and conjunctiva. Pharm. Pharmacol. Commun. 4, 339–343.

Krachmer, J.H., Mannis, M.J., Holland, E.J., 2011. Cornea. Mosby, St. Louis, Mo.

Law, S., Huang, K., Chiang, C., 2000. Acyclovir-containing liposomes for potential ocular delivery: corneal penetration and absorption. J. Controlled Release 63, 135–140.

Mahdi Jafari, S., He, Y., Bhandari, B., 2006. Nano-emulsion production by sonication and microfluidization—a comparison. Int. J. Food Prop. 9, 475–485.

Mains, J., Wilson, C.G., 2013. The vitreous humor as a barrier to nanoparticle distribution. J. Ocul. Pharmacol. Ther. 29, 143–150.

Masuda, I., Matsuo, T., Yasuda, T., Matsuo, N., 1996. Gene transfer with liposomes to the intraocular tissues by different routes of administration. Invest. Ophthalmol. Vis. Sci. 37, 1914–1920.

Maurice, D.M., 2002. Drug delivery to the posterior segment from drops. Surv. Ophthalmol. 47, 41–52.

Maurice, D., Mishima, S., 1984. Ocular pharmacokinetics. In: Anonymous Pharmacology of the Eye. Springer, pp. 19–116.

Mayhew, E., Lazo, R., Vail, W., King, J., Green, A., 1984. Characterization of liposomes prepared using a microemulsifier. Biochim. Biophys. Acta (BBA)-Biomembr. 775, 169–174.

Mordenti, J., Thomsen, K., Licko, V., Berleau, L., Kahn, J.W., Cuthbertson, R.A., Duenas, E.T., Ryan, A.M., Schofield, C., Berger, T.W., Meng, Y.G., Cleland, J., 1999. Intraocular pharmacokinetics and safety of a humanized monoclonal antibody in rabbits after intravitreal administration of a solution or a PLGA microsphere formulation. Toxicol. Sci. 52, 101–106.

Nagai, N., Kaji, H., Onami, H., Ishikawa, Y., Nishizawa, M., Osumi, N., Nakazawa, T., Abe, T., 2014. A polymeric device for controlled transscleral multi-drug delivery to the posterior segment of the eye. Acta Biomater. 10, 680–687.

Pautot, S., Frisken, B.J., Weitz, D., 2003. Production of unilamellar vesicles using an inverted emulsion. Langmuir 19, 2870–2879.

Prager, F., Michels, S., Kriechbaum, K., Georgopoulos, M., Funk, M., Geitzenauer, W., Polak, K., Schmidt-Erfurth, U., 2009. Intravitreal bevacizumab (Avastin) for macular oedema secondary to retinal vein occlusion: 12-month results of a prospective clinical trial. Br. J. Ophthalmol. 93, 452–456.

Ranta, V., Mannermaa, E., Lummepuro, K., Subrizi, A., Laukkanen, A., Antopolsky, M., Murtomäki, L., Hornof, M., Urtti, A., 2010. Barrier analysis of periocular drug delivery to the posterior segment. J. Controlled Release 148, 42–48.

Saheki, A., Seki, J., Nakanishi, T., Tamai, I., 2012. Effect of back pressure on emulsification of lipid nanodispersions in a high-pressure homogenizer. Int. J. Pharm. 422, 489–494.

Sani, S.N., Das, N.G., Das, S.K., 2009. Effect of microfluidization parameters on the physical properties of PEG-PLGA nanoparticles prepared using high pressure microfluidization. J. Microencapsul. 26, 556–561.
Siqueira, G., Bras, J., Dufresne, A., 2009. New process of chemical grafting of cellulose nanoparticles with a long chain isocyanate. Langmuir 26, 402–411.
Sorgi, F.L., Huang, L., 1996. Large scale production of DC-Chol cationic liposomes by microfluidization. Int. J. Pharm. 144, 131–139.
Sugasawa, K., Deguchi, J., Okami, T., Yamamoto, A., Omori, K., Uyama, M., Tashiro, Y., 1994. Immunocytochemical analyses of distributions of Na, K-ATPase and GLUT1, insulin and transferrin receptors in the developing retinal pigment epithelial cells. Cell Struct. Funct. 19, 21–28.
Sugita, A., Hamasaki, M., Higashi, R., 1982. Regional difference in fenestration of choroidal capillaries in Japanese monkey eye. Jpn. J. Ophthalmol. 26, 47–52.
Takahashi, M., Kitamoto, D., Asikin, Y., Takara, K., Wada, K., 2009. Liposomes encapsulating Aloe vera leaf gel extract significantly enhance proliferation and collagen synthesis in human skin cell lines. J. Oleo Sci. 58, 643–650.
Takashima, Y., Saito, R., Nakajima, A., Oda, M., Kimura, A., Kanazawa, T., Okada, H., 2007. Spray-drying preparation of microparticles containing cationic PLGA nanospheres as gene carriers for avoiding aggregation of nanospheres. Int. J. Pharm. 343, 262–269.
Thompson, A., Singh, H., 2006. Preparation of liposomes from milk fat globule membrane phospholipids using a microfluidizer. J. Dairy Sci. 89, 410–419.
Urtti, A., 2006. Challenges and obstacles of ocular pharmacokinetics and drug delivery. Adv. Drug Deliv. Rev. 58, 1131–1135.
Urtti, A., Pipkin, J.D., Rork, G., Sendo, T., Finne, U., Repta, A., 1990. Controlled drug delivery devices for experimental ocular studies with timolol 2. Ocular and systemic absorption in rabbits. Int. J. Pharm. 61, 241–249.
Voinea, M., Dragomir, E., Manduteanu, I., Simionescu, M., 2002. Binding and uptake of transferrin-bound liposomes targeted to transferrin receptors of endothelial cells. Vascul. Pharmacol. 39, 13–20.
Wang, J.L., Liu, Y.L., Li, Y., Dai, W.B., Guo, Z.M., Wang, Z.H., Zhang, Q., 2012. EphA2 targeted doxorubicin stealth liposomes as a therapy system for choroidal neovascularization in rats. Invest. Ophthalmol. Vis. Sci. 53, 7348–7357.
Washington, C., Davis, S., 1988. The production of parenteral feeding emulsions by microfluidizer. Int. J. Pharm. 44, 169–176.
Whittenton, J., Harendra, S., Pitchumani, R., Mohanty, K., Vipulanandan, C., Thevananther, S., 2008. Evaluation of asymmetric liposomal nanoparticles for encapsulation of polynucleotides. Langmuir 24, 8533–8540.
Yefimova, M.G., Jeanny, J.C., Guillonneau, X., Keller, N., Nguyen-Legros, J., Sergeant, C., Guillou, F., Courtois, Y., 2000. Iron, ferritin, transferrin, and transferrin receptor in the adult rat retina. Invest. Ophthalmol. Vis. Sci. 41, 2343–2351.
Ying, L., Tahara, K., Takeuchi, H., 2013. Drug delivery to the ocular posterior segment using lipid emulsion via eye drop administration: effect of emulsion formulations and surface modification. Int. J. Pharm. 453, 329–335.
Zook, J.M., Vreeland, W.N., 2010. Effects of temperature, acyl chain length, and flow-rate ratio on liposome formation and size in a microfluidic hydrodynamic focusing device. Soft Matter 6, 1352–1360.

6. Study II: Light induced cytosolic drug delivery from liposomes with gold nanoparticles

Journal of Controlled Release 203 (2015) 85–98

Contents lists available at ScienceDirect

Journal of Controlled Release

journal homepage: www.elsevier.com/locate/jconrel

Light induced cytosolic drug delivery from liposomes with gold nanoparticles

Tatu Lajunen [a,*,1], Lauri Viitala [b], Leena-Stiina Kontturi [a], Timo Laaksonen [a], Huamin Liang [c], Elina Vuorimaa-Laukkanen [c], Tapani Viitala [a], Xavier Le Guével [d], Marjo Yliperttula [a], Lasse Murtomäki [b], Arto Urtti [a,e]

[a] Centre for Drug Research, Division of Pharmaceutical Biosciences, University of Helsinki, P.O. Box 56, FI-00014, Helsinki, Finland
[b] Department of Chemistry, Aalto University, P.O. Box 16100, FI-00076 Aalto, Finland
[c] Department of Chemistry and Bioengineering, Tampere University of Technology, P.O. Box 541, FI-33101 Tampere, Finland
[d] The Andalusian Centre for Nanomedicine and Biotechnology, Parque Tecnológico de Andalucía c/ Severo Ochoa 35, 29590 Campanillas, Málaga, Spain
[e] School of Pharmacy, University of Eastern Finland, P.O. Box 1627, FI-70211 Kuopio, Finland

ARTICLE INFO

Article history:
Received 18 December 2014
Received in revised form 11 February 2015
Accepted 17 February 2015
Available online 19 February 2015

Chemical compounds studied in this article:
1,2-Dipalmitoyl-sn-glycero-3-phosphocholine (PubChem CID: 6138)
1,2-Distearoyl-sn-glycero-3-phosphocholine (PubChem CID: 94190)
1-Stearoyl-2-hydroxy-sn-glycero-3-phosphocholine (PubChem CID: 497299)
1,2-Distearoyl-sn-glycero-3-phosphoethanolamine-N-[methoxy(polyethylene glycol)-2000] (PubChem CID: 86278269)
1,3-Diolein (PubChem CID: 33120)
Cholesteryl hemisuccinate (PubChem CID: 65082)
Calcein (PubChem CID: 65079)
Gold (PubChem CID: 23985)

Keywords:
Light activation
Liposome
Gold nanoparticle
Intracellular delivery
Triggered release
Retinal pigment epithelium

ABSTRACT

Externally triggered drug release at defined targets allows site- and time-controlled drug treatment regimens. We have developed liposomal drug carriers with encapsulated gold nanoparticles for triggered drug release. Light energy is converted to heat in the gold nanoparticles and released to the lipid bilayers. Localized temperature increase renders liposomal bilayers to be leaky and triggers drug release. The aim of this study was to develop a drug releasing system capable of releasing its cargo to cell cytosol upon triggering with visible and near infrared light signals. The liposomes were formulated using either heat-sensitive or heat- and pH-sensitive lipid compositions with star or rod shaped gold nanoparticles. Encapsulated fluorescent probe, calcein, was released from the liposomes after exposure to the light. In addition, the pH-sensitive formulations showed a faster drug release in acidic conditions than in neutral conditions. The liposomes were internalized into human retinal pigment epithelial cells (ARPE-19) and human umbilical vein endothelial cells (HUVECs) and did not show any cellular toxicity. The light induced cytosolic delivery of calcein from the gold nanoparticle containing liposomes was shown, whereas no cytosolic release was seen without light induction or without gold nanoparticles in the liposomes. The light activated liposome formulations showed a controlled content release to the cellular cytosol at a specific location and time. Triggering with visual and near infrared light allows good tissue penetration and safety, and the pH-sensitive liposomes may enable selective drug release in the intracellular acidic compartments (endosomes, lysosomes). Thus, light activated liposomes with gold nanoparticles are an attractive option for time- and site-specific drug delivery into the target cells.

* Corresponding author at: Centre for Drug Research, Division of Pharmaceutical Biosciences, Faculty of Pharmacy, University of Helsinki, P.O. Box 56 (Viikinkaari 9), FI-00014 Helsinki, Finland.
E-mail addresses: tatu.lajunen@helsinki.fi (T. Lajunen), lauri.viitala@aalto.fi (L. Viitala), leena.kontturi@helsinki.fi (L.-S. Kontturi), timo.laaksonen@helsinki.fi (T. Laaksonen), huamin.liang@tut.fi (H. Liang), elina.vuorimaa@tut.fi (E. Vuorimaa-Laukkanen), tapani.viitala@helsinki.fi (T. Viitala), xleguevel@bionand.es (X. Le Guével), marjo.yliperttula@helsinki.fi (M. Yliperttula), lasse.murtomaki@aalto.fi (L. Murtomäki), arto.urtti@helsinki.fi (A. Urtti).
[1] Present address: (Until 31st of March 2015) Department of Biopharmaceutics and Drug Metabolism, Graduate School of Pharmaceutical Sciences, Kyoto University, 46-29 Yoshidashimoadachi-cho, Sakyo-ku, Kyoto 606-8501, Japan.

http://dx.doi.org/10.1016/j.jconrel.2015.02.028
0168-3659/

1. Introduction

Target sites of many drugs are located intracellularly. For example, transcription factors, RNAi compounds, DNA, and modulators of intracellular proteins must be delivered into the target cells. Therefore, intracellular delivery is a prerequisite for the efficacy of many important drug classes.

Liposomes are effectively endocytosed into the target cells, but drug release from the liposomes in the cells is often sub-optimal. Different approaches have been used to facilitate intracellular drug release from the liposomes and other nanomedicines. For example, pH-sensitive [1,2], thermosensitive [3–6], photosensitive [7,8], ultrasonically [9,10] and electromagnetically triggered [11–13] formulations have been used. Biological triggers, such as enzymes [14] or microbes [15], have also been utilized in some experiments. Paasonen et al. [5,6] and later publications [16–21] show a light triggered content release from the liposomes with gold nanoparticles. The triggered release is based on the absorption of light energy by gold nanoparticles. The absorbed light energy is released as heat to the lipid bilayers causing phase transition in the lipid bilayers and content release from the liposomes [22–24].

In principle, the light triggered drug release from the liposomes can be used in the tissues that can be reached with the light irradiation. The light induced drug release from liposomes may be applicable in the treatment of the diseases affecting the eyes, gastrointestinal tract, skin, lungs, nasal cavity, ears or superficial tissues. For example, the tissues in the back of the eye (retina, choroid) are commonly treated in the clinics with lasers that could also be used to trigger drug release in the eye. Examples of the diseases affecting the posterior eye segment include glaucoma [25], retinopathies [26–28], choroidopathy [29], Coat's disease [30], retinoblastoma [31], and age-related macular degeneration [32,33].

Light penetration into the human tissues depends on the wavelength: penetration at 700–900 nm is at least 20 times more effective than at wavelengths below 400 nm [34–38]. In addition, the wavelength has important safety implications, since ultraviolet (UV) light may be harmful to the retina and other human tissues [39]. Previous proof-of-concept studies on light activated liposomes utilized small gold nanoparticles (1.5–3 nm) that are activated with UV light [5,6]. The absorption wavelength of gold nanoparticles depends on the shape and diameter of the nanoparticles. This allows the design of liposome formulations that are activated at visible and near infrared wavelengths, since larger gold nanoparticles (30–50 nm) absorb light at visible and near infrared regions [40–43].

Endocytosis and phagocytosis are the principal cellular uptake mechanisms of liposomes [44]. After cellular internalization, liposomes are entrapped within the endosomes and they may be re-circulated back to the extracellular space or trafficked to the lysosomes [45]. However, drug escape from the endosomes is needed for intracellular drug action. Otherwise, the liposomes will be trafficked to the lysosomes where drug may be degraded [45]. Distribution of liposomal drug from the endosomes to the cytosol can be facilitated with membrane active peptides [46] and pH-sensitive liposomes [1,2]. Previously, light activation of liposomes did not result in the distribution of liposomal contents to the cytosol [6], but synergistic effects of light activation and pH sensitivity might result in cytosolic delivery of the liposomal cargo.

In this study, we investigated light activated liposomes with important new features. Firstly, we loaded the liposomes with gold nanoparticles that can be triggered with visible and near infrared light. Secondly, lipid composition of Ickenstein et al. [47–50] was optimized to allow highly effective light triggering of drug release. Thirdly, we developed pH-sensitive liposomes that showed a fast content release at the acidic endosomal pH, that may enhance the therapeutic effect without exposing the surrounding tissues to the medication. The functionality of the formulations was studied with physicochemical methods, release tests, and cell culture studies. Overall, the new light activated liposomes showed a triggered content release at safe wavelengths (near infrared) that penetrate the human tissues. Furthermore, the light induction resulted in efficient intracellular delivery of the liposomal contents to the cell cytosol.

2. Material and methods

2.1. Preparation of light activated thermosensitive liposomes

1,2-Dipalmitoyl-sn-glycero-3-phosphocholine (DPPC), 1,2-distearoyl-sn-glycero-3-phosphocholine (DSPC), 1-stearoyl-2-hydroxy-sn-glycero-3-phosphocholine (Lyso PC) and 1,2-distearoyl-sn-glycero-3-phosphoethanolamine-N-[methoxy(polyethylene glycol)-2000] (DSPE-PEG) were bought from Avanti Polar Lipids, Inc. (Alabaster, AL, USA). The lipids were dissolved in chloroform (Sigma-Aldrich, St. Louis, MO, USA). The liposomes were prepared using the reverse-phase evaporation method (REV) [5,6] with a few modifications. Briefly, the lipids in chloroform solutions were mixed in a glass tube (10 μmol of total lipids). The tube was placed in a water bath within a larger glass tube and attached to a vacuum rotary evaporation system (Büchi R-114, Büchi Labortechnik AG, Flawil, Switzerland). Chloroform was evaporated by heating the tube up to 60 °C and gradually reducing the pressure to 70 mbar under a nitrogen flow. The resulting thin lipid layer was dissolved in 1.2 ml of di-isopropylether (DIPE) (Sigma-Aldrich). A calcein solution (60 mM, 280 mOsm) was prepared by dissolving 374 mg of calcein (Sigma-Aldrich) and 17 mg of sodium chloride (Sigma-Aldrich) in 10 ml of milli-Q water, and the pH was adjusted to 7.4 with sodium hydroxide.

Hydrophilic gold nanorods (width 25 nm; length 60 nm; relative SD ± 10%; cetyltrimethylammonium bromide (CTAB) stabilized) were purchased from Sigma-Aldrich. Hydrophilic gold nanostars (diameter 50–60 nm; polyethylene glycol (PEG) coated) were prepared by the protocol described by Barbosa et al. [51] The nanorods have a light absorption maximum at 650 nm and the nanostars have a wide absorption peak at 700–900 nm. The gold nanoparticle solutions were concentrated by centrifugation and careful removal of the supernatant. The final nanoparticle concentration was 15 μg/μl.

The solutions of calcein (480 μl), gold nanoparticles (20 μl) and lipid-DIPE were heated to 60 °C and mixed in a glass tube. After brief vortexing the mixture was sonicated in a heated bath ultrasonicator (Elma Schmidbauer GmbH, Singen, Germany) at 60 °C until a homogeneous solution without separate phases was obtained. The glass tube was quickly transferred to a larger tube with 2.5 ml of milliQ water. The organic solvent was evaporated in vacuum in a 60 °C water bath under a nitrogen atmosphere. The pressure was gradually reduced to 180 mbar during 2 h while avoiding the formation of excessive bubbles and foaming in the sample. The sample was kept at 180 mbar for 10 min to ensure complete evaporation of the organic solvent and formation of liposomes with encapsulated gold nanoparticles in the aqueous core. The size of the liposomes was reduced by ultra-sonication for 10 min above the transition temperature of the lipids. The liposome samples were purified by gel filtration in a Sephadex G-50 (Sigma-Aldrich) column where samples were eluted with a buffer solution of 20 mM HEPES (Sigma-Aldrich) and 140 mM sodium chloride (pH 7.4, 280 mOsm). Gold nanoparticle concentration was analyzed using Inductively Coupled Plasma-Optical Emission Spectrometry (7100 DV-ICP-OES, Perkin Elmer, Waltham, MA, USA) and the gold concentration of the samples was adjusted to 50 μM with the buffer solution. Liposomes without gold nanoparticles were prepared as control samples. Light absorption spectra of the gold nanoparticles and liposomes were analyzed with a Varioskan Flash plate reader (Thermo Fisher Scientific Inc., Waltham, MA, USA).

2.2. Preparation of light activated thermo- and pH-sensitive liposomes

1,3-Diolein (diolein) and cholesteryl hemisuccinate (CHEMS) were purchased from Sigma-Aldrich. 1,2-Dioleoyl-sn-glycero-3-phosphoethanolamine (DOPE) was bought from Avanti Polar Lipids. Two

pH-sensitive lipid combinations, DOPE/CHEMS [52,53] and diolein/CHEMS [54,55], were studied as pH-sensitive components in the liposomes. A combination of diolein and CHEMS was more suitable for our formulations than DOPE/CHEMS combination (data not shown). Polyethylene glycol (PEG) was not used, because it may reduce pH-sensitivity of liposomes [56]. Different molar ratios of DPPC, DSPC, Lyso PC, diolein and CHEMS were mixed in a glass tube and the liposomes were prepared as described above. Gold nanorods were used as the light absorbing components in these formulations.

2.3. Size analysis of liposomes

The size distributions of the liposomes were analyzed with a Zetasizer APS dynamic light scattering automated plate sampler (Malvern Instruments, Malvern, United Kingdom). The sizes were analyzed based on the signal intensities.

2.4. Content release from the liposomes

2.4.1. Temperature induced release

Calcein release from the liposomes was studied at increasing temperatures up to 45 °C. Fluorescence emission of calcein was quenched at high concentrations within liposomes. Upon release, dilution of calcein took place and strong fluorescence signal was detected. The release measurements were performed at excitation and emission wavelengths at 495 nm and 515 nm, respectively, using a Varioskan Flash plate reader. Temperature had no significant effect on the emission of calcein (see the Supplementary data).

Liposome solutions (5 μl) were transferred into 250 μl of HEPES buffer (pH 7.4) in the wells of Black/White Isoplate-96 plates (Perkin Elmer). Fluorescence emission in the wells was measured at 5 minute intervals while temperature was increased stepwise (2.5 °C each time) from 25 °C to 45 °C. Then, the samples were incubated for 15 min at 45 °C and the fluorescence was measured at 5 minute intervals. Finally, 10 μl of 10% Triton X-100 was added to dissolve the liposomes for complete calcein release. At each step, the fluorescence emission of calcein was measured with a Varioskan Flash plate reader and calcein release percentage (R) was calculated as:

$$R = \frac{F - F_0}{F_{100} - F_0} \times 100\%$$

where F is the fluorescence in the specific sample, F_0 is the background fluorescence and F_{100} is the fluorescence after a complete calcein release. Temperature induced calcein release from pH-sensitive liposomes was determined in buffer solutions with pH values ranging from 4.5 to 7.4. Separate standard curves of calcein fluorescence emission were generated for each pH.

2.4.2. Light induced calcein release

A test platform was assembled to precisely control the experimental conditions in the light activation experiments (Fig. 1). The system consisted of a WheeLED Wavelength-Switchable LED light source (Mightex Systems, Pleasanton, CA, USA) equipped with a liquid light guide and a collimator with a lens that focused the light beam to the individual wells in 96-well plates. The light intensities at different feed currents were measured with a Coherent Fieldmax II-TOP with LM-10 power head (range 10 mW–10 W) (Coherent Inc., Santa Clara, CA, USA). The light source was mounted in an automatic plate-handling robot (Tecan Genesis Workstation 150, Tecan Group Ltd., Männedorf, Switzerland) that was equipped with an adjustable temperature stand for 96-well plates. The temperature of the samples was adjusted to 37 °C and verified with a thermometer. The testing platform was located in a dark room thereby allowing exact control of the light exposure conditions.

Liposome solution (5 μl) was transferred into 250 μl of HEPES buffer (pH 7.4) in Black/White Isoplate-96 (Perkin Elmer) wells. The samples were exposed to light (6 W/cm^2) at wavelengths of 656 nm and 850 nm for liposomes with gold nanorods and gold nanostars, respectively. The samples were irradiated for 5, 10, 20 and 30 min, while blocking the light exposure to the control samples. Immediately after light activation of the liposomes, calcein release was analyzed using excitation and emission wavelengths of 495 nm and 515 nm, respectively (Varioskan Flash). The light activation studies were performed at two pH conditions, i.e. pH 5.0 and 7.4. The acidic pH 5.0 simulates the conditions in the endosomes and pH 7.4 simulates the situation in the extracellular space. Control experiments were carried out with liposomes without gold nanoparticles.

2.5. Liposome phase transition and stability studies

Differential scanning calorimetry (Mettler Toledo DSC823e, Mettler-Toledo GmbH, Greifensee, Switzerland) was used to determine the phase transition temperatures of the liposomes. Briefly, 20 μl of the undiluted liposome sample was pipetted on an aluminum pan and sealed by an aluminum lid with two small holes to prevent pressure buildup. The sample pan was heated in a linear gradient alongside with a reference pan in a nitrogen environment. The phase transitions were seen as peaks on the enthalpy graphs (analyzed with the STARe software, Mettler-Toledo). The measurements were performed at pH 5.0 and/or 7.4.

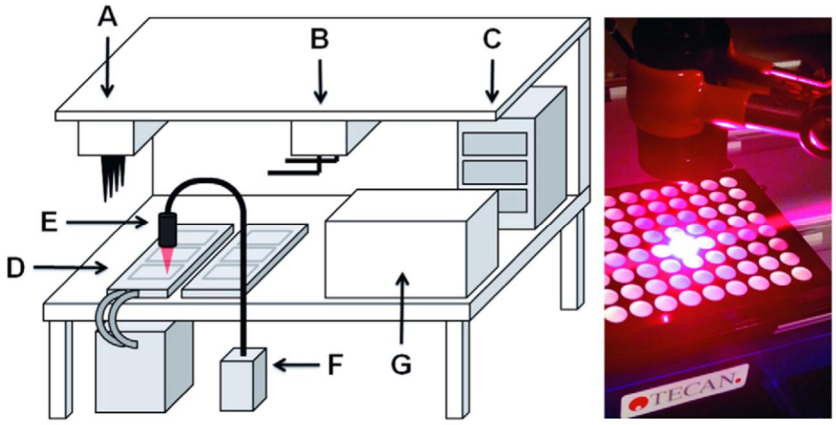

Fig. 1. Left: Schematic presentation of the light activation test platform with a pipetting robot (A), a plate handling robot (B), a well plate incubator (C), a temperature controlled plate stand (D), a light collimator and a focusing lens (E), a wavelength selectable light source with a liquid light guide (F) and a well plate rack (G). Right: Collimator and focusing lens assembly over a well plate.

Brewster angle microscope (BAM) images and Langmuir isotherms of lipid mixtures were measured simultaneously with a KSV OPTREL BAM300 mounted on a KSV minitrough Langmuir film balance (KSV Instruments Ltd., Helsinki, Finland) equipped with a double barrier system. The sub-phase was 20 mM HEPES and 140 mM sodium chloride in milli-Q water. The temperature of the sub-phase was 21 ± 1 °C and the compression speed was 3 mm/min i.e. 2.25 cm^2 min^{-1}. The BAM instrument was equipped with a 10 mW HeNe laser (633 nm) that was linearly polarized in the plane of incidence by a Glan–Thomson polarizer. The reflection from the interface passed through a second Glan–Thomson polarizer and it was monitored with a CCD camera. The microscope was adjusted so that reflection from the bare air–water interface was minimal. Therefore, it was sensitive to local changes in the optical properties of the interface. The spatial resolution of the system was approximately 2 μm. The image processing procedure included a geometrical correction of the image as well as a filtering operation for noise reduction. Furthermore, the brightness of each image was scaled to improve contrast.

2.6. Cell experiments

Cellular uptake of the liposomes and the light induced release of calcein were studied in a human retinal pigment epithelial cell line (ARPE-19, P15–P25) and in human umbilical vein endothelial cells (HUVEC, P9–P15). ARPE-19 cells were cultured in DMEM/F-12 medium with 10% fetal bovine serum (FBS), 1% L-glutamine, and 1% penicillin–streptomycin. HUVEC cells were cultured in Ham's F-12K medium with heparin (0.1 mg/ml), endothelial cell growth supplement (ECGS) (0.05 mg/ml), 10% FBS, 1% L-glutamine, and 1% penicillin–streptomycin. All cell culture media and supplements were purchased from Gibco (Invitrogen, CA, USA) except heparin and ECGS that were bought from Sigma-Aldrich.

2.6.1. Cellular uptake

We seeded 10,000 ARPE-19 cells or 5000 HUVEC cells per well in tissue culture treated Black/White Isoplate-96 plates and cultured the cells for 48 h in an incubator (37 °C, 5% CO_2). The growth medium was replaced with 150 μl of serum-free medium. Then, 50 μl of purified liposome samples was added to the wells and incubated at 37 °C for 20 min. Thereafter, 150 μl of serum free medium was replaced into the wells and light was projected to the individual wells for 20 min. The well plates included also samples without light exposure and control samples without liposomes. After light activation the medium was removed and the wells were washed with phosphate buffered saline (PBS, Gibco). The cells were detached by incubation in 100 μl of trypsin–EDTA for 10 min at 37 °C. Thereafter, the cells were fixed with 100 μl of 2% paraformaldehyde (PFA, Sigma-Aldrich) and further incubated for 10 min at 25 °C. In order to ensure a sufficient amount of cells for flow cytometry measurements, several wells were pooled together into a single eppendorf tube (3 wells for ARPE-19 cells and 5 wells for HUVEC cells). The eppendorf tubes were centrifuged at 4 °C (1000 *g*, 10 min), supernatants were carefully discarded and the cells were re-suspended with 200 μl of 2% PFA. The centrifugation and resuspension of the samples were repeated. The tubes were stored at 4 °C until further analyses.

For fluorescence-activated cell sorting (FACS) flow cytometry analyses, the samples were diluted with 500 μl of PBS and vortexed. Then, the cellular uptake of the liposomes was determined (BD LSR II flow cytometer, Becton Dickinson, Franklin Lakes, NJ, USA). Live cell population was gated based on forward scatter (FSC) and side scatter (SSC) characteristics from cell debris and aggregates and the internalized calcein was detected based on fluorescence intensity (ex: 494 nm, em: 519 nm). The event data was analyzed with the FACS Diva software (Becton Dickinson). The fluorescence threshold was set at the upper end of the fluorescence peak of the untreated control cells (FITC-A value of 10^2) and the cells with fluorescence levels above the threshold were considered to include liposomes.

2.6.2. Intracellular distribution

Confocal laser scanning microscopy was used to determine the localization of the calcein in the cells. 15,000 ARPE-19 cells or 8000 HUVEC cells were seeded on a center glass of MatTek dishes coated with cell adhesion promoters (dish diameter of 35 mm, glass diameter of 14 mm, glass thickness of 0.16–0.19 mm) (MatTek Corporation, Ashland, MA, USA). The plates for ARPE-19 cells had poly-D-lysine coating, while collagen coating was used for HUVEC cells. The cells were cultured for 48 h in an incubator (37 °C, 5% CO_2), and then the cells were rinsed with serum-free medium. Thereafter, 100 μl of purified liposomes and 100 μl of serum-free medium were added on the center the glass and incubated for 20 min at 37 °C. Then, the cells were incubated at 37 °C with 1 ml of Hoechst 33258 (Sigma-Aldrich, 5 μg/ml) and 1 ml of serum-free medium for 10 min. The dish was placed on a small water bath (37 °C) and exposed to light with an appropriate wavelength for 20 min. Finally, the cells were washed twice with PBS and 1 ml of serum-free medium was added to the dish. The localization of calcein was examined using a Leica SP5 II HCS A inverted microscope (Leica Microsystems GmbH, Wetzlar, Germany) equipped with a 63×/1.2 W Corr/0.17 CS water objective (lasers: Ar 488 nm and UV 364 nm). Multichannel image processing was performed using the Leica LAS AF software (Leica Microsystems). Control experiments were performed using liposomes without gold nanoparticles and incubations without light exposure.

2.6.3. Cell viability

The effects of the materials and the light activation on the cell viability were studied using an Alamar Blue assay (Thermo Fisher Scientific). Firstly, 10,000 ARPE-19 cells or 5000 HUVEC cells per well were seeded on a tissue culture treated Black/White Isoplate-96 plates and cultured for 48 h in an incubator (37 °C, 5% CO_2). The medium was replaced with 150 μl of serum-free medium and 50 μl of purified liposomes with gold nanoparticles or only gold nanoparticles (50 μM). The cells were incubated for 24 h in an incubator. The light exposure effects were investigated using 48 h of culturing the cells in the growth medium. Then, the medium was replaced with 100 μl of serum-free medium and the individual wells were exposed to light conditions that were used in the cellular calcein distribution studies. After their exposure to the liposomes, gold nanoparticles, or light, the cells were washed with PBS. Then, 100 μl of fresh serum-free medium and 10 μl of Alamar Blue reagent were added to the wells. The cells were incubated for 3 h at 37 °C and their viability was analyzed with a Varioskan Flash plate reader (Thermo Fisher Scientific) (excitation and emission wavelengths of 570 and 585 nm, respectively, and a bandwidth of 5 nm). Untreated cells were used as controls.

2.7. Statistical analysis

Student's t-test was used to evaluate the statistical significance between two sample groups. The differences between the results were considered to be significant when the p-values were less than 0.05.

3. Results

3.1. Light activated thermosensitive liposomes

The liposomes consisting of DPPC/Lyso PC/DSPE-PEG (DLD; molar ratio 90:10:4) and DSPC/DPPC (DD; molar ratio 9:1) with gold nanorods or gold nanostars were produced and tested (for compositions, see Table 1). Previously published [5,6,57,58] DD liposomes were used as a benchmark system. The sizes of liposomes and absorption spectra of liposomes and gold nanoparticles are shown in Fig. 2.

Table 1
List of lipid formulations.

Abbreviation	Lipid formulation (molar ratio)	
DLD	DPPC/Lyso PC/DSPE-PEG (90:10:4)	Light activated thermosensitive liposomes
DD	DSPC/DPPC (9:1)	
D100pH	DPPC/DSPC/Lyso PC/diolein/CHEMS (100:0:15:15:10)	Light activated pH- and thermosensitive liposomes
D90pH	DPPC/DSPC/Lyso PC/diolein/CHEMS (90:10:15:15:10)	
D50pH	DPPC/DSPC/Lyso PC/diolein/CHEMS (50:50:15:15:10)	
D10pH	DPPC/DSPC/Lyso PC/diolein/CHEMS (10:90:15:15:10)	

3.1.1. Temperature and light induced calcein release

DLD liposomes with nanorods and nanostars released calcein in a few minutes at temperatures over 40 °C, whereas calcein release was considerably slower below 40 °C (Fig. 3A). Temperature induced release of calcein was moderate from DD liposomes (Fig. 3A). The DLD liposomes released all calcein after 5 min at 45 °C, whereas only 40% was released from the DD liposomes. Further incubation of the DD liposomes for 15 min at 45 °C resulted in calcein release up to 80%. The DLD formulation with nanostars was more leaky at lower temperatures than the liposomes with nanorods.

Both light exposure and gold nanoparticles were required for an efficient content release from the liposomes at 37 °C (Fig. 3B–D). Only low calcein release was seen from the liposomes without light exposure or without gold nanoparticles, whereas the DLD liposomes with gold nanoparticles showed an efficient calcein release during the light exposure (Fig. 3B–D). The DLD liposomes with gold nanorods released 75% of calcein in 20 min and 88% in 30 min of light exposure (Fig. 3C). The DLD liposomes with gold nanostars released 86% of calcein within 20 min and 99% within 30 min of light exposure (Fig. 3D). On the other hand, calcein from the DD liposomes with gold nanorods was only 34% in 30 min (Fig. 3B). All formulations showed some passive leakage without light exposure.

3.2. Light activated liposomes with pH- and thermosensitivity

The thermosensitive liposomes were further modified with a pH-sensitive lipid component (diolein/CHEMS) [54,55] to facilitate the release in the acidic environment of endosomes in the cells. DPPC/DSPC/Lyso PC/diolein/CHEMS-liposomes with gold nanorods were prepared at various molar ratios of the lipids (Table 1). Lipid composition and nanorods did not affect significantly the particle size of the liposomes (Fig. 2).

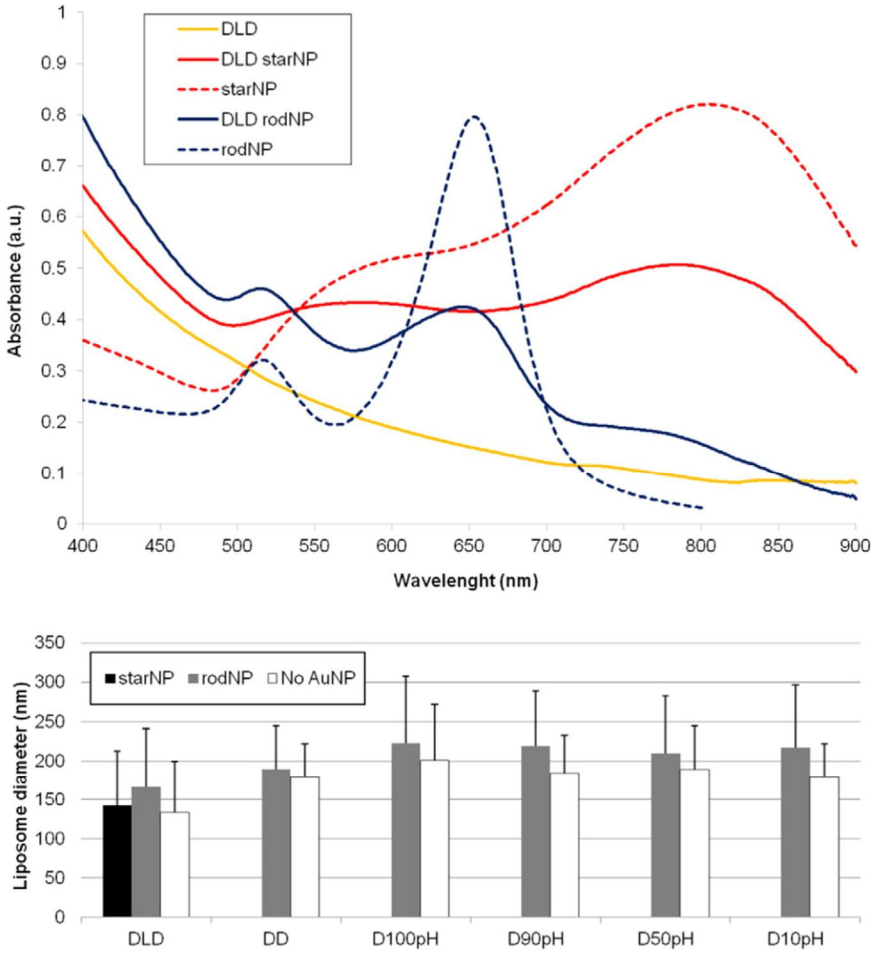

Fig. 2. Top: Absorbance spectra of DLD liposomes with and without gold nanoparticles. Spectra of plain nanoparticles are also shown (dotted lines). starNP = gold nanostars, rodNP = gold nanorods, a.u. = arbitrary units. Bottom: Average diameters of thermosensitive and pH-sensitive liposomes with or without gold nanoparticles. See Table 1 for abbreviations of the liposome formulations. starNP = gold nanostars, rodNP = gold nanorods, No AuNP = liposomes without gold nanoparticles. The error bars indicate the standard deviations. The differences between the liposome sizes were not significant.

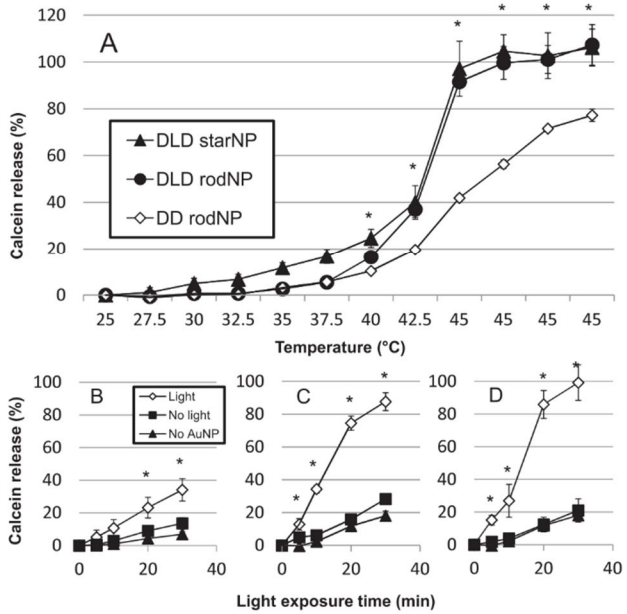

Fig. 3. A: Calcein release from the DLD liposomes with nanostars (black triangles, DLD starNP) and nanorods (black circles, DLD rodNP), and from the DD liposomes with nanorods (open diamonds, DD rodNP). Temperature was increased by 2.5 °C every 5 min of incubation and calcein release was followed as a function of temperature. Error bars indicate the standard deviations (n = 5). Statistical analysis: *p < 0.05; DLD liposomes were compared with DD liposomes. B–D: Effect of light exposure on calcein release from DD liposomes with nanorods (B), DLD liposomes with nanorods (C) and nanostars (D). Light exposed samples (open diamonds), samples without light exposure (black squares) and samples with light exposure, but without gold nanoparticles (black triangles) are shown. Error bars indicate the standard deviations (n = 3). Statistical analysis: *p < 0.05; light activated liposomes (Light) were compared with the liposomes without light exposure (No light) and with the liposomes without gold nanoparticles (No AuNP). The light activation tests (B–D) were carried out at 37 °C.

3.2.1. Temperature dependent calcein release at different pH conditions

Calcein release from the liposomes with thermosensitive and pH-responsive properties was studied (Fig. 4). These liposomes were sensitive to the acidic conditions: in the temperature gradient experiment, calcein was released more efficiently at an acidic pH (4.5–5.5) than at a neutral pH (7.4). Also the release was substantially increased at temperatures above 37 °C. The D100pH liposomes, without DSPC, released calcein efficiently at 37 °C and, therefore, this formulation was not optimal for light triggered liposomes (Fig. 4A1).

DSPC has higher phase transition temperature than DPPC and, therefore, the inclusion of a small amount of DSPC in the formulations did increase the threshold temperature of efficient calcein release, but the pH-sensitive properties were still maintained (Fig. 4A2). At pH 7.4, only 5.5% of calcein was released at 37.5 °C and 20% of calcein was released at 42.5 °C and above. At pH 5.5, 10% of calcein was released at 37.5 °C and 24% was released at 42.5 °C. At pH 4.5, the release was higher than at pH 5.5. Overall, D90pH liposomes showed an increased release above 37 °C, particularly at acidic conditions.

Further increase of the DSPC concentration in the formulations (D50pH, D10pH) did not alter the release inducing threshold temperature, but the extent of calcein release from the liposomes was increased (Fig. 4A3, A4). In these formulations, the levels of released calcein at acidic pH conditions (pH 4.5–5.5) were increased at temperatures of 42.5–45 °C up to 80%, but the release at pH 7.4 was about 20–25%.

In case of liposomes without DPPC (i.e. DSPC/Lyso PC/diolein/CHEMS; 100:15:15:10 molar ratios), the threshold temperature was too high for selective light activation purposes (data not shown). Overall, the D10pH liposomes showed the most promising properties for light triggered drug release.

3.2.2. Light induced and pH dependent calcein release

The thermosensitive and pH-responsive liposomes were further studied in light activation experiments at pH 5.0 and 7.4 (Fig. 4B). The release of calcein from D100pH liposomes was not facilitated by light activation (Fig. 4B1), but it was pH dependent showing a higher release at pH 5.0 than at pH 7.4. At pH 5.0, the D90pH liposomes showed a light dependent release, but no pH dependence was seen without light induction (Fig. 4B2). The D50pH formulation showed a significant light induced calcein release at pH 5 (37% in 30 min), while release at neutral conditions was minimal (2% in 30 min without light induction and 7% in 30 min with light induction) (Fig. 4B3). At pH 5.0, the D10pH liposomes showed a more efficient calcein release in the presence of light activation (51% in 30 min), while calcein release at pH 7.4 was very low (1% without light induction and 6% with light induction) (Fig. 4B4). On the basis of these results, the D10pH liposomes were chosen for further experiments.

3.3. Phase transition temperatures and lipid layer stability

DLD, DD and D10pH liposomes were analyzed with differential scanning calorimetry (Fig. 5A). The DLD liposomes showed a phase transition peak at about 43 °C and the DD liposomes showed a peak at about 53 °C. At pH 7.4, the D10pH liposomes showed a shallow phase transition peak at about 50 °C indicating relatively stable bilayers at neutral pH. However, at an acidic pH, these liposomes showed an additional transition at about 42 °C suggesting disassembly of the pH-sensitive lipid domain (diolein/CHEMS). Another small transition peak was seen at 57 °C.

The pH effects on the stability of the D10pH monolayer were further examined with Langmuir film balance and Brewster angle microscopy (BAM). The surface pressure–area isotherms for the pH-insensitive lipid components (DSPC/DPPC/Lyso PC) did not show any differences in curvature shapes at pH 7.4 and 5.0 indicating a similar layer packing behavior (Fig. 5B). This was confirmed in BAM measurements that showed homogeneous films without any visible domains at both pH values (images in the Supplementary data). The sudden decrease in the area above 60 mN/m is attributed to the expulsion of the more liquid-like Lyso PC component from the monolayer.

Langmuir isotherm curve shapes of diolein/CHEMS lipid combination were different at pH 5.0 and 7.4 (Fig. 5B). The surface pressure values below 40 Å^2 were constantly lower at pH 5.0 than at pH 7.4. The transition point at a surface pressure around 29 mN/m at pH 5.0 was also much lower than at pH 7.4 (i.e. 35 mN/m). The BAM images of diolein/CHEMS monolayers become brighter around the transition points at 29 mN/m for pH 5.0 and at 35 mN/m for pH 7.4 indicating a formation of multilayers (images in the Supplementary data).

For the complete lipid composition of the D10pH liposomes, the isotherm at pH 7.4 showed a smooth pressure increase with a transition point at about 50 mN/m and a final collapse at about 66 mN/m (Fig. 5B).

Fig. 4. Left column (A1–A4): Calcein release from the liposomes at pH 7.4 (open diamonds), pH 5.5 (black squares), pH 5.0 (black triangles) and pH 4.5 (black circles). Temperature was elevated by 2.5 °C every 5 min during incubation until the temperature of 45 °C. The error bars indicate the standard deviations (n = 5). Statistical analysis: *p < 0.05; Release at different pH values was compared with each other at the temperature ranges that are indicated with the horizontal bars. Right column (B1–B4): Calcein release at pH 5.0 and pH 7.4 with light activation (open symbols) and without light activation (black symbols). The error bars indicate the standard deviations (n = 3). Statistical analysis: *p < 0.05; light activated liposomes at pH 5.0 compared with liposomes without light activation at pH 5.0. The light activation experiments were carried out at 37 °C.

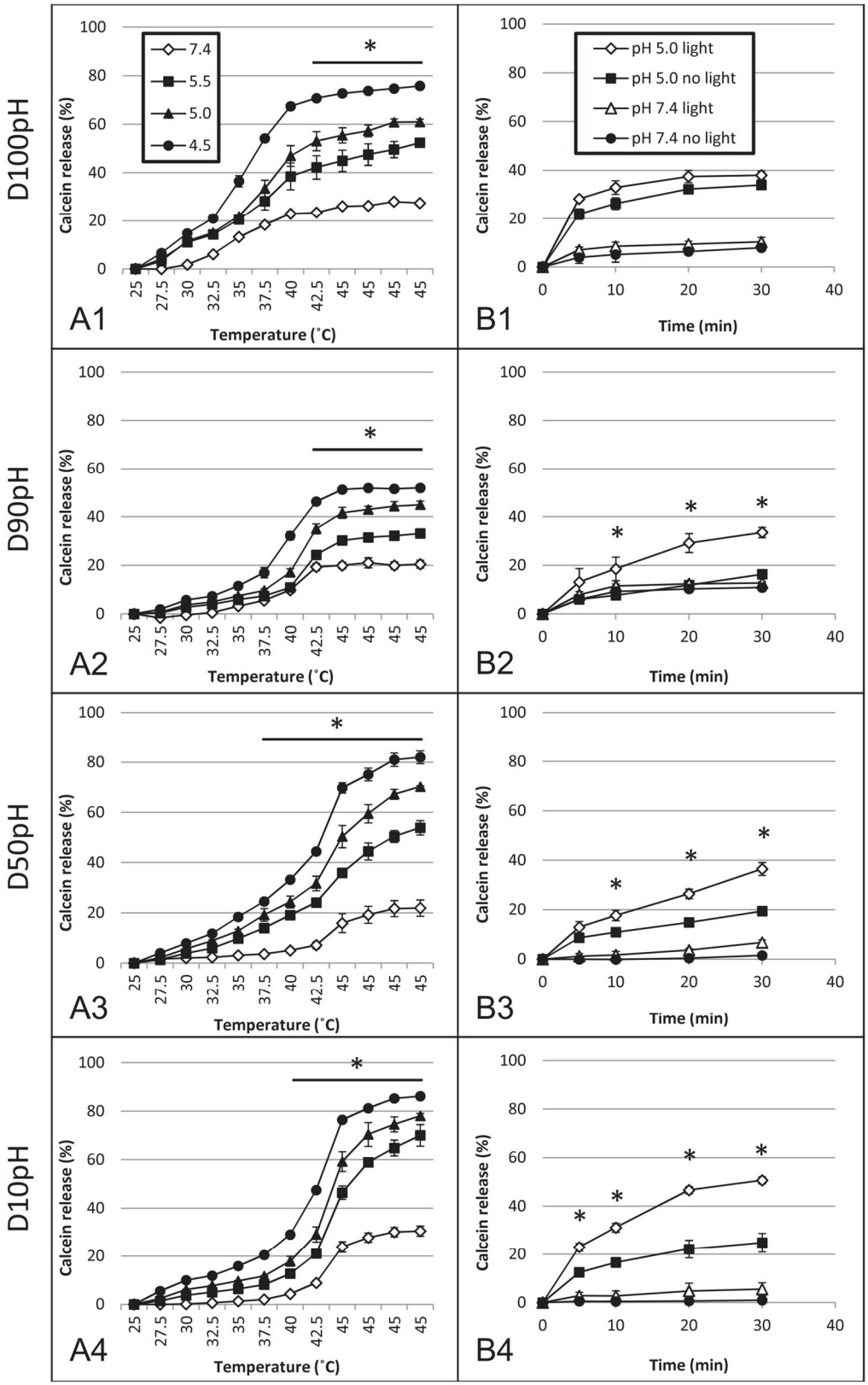
D100pH
D90pH
D50pH
D10pH
A1
A2
A3
A4
B1
B2
B3
B4
Calcein release (%)
Temperature (˚C)
Time (min)
7.4
5.5
5.0
4.5
pH 5.0 light
pH 5.0 no light
pH 7.4 light
pH 7.4 no light
*

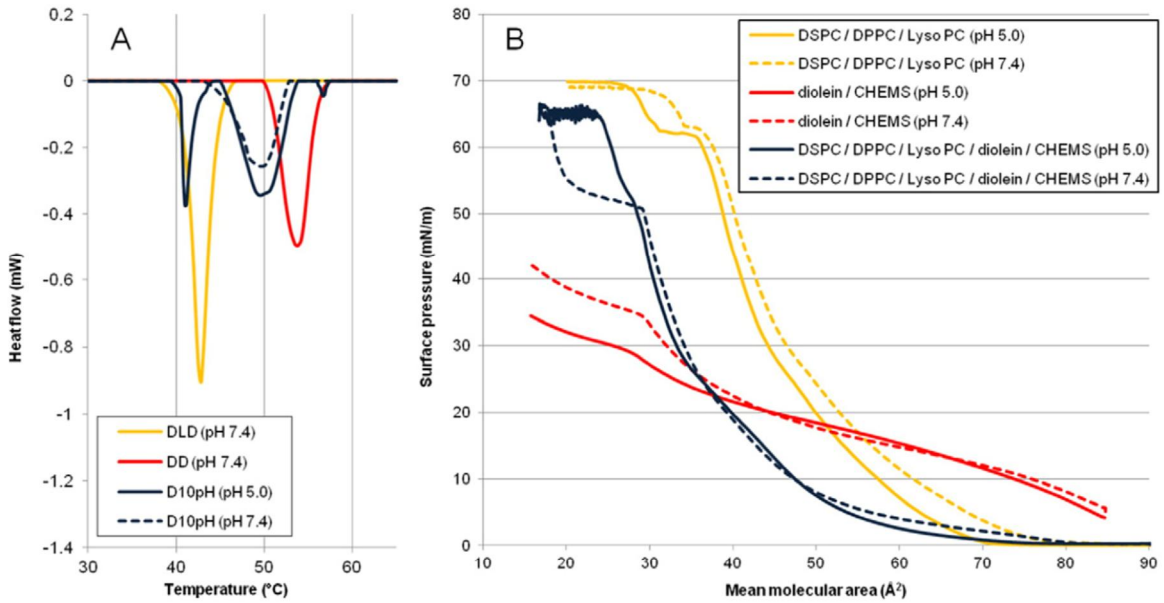

Fig. 5. A: Differential scanning calorimetry measurements with the liposomes. Heat flow graphs of DD liposomes (yellow line), DLD liposomes (red line), D10pH liposomes at pH 7.4 (blue dotted line) and D10pH liposomes at pH 5.0 (blue solid line). B: Langmuir surface pressure–area isotherms of DPPC/DSPC/Lyso PC (yellow), diolein/CHEMS (red) and DPPC/DSPC/Lyso PC/diolein/CHEMS (blue) monolayers. Measurements were carried out on top of a sub-phase with pH 5.0 (solid lines) and pH 7.4 (dotted lines), respectively.

The transition point at 50 mN/m is between the transition points of the DPPC/DSPC/Lyso PC and diolein/CHEMS monolayers at pH 7.4. It can be attributed to the expulsion of diolein, CHEMS and Lyso PC from the monolayer. At pH 5.0, the surface pressure–area isotherm of D10pH formulation showed a broad shoulder-like transition region between 30–50 Å^2 (surface pressure 7.5–25 mN/m), which was not visible at pH 7.4, and a transition point at 25 mN/m. This corresponds to the transition point found for the diolein/CHEMS isotherm at pH 5.0. Also a small change at a surface pressure of 50 mN/m followed by a final collapse at 66 mN/m was seen. This change at 50 mN/m was more subtle at pH 5.0 compared to pH 7.4.

A selection of BAM images of the D10pH monolayer at different surface pressures measured at pH 5 and pH 7.4 is shown in Fig. 6. At low surface pressures (i.e. 2 mN/m), there was a clear phase separation between solid lipid domains and the remaining liquid phase monolayer at pH 5.0 as indicated by the bright areas. This effect was not visible at pH 7.4. At pH 7.4, the D10pH lipids formed a completely homogeneous liquid-condensed/solid monolayer when reaching surface pressures of 20 mN/m. At pH 5.0, a phase separation between the solid lipid domains and the remaining liquid phase monolayer was still seen at surface pressures of 20 mN/m. The D10pH monolayer at pH 5.0 formed a homogeneous liquid-condensed/solid monolayer when reaching surface pressures of 25 mN/m (i.e. the transition point in the surface pressure–area isotherm at pH 5.0, Fig. 5B). At pH 7.4, faint lines were observed in the BAM images at 57 mN/m indicating that the monolayer formed multilayers on the air–water interface. Similar lines could not be seen for the monolayer at pH 5.0. The complete set of BAM images of D10pH monolayer is available in the Supplementary data.

3.4. Cell experiments

3.4.1. Cellular uptake

Uptake of the liposomes into the ARPE-19 and HUVEC cells was studied with flow cytometry (Fig. 7). Fluorescence of calcein was detected in the cells after incubation with the DLD liposomes (with nanorods and nanostars) and the D10pH liposomes (with nanorods). About 90–100% of the ARPE-19 and HUVEC cells showed fluorescence levels above the untreated control cells (Fig. 7, table). The light activated cell samples showed 1.29–1.75 times higher mean fluorescence emissions than the cell samples without light activation (Fig. 7, table).

3.4.2. Cytosolic delivery with light-triggering

Confocal laser scanning microscopy was used to elucidate the localization of calcein in the ARPE-19 and HUVEC cells after its liposomal delivery. In both cell types, calcein fluorescence was found in cellular vesicular structures after exposure to the DLD liposomes (with nanorods or nanostars) and D10pH liposomes (with nanorods). Fluorescence was seen as green bright dots in the images (Fig. 8, full resolution pictures in the Supplementary data). This pattern of calcein distribution was seen without light activation.

More intense and more diffuse cytoplasmic distribution of calcein was seen in the ARPE-19 and HUVEC cells after light activation of the gold nanoparticle containing liposomes (Fig. 8D–F, J–L). The extent of calcein distribution in the cells was more easily seen in the HUVEC cells due to the smaller number of cells and clearer cellular borders compared to the ARPE-19 cells (Fig. 8J–O). Without light activation, calcein remained in the vesicular structures (endosomes, lysosomes) of the cells and no cytosolic fluorescence was seen. Furthermore, light induction did not result in cytosolic calcein distribution from the control liposomes without gold nanoparticles (see the Supplementary data).

3.4.3. Cell viability

The Alamar Blue cell viability assay showed that the DLD and D10pH liposomes with gold nanoparticles did not reduce the viability of the ARPE-19 and HUVEC cells (Fig. 9A1, B1). Plain PEGylated nanostars did not have any effect on the cell viability. On the other hand, the nanorods reduced the cell viability to 6–7% of the control samples (Fig. 9A1, B1). Interestingly, identical nanorods did not decrease the cell viability when they were delivered in the liposomes. The light exposure (30 min at 6 W/cm^2, wavelengths 656 nm or 850 nm) did not affect the cell viability (Fig. 9A2, A3, B2, B3).

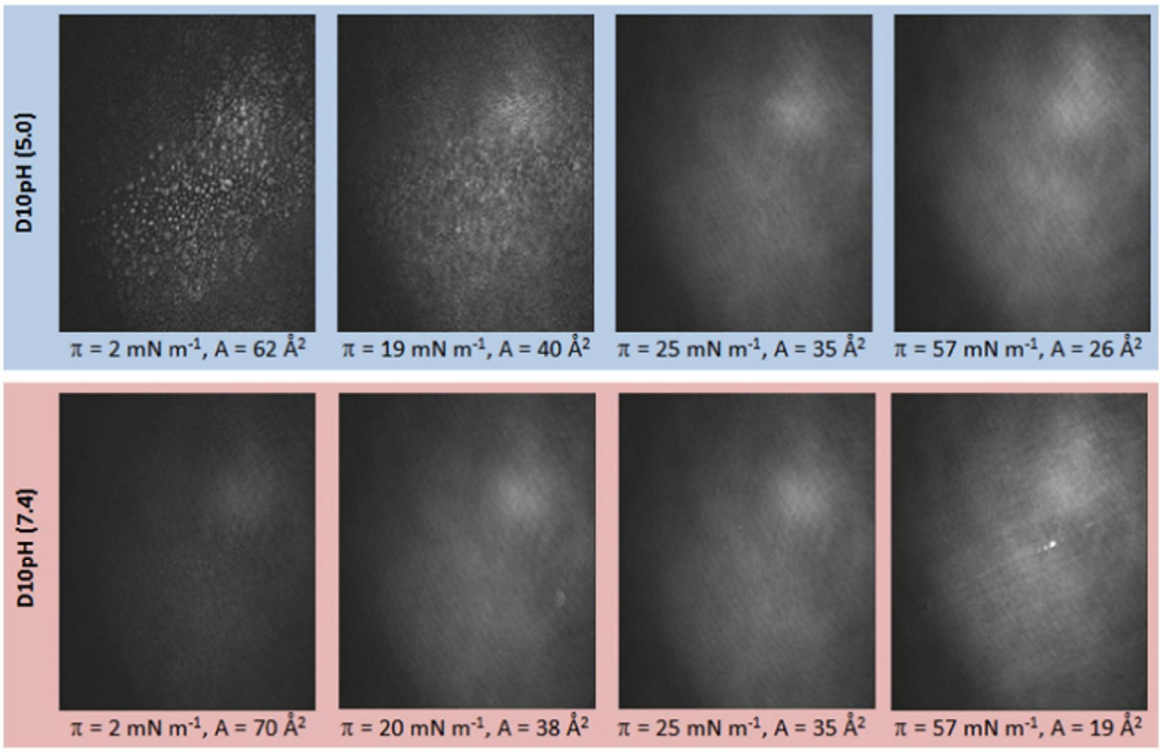

Fig. 6. Brewster angle microscopy images of D10pH monolayer at pH 5.0 (upper row) and pH 7.4 (lower row). The surface pressures (π) and the mean molecular areas (A) at the time of image capture are shown.

4. Discussion

In this study, we have developed light triggered and gold nanoparticle containing thermosensitive liposomes. Liposomes with and without pH-sensitive properties were studied. In principle, this approach allows spatial and temporal control of drug release with light signal. Compared to the earlier studies on light activated liposomes [5,6] these formulations enabled more efficient light induced drug release with visible and near infrared wavelengths. These wavelengths have better tissue penetration [38] and safety [39] than previously used UV light. The liposomes showed improved light and temperature sensitivity and they facilitated cytosolic delivery of the liposomal contents. Furthermore, the synergistic action of the light triggering and acidic endosomal pH targets the drug release to the intracellular space of the light exposed cells. Liposomal drug release after light triggering or acidification has been reported separately [1,59], but their synergistic use in a single drug delivery system has never been reported.

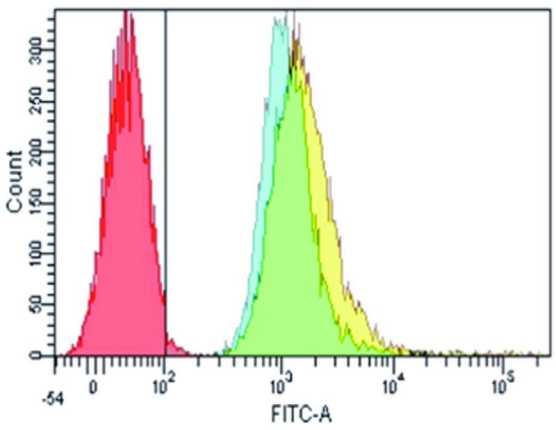

ARPE-19		Lipo% (MFI)	MFR
DLD rodNP	LA	**99.8** (2684)	1.75
	NA	**99.9** (1534)	
DLD starNP	LA	**100.0** (1143)	1.29
	NA	**99.9** (885)	
D10pH rodNP	LA	**100.0** (2365)	1.39
	NA	**99.9** (1702)	
HUVEC			
DLD rodNP	LA	**96.1** (9788)	1.57
	NA	**95.9** (6226)	
DLD starNP	LA	**90.2** (3044)	1.68
	NA	**90.3** (1812)	
D10pH rodNP	LA	**99.9** (11046)	1.54
	NA	**99.9** (7178)	

Fig. 7. Flow cytometry analysis histogram of ARPE-19 cells. The cells were exposed to DLD liposomes including nanorods and light activation (yellow), exposed to liposomes without light activation (cyan) or cultured without liposome or light treatment (red). Vertical axis represents the number of cells and horizontal axis represents the fluorescence intensity (FITC-A). Table: Cell population percentages with internalized liposomes (Lipo%) and mean fluorescence intensity (MFI) of cell lines treated with liposomes. LA = light activated samples. NA = samples without light activation. MFR = mean fluorescence intensity ratio between samples with light activation and samples without light activation.

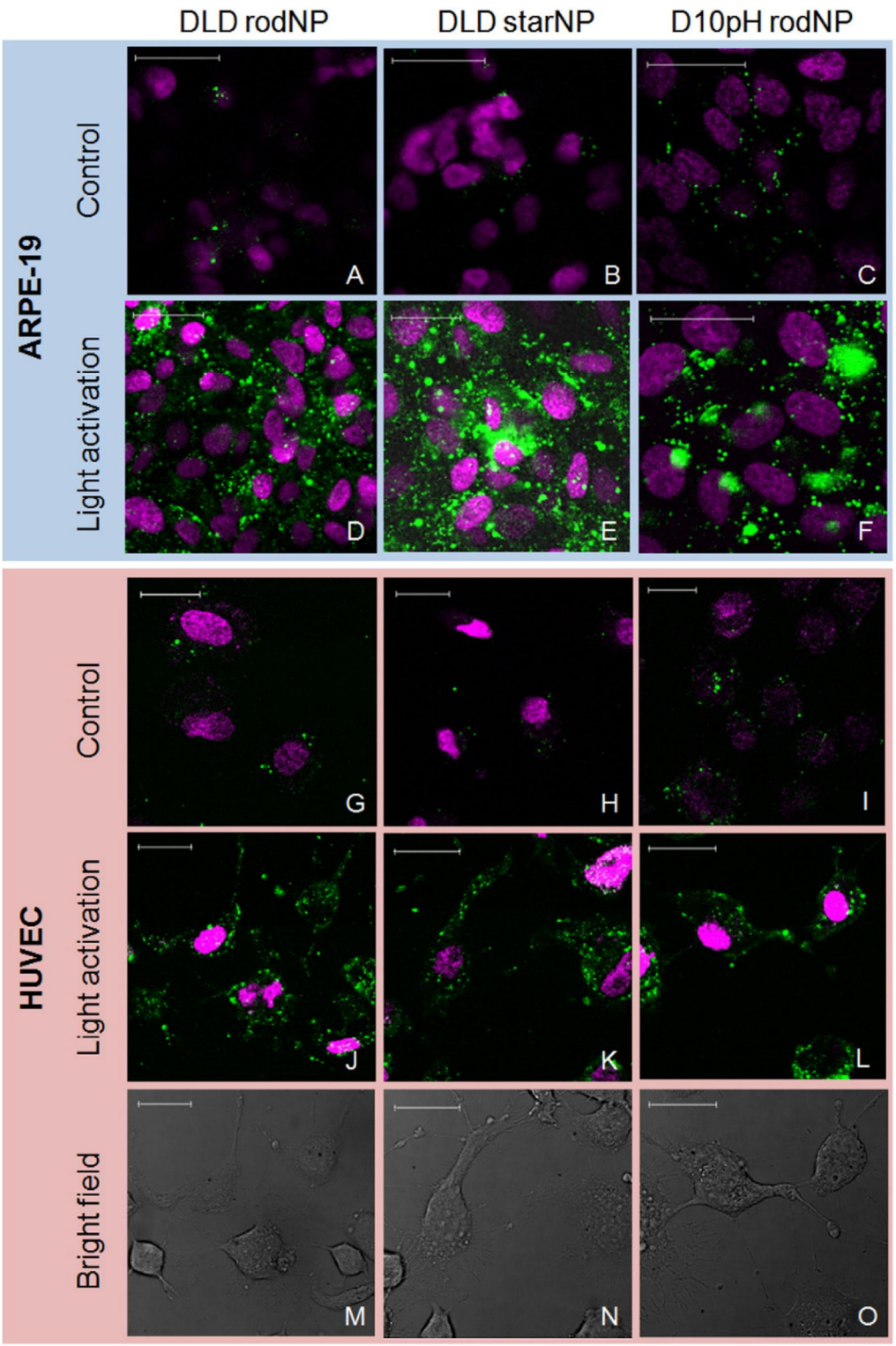

Fig. 8. Confocal microscope images of ARPE-19 (A–F) and HUVEC (G–O) cells after treatment with liposomes (DLD rodNP = DLD liposomes with gold nanorods; DLD starNP = DLD liposomes with gold nanostars; D10pH rodNP = D10pH liposomes with gold nanorods). The cells were exposed to the light activation for 20 min. Control cells without light activation were also examined. Nuclei are shown in magenta and calcein is shown in green. Bright field channel of fluorescent images J–L are represented in images M–O. Scale bar length is 30 μm.

The release data at different temperatures suggest that these liposomes may be relatively stable at body temperature (37 °C), but they release the contents upon light induced heating. Importantly, nanorods and nanostars absorb light at visible and near infrared wavelengths, respectively, and convert the absorbed energy to heat thereby triggering the content release. The formulations with DPPC, Lyso PC and

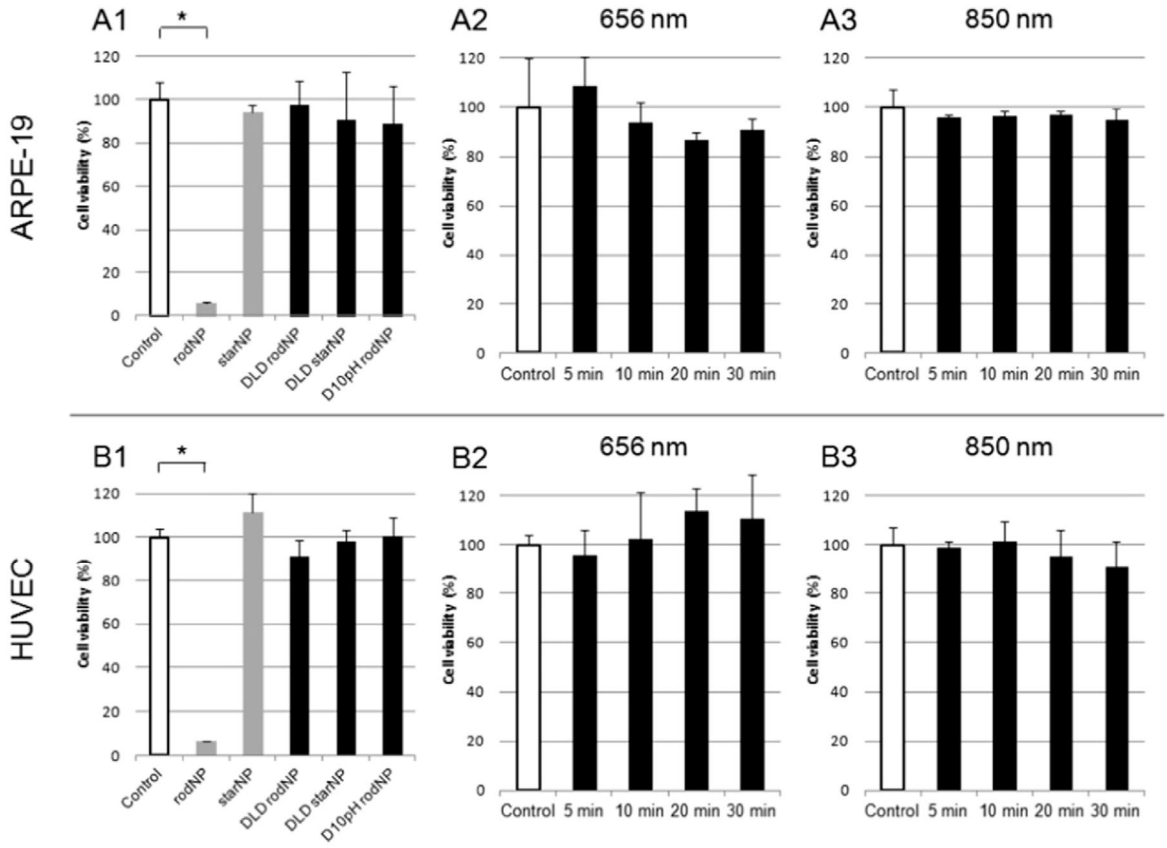

Fig. 9. A1, B1: Viability of the ARPE-19 and HUVEC cells after exposure to gold nanoparticles (gray bars; rodNP = gold nanorods, starNP = gold nanostars) and DLD liposomes with gold nanoparticles (black bars). The error bars represent the standard deviations (n = 4). Statistical analysis: *$p < 0.05$. A2, A3, B2, B3: Viability of the ARPE-19 and HUVEC cells after exposing the cells to light (6 W/cm^2; 656 nm or 850 nm) for different exposure periods. The error bars represent the standard deviations (n = 4).

DSPE-PEG were significantly more responsive to light activation than the previously studied liposomes of DSPC and DPPC [5,6]. The DLD liposomes with nanostars showed higher non-specific release than the liposomes with nanorods. This is possibly due to the larger size and the PEG coating of the gold nanostars. These factors may lead to a closer contact of gold nanoparticles with the lipids and interference of PEG chains with the lipid bilayer thereby affecting the order and barrier function of the phospholipids [60]. The increased fluidity caused by the Lyso PC might facilitate these processes.

Cholesterol is often used to stabilize liposomes and prevent content leakage [61], but it also reduces the sensitivity of the bilayer to changes in temperature [62], thus limiting the usefulness of this approach in a heat based drug release. Degradable stabilizing components may offer an improved light induced release in the presence of a suitable environment (e.g. pH or enzymes.) A decrease in the bilayer stability due to a pH change enables a selective content release in an acidic environment, such as endosomes, upon light induction.

Regarding the retinal treatment, orientation of the light signal enables selection of the desired site for drug release and the long wavelengths allow good tissue penetration in the eye. The size range of the liposomes in this study (140–300 nm) is suitable for their uptake into many cell types and this size range allows also their mobility in the vitreous after intravitreal injection [63]. However, the size of the liposomes may be too large for their access to the retina after systemic, topical and periocular administrations [64].

The main phase transition temperature of the DLD liposomes (43 °C) was significantly above the body temperature of 37 °C. The ordered gel phase of the liposomes at body temperature explains the reduced content leakage in these conditions. On the other hand, a moderate and localized increase of temperature due to light activation leads to a phase transition of the lipid layer to more leaky liquid crystalline phase thereby inducing content release. The phase transition of the DD liposomes was at a higher temperature (50 °C) than the DLD liposomes. There was a disparity between the temperatures of calcein leakage from the DD liposomes and the phase transition temperature in the DSC measurements. This is probably due to the formation of a leaky rippled phase below the actual phase transition temperature of the lipids [6,65,66]. This change was too subtle to be detected by the DSC instrument in this study. The DSC measurements also showed a stabilizing effect of the pH-sensitive diolein/CHEMS domains at pH 7.4, which is in line with the calcein release data. The pH-sensitive D10pH liposomes had a clear phase transition at 42 °C only in acidic medium, suggesting increased sensitivity of these liposomes in acidic intracellular compartments (endosomes and lysosomes).

Langmuir film and Brewster angle microscopy experiments elucidated many interesting lipid bilayer properties of the D10pH composition. At pH 7.4, the diolein/CHEMS components were homogeneously distributed within the gel phase monolayer as evidenced by the smooth surface pressure–area isotherm and BAM images. On the other hand, at pH 5.0 the diolein/CHEMS components induced lipid domains that caused a phase separation to liquid crystalline and gel phases in the monolayer. The BAM images and the lack of a clear collapse pressure indicated that diolein/CHEMS monolayer formed multilayers, underwent a partial collapse or formed soluble aggregates that were expelled from the monolayer. These results indicated that diolein/CHEMS monolayer was less stable or more soluble under acidic conditions. In case of D10pH formulation, the changes in Langmuir isotherm curvature and brightness of the microscope images corresponded to the transitions

seen in DSC measurements at 42 °C, 50 °C and 57 °C, for leaky liquid crystalline, gel phase and induced lipid domain transitions, respectively. Diolein and CHEMS probably induced lipid domains more readily at pH 5.0 than at pH 7.4, which was indicated by the broad shoulder-like transition between 30–50 Å^2 (Fig. 5B). These lipid domains seemed to be expelled from the bulk monolayer at pH 5.0, consequently leading to a smaller transition at 50 mN/m. Overall, the phase transition studies support the other data suggesting that the D10pH liposomes are more sensitive to the light induced heat at acidic conditions than at neutral pH.

Retinal pigment epithelium (RPE) and vascular endothelial cells of the retina and choroid are affected in many ocular diseases [26,27,29,32,33,67]. Thus, they are important drug targets in several diseases. The RPE has a vital role in enabling the normal functionality of the retina and as a barrier to protect the neural retina [68,69]. Therefore, abnormalities in the RPE give rise to several disease conditions in the posterior segment of the eye (e.g. the dry form of age-related macular degeneration). Uncontrolled formation of new blood vessels in exudative age-related degeneration is based on an abnormal phenotype of vascular endothelial cells [33]. The RPE cell line (ARPE-19) and vascular endothelial cells (HUVECs) were chosen as model cells to study the cellular uptake and distribution of the calcein cargo of the light activated liposomes.

Both cell types (ARPE-19, HUVEC) readily internalized the liposomes, as shown in the flow cytometry experiments. Fluorescence emission of liposomal calcein is self-quenched at high concentrations, but the fluorescence becomes more intense upon dilution that takes place during calcein release (see the Supplementary data). Elevated fluorescence signals in light activated cells suggest that calcein is released in the cells after light exposure and imaging with confocal microscope verified cytosolic delivery of calcein after light induction. All studied liposome formulations with gold nanoparticles showed cytosolic delivery upon light activation, whereas the experiments without light activation or liposomes without gold nanoparticles did not result in cytosolic delivery.

The pH-sensitive liposomes may facilitate calcein release and cytosolic delivery even without light activation, because they can destabilize the endosomal walls and cause pore formation [1]. In this case, the fluorescence intensity in the cytosol was, however, very low (see the Supplementary data). Much greater delivery of calcein to the cytosol was seen in the light activated D10pH liposomes with nanorods. Passive diffusion of the highly polar calcein across the endosomal membrane is unlikely. Therefore, the cytosolic delivery must be mediated by enhanced liposome fusion with the endosomal membrane or by the heat induced permeabilization of the endosomal wall. Obviously, the cytosolic release depends also on the drug properties. The value of this technology in cytosolic delivery of other compounds remains to be seen in the future.

Safety of drug delivery system is a prerequisite for its clinical use. The liposome formulations did not show toxic effects in the ARPE-19 and HUVEC cells. Only the plain nanorods reduced cell viability, probably due to the cationic surfactant CTAB (cetyltrimethylammonium bromide) that was used as a stabilizer in the particles [70,71]. The toxic effects may be due to the free CTAB in the solution. Although, contradicting results on CTAB toxicity have been reported [72]. Toxicity of the nanorods was masked when they were encapsulated in the liposomes. Chronic accumulation of gold nanoparticles might lead to negative outcomes in the cells, but unfortunately only short-term toxicity studies on gold nanoparticles have been published [73–75]. We chose long wavelength light to improve tissue penetration and safety of the light induction. Indeed, the near infrared light did not hamper the cell viability [76], and the light exposure in this study should be safe for the eyes also in vivo [39]. This is a major safety improvement compared to the previous technology that was based on the UV light [6].

The liposomes described in this paper showed a substantial light induced content release and strong endoplasmic escape to the cytosol compared to previous formulations [6]. In the case of the pH-sensitive liposomes, the light induced release of the contents took place preferentially in the acidic environment suggesting drug release primarily in the cellular endosomes and lysosomes. Combined pH- and light sensitivity facilitates selective drug release and delivery to cytosol, thereby increasing the drug bioavailability in the target cells and decreasing off-target effects. Preferential intracellular release from light induced liposomes is not expected without pH-sensitive lipid composition; on the contrary, drug release is triggered similarly in the cells and extracellular space. Intracellular drug release can be achieved also with regular pH-sensitive liposomes [1,2], but they do not have temporal and spatial control of drug release shown here. Finally, the extent of synergistic benefits of pH-sensitivity and light sensitivity in vivo remains to be studied in the future.

Liposomes have been shown to be efficient drug carriers although some problems and limitations remain, including inadequate control of intracellular drug delivery and distribution to the cytosol and nucleus [77]. Externally controlled time and location of drug release is an attractive concept, and it may be applicable for drug delivery to the target cells in the posterior eye tissues. This may increase the efficacy at the desired target and reduce off-target effects. In vivo, the liposomes would be delivered to the eye as intravitreal or intravenous injections. After intravitreal injection liposomes have been shown to distribute to the retina, where they can be phagocytosed by the RPE [78]. On the other hand, vascular endothelia in the choroid can be reached using intravenous injection. Light can be projected through transparent ocular tissues to the retina and choroid to activate drug release from the liposomes in the disease tissue site.

5. Conclusions

New light triggered and pH-sensitive liposomes with gold nanoparticles were developed. The content release from the liposomes was highly dependent on temperature, pH and light activation at near infrared region. Improved release triggering was shown, and synergistic impact of light activation and pH-sensitivity was demonstrated. After intracellular uptake the liposomes released their contents to the cytosol upon light activation. The results suggest a site-specific and light induced drug release in the target cells. The formulations and light activation were shown to be safe for the cells. This technology is an attractive option for the treatment of pathological conditions that benefit from specific control of location and timing of the drug release.

Acknowledgments

The Academy of Finland is acknowledged for funding via the Programmable Materials Program, project “Light Triggered Nanoparticles” (OMA, #263453). The corresponding author would like to acknowledge the financial support from Evald & Hilda Nissin Foundation, Sokeain Ystävät Foundation and Mary & Georg Ehrnrooth Foundation. T. Laaksonen and E. Vuorimaa-Laukkanen acknowledge funding from the Academy of Finland grants #258114 and #140357, respectively. T. Viitala acknowledges the Academy of Finland for academy research fellow funding (grants #137053 and #263861). The corresponding author would like to acknowledge H. Revitzer in Aalto University for the technical assistance during ICP-OES measurements.

Appendix A. Supplementary data

Supplementary data to this article can be found online at http://dx.doi.org/10.1016/j.jconrel.2015.02.028.

References

[1] S. Simões, J.N. Moreira, C. Fonseca, N. Düzgüneş, Maria C. Pedrosode Lima, On the formulation of pH-sensitive liposomes with long circulation times, Adv. Drug Deliv. Rev. 56 (2004) 947–965.
[2] I. Kim, Y. Kang, D.S. Lee, H. Park, E. Choi, Y. Oh, H. Son, J. Kim, Antitumor activity of EGFR targeted pH-sensitive immunoliposomes encapsulating gemcitabine in A549 xenograft nude mice, J. Control. Release 140 (2009) 55–60.

[3] L.H. Lindner, M.E. Eichhorn, H. Eibl, N. Teichert, M. Schmitt-Sody, R.D. Issels, M. Dellian, Novel temperature-sensitive liposomes with prolonged circulation time, Clin. Cancer Res. 10 (2004) 2168–2178.
[4] L. Paasonen, B. Romberg, G. Storm, M. Yliperttula, A. Urtti, W.E. Hennink, Temperature-sensitive poly(N-(2-hydroxypropyl) methacrylamide mono/dilactate)-coated liposomes for triggered contents release, Bioconjug. Chem. 18 (2007) 2131–2136.
[5] L. Paasonen, T. Laaksonen, C. Johans, M. Yliperttula, K. Kontturi, A. Urtti, Gold nanoparticles enable selective light-induced contents release from liposomes, J. Control. Release 122 (2007) 86–93.
[6] L. Paasonen, T. Sipilä, A. Subrizi, P. Laurinmäki, S.J. Butcher, M. Rappolt, A. Yaghmur, A. Urtti, M. Yliperttula, Gold-embedded photosensitive liposomes for drug delivery: triggering mechanism and intracellular release, J. Control. Release 147 (2010) 136–143.
[7] P. Shum, J. Kim, D.H. Thompson, Phototriggering of liposomal drug delivery systems, Adv. Drug Deliv. Rev. 53 (2001) 273–284.
[8] A. Yavlovich, A. Singh, S. Tarasov, J. Capala, R. Blumenthal, A. Puri, Design of liposomes containing photopolymerizable phospholipids for triggered release of contents, J. Therm. Anal. Calorim. 98 (2009) 97–104.
[9] S. Hernot, A.L. Klibanov, Microbubbles in ultrasound-triggered drug and gene delivery, Adv. Drug Deliv. Rev. 60 (2008) 1153–1166.
[10] A. Schroeder, J. Kost, Y. Barenholz, Ultrasound, liposomes, and drug delivery: principles for using ultrasound to control the release of drugs from liposomes, Chem. Phys. Lipids 162 (2009) 1–16.
[11] E. Viroonchatapan, H. Sato, M. Ueno, I. Adachi, K. Tazawa, I. Horikoshi, Release of 5-fluorouracil from thermosensitive magnetoliposomes induced by an electromagnetic field, J. Control. Release 46 (1997) 263–271.
[12] L. Zhu, Z. Huo, L. Wang, X. Tong, Y. Xiao, K. Ni, Targeted delivery of methotrexate to skeletal muscular tissue by thermosensitive magnetoliposomes, Int. J. Pharm. 370 (2009) 136–143.
[13] B.P. Timko, T. Dvir, D.S. Kohane, Remotely triggerable drug delivery systems, Adv. Mater. 22 (2010) 4925–4943.
[14] J. Heller, S. Pangburn, K. Roskos, Development of enzymatically degradable protective coatings for use in triggered drug delivery systems: derivatized starch hydrogels, Biomaterials 11 (1990) 345–350.
[15] V. Sinha, R. Kumria, Microbially triggered drug delivery to the colon, Eur. J. Pharm. Sci. 18 (2003) 3–18.
[16] G. Wu, A. Mikhailovsky, H.A. Khant, C. Fu, W. Chiu, J.A. Zasadzinski, Remotely triggered liposome release by near-infrared light absorption via hollow gold nanoshells, J. Am. Chem. Soc. 130 (2008) 8175–8177.
[17] T.S. Troutman, J.K. Barton, M. Romanowski, Biodegradable plasmon resonant nanoshells, Adv. Mater. 20 (2008) 2604–2608.
[18] Y. Jin, X. Gao, Spectrally tunable leakage-free gold nanocontainers, J. Am. Chem. Soc. 131 (2009) 17774–17776.
[19] D.B. Chithrani, M. Dunne, J. Stewart, C. Allen, D.A. Jaffray, Cellular uptake and transport of gold nanoparticles incorporated in a liposomal carrier, Nanomed. Nanotechnol. Biol. Med. 6 (2010) 161–169.
[20] F. El-Hamed, N. Dave, J. Liu, Stimuli-responsive releasing of gold nanoparticles and liposomes from aptamer-functionalized hydrogels, Nanotechnology 22 (2011) 494011.
[21] N. Nombona, K. Maduray, E. Antunes, A. Karsten, T. Nyokong, Synthesis of phthalocyanine conjugates with gold nanoparticles and liposomes for photodynamic therapy, J. Photochem. Photobiol. B Biol. 107 (2012) 35–44.
[22] P. Mulvaney, Surface plasmon spectroscopy of nanosized metal particles, Langmuir 12 (1996) 788–800.
[23] J. Wilcoxon, J. Martin, F. Parsapour, B. Wiedenman, D. Kelley, Photoluminescence from nanosize gold clusters, J. Chem. Phys. 108 (1998) 9137–9143.
[24] N. Harris, M.J. Ford, M.B. Cortie, Optimization of plasmonic heating by gold nanospheres and nanoshells, J. Phys. Chem. B 110 (2006) 10701–10707.
[25] Y.H. Yücel, Q. Zhang, R.N. Weinreb, P.L. Kaufman, N. Gupta, Effects of retinal ganglion cell loss on magno-, parvo-, koniocellular pathways in the lateral geniculate nucleus and visual cortex in glaucoma, Prog. Retin. Eye Res. 22 (2003) 465–481.
[26] M. Spitznas, Pathogenesis of central serous retinopathy: a new working hypothesis, Graefes Arch. Clin. Exp. Ophthalmol. 224 (1986) 321–324.
[27] D. Callanan, J.D. Gass, Multifocal choroiditis and choroidal neovascularization associated with the multiple evanescent white dot and acute idiopathic blind spot enlargement syndrome, Ophthalmology 99 (1992) 1678–1685.
[28] A. Keech, P. Mitchell, P. Summanen, J. O'Day, T. Davis, M. Moffitt, M. Taskinen, R.J. Simes, D. Tse, E. Williamson, Effect of fenofibrate on the need for laser treatment for diabetic retinopathy (FIELD study): a randomised controlled trial, Lancet 370 (2007) 1687–1697.
[29] J. Brown Jr., J.C. Folk, C.V. Reddy, A.E. Kimura, Visual prognosis of multifocal choroiditis, punctate inner choroidopathy, and the diffuse subretinal fibrosis syndrome, Ophthalmology 103 (1996) 1100–1105.
[30] B.G. Haik, Advanced Coats' disease, Trans. Am. Ophthalmol. Soc. 89 (1991) 371–476.
[31] M. Rubenfeld, D.H. Abramson, R.M. Ellsworth, F.D. Kitchin, Unilateral vs. bilateral retinoblastoma. Correlations between age at diagnosis and stage of ocular disease, Ophthalmology 93 (1986) 1016–1019.
[32] J. Ambati, B.K. Ambati, S.H. Yoo, S. Ianchulev, A.P. Adamis, Age-related macular degeneration: etiology, pathogenesis, and therapeutic strategies, Surv. Ophthalmol. 48 (2003) 257–293.
[33] R.D. Jager, W.F. Mieler, J.W. Miller, Age-related macular degeneration, N. Engl. J. Med. 358 (2008) 2606–2617.
[34] W. Geeraets, R. Williams, G. Chan, W. Ham, D. Guerry, F. Schmidt, The loss of light energy in retina and choroid, Arch. Ophthalmol. 64 (1960) 606–615.
[35] E.M. Beems, J.A. Van Best, Light transmission of the cornea in whole human eyes, Exp. Eye Res. 50 (1990) 393–395.
[36] T.J.T.P. van den Berg, H. Spekreijse, Near infrared light absorption in the human eye media, Vision Res. 37 (1997) 249–253.
[37] J. Doutch, A.J. Quantock, V.A. Smith, K.M. Meek, Light transmission in the human cornea as a function of position across the ocular surface: theoretical and experimental aspects, Biophys. J. 95 (2008) 5092–5099.
[38] J. Eichler, J. Knof, H. Lenz, Measurements on the depth of penetration of light (0.35–1.0 μm) in tissue, Radiat. Environ. Biophys. 14 (1977) 239–242.
[39] F.C. Delori, R.H. Webb, D.H. Sliney, Maximum permissible exposures for ocular safety (ANSI 2000), with emphasis on ophthalmic devices, JOSA A 24 (2007) 1250–1265.
[40] S. Link, M.A. El-Sayed, Size and temperature dependence of the plasmon absorption of colloidal gold nanoparticles, J. Phys. Chem. B 103 (1999) 4212–4217.
[41] P.K. Jain, K.S. Lee, I.H. El-Sayed, M.A. El-Sayed, Calculated absorption and scattering properties of gold nanoparticles of different size, shape, and composition: applications in biological imaging and biomedicine, J. Phys. Chem. B 110 (2006) 7238–7248.
[42] F. Hao, C.L. Nehl, J.H. Hafner, P. Nordlander, Plasmon resonances of a gold nanostar, Nano Lett. 7 (2007) 729–732.
[43] P.S. Kumar, I. Pastoriza-Santos, B. Rodriguez-Gonzalez, F.J. García De Abajo, L.M. Liz-Marzan, High-yield synthesis and optical response of gold nanostars, Nanotechnology 19 (2008) 015606.
[44] R.M. Straubinger, K. Hong, D.S. Friend, D. Papahadjopoulos, Endocytosis of liposomes and intracellular fate of encapsulated molecules: encounter with a low pH compartment after internalization in coated vesicles, Cell 32 (1983) 1069–1079.
[45] L. Medina-Kauwe, J. Xie, S. Hamm-Alvarez, Intracellular trafficking of nonviral vectors, Gene Ther. 12 (2005) 1734–1751.
[46] C. Plank, W. Zauner, E. Wagner, Application of membrane-active peptides for drug and gene delivery across cellular membranes, Adv. Drug Deliv. Rev. 34 (1998) 21–35.
[47] L.M. Ickenstein, M.C. Arfvidsson, D. Needham, L.D. Mayer, K. Edwards, Disc formation in cholesterol-free liposomes during phase transition, Biochim. Biophys. Acta Biomembr. 1614 (2003) 135–138.
[48] G.N. Chiu, S.A. Abraham, L.M. Ickenstein, R. Ng, G. Karlsson, K. Edwards, E.K. Wasan, M.B. Bally, Encapsulation of doxorubicin into thermosensitive liposomes via complexation with the transition metal manganese, J. Control. Release 104 (2005) 271–288.
[49] J. Woo, G.N. Chiu, G. Karlsson, E. Wasan, L. Ickenstein, K. Edwards, M.B. Bally, Use of a passive equilibration methodology to encapsulate cisplatin into preformed thermosensitive liposomes, Int. J. Pharm. 349 (2008) 38–46.
[50] J.P. May, M.J. Ernsting, E. Undzys, S. Li, Thermosensitive liposomes for the delivery of gemcitabine and oxaliplatin to tumors, Mol. Pharm. 10 (2013) 4499–4508.
[51] S. Barbosa, A. Agrawal, L. Rodríguez-Lorenzo, I. Pastoriza-Santos, R.A. Alvarez-Puebla, A. Kornowski, H. Weller, L.M. Liz-Marzán, Tuning size and sensing properties in colloidal gold nanostars, Langmuir 26 (2010) 14943–14950.
[52] C. Chu, J. Dijkstra, M. Lai, K. Hong, F.C. Szoka, Efficiency of cytoplasmic delivery by pH-sensitive liposomes to cells in culture, Pharm. Res. 7 (1990) 824–834.
[53] D.S. Collins, K. Findlay, C.V. Harding, Processing of exogenous liposome-encapsulated antigens in vivo generates class I MHC-restricted T cell responses, J. Immunol. 148 (1992) 3336–3341.
[54] W. Guo, M.A. Gosselin, R.J. Lee, Characterization of a novel diolein-based LPDII vector for gene delivery, J. Control. Release 83 (2002) 121–132.
[55] M.A. Gosselin, W. Guo, R.J. Lee, Incorporation of reversibly cross-linked polyplexes into LPDII vectors for gene delivery, Bioconjug. Chem. 13 (2002) 1044–1053.
[56] V.A. Slepushkin, S. Simoes, P. Dazin, M.S. Newman, L.S. Guo, M.C. Pedroso de Lima, N. Duzgunes, Sterically stabilized pH-sensitive liposomes. Intracellular delivery of aqueous contents and prolonged circulation in vivo, J. Biol. Chem. 272 (1997) 2382–2388.
[57] K. Iga, N. Hamaguchi, Y. Igari, Y. Ogawa, K. Gotoh, K. Ootsu, H. Toguchi, T. Shimamoto, Enhanced antitumor activity in mice after administration of thermosensitive liposome encapsulating cisplatin with hyperthermia, J. Pharmacol. Exp. Ther. 257 (1991) 1203–1207.
[58] K. Maruyama, S. Unezaki, N. Takahashi, M. Iwatsuru, Enhanced delivery of doxorubicin to tumor by long-circulating thermosensitive liposomes and local hyperthermia, Biochim. Biophys. Acta Biomembr. 1149 (1993) 209–216.
[59] N. Fomina, J. Sankaranarayanan, A. Almutairi, Photochemical mechanisms of light-triggered release from nanocarriers, Adv. Drug Deliv. Rev. 64 (2012) 1005–1020.
[60] M. Stepniewski, M. Pasenkiewicz-Gierula, T. Róg, R. Danne, A. Orlowski, M. Karttunen, A. Urtti, M. Yliperttula, E. Vuorimaa, A. Bunker, Study of PEGylated lipid layers as a model for PEGylated liposome surfaces: molecular dynamics simulation and Langmuir monolayer studies, Langmuir 27 (2011) 7788–7798.
[61] C. Kirby, J. Clarke, G. Gregoriadis, Effect of the cholesterol content of small unilamellar liposomes on their stability in vivo and in vitro, Biochem. J. 186 (1980) 591–598.
[62] R. Magin, M. Niesman, Temperature-dependent drug release from large unilamellar liposomes, Cancer Drug Deliv. 1 (1984) 109–117.
[63] Q. Xu, N.J. Boylan, J.S. Suk, Y. Wang, E.A. Nance, J. Yang, P.J. McDonnell, R.A. Cone, E.J. Duh, J. Hanes, Nanoparticle diffusion in, and microrheology of, the bovine vitreous ex vivo, J. Control. Release 167 (2013) 76–84.
[64] T. Lajunen, K. Hisazumi, T. Kanazawa, H. Okada, Y. Seta, M. Yliperttula, A. Urtti, Y. Takashima, Topical drug delivery to retinal pigment epithelium with microfluidizer produced small liposomes, Eur. J. Pharm. Sci. 62 (2014) 23–32.
[65] M. Rappolt, G. Rapp, Structure of the stable and metastable ripple phase of dipalmitoylphosphatidylcholine, Eur. Biophys. J. 24 (1996) 381–386.
[66] S. Park, S. Oh, J. Mun, S. Han, Loading of gold nanoparticles inside the DPPC bilayers of liposome and their effects on membrane fluidities, Colloids Surf. B: Biointerfaces 48 (2006) 112–118.
[67] D.F. Williams, W.F. Mieler, Long-term follow-up of acute multifocal posterior placoid pigment epitheliopathy, Br. J. Ophthalmol. 73 (1989) 985–990.

[68] R.W. Young, D. Bok, Participation of the retinal pigment epithelium in the rod outer segment renewal process, J. Cell Biol. 42 (1969) 392–403.
[69] O. Strauss, The retinal pigment epithelium in visual function, Physiol. Rev. 85 (2005) 845–881.
[70] S. Wang, W. Lu, O. Tovmachenko, U.S. Rai, H. Yu, P.C. Ray, Challenge in understanding size and shape dependent toxicity of gold nanomaterials in human skin keratinocytes, Chem. Phys. Lett. 463 (2008) 145–149.
[71] I.P. Lau, H. Chen, J. Wang, H.C. Ong, K.C. Leung, H.P. Ho, S.K. Kong, In vitro effect of CTAB-and PEG-coated gold nanorods on the induction of eryptosis/erythroptosis in human erythrocytes, Nanotoxicology 6 (2012) 847–856.
[72] E.E. Connor, J. Mwamuka, A. Gole, C.J. Murphy, M.D. Wyatt, Gold nanoparticles are taken up by human cells but do not cause acute cytotoxicity, Small 1 (2005) 325–327.
[73] J.J. Li, L. Zou, D. Hartono, C. Ong, B. Bay, L. Lanry Yung, Gold nanoparticles induce oxidative damage in lung fibroblasts in vitro, Adv. Mater. 20 (2008) 138–142.
[74] C.J. Murphy, A.M. Gole, J.W. Stone, P.N. Sisco, A.M. Alkilany, E.C. Goldsmith, S.C. Baxter, Gold nanoparticles in biology: beyond toxicity to cellular imaging, Acc. Chem. Res. 41 (2008) 1721–1730.
[75] W. Cho, M. Cho, J. Jeong, M. Choi, H. Cho, B.S. Han, S.H. Kim, H.O. Kim, Y.T. Lim, B.H. Chung, Acute toxicity and pharmacokinetics of 13 nm-sized PEG-coated gold nanoparticles, Toxicol. Appl. Pharmacol. 236 (2009) 16–24.
[76] M.S. Yavuz, Y. Cheng, J. Chen, C.M. Cobley, Q. Zhang, M. Rycenga, J. Xie, C. Kim, K.H. Song, A.G. Schwartz, Gold nanocages covered by smart polymers for controlled release with near-infrared light, Nat. Mater. 8 (2009) 935–939.
[77] V.P. Torchilin, Recent advances with liposomes as pharmaceutical carriers, Nat. Rev. Drug Discov. 4 (2005) 145–160.
[78] E.M. Del Amo, A. Urtti, Current and future ophthalmic drug delivery systems: a shift to the posterior segment, Drug Discov. Today 13 (2008) 135–143.

7. Study III: Photothermally triggered Lipid Bilayer Phase Transition and Drug Release from Gold Nanorod and Indocyanine Green Encapsulated Liposomes

LANGMUIR

Article

pubs.acs.org/Langmuir

Photothermally Triggered Lipid Bilayer Phase Transition and Drug Release from Gold Nanorod and Indocyanine Green Encapsulated Liposomes

Lauri Viitala,[†] Saija Pajari,[†] Tatu Lajunen,[‡] Leena-Stiina Kontturi,[‡,⊥] Timo Laaksonen,[‡] Päivi Kuosmanen,[†] Tapani Viitala,[‡] Arto Urtti,[‡,§] and Lasse Murtomäki*[,†]

[†]Department of Chemistry, Aalto University, P.O. Box 16100, FI-00076 Aalto, Finland

[‡]Faculty of Pharmacy, University of Helsinki, P.O. Box 56, FI-00014 Helsinki, Finland

[§]School of Pharmacy, University of Eastern Finland, P.O. Box 1627, FI-70211 Kuopio, Finland

[⊥]Department of Pharmaceutics, Utrecht University, Universiteitsweg 99, 3584 CG, Utrecht, The Netherlands

ABSTRACT: In light-activated liposomal drug delivery systems (DDSs), the light sensitivity can be obtained by a photothermal agent that converts light energy into heat. Excess heat increases the drug permeability of the lipid bilayer, and drug is released as a result. In this work, two near-IR responsive photothermal agents in a model drug delivery system are studied: either gold nanorods (GNRs) encapsulated inside the liposomes or indocyanine green (ICG) embedded into the lipid bilayer. The liposome system is exposed to light, and the heating effect is studied with fluorescent thermometers: laurdan and CdSe quantum dots (QDs). Both photothermal agents are shown to convert light into heat in an extent to cause a phase transition in the surrounding lipid bilayer. This phase transition is also proven with laurdan generalized polarization (GP). In addition to the heating results, we show that the model drug (calcein) is released from the liposomal cavity with both photothermal agents when the light power is sufficient to cause a phase transition in the lipid bilayer.

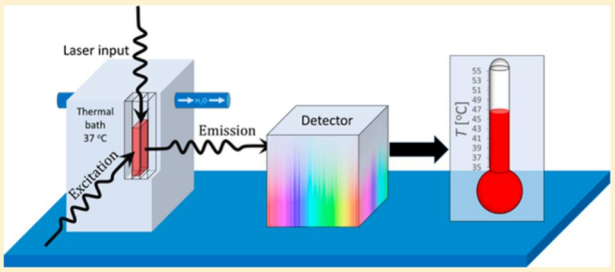

INTRODUCTION

Drug delivery systems (DDSs) are developed to optimize drug concentrations and duration of action in the target cells. The functions of a DDS can be divided into three key points. First, it must provide protection to the drug against the biochemical conditions, for example, catalytic enzymes. Second, DDSs should deliver drug to the specific target site and release the drug in a controlled manner with sufficient amounts. In other words, DDS should stay mute or in the "stealth mode" outside the target but switch to "release mode" instantly at the target site. Third, DDS must always be nontoxic and biodegradable if it is given parenterally.[1] The development of next-generation DDSs is not a trivial matter; in many cases the drug carrier finds its way to the target, but the drug release dose remains insufficient.[2] This usually stems from too stable a DDS in the target site. That is why there is a keen interest in DDSs with external triggering mechanisms where the trigger can be either exogenous (i.e., light, temperature, magnetic fields, etc.) or endogenous (i.e., pH, enzymatic concentrations, etc.).[3]

Liposomal DDSs provide excellent biocompatibility and ability to be engineered to respond to various types of release mechanisms. Liposomal DDSs are readily endocytosed to many target cells, where the drug release can be triggered with e.g. pH change[4] (during the endocytosis), temperature,[5] or light-to-heat conversion with a photothermal agent, e.g., gold nanoparticles.[6−9] All of these triggers are of potential use, for instance, in the treatment of diseases at the posterior segment of the eye.[10]

This paper deals with the light-to-heat conversion that would trigger the drug release from liposomes in the target site (e.g., the eye), where light (especially in the near-IR region) penetrates the tissue effectively. Light-to-heat conversion has been done by encapsulating hydrophilic gold nanoparticles (GNPs) inside the liposomes or hydrophobic GNPs into the bilayer of the liposomes.[6,11] As the GNP turns absorbed light energy into heat, heat is transported to the surrounding lipid bilayer (MD simulation; see e.g. ref 12) and the lipids undergo a phase transition[8,13] followed by drug release.[6,9] The underlying mechanism of action is no different than in thermotherapy, where GNPs are heated by light in order to kill cancer cells.[14] In addition to gold colloids, some organic dyes such as indocyanine green (ICG) and IR820 act as a photothermal agent and can also be used in thermal therapy.[15,16] Remarkably, these dyes have so far not been used in drug release from liposomes.

Received: February 24, 2016
Revised: April 11, 2016
Published: April 18, 2016

The heating effect of a photothermal agent is directly dependent on the absorptivity at a given wavelength. In most cases, interest lies in the region between 700 and 900 nm, i.e., "the physiological window", as lower wavelengths (i.e., UV and visible light region) pose a risk to the retina and other tissues. In the near-IR region, light penetrates tissue effectively and causes less damage to the cells and tissues.[11,17,18] With ICG, the absorption maximum is in the physiological window. With GNPs, the surface plasmon peak at the absorption spectrum can be optimized to this region by changing the GNP dimensions. In the case of GNRs, the surface plasmon peak is readily tunable by changing the corresponding aspect ratio, η, i.e., the ratio of length versus diameter of the rod.

Two fluorescent thermometers are used in this paper. First, laurdan is a fluorescent probe that exhibits two distinguishable energy states that are called locally excited state and charge transfer state (or ground state and excited state). These two states are distributed according to the statistical average that is an expression of the polarity of the surroundings.[19−21] More profoundly, they emit different wavelengths under excitation. Therefore, laurdan can be used in various systems that experience changes in the dipolar interactions. One of the most commonly used application is the study of a lipid bilayer. The lipid order and the lipid phase behavior at different temperatures can be measured with a so-called laurdan generalized polarization:

$$\mathrm{GP} = \frac{I_g - I_{lc}}{I_g + I_{lc}} \quad (1)$$

where I_g and I_{lc} represent laurdan emission intensities at the maximum intensity wavelengths of gel order and liquid crystal order in the bilayer, respectively.[19,20,22] This approach allows laurdan to be used in the determination of lipid phase diagrams and phase separation directly by using microscopic techniques or by simple spectroscopic measurements.[23,24] Because of the fact that the phase transition in a single-lipid system occurs at fixed temperature and the shape of the GP is easy to obtain, it is also possible to use laurdan as a temperature probe.[25]

CdSe quantum dots (QDs) are the second fluorescent thermometer used in this paper. In general, QDs are nanocrystals that are made of semiconducting materials. The electron−hole pairs in the conjunction points in the QD volume result in a bright and narrow emission band that can be excited with a wide range of wavelengths. This is very beneficial in e.g. flow cytometry[26] and fluorescence imaging.[27] The spectral position of the emission band is mainly dependent on the size and the geometry of the QDs. Some QDs can be used as nanothermometers because the temperature increment causes a red-shift in the emission maximum along with the reduction of the emission intensity.[28] These QDs usually consist of CdSe[29−31] or CdTe.[28] Because of their small size and high quantum yield, QD nanothermometers can sense very local temperature changes and are highly applicable to various applications where the interest is in the thermometry at small scale. A drawback for the QD nanothermometers is that the spectral position can require some line of work to be determined with high accuracy. Nonetheless, the accuracy of a QD nanothermometer (ca. 1 °C) is rather similar when compared with normal ratiometric fluorescent thermometers in physiological conditions. Hence, QD nanothermometers can be used in various conditions to track down small-scale effects with very low concentration.[32,33]

In this paper, we give new insight into the light-to-heat conversion of the GNRs and ICG. Temperature increment is determined with fluorescent probes laurdan and CdSe QDs that are used jointly to provide double reading of the temperature and the phase order in the bilayer (by laurdan). The photothermal heat conversion is measured with and without the liposome systems, and the results are compared. The liposomes used in this paper constitute of large unilamellar vesicles (LUV) that could be utilized in targeted delivery via e.g. macrophage uptake in terms of their size. However, as we focus on the light triggered phase transition that takes place in the lipid bilayer, the liposome size is irrelevant, and the results here should be taken beyond any specific application.

This paper couples the photothermal effects that have been studied separately in the previous publications. These can be listed in terms of (1) heating efficiency with GNPs,[30,31,34−37] (2) heating efficiency with ICG,[15] and (3) the enhancement of drug release with GNPs.[6,7,9] In addition to these, we have showed that GNPs were able to cause phase transition in liposomes under steady UV illumination on a QCM sensor[13] and in a solution[8] (measured with small-angle X-ray scattering, SAXS). In this paper, we continue this line of work by introducing fluorescent probes laurdan and CdSe QDs to measure light-inflicted temperature changes in systems containing GNRs and ICG. These elevated temperatures cause phase transition in the lipid bilayer, and it is proven with laurdan. Hence, we would like to state that this publication is the first paper to show the heating effect and the drug carrier phase transition in a buffer solution at the same time, underlining the relevance of the phase behavior in drug release from a drug carrier during the illumination. Furthermore, this is the first paper having ICG as the photothermal agent for the drug release from liposomes.

EXPERIMENTAL SECTION

Materials. DPPC (1,2-dipalmitoyl-*sn*-glycero-3-phosphocholine) solutions (25 mg/mL of lipid diluted in chloroform) and DPPC powder were purchased from Avanti Polar Lipids. GNRs with citrate as a stabilizing agent with the aspect ratio around 4.1 (length around 41 nm) were purchased from Nanopartz. PEGylated CdSe QDs with emission maximum at 565 nm were purchased from Invitrogen. Ethanol was a product of Altia. Laurdan, indocyanine green (ICG), calcein, and the rest of the chemicals were purchased from Sigma-Aldrich.

Light-to-Heat Conversion in Photothermal Liposomes. All liposome samples were prepared in a similar manner. First, 1.5 μmol (44 μL) of DPPC in chloroform (25 mg/mL) was added to a round flask with 5.7 nmol of laurdan in pure ethanol (10 μL of 0.2 mg/mL). The organic solution was evaporated under a stream of nitrogen initially at room temperature but slowly heated to around 60 °C where it was kept for another 30 min. Next, the lipid film was hydrated with slow addition of a buffer solution containing 10 mM TRIS-HCl and 100 mM NaCl at pH 7.4 with or without the photothermal agent (GNRs and/or ICG with or without 100 mM sodium ascorbate) while sonicating the mixture in a 60 °C water bath. The total volume of the added solution was 750 μL. Liposomes were then extruded 11 times ($T \approx 60$ °C) through two-stacked polycarbonate membranes with a pore size of 400 nm. During the extrusion, multilamellar liposomes and larger liposomes break down and reassemble to form unilamellar liposomes with a given size range. This provides more encapsulation volume, as the degree of multilamellarity in liposomes is reduced. After the last extrusion, the syringe content was injected carefully onto a Sephadex G-50 gel column, and the sample was slowly eluted with buffer solution. Roughly 550 μL aliquots were collected after the fluorescent part of the sample front (laurdan is visible in the UV light) was eluted to around 5 mm from the gel filter bottom. The third

aliquot (see Figure 1) was used in further experiments. In the case of ICG samples, the gel filtration step was not conducted. Instead, the

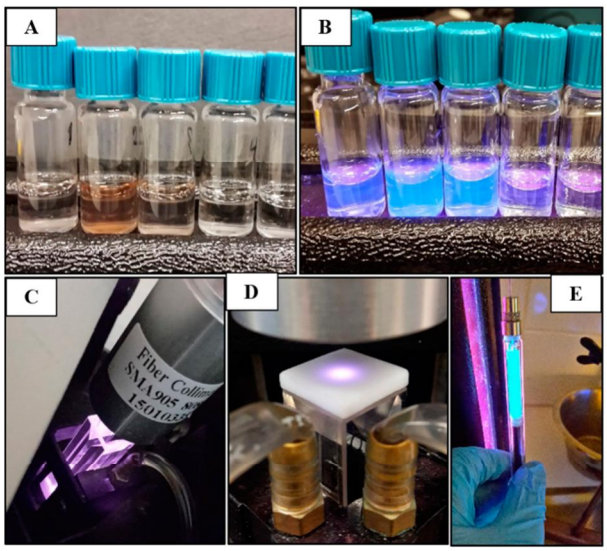

Figure 1. Sephadex G-50 gel-filtrated aliquots of laurdan–DPPC liposomes with GNRs in normal room light (A) and under the low-intensity UV irradiation (B). Sample 3 (third from the left) was used in further experiments. This sample showed less GNRs but rather equal Laurdan emission intensities observed by naked eye under the UV irradiation. Experimental setup is shown under the sample images. The alignment was done with a camera with visibility to near-IR (C, D). The sample before the gel filtration is shown in (E).

ICG-liposome concentration was diluted to 1 mM. Finally, ca. 64 nM of QDs was added to the sample dispersion so that in the final stage GNRs (if any) were encapsulated inside the liposomes, laurdan and ICG (if any) were located inside the lipid bilayer, and QDs were located outside of the liposomes.

Fluorescence measurements were carried out with a PerkinElmer LS5 fluorescence spectrometer with excitation wavelength 365 nm. The external trigger was provided with a 5 W diode laser (808 nm, Dragon Lasers) with a circular beam diameter of 4 mm after the fiber and the collimator. The alignment of the heating laser was done manually with the help of a near-IR-detecting camera (see Figure 1). The sample volume was exactly 450 μL in every measurement, independent of the sample concentration. All measurements were performed in a four-window fluorescence cuvette (total volume 700 μL, Thorlabs) with inner dimensions of 0.2 cm × 1 cm × 3.5–4 cm. Hence, the path length of light was ca. 2.25 cm for the heating laser and 1 cm for the excitation beam. All further analyses were performed in Matlab.

Calcein Release from the Photothermally Heated Liposomes. At first, 1.5 μmol (110 μL) of DPPC in chloroform (10 mg/mL) was added to a glass tube. Organic solution was evaporated under a stream of nitrogen at 60 °C in a vacuum rotary evaporation system (Büchi R-114, Büchi Labortechnik AG, Flawil, Switzerland). The pressure was slowly reduced to 100 mbar and kept at that level for 10 min. A calcein solution (60 mM) was prepared by dissolving 374 mg of calcein and 17 mg of sodium chloride in 10 mL of Milli-Q water, and the pH was adjusted to 7.4 with sodium hydroxide. 3 pmol of GNRs or 30 nmol of ICG was added to the solution. Next, the lipid film was hydrated with 750 μL of the calcein solution at 60 °C with gentle stirring for 30 min. The formed liposomes were then extruded 11 times ($T \approx 60$ °C) through polycarbonate membranes with a pore size of 400 nm. The liposome samples were purified by gel filtration in a Sephadex G-50 column where samples were eluted with a buffer solution of 20 mM HEPES and 140 mM sodium chloride (pH 7.4).

500 μL of the purified sample was placed in a Thermomixer C heating device (Eppendorf AG, Hamburg, Germany) and heated to 37 °C. The light triggered sample was exposed to light for 15 min with a power density of 6 or 18 W cm^{-2} (or light power of 1 and 3 W). At the same time, a control sample on the same heating device was shielded from the light exposure. Next, 5 μL of triggered sample, control sample, and baseline sample (no heating or light exposure) was transferred to 250 μL of HEPES buffer solution (n = 4) on an Optiplate-96 well plate (PerkinElmer, Waltham, MA). Fluorescence emission of calcein was quenched at high concentrations within liposomes. Upon release, dilution of calcein took place and a strong fluorescence signal was detected. The release measurements were performed at excitation and emission wavelengths of 495 and 515 nm, respectively, using a Varioskan Flash plate reader (Thermo Fisher Scientific Inc., Waltham, MA). After measuring the fluorescence, 10 μL of 10% Triton X-100 was added to dissolve the liposomes for complete calcein release, and the wells were measured again. The calcein release percentage (R) was calculated as

$$R = \frac{F - F_0}{F_{100} - F_0} \times 100\% \quad (2)$$

where F is the fluorescence in the sample, F_0 is the fluorescence of the baseline sample, and F_{100} is the fluorescence after a complete calcein release. The release study was repeated thrice, and the mean calcein release percentage and standard deviation were calculated.

RESULTS AND DISCUSSION

Light-to-Heat Conversion by the Photothermal Agents. *Free GNRs in Buffer Solution.* Temperature changes in the GNR-containing buffer solutions were determined by making a calibration curve from the QD emission maximum (λ_{ex} = 365 nm) in temperatures between 25 and 70 °C (25, 30, 35, 37, 45, 55, 65, and 70 °C from left to right in Figures 2A and 2C with and without temperature control). During the illumination, temperature was rapidly increased in all GNR solutions (0.5, 1.0, and 2.0 nM). With thermal bath at 37 °C (Figure 2B), the temperature increased ca. 10–12 °C. When no temperature control was used, the illumination caused a greater shift in the QD spectrum, and the temperature increment was around 20 °C (Figure 2D). Figures 2E and 2F show these temperature increments as a function of concentration. Surprisingly, all three concentrations of GNR gave similar responses. Only small differences were detected between samples that had no temperature control. In other words, temperature increment is not a linear function of the GNR concentration, although the temperature increment followed the concentration in some moderation. Jang et al.[38] obtained similar results when they compared temperature increments caused by GNRs under steady illumination in different depths inside a polymer matrix (with no external temperature control). In more concentrated samples, the temperature increment was greater closer to the surface toward the incident wave, whereas more dilute samples had more homogeneous effect and the heating was extended deeper inside the matrix. At around 6 mm depth, the temperature was rather equal for all samples containing 0.5, 1.0, and 2.0 nM of GNRs. Although the temperature was of the same magnitude, the temperature gradients became larger when the concentration was increased. Hence, it was concluded that the adjustability and the homogeneity of the temperature increase inside the whole target site are best obtained with a low concentration of GNRs, whereas the actual temperature increase and the penetration depth of the incident beam can be controlled by adjusting the laser power.[38]

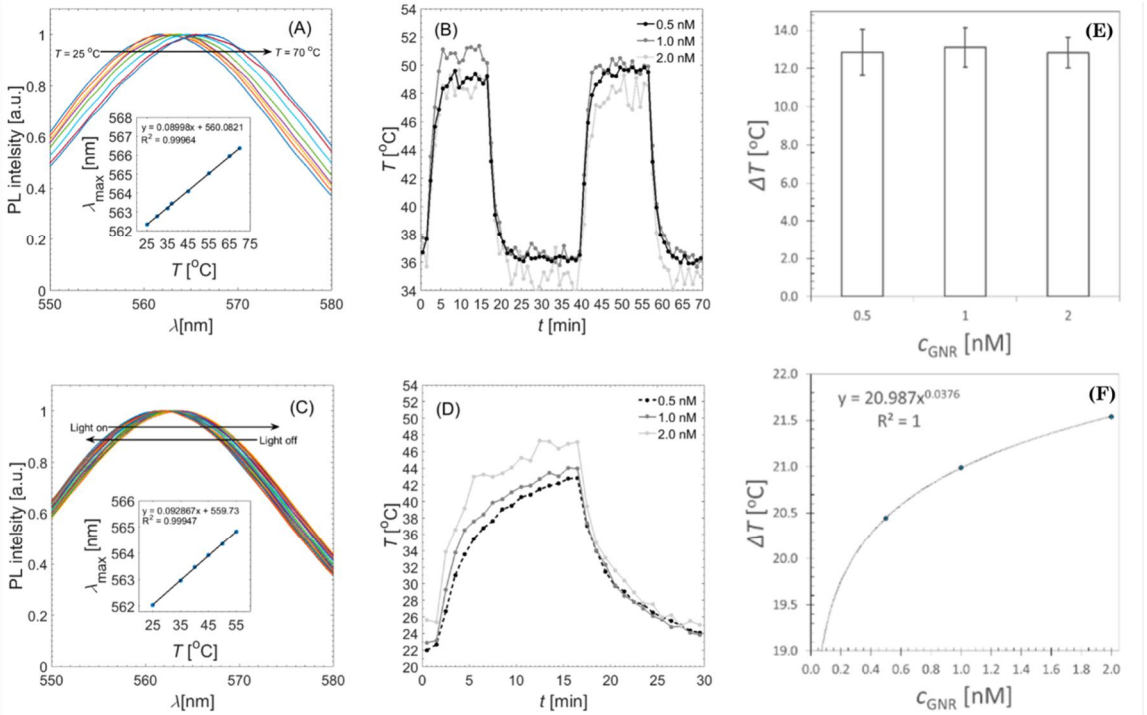

Figure 2. (A) Temperature dependency of QD emission in TRIS buffered GNR (1 nM) solution. (B) Temperature increment during the illumination (2–17 and 40–57 min) for 0.5, 1.0, and 2.0 nM GNR solutions. (C) Emission spectrum of QDs during the illumination and temperature dependency of the maximum intensity wavelength calibration curve (inset). (D) Temperature increment during the illumination (2–17 min) for 0.5, 1.0, and 2.0 nM GNR solutions without temperature control. Increase in the mean temperature during the illumination in a water circulated system (E, $T_{bath} \approx 37$ °C) and in a system without external temperature control (F) as a function of GNR concentration.

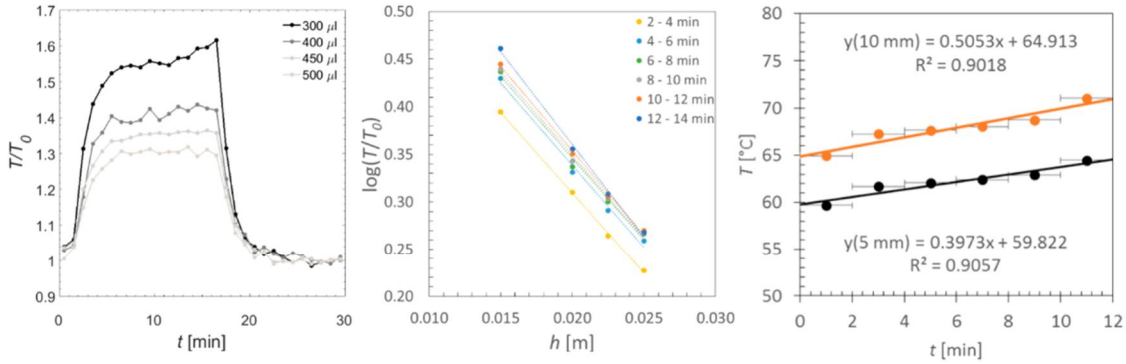

Figure 3. Left: temperature increase (with water circulation at 37 °C) in relation to the equilibration temperature as a function of time (illumination starts after 2 min) for different sample volumes. Center: natural logarithm of the temperature increase respect to the initial temperature as a function of the length of which light travels through the sample in different time slots (i.e., average of three time points, e.g., 2, 3, and 4 min, from the starting time of the light irradiation). Right: the estimated temperature increase during illumination starting at $t = 0$. The excitation beam is at height $z = 5$ mm (black) and $z = 10$ mm (orange). In reality, the beam center, z, is located between these values.

From a general perspective, light attenuation in more concentrated GNR samples cause heterogeneous heating in the GNR samples. This is rather common outcome when a light beam is directed through an absorbing and scattering media, and the phenomenon can be expressed with the well-known Beer–Lambert–Bouguer law. In our results, the signal noise was slightly increased when the GNR concentration was increased. This implies that, similarly, a high concentration of GNRs may cause a steeper temperature gradient as the light is attenuated in its path throughout the sample. The mean temperature rise had then only a minor correlation with the concentration of the GNRs inside the system. Another way of looking at the Beer–Lambert–Bouguer effect is to measure the temperature rise with different sample volumes. The attenuation of light intensity is an exponential function of the sample thickness or the path length of light. Hence, logarithm of the temperature increase, that is proportional to the light power being absorbed, is a linear function of the sample thickness (see Figure 3). Thus, obviously, homogeneously diluted GNRs with a large absorption cross section warm up as a function of the intensity of light they absorb, which depends on the geometry of the sample. This is an important point that distinguishes a

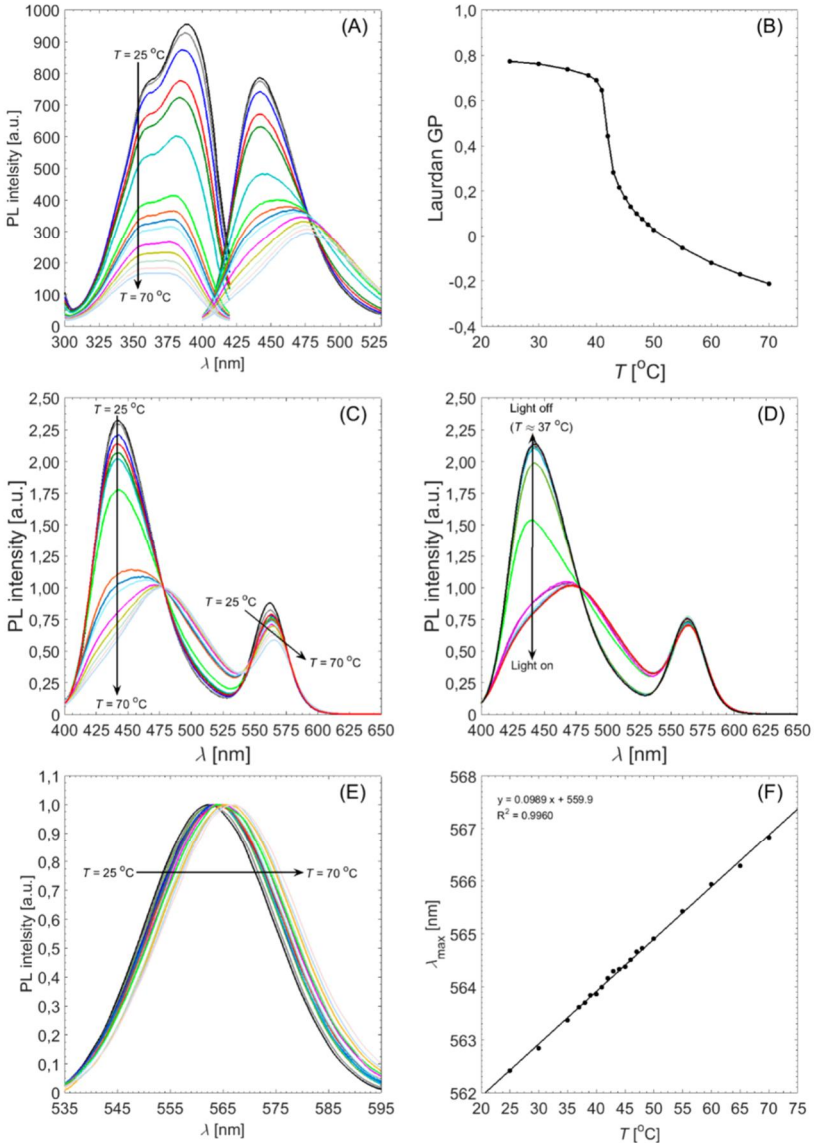

Figure 4. (A) Laurdan excitation (λ_{em} = 440 nm) and emission (λ_{ex} = 365 nm) spectra in different temperatures in the intensity-descending order (with respect to temperature increment). (B) Laurdan GP as a function of temperature. (C) Normalized GNR–laurdan–DPPC–QD emission spectra in different temperatures. (D) GNR–laurdan–DPPC–QD emission spectra during the illumination experiment (initial temperature ca. 37 °C; measurement in 1 min intervals). (E) Baseline corrected QD spectrum as a function of temperature. (F) Maximum emission wavelength from (E) as a function of temperature.

macroscopic measurement from a nanosized one. To get actual information on such small scales, both the geometry and the time scale of the system should be very small, and the intensity of the incident beam should be sufficient (i.e., decades larger what is required in the macroscopic system). This is mainly due to the fact that heat transport in water phase is very rapid and the rate of temperature equilibration is ca. 100 nm/ns. We do not go deeper into this matter in this paper (some details are available in refs 39 and 40), as we focus on describing the macroscopic system that is relevant in the drug delivery systems. However, we can make a rough estimate of the temperature near the nanoparticle surface by assuming that the value corresponds to a point where the maximum intensity of light is at z (i.e., the height of the excitation beam center):

$$\frac{T}{T_0} = \exp(k_1 z + k_2) \tag{3}$$

where k_1 and k_2 are the slope and the intersect of the $\log(T/T_0^{-1})$ vs h fit.

GNR Encapsulated Liposomes. Laurdan–DPPC (1,2-dipalmitoyl-*sn*-glycero-3-phosphocholine) excitation and emission spectra are shown in Figure 4A. In both, the shape of the curve changes when laurdan is exposed to a more polar environment due to the temperature increase and change in the lipid order inside the lipid bilayer.[19−21] At ca. 41−43 °C, the emission intensity drops down rapidly at 430 nm and increases at 510 nm. This is caused by the phase transition, which becomes more observable when the intensity data are converted to GP (eq 1) at the given temperature. The GP

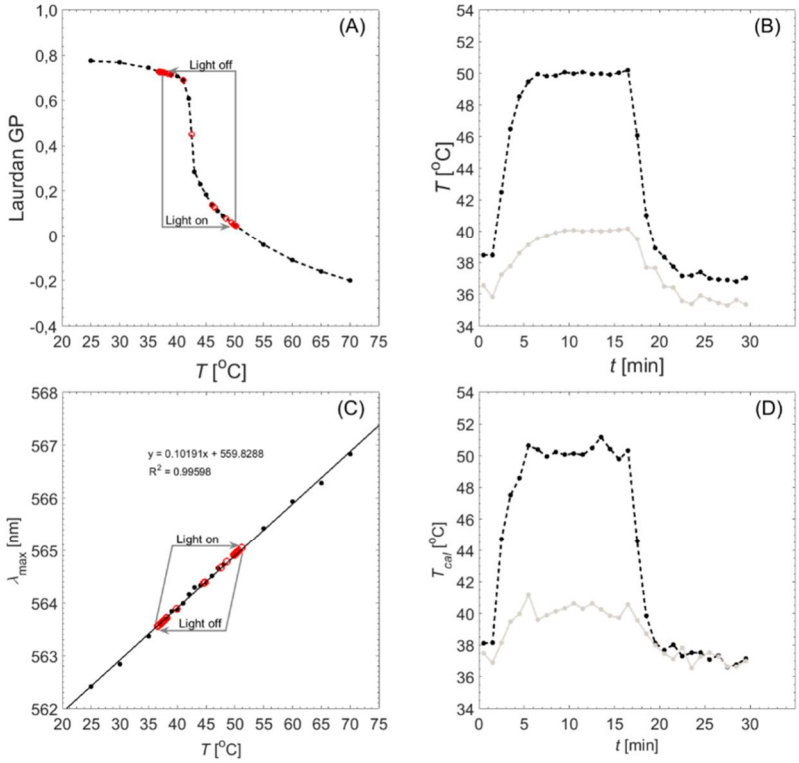

Figure 5. Illumination response of GNRs encapsulated laurdan–DPPC liposomes. System is cooled down with a water circulation that is set to maintain the temperature at 37 °C. In (A), black dots represent the laurdan GP as a function of temperature, and red dots are the corresponding GP values during the illumination experiment. In (B), temperature is obtained from (A) as a function of time during the illumination. (C) QD emission maximum wavelengths as a function of temperature and during the illumination (red points). In (D), temperature is obtained from (C) as a function of time during the illumination. Gray curves in (B) and (D) represent the illumination experiment without GNRs.

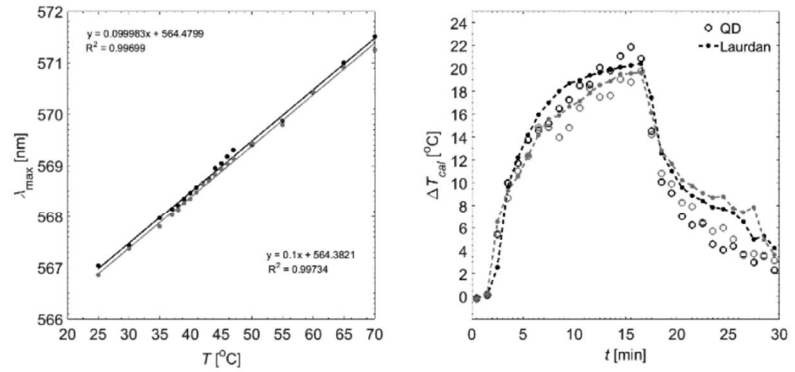

Figure 6. Left: QD temperature calibration curve for the sample under study. Right: temperature increment of a GNR encapsulated liposomes without water circulation measured with QDs and with laurdan GP.

curve for DPPC is shown in Figure 4B. Figures 4C and 4D show respectively the emission spectra of the sample when it was slowly heated from 25 to 70 °C (T = 25, 30, 35, 37, 40, 41, 42, 43, 44, 45, 50, 55, 60, 65, and 70 °C in the intensity-descending order) and the emission spectra of the illuminated sample containing GNRs with the initial temperature of 37 °C (data collected in 1 min intervals with 300 nm/min). During illumination, laurdan emission shifts rapidly toward the normal response of a DPPC bilayer of a liquid crystalline phase. It shows that the heating effect even with a small concentration of GNRs is sufficient to cause the phase transition in the bilayer. In addition, laurdan GP information can be used as a thermometer. This is depicted in Figures 5A and 5B, where the result of the illumination experiment is shown as a function of time.

In addition to the laurdan results, QDs denote the temperature change by red-shifting their maximum emission wavelength. This is more distinguishable from Figures 4E and 4F where the baseline curve (i.e., laurdan without QDs) is subtracted from the measured curve (Figure 4C). In the illumination experiment, measured temperature increments (see Figures 5C and 5D) were conclusively the same for laurdan and QDs, and the temperature increment in the system (containing less than 1 nM of GNRs) was ca. 11–13 °C over

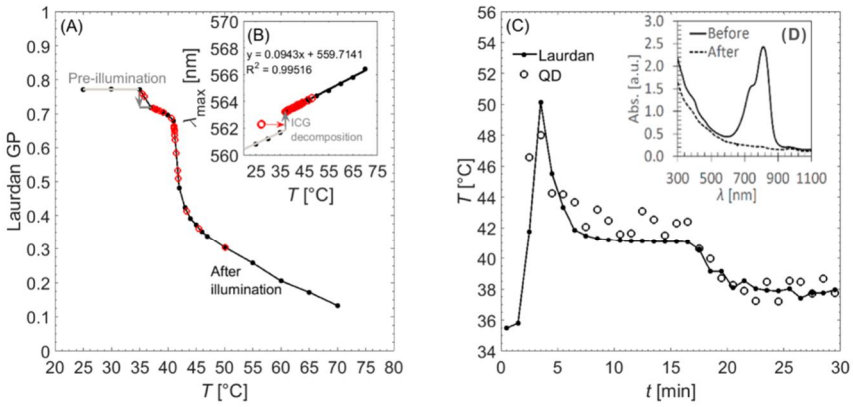

Figure 7. Temperature change in laurdan–DPPC–QD system with 80 μM of ICG during the illumination (C) that was obtained from the laurdan GP and QD calibration curves (A and B, respectively). In both cases, a shift in the calibration curves took place after introducing the incident beam. Because of this shift, there is some inaccuracy in the beginning of the illumination. Shortly after, however, both thermometers converged to the same reading, indicating a re-equilibration of the system after a rapid temperature increase that was encompassed with a decomposition of ICG (see the absorption spectrum in (D)).

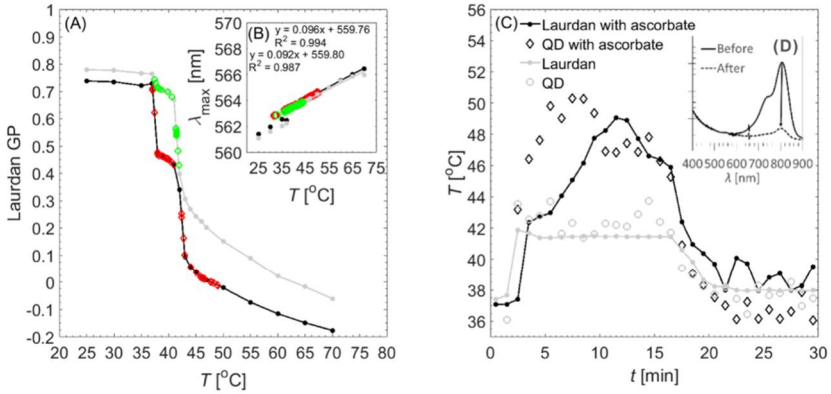

Figure 8. Temperature change in the laurdan–DPPC–QD system with 40 μM of ICG and with 100 mM sodium ascorbate (black curve and black points in (C)) and without sodium ascorbate (gray curves and gray points in (C)) during the illumination. The temperature readings were obtained from the laurdan GP and QD calibration curves (A and B, respectively). Black curve and red points and gray curve and green points represent the calibration curves and the light illumination points for the ascorbate and the ascorbate-free case, respectively. A shift in the curves took place after introducing an incident beam due to a photochemical decomposition of photoactive substances (ICG and ascorbate) that is evident from the absorption spectrum in (D). Nonetheless, temperature increased rapidly in the ascorbate sample, and the temperature remained at around 50 °C before gradual decrease in the QD determination. Laurdan seemed to react slower due to stronger ICG interactions. In the ascorbate-free case, the temperature increase and the decomposition of ICG were probably too rapid a phenomenon to be registered by either probe.

the thermal bath at 37 °C. As a comparison, Figures 5B and 5D show the illumination-caused temperature increment without GNRs (gray curves). In the GNR-free cases, the temperature was increased by 3–4 °C. Hence, the temperature change was more than 3 times higher with GNRs compared to the system without GNRs.

Heat generation with encapsulated GNRs was also studied without water circulation to compare heating efficiency of GNR encapsulated liposomes with free GNRs. These results are shown in Figure 6. In this case, the temperature increment was approximately 20 °C, and no real distinction to the case of free GNRs (see Figure 2) was detected. Thus, neither the bilayer nor the GNR packing order had an effect on the heat transport in the macroscopic limit. This is not a surprise since the lipid bilayer is only 5 nm thick. The same conclusion can also be drawn from the water circulated system, where the temperature increase was also very similar to that of a sample with free GNRs. Finally, heat production of temperature controlled and uncontrolled systems would have been sufficient to initiate drug release.

ICG Embedded Liposomes. ICG is an amphiphilic molecule that is located inside the lipid bilayer with laurdan. The close proximity means that laurdan detects the ICG molecule in the bilayer, and the laurdan GP is thus easily affected by physical transformations in the system. Unfortunately, ICG is a photosensitive molecule that decomposes when it is illuminated at its responsive frequency. This is followed by a shift in the laurdan calibration curve as the system experiences a change in the physical state. ICG was rapidly decomposed when the system was illuminated at 808 nm with power density of 18 W cm^{-2} (3 W). This is readily seen from the absorption spectra of the ICG system before and after the illumination that is shown in Figure 7D. In addition to this, a shift in the laurdan GP was also obtained (see Figure 7A), and the first two temperature readings were no longer comparable to the rest of the system readings. A similar shift occurred also in the QD thermometer (Figure 7B). This discontinuation was probably caused by the

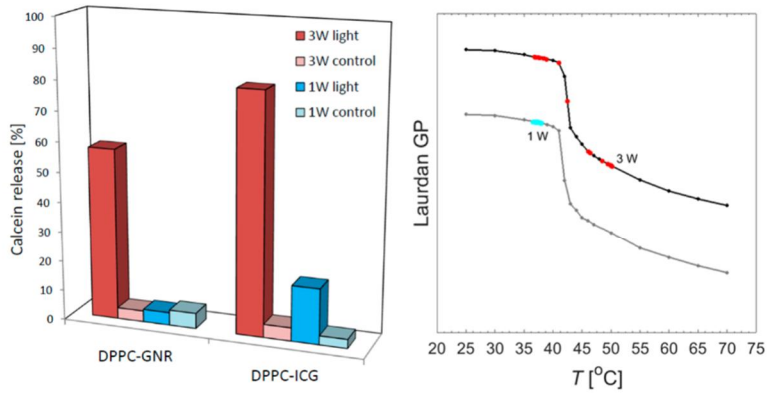

Figure 9. Left: relative amount of released calcein from DPPC liposomes after 15 min of illumination with 6 W cm^{-2} (1 W) and 18 W cm^{-2} (3 W) power density. Left columns represent the system with GNRs, and right ones are systems with ICG. The leftmost of the columns is the illumination of photothermal solution with 3 W; next, control sample with 3 W; illumination of photothermal solution with 1 W; and finally, control with 1 W. Right: laurdan generalized polarization shows that during illumination with 3 W the lipid bilayer goes through a phase transition while illumination with 1 W does not provide enough power to cause this effect. The calibration curves are manually separated to give better illustration of the action taking place.

enhanced interaction with the particles produced in the decomposition of ICG. In first couple minutes in Figure 7C, the system had a peak in the values of both temperature probes during which the temperature increased to approximately 48–50 °C, a temperature considerably higher than the drug release temperature (41.5 °C for DPPC). Because of the slow rate of the measurement, the peak value represents an average of a 1 min time interval, and the actual peak value may have been even higher. The peak also remained narrow, meaning that the decomposition of ICG was very rapid and exhaustive.

A physical transformation in the system makes temperature determination rather difficult. In the case of photochemical decomposition, one may inhibit the rate of the radical reactions by e.g. adding a singlet-oxygen quencher (e.g., sodium azide[41]) into the system. In this paper, 100 mM of water-soluble sodium ascorbate was added to hinder the ICG decomposition. This enhanced the observed temperature rise in smaller concentrations and seemed to stabilize the ICG molecule for a longer period of time (see Figure 8C). However, it did not stop ICG from decomposing, and due to the photochemistry of the ascorbate, laurdan and QD calibration curves were shifted even more than in the unhindered measurements (see Figures 8A and 8B). Nonetheless, the temperature was rapidly balanced at around 50 °C before it was slowly decreased as the irradiation continued. The ICG molecule is likely to affect the laurdan molecule in the bilayer more than the QD probe that is located outside of the liposomes. Hence, the QD thermometer reacts faster to the changes of temperature and laurdan only after gradual degradation of ICG. After some 10 min, however, both thermometers gave the same value, and at the end, most of the ICG was decomposed. This can be seen from the inset in Figure 8D.

Photothermally Triggered Drug Release. Figure 9 represents photothermally released amounts of calcein in GNR encapsulated DPPC liposomes and in ICG embedded DPPC liposomes with 6 W cm^{-2} (1 W) and 18 W cm^{-2} (3 W). With the higher light intensity, an effective release of calcein is obtained with both photothermal agents. With GNRs, approximately 57% of drug is released, whereas almost 80% of calcein was released from ICG embedded system. In the lower incident beam intensity, the GNR system had calcein release indistinguishable from the control sample, whereas some calcein (around 18.5%) was released in the ICG system. The difference between ICG and GNR samples stems probably from the fact that ICG stands inside the lipid bilayer, and from there, it may cause destabilization to the bilayer with closer proximity when compared with the heat produced from GNRs inside the liposome. As the intensity is increased, more heat is provided to the bilayer, and the physical deformations become a global phenomenon in the drug vesicle solution. This affects the liposomes that are burst open so that the drug is released. This is also shown in the right panel in Figure 9, where the undoubted phase transition occurs when the GNR encapsulated liposomes are illuminated with light power of 3 W.

Safety Aspects of Photothermal Drug Delivery. In this paper, we have studied the light-to-heat conversion that is incorporated with the phase transition of the drug carrier, resulting in drug release. The results shown here are not designed to any specific applications. However, these types of DDSs could be used in e.g. transdermal and transscleral drug delivery in addition to ablation of cancer cells. Hence, to avoid any fatal *en passants* in the future, some potential issues should be taken into account. First, there are limitations in the light power dosage, with the exposure time t, what the target organ can bear. As the eyes are especially sensitive, we will limit our discussion to the following. In the ocular tissue, the power limit for the incident at near-infrared region is given by the equation[17]

$$\frac{P}{(\mathrm{W})} = 6.93 \times 10^{-4} C_T C_E \left(\frac{t}{(\mathrm{s})}\right)^{-1/4} \quad (4)$$

where, in our case, $C_T = 10^{0.002(\lambda-700)} = 1.644$ (for $\lambda = 808$ nm) and $C_E = 66.7$ (depending on the visual angle). As the value is obtained for an incident beam of 1.7 mm in diameter, the power density of 18 W cm^{-2} (3 W in our case) should not be applied longer than for 1 ms at a time. It is notable that we have used CW laser with a lot longer exposure times to reach the macroscopic limits in this paper. However, it should be also noted that the system presented here is constituted of randomly dispersed photothermal agents. Hence, the light power demand of our studies rely on the size of the system, as the light is absorbed and scattered by the random media. In

other words, the heat is produced through light localization.[38,42] Earlier, it has been shown that already the aggregation of the photothermal agent, GNRs, can have a sufficient endorsement in the photothermal cancer therapy *in vitro* when compared with more loosely packed photothermal agents.[43] This makes the estimation of the power demand in a biological system difficult and underlines the need of good *in vivo* studies to further clarify the operation limits of such systems in different biological target locations. In any case, as the microscopic effect should be rather instantaneously near the photothermal agent, the drug release at the target site could be achieved with a pulsed laser by optimizing the pulse frequency, duty cycle, and power to suit the given target. In addition to this, the light power density can be adjusted by engineering the drug carrier system and the photothermal agent. For the former, the carrier can be made more responsive to e.g. pH and temperature.[9]

The toxicity of the photothermal agents is another issue related to the applicability of the photothermal DDSs. The main obstacle with GNPs is the lack of long-term clinical studies *in vivo*. Also, there are some contradictive studies in the field on the acute causation due to the GNPs in different biological target sites.[44] In the eye, for instance, citrate stabilized GNPs have been shown to cause adverse effects in retina[45] and to permeate through the blood–brain barrier after an intravitreous injection in mice.[46,47] At the same time, Sharma et al.[48] have shown that the polyethylenimine-conjugated GNPs had no notable toxicity effect in rabbit cornea *in vivo* and in human cornea *in vitro*. Although some discouraging results in the field have been published, there are still multiple ways to make GNPs more biocompatible and biodegradable by engineering e.g. the surface of the colloids.[44] With this in mind, only time will tell whether the GNPs really are the promised golden bullet for the future controlled release. ICG, on the other hand, is a widely used fluorescent marker that has been already approved by the European Medicines Agency (EMA) and the U.S. Food and Drug Administration (FDA).[49,50] Therefore, it offers a very interesting option for the photothermal therapy of various systems in addition to drug release as the only thinkable cause of concern is the photodegradation[41] which has been shown to produce five toxic decomposition compounds.[41,51] This may not be the major issue, since many cells have an inherent clearance system against various hazardous compounds. For instance, retinal pigment epithelia cells (RPE-cells) have well-adapted clearance mechanisms against oxidative stress (relating to the mechanism that photodegrades ICG).[52] In any case, further studies are still needed to determine the full potential of these photothermal agents.

■ CONCLUSIONS

Two fluorescent thermometers, laurdan and CdSe quantum dots (QDs), have been used to give double reading of the temperature and to study the photothermal agents gold nanorods (GNRs) and indocyanine green (ICG) in a model drug delivery application. Three important conclusions were reached. First, when exposed to 808 nm laser with the power density of 18 W cm^{-2}, both photothermal agents were shown to warm up and, even more importantly, over the phase transition temperature of the lipids. Second, a phase transition in the lipid bilayer took place during the illumination, as proven with laurdan generalized polarization (GP). Third, most of the model compound, calcein, was shown to be released when the system was illuminated with an incident beam sufficient to cause a phase transition. Hence, we can conclude that the drug release was driven by heat production of the photothermal agents in the drug delivery system but not without a threshold value needed to cause a phase transition in the lipid bilayer.

■ AUTHOR INFORMATION

Corresponding Author

*E-mail lasse.murtomaki@aalto.fi; tel +358 50 5706352 (L.M.).

Notes

The authors declare no competing financial interest.

■ ACKNOWLEDGMENTS

The Academy of Finland is acknowledged for funding via the Programmable Materials Program "Light Triggered Nanoparticles" (OMA, #263453). T.V. acknowledges Academy of Finland for academy research fellow funding (Grants 137053 and 263861). The authors thank Dr. Vladimir Chukharev and Dr. Elina Vuorimaa-Laukkanen for their help in designing the experimental setup. The authors also thank Prof. Sakari Kulmala for allowing us to use the fluorescence spectroscope in his laboratory.

■ REFERENCES

(1) Alvarez-Lorenzo, C.; Concheiro, A. Smart Drug Delivery Systems: From Fundamentals to the Clinic. *Chem. Commun.* **2014**, *50*, 7743–7765.

(2) Gilleron, J.; et al. Image-Based Analysis of Lipid Nanoparticle–mediated siRNA Delivery, Intracellular Trafficking and Endosomal Escape. *Nat. Biotechnol.* **2013**, *31*, 638–646.

(3) Mura, S.; Nicolas, J.; Couvreur, P. Stimuli-Responsive Nanocarriers for Drug Delivery. *Nat. Mater.* **2013**, *12*, 991–1003.

(4) Simões, S.; Moreira, J. N.; Fonseca, C.; Düzgüneş, N.; Pedroso de Lima, M. C. On the Formulation of pH-Sensitive Liposomes with Long Circulation Times. *Adv. Drug Delivery Rev.* **2004**, *56*, 947–965.

(5) Lindner, L. H.; Eichhorn, M. E.; Eibl, H.; Teichert, N.; Schmitt-Sody, M.; Issels, R. D.; Dellian, M. Novel Temperature-Sensitive Liposomes with Prolonged Circulation Time. *Clin. Cancer Res.* **2004**, *10*, 2168–2178.

(6) Paasonen, L.; Laaksonen, T.; Johans, C.; Yliperttula, M.; Kontturi, K.; Urtti, A. Gold Nanoparticles Enable Selective Light-Induced Contents Release from Liposomes. *J. Controlled Release* **2007**, *122*, 86–93.

(7) Troutman, T. S.; Leung, S. J.; Romanowski, M. Light-Induced Content Release from Plasmon-Resonant Liposomes. *Adv. Mater.* **2009**, *21*, 2334–2338.

(8) Paasonen, L.; Sipilä, T.; Subrizi, A.; Laurinmäki, P.; Butcher, S. J.; Rappolt, M.; Yaghmur, A.; Urtti, A.; Yliperttula, M. Gold-Embedded Photosensitive Liposomes for Drug Delivery: Triggering Mechanism and Intracellular Release. *J. Controlled Release* **2010**, *147*, 136–143.

(9) Lajunen, T.; Viitala, L.; Kontturi, L.; Laaksonen, T.; Liang, H.; Vuorimaa-Laukkanen, E.; Viitala, T.; Le Guével, X.; Yliperttula, M.; Murtomäki, L.; Urtti, A. Light Induced Cytosolic Drug Delivery from Liposomes with Gold Nanoparticles. *J. Controlled Release* **2015**, *203*, 85–98.

(10) Lajunen, T.; Hisazumi, K.; Kanazawa, T.; Okada, H.; Seta, Y.; Yliperttula, M.; Urtti, A.; Takashima, Y. Topical Drug Delivery to Retinal Pigment Epithelium with Microfluidizer Produced Small Liposomes. *Eur. J. Pharm. Sci.* **2014**, *62*, 23–32.

(11) Timko, B. P.; Dvir, T.; Kohane, D. S. Remotely Triggerable Drug Delivery Systems. *Adv. Mater.* **2010**, *22*, 4925–4943.

(12) Potdar, D.; Sammalkorpi, M. Asymmetric Heat Transfer from Nanoparticles in Lipid Bilayers. *Chem. Phys.* **2015**, *463*, 22–29.

(13) Viitala, L.; Lajunen, T.; Urtti, A.; Viitala, T.; Murtomäki, L. Detection of Phase Transition in Photosensitive Liposomes by Advanced QCM. *J. Phys. Chem. C* **2015**, *119*, 21395–21403.

(14) Huang, X.; El-Sayed, I.; Qian, W.; El-Sayed, M. Cancer Cell Imaging and Photothermal Therapy in the Near-Infrared Region by using Gold Nanorods. *J. Am. Chem. Soc.* **2006**, *128*, 2115−2120.
(15) Fernandez-Fernandez, A.; Manchanda, R.; Lei, T.; Carvajal, D. A.; Tang, Y.; Raza Kazmi, S. Z.; McGoron, A. J. Comparative Study of the Optical and Heat Generation Properties of IR820 and Indocyanine Green. *Mol. Imaging* **2012**, *11*, 99−113.
(16) Zheng, M.; Yue, C.; Ma, Y.; Gong, P.; Zhao, P.; Zheng, C.; Sheng, Z.; Zhang, P.; Wang, Z.; Cai, L. Single-Step Assembly of DOX/ICG Loaded Lipid−polymer Nanoparticles for Highly Effective Chemo-Photothermal Combination Therapy. *ACS Nano* **2013**, *7*, 2056−2067.
(17) Delori, F. C.; Webb, R. H.; Sliney, D. H. Maximum Permissible Exposures for Ocular Safety (ANSI 2000), with Emphasis on Ophthalmic Devices. *J. Opt. Soc. Am. A* **2007**, *24*, 1250−1265.
(18) American National Standards Institute. In *American National Standard for the Safe Use of Lasers*; Laser Institute: Orlando, FL, 1993; Vol. ANSI Z136 1-1993.
(19) Parasassi, T.; De Stasio, G.; d'Ubaldo, A.; Gratton, E. Phase Fluctuation in Phospholipid Membranes Revealed by Laurdan Fluorescence. *Biophys. J.* **1990**, *57*, 1179−1186.
(20) Parasassi, T.; Krasnowska, E.; Bagatolli, L.; Gratton, E. Laurdan and Prodan as Polarity-Sensitive Fluorescent Membrane Probes. *J. Fluoresc.* **1998**, *8*, 365−373.
(21) Kawski, A.; Kukliński, B.; Bojarski, P.; Diehla, H. Ground and Excited State Dipole Moments of LAURDAN Determined from Solvatochromic and Thermochromic Shifts of Absorption and Fluorescence Spectra. *Z. Naturforsch., A: Phys. Sci.* **2000**, *55*, 817−822.
(22) Parasassi, T.; Gratton, E. Membrane Lipid Domains and Dynamics as Detected by Laurdan Fluorescence. *J. Fluoresc.* **1995**, *5*, 59−69.
(23) Bagatolli, L. A.; Sanchez, S. A.; Hazlett, T.; Gratton, E. Giant Vesicles, Laurdan, and Two-Photon Fluorescence Microscopy: Evidence of Lipid Lateral Separation in Bilayers. *Methods Enzymol.* **2003**, *360*, 481−500.
(24) Harris, F. M.; Best, K. B.; Bell, J. D. Use of Laurdan Fluorescence Intensity and Polarization to Distinguish between Changes in Membrane Fluidity and Phospholipid Order. *Biochim. Biophys. Acta, Biomembr.* **2002**, *1565*, 123−128.
(25) Chapman, C. F.; Liu, Y.; Sonek, G. J.; Tromberg, B. J. The use of Exogenous Fluorescent Probes for Temperature Measurement in Single Living Cells. *Photochem. Photobiol.* **1995**, *62*, 416−425.
(26) Chattopadhyay, P. K.; Price, D. A.; Harper, T. F.; Betts, M. R.; Yu, J.; Gostick, E.; Perfetto, S. P.; Goepfert, P.; Koup, R. A.; De Rosa, S. C.; Bruchez, M. P.; Roederer, M. Quantum Dot Semiconductor Nanocrystals for Immunophenotyping by Polychromatic Flow Cytometry. *Nat. Med.* **2006**, *12*, 972−977.
(27) Michalet, X.; Pinaud, F. F.; Bentolila, L. A.; Tsay, J. M.; Doose, S.; Li, J. J.; Sundaresan, G.; Wu, A. M.; Gambhir, S. S.; Weiss, S. Quantum Dots for Live Cells, in Vivo Imaging, and Diagnostics. *Science* **2005**, *307*, 538−544.
(28) Jaque, D.; Vetrone, F. Luminescence Nanothermometry. *Nanoscale* **2012**, *4*, 4301−4326.
(29) Walker, G. W.; Sundar, V. C.; Rudzinski, C. M.; Wun, A. W.; Bawendi, M. G.; Nocera, D. G. Quantum-Dot Optical Temperature Probes. *Appl. Phys. Lett.* **2003**, *83*, 3555−3557.
(30) Maestro, L. M.; Haro-González, P.; Coello, J. G.; Jaque, D. Absorption Efficiency of Gold Nanorods Determined by Quantum Dot Fluorescence Thermometry. *Appl. Phys. Lett.* **2012**, *100*, 201110.
(31) Maestro, L. M.; Haro-González, P.; Sánchez-Iglesias, A.; Liz-Marzán, L. M.; García Solé, J.; Jaque, D. Quantum Dot Thermometry Evaluation of Geometry Dependent Heating Efficiency in Gold Nanoparticles. *Langmuir* **2014**, *30*, 1650−1658.
(32) Kucsko, G.; Maurer, P. C.; Yao, N. Y.; Kubo, M.; Noh, H. J.; Lo, P. K.; Park, H.; Lukin, M. D. Nanometre-Scale Thermometry in a Living Cell. *Nature* **2013**, *500*, 54−58.
(33) Alicki, R.; Leitner, D. M. Size-Dependent Accuracy of Nanoscale Thermometers. *J. Phys. Chem. B* **2015**, *119*, 9000−9005.
(34) Baffou, G.; Berto, P.; Bermúdez Ureña, E.; Quidant, R.; Monneret, S.; Polleux, J.; Rigneault, H. Photoinduced Heating of Nanoparticle Arrays. *ACS Nano* **2013**, *7*, 6478−6488.
(35) Baffou, G.; Polleux, J.; Rigneault, H.; Monneret, S. Super-Heating and Micro-Bubble Generation Around Plasmonic Nanoparticles Under Cw Illumination. *J. Phys. Chem. C* **2014**, *118*, 4890−4898.
(36) Govorov, A. O.; Zhang, W.; Skeini, T.; Richardson, H.; Lee, J.; Kotov, N. A. Gold Nanoparticle Ensembles as Heaters and Actuators: Melting and Collective Plasmon Resonances. *Nanoscale Res. Lett.* **2006**, *1*, 84−90.
(37) Keblinski, P.; Cahill, D. G.; Bodapati, A.; Sullivan, C. R.; Taton, T. A. Limits of Localized Heating by Electromagnetically Excited Nanoparticles. *J. Appl. Phys.* **2006**, *100*, 054305.
(38) Jang, B. Effects of Gold Nanorod Concentration on the Depth-Related Temperature Increase during Hyperthermic Ablation. *Small* **2010**, *7*, 265.
(39) Baffou, G.; Quidant, R. Thermo-plasmonics: Using Metallic Nanostructures as Nano-sources of Heat. *Laser Photon. Rev.* **2013**, *7*, 171−187.
(40) Chen, Z.; Shan, X.; Guan, Y.; Wang, S.; Zhu, J.; Tao, N. Imaging Local Heating and Thermal Diffusion of Nanomaterials with Plasmonic Thermal Microscopy. *ACS Nano* **2015**, *9*, 11574−11581.
(41) Engel, E.; Schraml, R.; Maisch, T.; Kobuch, K.; König, B.; Szeimies, R.; Hillenkamp, J.; Bäumler, W.; Vasold, R. Light-Induced Decomposition of Indocyanine Green. *Invest. Ophthalmol. Visual Sci.* **2008**, *49*, 1777−1783.
(42) Hogan, N. J.; Urban, A. S.; Ayala-Orozco, C.; Pimpinelli, A.; Nordlander, P.; Halas, N. J. Nanoparticles Heat through Light Localization. *Nano Lett.* **2014**, *14*, 4640−4645.
(43) Nam, J.; Won, N.; Jin, H.; Chung, H.; Kim, S. pH-Induced Aggregation of Gold Nanoparticles for Photothermal Cancer Therapy. *J. Am. Chem. Soc.* **2009**, *131*, 13639−13645.
(44) Alkilany, A. M.; Murphy, C. J. Toxicity and Cellular Uptake of Gold Nanoparticles: What we have Learned so Far? *J. Nanopart. Res.* **2010**, *12*, 2313−2333.
(45) Söderstjerna, E.; Bauer, P.; Cedervall, T.; Abdshill, H.; Johansson, F.; Johansson, U. E. Silver and Gold Nanoparticles Exposure to in Vitro Cultured Retina−studies on Nanoparticle Internalization, Apoptosis, Oxidative Stress, Glial-and Microglial Activity. *PLoS One* **2014**, *9*, e105359.
(46) Kim, J. H.; Kim, J. H.; Kim, K.; Kim, M. H.; Yu, Y. S. Intravenously Administered Gold Nanoparticles Pass through the Blood? Retinal Barrier Depending on the Particle Size, and Induce no Retinal Toxicity. *Nanotechnology* **2009**, *20*, 505101.
(47) Khlebtsov, N.; Dykman, L. Biodistribution and Toxicity of Engineered Gold Nanoparticles: A Review of in Vitro and in Vivo Studies. *Chem. Soc. Rev.* **2011**, *40*, 1647−1671.
(48) Sharma, A.; Tandon, A.; Tovey, J. C. K.; Gupta, R.; Robertson, J. D.; Fortune, J. A.; Klibanov, A. M.; Cowden, J. W.; Rieger, F. G.; Mohan, R. R. Polyethylenimine-Conjugated Gold Nanoparticles: Gene Transfer Potential and Low Toxicity in the Cornea. *Nanomedicine* **2011**, *7*, 505−513.
(49) EMA Evaluation of the Pharmacokinetics of Medicinal Products in Patients with Impaired Hepatic Function. http://www.ema.europa.eu/docs/en_GB/document_library/scientific_guideline/2009/09/WC500003122.pdf (accessed 4/6/2016).
(50) FDA Product Insert: Indocyanine Green (IC-Green). http://www.accessdata.fda.gov/drugsatfda_docs/label/2006/011525s017lbl.pdf (accessed 4/6/2016).
(51) Sato, T.; Ito, M.; Ishida, M.; Karasawa, Y. Phototoxicity of Indocyanine Green Under Continuous Fluorescent Lamp Illumination and its Prevention by Blocking Red Light on Cultured Müller Cells. *Invest. Ophthalmol. Visual Sci.* **2010**, *51*, 4337−4345.
(52) Cai, J.; Nelson, K. C.; Wu, M.; Sternberg, P., Jr.; Jones, D. P. Oxidative Damage and Protection of the RPE. *Prog. Retinal Eye Res.* **2000**, *19*, 205−221.

8. Study IV: Indocyanine green-loaded liposomes for light-triggered drug release

molecular pharmaceutics

Article

pubs.acs.org/molecularpharmaceutics

Indocyanine Green-Loaded Liposomes for Light-Triggered Drug Release

Tatu Lajunen,[*,†] Leena-Stiina Kontturi,[†,¶] Lauri Viitala,[‡] Moutusi Manna,[§] Oana Cramariuc,[§] Tomasz Róg,[§,∥] Alex Bunker,[†] Timo Laaksonen,[†,⊥] Tapani Viitala,[†] Lasse Murtomäki,[‡] and Arto Urtti[†,#]

[†]Centre for Drug Research, Division of Pharmaceutical Biosciences, University of Helsinki, P.O. Box 56, FI-00014 Helsinki, Finland

[‡]Department of Chemistry, Aalto University, P.O. Box 16100, FI-00076 Aalto, Finland

[§]Department of Physics, Tampere University of Technology, P.O. Box 692, FI-33101 Tampere, Finland

[∥]Department of Physics, University of Helsinki, P.O. Box 64, FI-00014 Helsinki, Finland

[⊥]Department of Chemistry and Bioengineering, Tampere University of Technology, P.O. Box 541, FI-33101 Tampere, Finland

[#]School of Pharmacy, University of Eastern Finland, P.O. Box 1627, FI-70211 Kuopio, Finland

[¶]Department of Pharmaceutics, Utrecht Institute of Pharmaceutical Sciences (UIPS), Utrecht University, Universiteitsweg 99, 3584 CG Utrecht, The Netherlands

Supporting Information

ABSTRACT: Light-triggered drug delivery systems enable site-specific and time-controlled drug release. In previous work, we have achieved this with liposomes containing gold nanoparticles in the aqueous core. Gold nanoparticles absorb near-infrared light and release the energy as heat that increases the permeability of the liposomal bilayer, thus releasing the contents of the liposome. In this work, we replaced the gold nanoparticles with the clinically approved imaging agent indocyanine green (ICG). The ICG liposomes were stable at storage conditions (4−22 °C) and at body temperature, and fast near-infrared (IR) light-triggered drug release was achieved with optimized phospholipid composition and a 1:50 ICG-to-lipid molar ratio. Encapsulated small molecular calcein and FITC-dextran (up to 20 kDa) were completely released from the liposomes after light exposure for 15 s. Location of ICG in the PEG layer of the liposomes was simulated with molecular dynamics. ICG has important benefits as a light-triggering agent in liposomes: fast content release, improved stability, improved possibility of liposomal size control, regulatory approval to use in humans, and the possibility of imaging the in vivo location of the liposomes based on the fluorescence of ICG. Near-infrared light used as a triggering mechanism has good tissue penetration and safety. Thus, ICG liposomes are an attractive option for light-controlled and efficient delivery of small and large drug molecules.

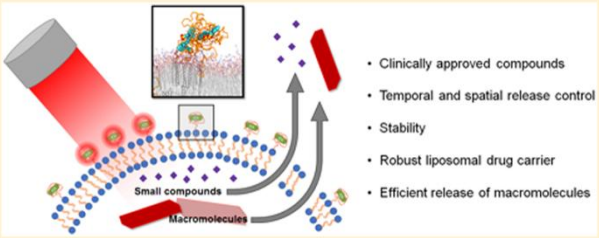

KEYWORDS: *liposome, indocyanine green, light activation, triggered release, macromolecules, molecular dynamics*

1. INTRODUCTION

In principle, nanocarriers offer distinct advantages over traditional drug formulations, including enhanced water solubility, controlled biodistribution, and optimized pharmacokinetics.[1−3] Typical nanocarriers release the drug passively, but the release in the target tissues is often incomplete and poorly controlled. Over the past few years, light-based[4−8] and other stimuli-responsive[9−11] drug release mechanisms have been studied because those approaches may improve drug release in the target site while minimizing off-target drug exposure. The overall goal is to have complete spatial and temporal control of drug release.[12]

Liposomes are nanocarriers that are already in clinical use; they are biocompatible, and their surface and lipid wall properties can be modified in a versatile manner.[13] Previously, light-activated release from liposomes has been achieved using gold nanoparticles as a light-triggering component.[4,5,8,14] Gold nanoparticles convert absorbed light energy to heat, permeabilizing the liposomal membrane and enabling drug release to the surrounding tissue.[4,5,15,16] The maximum absorption wavelength of the gold nanoparticles depends on the size and shape of the particles.[17−19] Small gold nanoparticles absorb light in the ultraviolet range (<400 nm), but such short wavelengths penetrate tissues poorly and may cause DNA damage to the cells.[20−22] Larger gold nanoparticles absorb light in the near IR range (700−900 nm),[8,19] the "phototherapeutic window". These wavelengths are safer to the tissues and show

Received: March 9, 2016
Revised: April 5, 2016
Accepted: April 20, 2016
Published: April 20, 2016

maximal tissue penetration.[20,23] Therefore, the use of near IR light is a promising approach for light-triggered drug delivery and phototherapy.[8,24−27]

Previous light-triggered systems have been suboptimal due to unsatisfactory physical qualities and unknown long-term toxicity of gold nanoparticles.[28−30] First, the required size of the gold nanoparticles (50−80 nm) for optimal near IR light absorption sets limits to the final size of the nanocarrier. Several tissues in the body have relatively small pores through which nanocarriers must pass. For example, the fenestrations in the choroid of the eye have a diameter of 75−85 nm that prevents ocular distribution of typical liposomes with gold nanoparticles (size range of 100−400 nm).[31,32] Second, gold nanoparticles are not biodegradable, they may cause cell death, and their long-term toxicity in various tissues is poorly understood.[29,30] Other inorganic nanoparticles, e.g., carbon, silica, and copper sulfide, have similar problems.[33−35] So far, no drug delivery system based on nonbiodegradable nanoparticles has received regulatory approval for therapeutic use in patients.[36]

Indocyanine green (ICG) is an amphiphilic fluorescent dye that is the only near IR imaging agent for clinical use approved by the European Medicines Agency (EMA) and the U.S. Food and Drug Administration (FDA).[37,38] The ICG molecule is reported to have a low toxicity at therapeutic concentrations.[39−41] It has an absorption maximum at around 780 nm in aqueous solution and slightly greater than 800 nm in the lipid environment.[39,42,43] The fluorescence emission peak of ICG is around 810−830 nm; at this wavelength, fluorescent interference from blood and tissue (500−600 nm) is minimal.[44,45] In addition to being a fluorescent compound, ICG can also convert near IR light into heat.[46−50] ICG degrades rapidly in aqueous solutions due to the oxidation of double bonds; it is highly bound to plasma proteins (98%) and quickly cleared by the liver ($t_{1/2} \approx 2-4$ min).[51,52] Free ICG is not useful in therapy and diagnostics because it is prone to aggregation and shows fluorescence quenching due to protein binding, thermal degradation, and photobleaching.[42,53] The stability of the ICG can be greatly improved by encapsulating it into liposomes or other nanoparticles.[43,54−58] Packing ICG with phospholipids reduces the self-quenching of the dye and increases the fluorescence yield compared to the free compound.[58,59] ICG has traditionally been used as an imaging agent, and lately, it has been of great interest in photothermal destruction of cancer cells.[46,47,49,50] However, the application of ICG as a sensitive drug release system for noncancer target sites has not, as of yet, been explored. In comparison with gold nanoparticle-based light-triggered liposomes, the ICG liposomes are expected to have important advantages, including safety, imaging possibilities, and manufacturing of smaller size controlled liposomes.

In this work, we report light-activated liposomes with ICG as the triggering compound. We optimized liposomal composition and ICG to yield effective light-triggered release of both small and large molecular contents from the ICG liposomes that are otherwise stable. Furthermor, all atom molecular dynamics simulations were used to gain additional insight into the location of ICG in the liposomes.

2. MATERIALS AND METHODS

2.1. Materials. 1,2-Dipalmitoyl-*sn*-glycero-3-phosphocholine (DPPC), 1,2-distearoyl-*sn*-glycero-3-phosphocholine (DSPC), 1-stearoyl-2-hydroxy-*sn*-glycero-3-phosphocholine (Lyso PC), and 1,2-distearoyl-*sn*-glycero-3-phosphoethanolamine-*N*-[methoxy(polyethylene glycol)-2000] (DSPE-PEG) were bought from Avanti Polar Lipids, Inc. (Alabaster, AL, USA). All other compounds were bought from Sigma-Aldrich (St. Louis, MO, USA).

2.2. ICG in Buffer Solution. ICG powder was dissolved in a buffer solution of 20 mM HEPES (Sigma-Aldrich) and 140 mM sodium chloride (pH 7.4, 280 mOsm) at a concentration of 20 μg/mL (25.8 μM) and diluted to concentrations in a range of 0.156−10 μg/mL (0.2−12.9 μM).

2.3. Preparation of Light-Activated ICG Liposomes. The lipids were dissolved in chloroform prior to the liposome preparation. The liposomes were formed by thin film hydration method followed by extrusion through a polycarbonate membrane. Briefly, the lipids in various molar ratios were mixed in a glass tube (10 μmol of total lipids). The tube was placed in a water bath within a larger glass tube and attached to a vacuum rotary evaporation system (Büchi R-114, Büchi Labortechnik AG, Flawil, Switzerland). Chloroform was evaporated by heating the tube to 60 °C and gradually reducing the pressure to 70 mbar under a nitrogen flow. The resulting thin lipid layer was hydrated with 500 μL of the HEPES buffer solution or calcein solution (60 mM, 280 mOsm, pH 7.4), including ICG (0.05−0.4 μmol), by gently stirring the tube in a water bath (60 °C) for 1 h. The sample was then extruded 11 times (60 °C) through polycarbonate membrane (pore sizes of 30, 100, 200, or 400 nm) with a syringe extrusion device (Avanti Polar Lipids) after which the sample was quickly cooled down and stored in a refrigerator. The cooled solution was purified by gel filtration with a Sephadex G-50 (Sigma-Aldrich) column, where the sample was eluted with the HEPES buffer solution. After the purification, the lipid concentration in the samples was 1.5 mM, and the ICG concentration was 7.5−60 μM.

ICG liposomes with FITC-dextran (4, 10, and 20 kDa) were also prepared by thin film hydration and extrusion replacing the calcein with FITC-dextran in the buffer solution (200 mg/mL). The size range of FITC-dextran was chosen to cover a wide range of therapeutic macromolecules. A 400 nm extrusion membrane was used because of the higher viscosity of the samples. Ultracentrifugation was used instead of gel filtration for the purification of free FITC-dextran from the liposome samples. Briefly, the sample was placed into an ultracentrifuge tube with 35 mL of HEPES buffer. The samples were centrifuged in swing buckets for 1 h (100,000*g*, 4 °C, vacuum conditions) with an Optima L-80 XP Ultracentrifuge (Beckman Coulter, Brea, CA, USA). Finally, the supernatant was discarded, and the liposome pellet was suspended and diluted to an appropriate concentration with HEPES buffer.

2.4. Differential Scanning Calorimetry. Differential scanning calorimetry (Mettler Toledo DSC823e, Mettler-Toledo GmbH, Greifensee, Switzerland) was used to determine the phase transition temperatures of the liposomes. Briefly, 20 μL of the liposome sample was pipetted on an aluminum pan and sealed by an aluminum lid with two small holes to prevent pressure buildup. The sample pan was heated in a linear gradient alongside a reference pan in a nitrogen environment. The phase transitions were seen as peaks on the enthalpy graphs (analyzed with STARe software, Mettler Toledo).

2.5. Temperature-Induced Content Release. Content release from the liposomes was studied at temperatures ranging from 35 to 50 °C on a thermomixer with an Eppendorf heating block (Eppendorf AG, Hamburg, Germany). The samples were heated for 10 min while shaking at 300 rpm, and then their

fluorescence was measured. Calcein exists as dimers at high concentrations and is thus a self-quenching fluorescent compound. Therefore, its emission is greatly reduced at high concentrations present in the liposomes. Upon calcein release, dilution takes place and a strong monomeric fluorescence signal is detected. Five microliters of the heated sample was mixed with 250 μL of the HEPES buffer solution on a white Optiplate-96 well plate (PerkinElmer, Waltham, MA, USA), and calcein release measurements were performed in the linear range of monomeric fluorescence relative to concentration plot using a Varioskan Flash plate reader (Thermo Fisher Scientific Inc., Waltham, MA, USA) at excitation and emission wavelengths of 495 and 515 nm, respectively. After measurement of the samples, 10 μL of 10% Triton X-100 was added to dissolve the liposomes for complete calcein release. Similarly, FITC-dextran, a self-quenching fluorescent macromolecule, with three molecular weights was studied. The excitation and emission wavelengths of FITC-dextran were 490 and 520 nm, respectively. Because Triton X-100 was found to reduce the fluorescence of FITC-dextran by more than 20%, complete compound release was achieved by incubating the sample in an 80 °C water bath for 5 min instead of Triton X-100 addition. Fluorescence was measured with the plate reader, and the release percentage (R) was calculated as

$$R = \frac{F - F_0}{F_{100} - F_0} \times 100\%$$

where F is the fluorescence of the sample at a specific measurement point, F_0 is the background fluorescence of the sample, and F_{100} is the fluorescence of complete release of the model drug compound. The content release temperature was determined from the linear part of burst increase of the fluorescence in the release graph.

2.6. Size Analysis of Liposomes. The size of the liposomes was analyzed with a Zetasizer APS dynamic light scattering automated plate sampler (Malvern Instruments, Malvern, United Kingdom) and reported as particle size distributions and polydispersity index (PdI).

2.7. Absorbance and Fluorescence of ICG. Light absorption and fluorescence spectra of the ICG samples were analyzed with a Varioskan Flash plate reader. For absorption spectrum, 300 μL of the sample was put into a black Costar clear bottom 96-well plate (Corning Inc., Corning, NY, USA), and the spectrum was analyzed with a bandwidth of 5 nm. For the fluorescence of free ICG in HEPES buffer, 300 μL of the sample was put into a white Optiplate-96 well plate and excited at 770 nm with a bandwidth of 12 nm, and emission was measured at a peak wavelength of 810 nm. For the fluorescence of liposomal ICG, the sample was analyzed with excitation and emission peak wavelengths of 790 and 815 nm, respectively.

2.8. Stability Studies. Storage stability of formulations with three different lipid compositions with ICG (0.2 μmol) and encapsulated calcein was studied for a duration of one month. The liposomes were stored in HEPES buffer at 4, 22, 37, and 42 °C. The size of the liposomes, calcein release, and ICG fluorescence were measured at time points of up to 4 weeks.

The liposomal size and calcein release were measured as described above. The chemical stability of ICG was measured by scanning the fluorescence of ICG with a Varioskan Flash plate reader. Briefly, 150 μL of undiluted sample was put into an Optiplate-96 (n = 3). The ICG fluorescence scan was performed with an excitation wavelength of 800 nm (bandwidth: 12 nm) and emission wavelengths of 820−840 nm. Because of a possible shift in the peak fluorescence emission wavelength during storage,[42] the maximum value of the fluorescence scan was reported.

2.9. Molecular Dynamics Simulation of the ICG and Lipid Bilayer. Two sets of simulations were performed with different initial location of ICG molecules with respect to the lipid bilayer. In the first set, **Set 1**, eight ICG molecules were placed in the water phase such that there was initially no interaction between the ICG and the lipid membrane. In the second set, **Set 2**, ICG (eight molecules) was initially placed in the gap between two bilayer leaflets. The lipid bilayer used in the study was composed of 22 DSPE-PEG, 78 DSPC, 52 Lyso PC, and 360 DPPC lipid molecules. The bilayer was solvated by 52447 water molecules, and sodium chloride (172 Na and 142 Cl) was added to maintain electroneutrality and physiological salt concentration. First, each system was simulated at 60 °C for 500 ns. Systems were then slowly cooled to 37 °C in 5 consecutive steps (55, 50, 45, 40, and 37 °C), each simulated for 200 ns. The total simulation time of each system thus covered 1.5 μs.

For parameterizing all lipid molecules, ICG, and ions, the all-atom optimized potentials for liquid simulations (OPLS-AA) force field were used.[60] For lipids, additional parameters describing head groups, glycerol backbone, long hydrocarbons, and unsaturated bonds were taken from our previous studies.[61,62] For water, the TIP3P model that is compatible with the OPLS-AA force field was used.[63] Partial atomic charges for ICG were derived in accordance with the OPLS-AA methodology by fitting to the electrostatic potential using the RESP procedure.[64] First, the geometry was optimized at the density functional theory (DFT) level using the Becke B3LYP exchange-correlation function and the 6-31G** basis set within the Gaussian 09 program. SCF convergence proved to be difficult due to the presence of sulfonate groups. For ensuring convergence, shifting of the orbital energies had to be increased to 300 milli-Hartrees. The molecular electrostatic potential was computed for the optimized molecule structure at the same level of theory. The obtained potential was used to calculate the partial atomic charges according to the RESP procedure implemented in ANTECHAMBER.[65] Supporting Information Figure S1A shows the electrostatic potential mapped on the van der Waals surface. An ICG simulation structure file for GROMACS in pdb format is also in the Supporting Information. All simulations were carried out using the GROMACS 4.6.6 software package.[66]

The time step was set to 2 fs, and the productive simulation runs were carried out at 1 bar. The v-rescale method was used to couple the temperature with separate heat baths for the membrane and the rest of the system with a time constant of 0.1 ps.[67] The reference pressure was maintained through the semi-isotropic Parrinello−Rahman barostat.[68] For long-range electrostatic interactions, the particle-mesh Ewald (PME) method was used.[69] The linear constraint solver (LINCS) algorithm was used to preserve covalent bond lengths.[70] Prior to all molecular dynamics simulations, the steepest-descent algorithm was used to minimize the energy of the initial configurations. The last 100 ns trajectory at 37 °C was used for the analysis. Solvent accessible surface area (SASA) calculations were performed using g_{sas} tool and a default probe radius of 0.14 nm. Hydrogen bonding was judged to occur when the acceptor−donor distance was ≤0.325 nm and the angle

between the acceptor−donor vector and the covalent bond donor−hydrogen was ≤35°.[71] Charge pairs were defined based on a distance cutoff of 0.4 nm between negatively charged oxygen and positively charged methyl group.[72] ICG molecule locations in the bilayer were calculated by the number of carbon atoms of sn-1 hydrocarbon chain of DPPC being neighbors of ICG heavy atoms. Neighbors were recognized when two heavy atoms were located at a distance equal to or shorter than 0.6 nm (0.6 nm is the approximate position of the maximum of the radial distribution function of carbon atoms in the membrane core).[73] Calculations were performed separately for each carbon along the sn-1 tail.

2.10. Light-Induced Content Release. The purified liposome sample (500 μL) was placed in a Thermomixer C heating device (Eppendorf AG, Hamburg, Germany) and heated to 37 °C. The light-triggered sample was exposed to 808 nm light for 5 s to 10 min with a laser power of 1 or 3 W (6 or 18 W cm^{-2}, Dragon Lasers, Chang Chun, China). The light source with a circular beam diameter of 4 mm was placed 3 cm above the surface of the 500 μL sample in an open 1.5 mL Eppendorf tube. At the same time, a control sample on the same heating device was shielded from the light exposure. Next, 5 μL of triggered sample, control sample, and background sample (no heating or light exposure) was transferred to 250 μL of HEPES buffer solution (n = 4) on an Optiplate-96 well plate, and the fluorescence (calcein, FITC-dextran) was measured with a Varioskan Flash plate reader as described earlier. The experiment was repeated three times, and the mean release percentage and the standard deviation were calculated.

2.11. Statistical Analysis. Student's t test was used to evaluate the statistical significance between two sample groups. The differences between the results were considered to be significant when the p-values were less than 0.05.

3. RESULTS

3.1. Differential Scanning Calorimetry and Temperature-Induced Content Release. Three different liposome compositions (Table 1) with 30 μM of ICG were prepared, and their transition temperatures were analyzed (Figure 1). Onsets of phase transitions were approximately 41, 42, and 45 °C for formulations A−C, respectively. The half widths of the glass transition peaks also increased slightly with increasing DSPC content in the formulations (Table 1). Because transition temperature does not accurately indicate the actual release temperature, the release was analyzed throughout a broad temperature range. Burst release of calcein from formulations A−C occurred 1−2 degrees below the phase transition at 39, 41, and 44 °C, respectively. Liposomes (composition B) with FITC-dextran (4, 10, and 20 kDa) were analyzed to study the effect of the cargo on the transition temperature and content release. The onset of the phase transition in the liposomes did not change with cargo (42−42.5 °C) (Figure 1). The apexes of phase transition peaks were at 45 °C, as was the case for calcein liposomes with the same lipid composition (Table 1). The release of FITC-dextran took place at 40−41 °C.

Table 1. Liposome Compositions, Differential Scanning Calorimetry Data, and Content Release Temperatures

molar ratio lipid composition (DPPC/DSPC/Lyso PC/DSPE-PEG)	cargo	transition peak apex (°C)	transition peak half width (°C)	content release temperature (°C)
A (90:0:10:4)	calcein	43	1.6	39
B (75:15:10:4)	calcein	45	2.2	41
C (50:40:10:4)	calcein	48	2.8	44
B (75:15:10:4)	FITC-dextran 4 kDa	45	2.0	41
B (75:15:10:4)	FITC-dextran 10 kDa	45	2.0	40
B (75:15:10:4)	FITC-dextran 20 kDa	45	1.8	40

3.2. Stability Studies. The physical and chemical stabilities of formulations A−C were determined over a period of one month (Figure 2). In a refridgerator and at room temperature, the particle sizes of the formulations remained stable for one month. At 37 °C, formulation A (with the highest DPPC content) showed an increase in liposome size at 2 weeks, whereas the other formulations were stable for one month. At 42 °C, formulation C was stable for one month, whereas formulations A and B showed increasing particle size after 2 weeks.

Differences in calcein release were seen between the formulations. At 42 °C, formulations A and B released essentially all calcein in 24 h, whereas formulation C released approximately 20% of the contents over 4 weeks. At 37 °C, formulations A and B leaked approximately 30 and 8% of the calcein in 24 h, whereas the release from formulation C was much slower. None of the formulations showed significant calcein release at 4 or 22 °C over one month.

Chemical integrity of ICG was measured by analyzing the fluorescence from the storage samples. A decrease in ICG fluorescence was seen at 42 °C in all formulations with formulation C having onset after 2 weeks and formulations A and B after 3 days. Formulation A also had a decrease in fluorescence at 37 °C. Only small changes in fluorescence emissions were seen over one month at 4 and 22 °C.

Formulation A was deemed to be too unstable. On the other hand, high transition temperature and minimal calcein leakage at 42 °C from formulation C does not enable efficient photothermal content release. Thus, formulation B was used in further experiments.

3.3. Influence of ICG Concentration. The maximal absorbance of free ICG in aqueous HEPES buffer was seen at around 780 nm (Figure 3A) with a shoulder at 710 nm. The intensity of ICG absorbance was directly proportional to its concentration in the solution. ICG was encapsulated into the liposomes at different ICG/total lipid molar ratios of 1:200, 1:100, 1:50, and 1:25 (0.05−0.4 μmol of ICG). Encapsulation of ICG into liposomes slightly shifted the absorption maximum to longer wavelengths, peaking at approximately 800 nm (shoulder at 730 nm) (Figure 3C and E). Increased concentration of ICG in the liposomes also increased the absorbance.

Increase of free ICG concentration in the solution generally caused an increase in fluorescence, but the self-quenching properties of ICG became evident at high concentrations (Figure 3B). The self-quenching phenomenon was even more evident with ICG in the liposomes (Figure 3D). Increase of the molar ratio of ICG within the liposomes dramatically decreased the fluorescence signal from over 600 units to less than 20 for 1:200 and 1:25 ratio samples, respectively.

ICG did not affect the phase transition temperature of the liposomes (Figure 3F). The onsets of phase transition

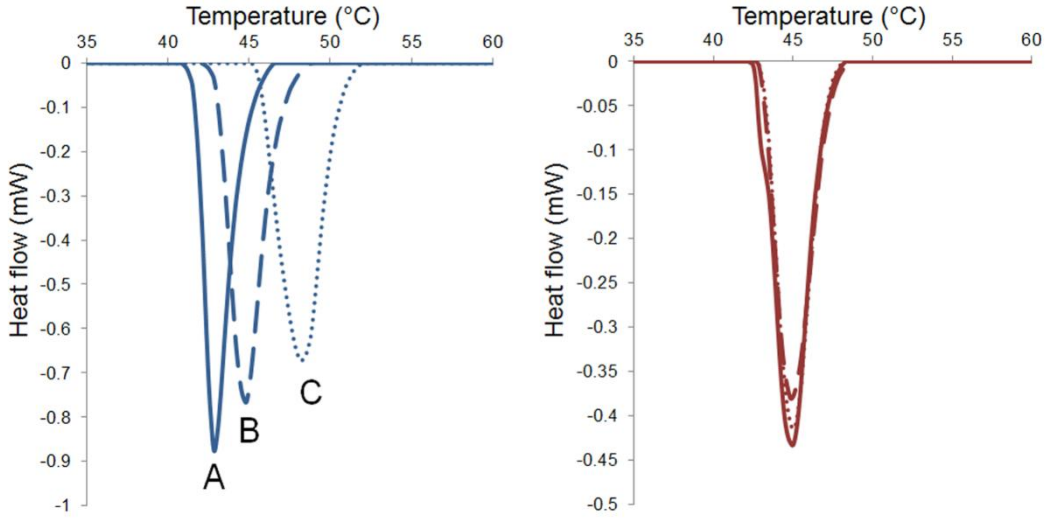

Figure 1. Differential scanning calorimetry measurements with liposome formulations. (Left) Heat flow graphs of formulations A (solid line), B (dashed line), and C (dotted line) with encapsulated calcein. (Right) Heat flow graphs of formulation B with encapsulated FITC-dextran at 4 kDa (solid line), 10 kDa (dashed line), and 20 kDa (dotted line).

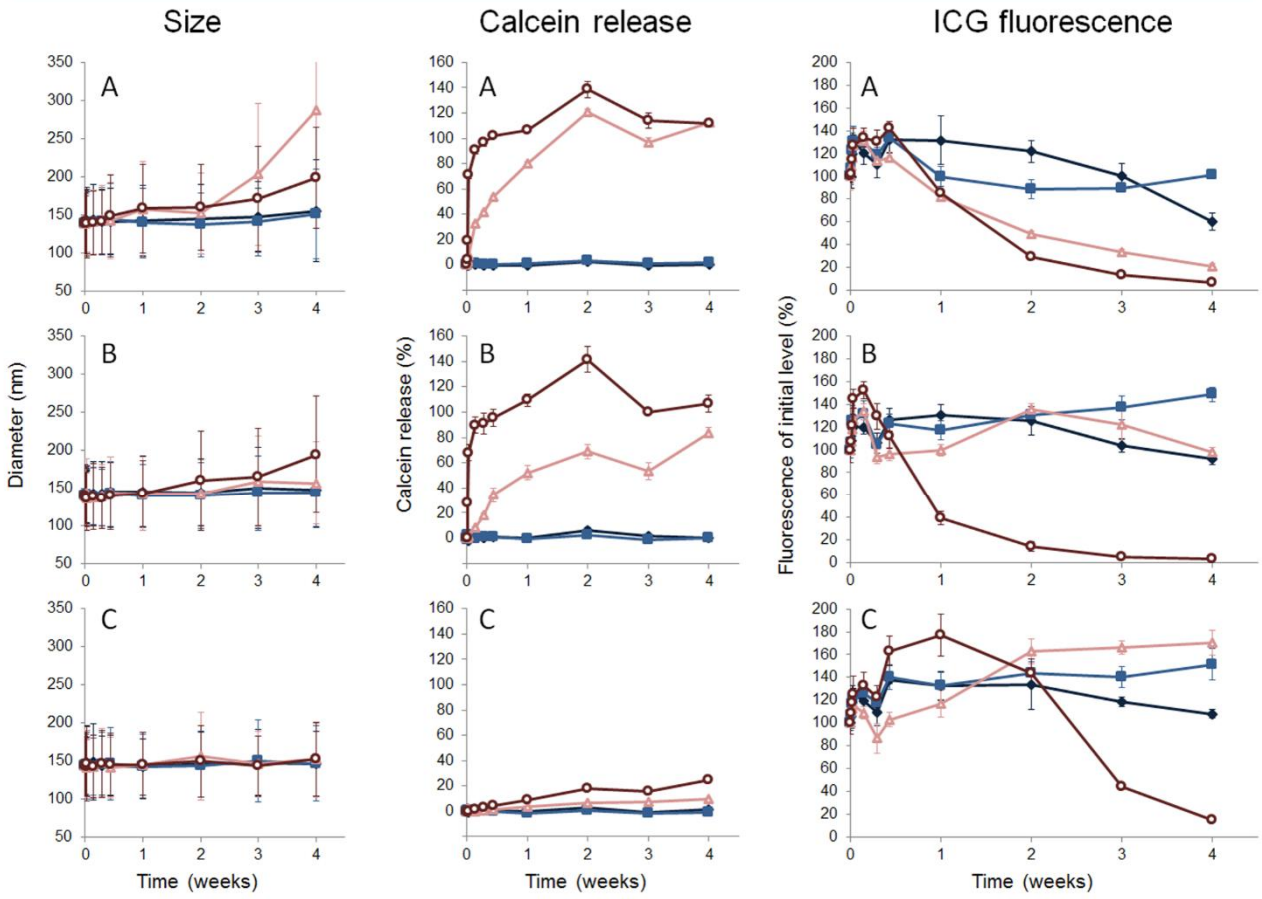

Figure 2. Stability of formulations A (top), B (middle), and C (bottom) during 4 weeks at 4 °C (solid diamonds), 22 °C (solid squares), 37 °C (open triangles), and 42 °C (open circles). Mean size of the liposomes (left), calcein release (center), and stability of ICG (right) were measured. Mean ± standard deviations (n = 3) are shown.

happened at approximately 41 °C with peaks at approximately 45 °C. Similarly, ICG did not have an influence on the final liposome size after extrusion through a membrane with a pore size of 100 nm (Table 2). The resulting liposomes had a mean diameter in the range of 82−103 nm and low polydispersity indexes (PdI) of 0.1 or less indicating a uniform size

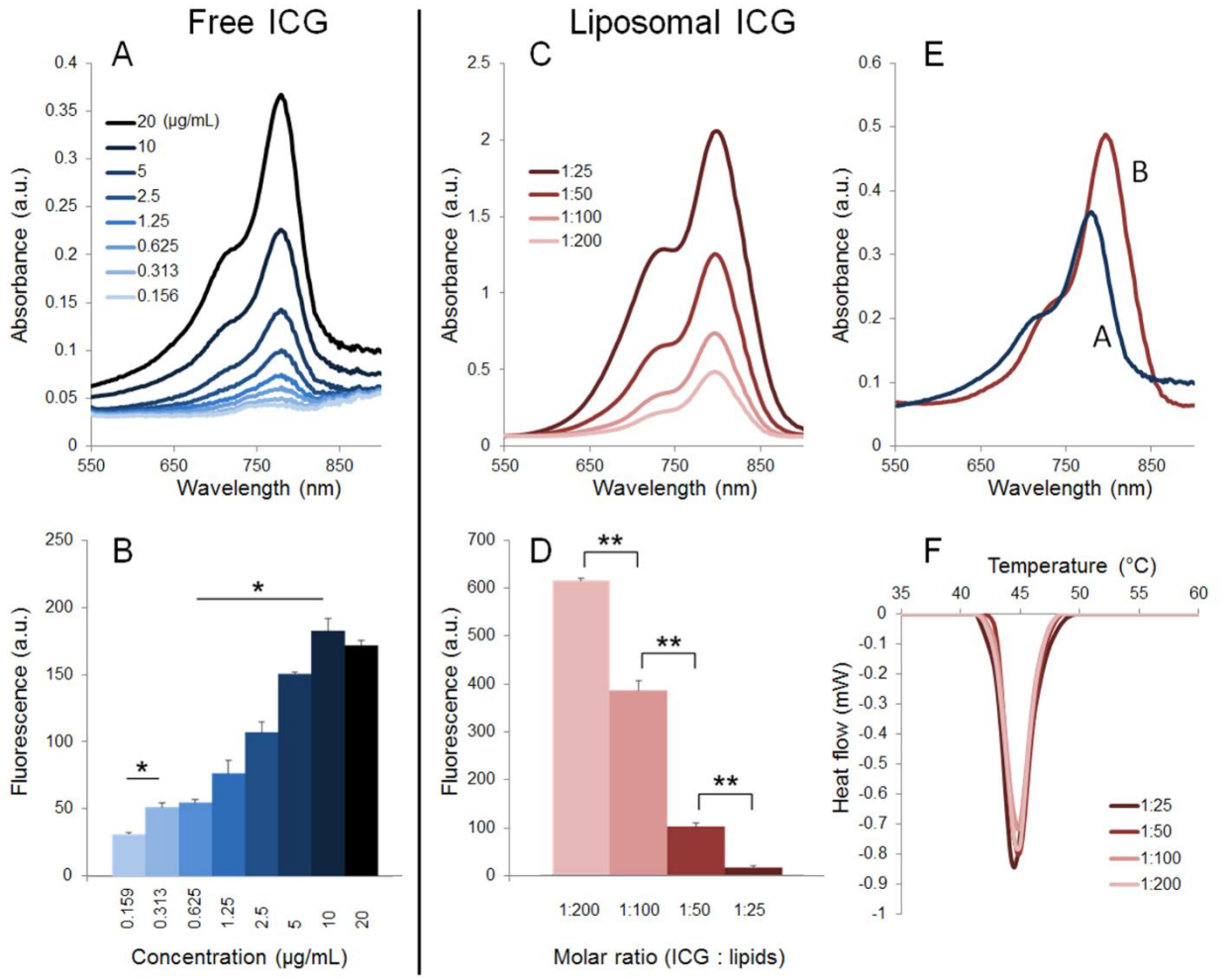

Figure 3. (A) Absorbance spectra of free ICG in buffer solution (n = 4). (B) Fluorescence emission intensities of free ICG in buffer solution (n = 4). (C) Absorbance spectra of ICG liposomes at various ICG/lipid molar ratios (n = 4). (D) Fluorescence emission intensities of ICG liposomes at various ICG/lipid molar ratios (n = 4). (E) Absorbance spectra of free ICG 25.8 μM (A) and liposomal ICG 7.5 μM (B) (n = 4). (F) Differential scanning calorimetry heat flow graphs of ICG liposomes at various ICG/lipid molar ratios. Error bars indicate the standard deviations. Statistical analysis: *p < 0.05 in the concentration range indicated by the horizontal lines and **p < 0.005.

Table 2. Sizes of Liposomes (Formulation B) with Calcein or FITC-Dextran and Various Molar Amounts of ICG[a]

fluorescent compound and extrusion pore size		ICG/lipid molar ratio	liposome mean diameter (nm ± SD)	PdI
calcein (100 nm)		1:25	82 ± 23	0.104
		1:50	98 ± 25	0.061
		1:100	98 ± 23	0.043
		1:200	96 ± 23	0.032
		no ICG	103 ± 24	0.044
calcein (30 nm)		1:50	63 ± 17	0.094
FITC-dextran (400 nm)	4 kDa	1:50	235 ± 118	0.279
	10 kDa	1:50	220 ± 93	0.137
	20 kDa	1:50	254 ± 93	0.094

[a]The molecular weights of FITC-dextrans are indicated in the sample names. SD = standard deviation, PdI = polydispersity index.

distribution. Extrusion of 1:50 ICG-ratio liposomes through a 30 nm pore sized membrane resulted in a liposomal diameter of 63 nm and PdI of 0.094. Because of their higher viscosity, the FITC-dextran samples were extruded through a 400 nm pore sized membrane. The resulting mean liposomal size was thus larger at around 250 nm with higher PdI in the case of 4 kDa FITC-dextrans.

3.4. Molecular Dynamics Simulation of the ICG and Lipid Bilayer. For the case of the bilayer with ICG molecules placed in the water phase (**Set 1**), a fast clustering of the ICG molecules and wrapping of the PEG chains around these clusters was observed. Two stable clusters were formed with 6 and 2 ICG molecules (Figure 4A and B). Stability of the ICG clusters is related to the limited accessibility of hydrophobic ICG surface to the water (Figure 5). The solvent accessible surface area (SASA) calculations indicate that, out of 9.7 ± 0.1 nm^2 of the ICG total area, 8.78 ± 0.08 nm^2 is hydrophobic and 2.87 ± 0.05 nm^2 is hydrophilic. In the simulation, 60% of the hydrophobic area was covered by PEG chains, and 19% was covered by other ICG molecules in cluster. Lipids covered 1%, and the remaining 20% was accessible to water. In the case of the hydrophilic area, 50% was exposed to water, 29% was covered by PEG, 12% by lipids, and 9% by other ICG molecules in the cluster. ICG molecules 3 and 4 did not form

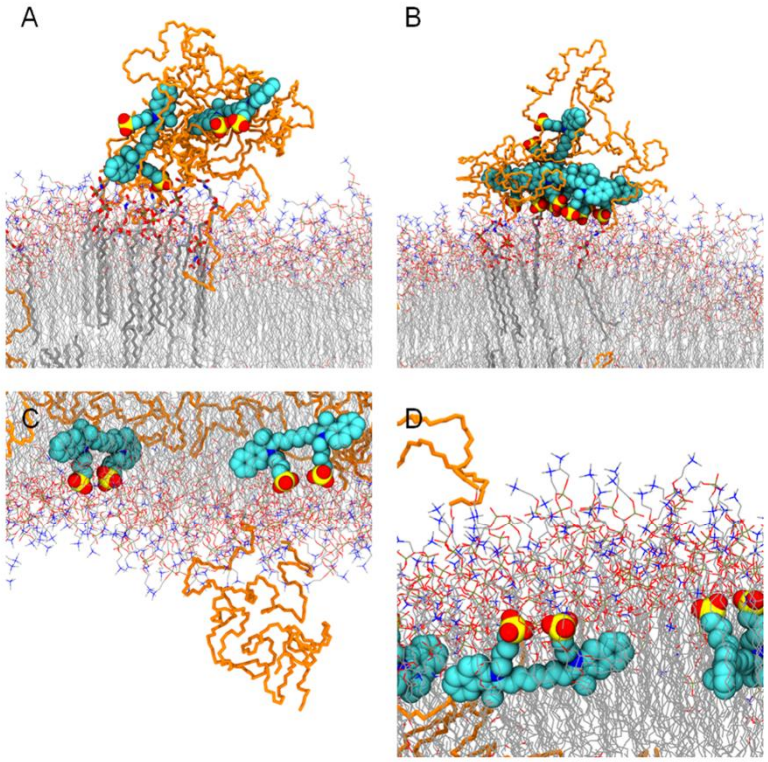

Figure 4. Snapshots of ICG clusters in PEG corona and ICG molecules in the lipid bilayer with PEG shown in orange, lipids as thin sticks, and the ICG molecules as van der Waals spheres for the cases of **Set 1** (A, B) and **Set 2** (C, D).

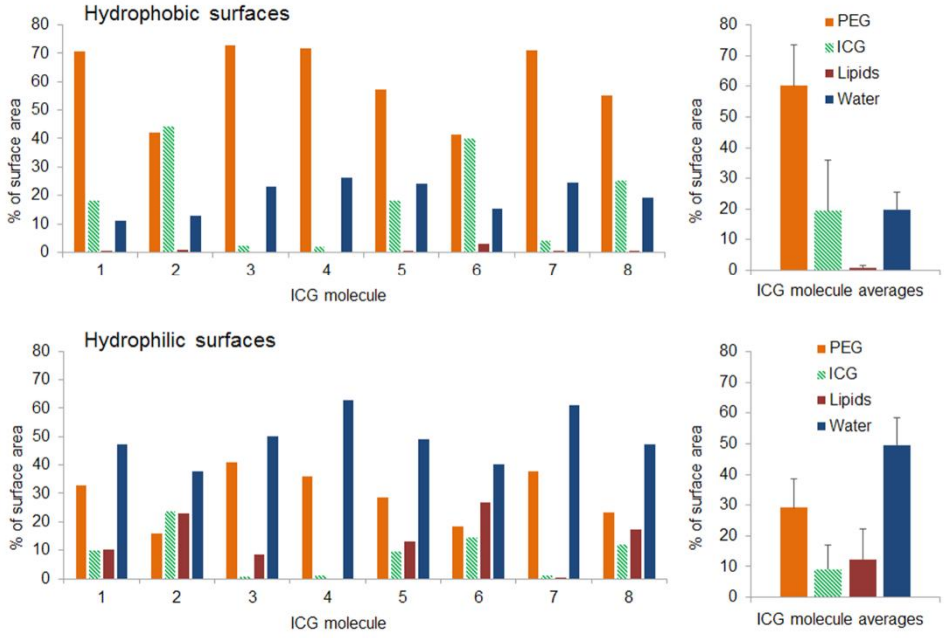

Figure 5. SASA analysis of ICG molecules in **Set 1** indicating the surface area coverage percentages of surrounding molecules with hydrophilic (top) and hydrophobic (bottom) ICG surfaces covered by PEG (orange), other ICG molecules (green), phospholipids (red), and water (blue). On the right, averaged data of individual ICG molecules. Error bars indicate standard deviation (n = 8).

oligomers and had little contact with other ICG molecules (Figures 4A and 5). In this arrangement, the sulfonic group of ICG forms 6.00 ± 0.04 hydrogen bonds with water being well-hydrated. In addition, sulfonic groups formed charge pairs with positively charged choline methyl groups (1.42 per sulfonic group).

After ICG insertion into the bilayer core (**Set 2**), ICG molecules quickly translocated toward the membrane water

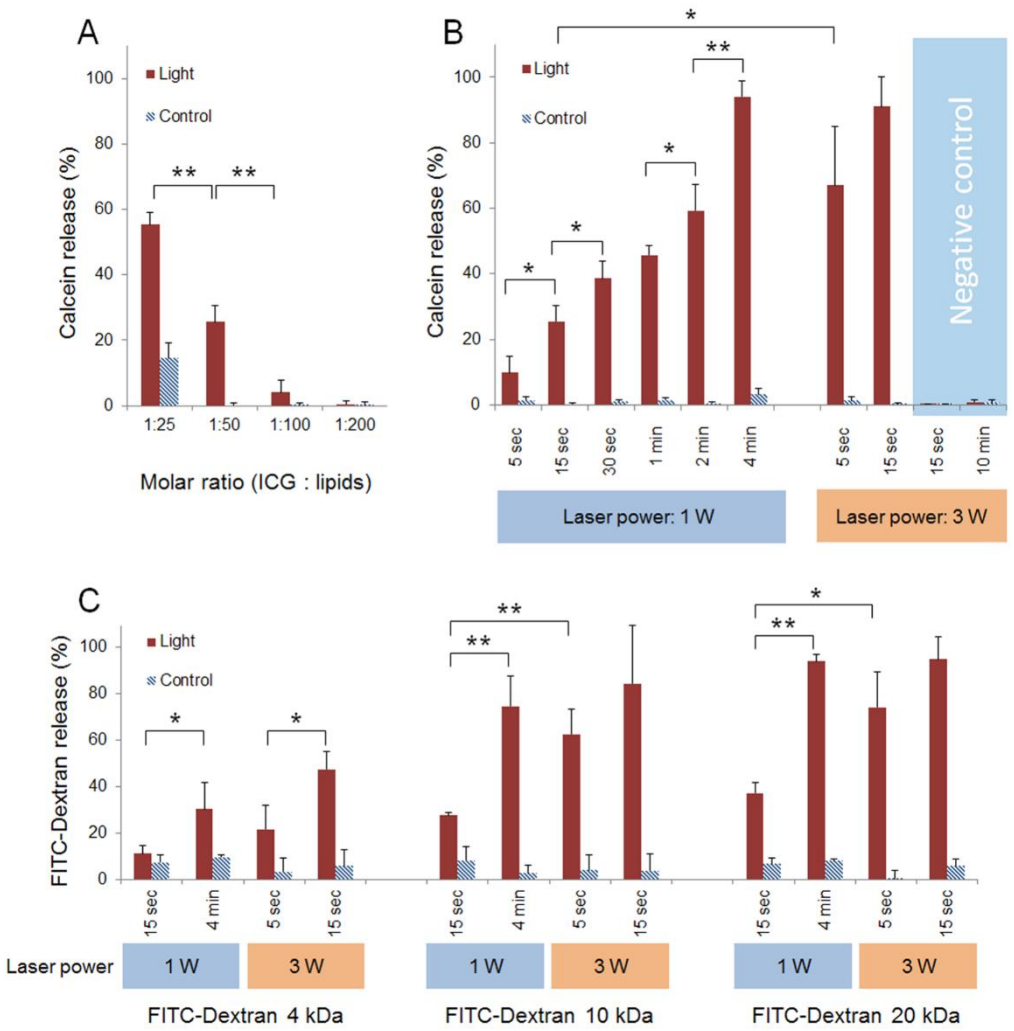

Figure 6. (A) Calcein release from the liposomes with various ICG/lipid molar ratios. The samples were heated to 37 °C, and light-triggered samples were exposed to 808 nm 1 W laser light for 15 s. (B) Calcein release from the liposomes with 1:50 ICG/lipid molar ratio and negative control liposomes without ICG. Exposure times and 808 nm laser powers of light are shown on the horizontal axis. (C) FITC-dextran release from liposomes with 1:50 ICG/lipid molar ratio. Exposure times and 808 nm laser powers of light-triggered samples on the horizontal axis. Error bars indicate the standard deviations (n = 3). Statistical analysis between the light-triggered samples: *p < 0.05 and **p < 0.005.

interface and exposed its sulfonic groups to the water phase, whereas the hydrophobic part of the molecule remained buried among the hydrocarbon chains. In this location, the long axis of the ICG molecule was oriented parallel to the membrane surface (Figure 4C and D). A larger degree of PEG chain insertion into the lipid bilayer was also observed. The profile of the number of contacts along the sn-1 tail of DPPC is shown in the Supporting Information Figure S1B. The obtained profile indicates that the ICG molecules are localized at a depth of 5−9 carbons in the lipid bilayer.

Finally, the polar interactions in which sulfonic groups participate was evaluated. The results showed that each sulfonic group forms 4.94 ± 0.03 hydrogen bonds with water; thus, they are well-hydrated but less than in the system with the ICG cluster wrapped by PEG. Formation of H-bonds with the amide group of DSPE-PEG was not observed, and only a very small number of H-bonds (0.01 per ICG molecule) with the hydroxyl group of Lyso PC was seen. Sulfonic groups forming charge pairs with the choline groups were seen; the number of observed charge pairs was 0.63 ± 0.02 per sulfonic group; 60% of the charge pair is formed with DPPC, 13% with DSPC, and 27% with Lyso PC. This indicates that interactions with Lyso PC are more favorable than with two other lipids, as from the ratios of the concentrations of these three lipids, only 11% of the interactions would be expected to form with Lyso PC. This observation can be explained by larger free volume below the Lyso PC headgroup that covers only 1 hydrocarbon chain.

3.5. Light-Induced Calcein Release. After exposure to 1 W laser light for 15 s, calcein was released from the liposomes, and the release was increased with higher ICG content (Figure 6A). Only the 1:25 (ICG/lipid) formulation showed significant passive leakage of calcein without light induction from the liposomes (Figure 6A). Additionally, the high concentration of ICG reduced the encapsulation efficiency of calcein in the liposomes such that 1:25 of ICG reduced encapsulation to 14% of the levels without ICG. In other ICG liposomes, encapsulation was reduced by 10% or less as compared to

the liposomes without ICG. The 1:50 formulation was chosen for further light-triggered release experiments.

At 1 W laser power, a steady increase in calcein release could be seen with increasing light exposure time (Figure 6B). Nearly complete calcein release (94%) was achieved in 4 min, and approximately half of the calcein (46%) was released in 1 min of light activation. No significant difference ($p > 0.05$) in calcein release during a 15 s exposure was seen between the samples extruded through 100 and 30 nm pore sized membranes (25 ± 5% and 20 ± 6%, respectively). The release of calcein was quite fast initially and slowed at longer light-triggering times. The relationship of calcein release to light exposure time was calculated to be

$$CR = 5.00 \times t^{0.54}$$

where CR is the calcein release percentage, and t is the light exposure time in seconds ($R^2 = 0.96$).

Increasing the laser power to 3 W caused significantly faster calcein release from the liposomes (Figure 6B). Then, 91% of the calcein was released after light exposure of 15 s. Calcein release from the control samples at the same temperature (37 °C) without light activation showed only minimal calcein release (0−2%). Similarly, the negative control liposomes without ICG being exposed released less than 1% of the calcein after laser light exposure (Figure 6B).

3.6. Light-Induced FITC-Dextran Release. Content release from ICG liposomes with FITC-dextrans (4, 10, and 20 kDa) was also analyzed (Figure 6C). All laser irradiated samples, with the exception of the 1 W, 15 s exposure on 4 kDa FITC-dextran liposomes, released more contents than that of the corresponding control samples without laser exposure. The content release was slower with 1 W than with 3 W laser exposure. The release of 4 kDa FITC-dextran was slower than the release of 10 and 20 kDa FITC-dextrans in all experiments. Importantly, 15 s triggering with 3 W laser released 47, 84, and 95% of 4, 10, and 20 kDa FITC-dextrans, respectively.

4. DISCUSSION

Light-triggered ICG liposomes were developed. The liposome formulation was optimized for in vivo applications, and the localization of ICG in lipid bilayers was simulated for the first time. Effective light-triggered release of small and large molecules from the ICG liposomes was proven in extensive light exposure experiments.

The transition temperature and drug permeability in the liposomal wall at 37 °C are critical properties in photothermal drug release because passive drug release at body temperature should be minimized. All test formulations had an onset of phase transition above 37 °C, thereby providing the possibility of selective drug release only after a light-induced rise in liposomal temperature. As expected, the higher DSPC concentrations in the bilayer elevated the phase transition temperatures and release temperatures, but the release temperature was always slightly lower than the phase transition temperature. This is due to the formation of a leaky ripple phase below the transition temperature.[5,74] The width of the half peak in DSC scans reflects the speed and cooperativity of the phase transition; narrow peaks represent a fast and uniform transition from the gel phase to the liquid crystalline phase.[75] In our results, DSPC shifted the phase transition to a higher temperature and slowed the transition speed. Importantly, the cargo (FITC-dextran, calcein) did not affect the liposomal phase transition, making the design of light-activated liposomes easier.

All test formulations were both physically and chemically stable at 4 and 22 °C for up to one month, but at higher temperatures (37 and 42 °C), changes were seen in some cases (Figure 2). Work with formulation A was not continued further because the passive leakage of calcein A was quite extensive at 37 °C (over 30% in 24 h). Formulation C had the highest DSPC content, and it was stable in all tests but also too stable for photothermal content release. Formulation B showed sufficient stability in the therapeutic timeframes from injection to light triggering and efficient photothermal content release.[32,76,77] Therefore, this formulation was chosen for further development.

One of the advantages of ICG-mediated photothermal triggering is the range of the absorbance wavelengths (700−900 nm) that enable deep light penetration to the tissues.[44,45] The absorbance of free and liposomal ICG increased with concentration. Additionally, the liposomal ICG showed a higher absorbance than that of free ICG (Figure 3E). This is in line with a previous report on ICG in liposomal systems.[78] The shift in the peak absorbance of liposomal ICG to longer wavelengths was probably due to conformational changes of ICG based on its interactions with the liposomal components via van der Waals forces. However, this shift is insignificant for the functionality of the light-activated liposomes. Our results show a fluorescence maximum of free ICG at 10 μg/mL (Figure 3B), which is higher than the previously reported concentration of 2 μg/mL.[51] Interactions with other compounds, e.g., HEPES buffer, may reduce dimer formation and self-quenching of ICG.[42] The ICG fluorescence emission was enhanced approximately 4-fold by liposomal encapsulation. This feature and minimal autofluorescence of deoxy- and oxyhemoglobin and lipids at the excitation wavelengths are beneficial for the imaging of ICG-containing liposomes. Self-quenching of the ICG fluorescence at the highest concentrations is not a problem in light-activated drug release because the heat production of ICG is not dependent on the fluorescence emission but rather on the energy conversion related to the absorbance.

ICG has been hypothesized to insert itself into the liposomal bilayer, allowing efficient heat transfer upon light triggering.[58,78] The possible effects of ICG concentration on the bilayer properties needed to be studied. Interestingly, ICG did not significantly affect the transition temperature (onset at 41 °C) or the size (~100 nm) of the liposomes (Figure 3F, Table 2), indicating that ICG did not compromise the integrity of the lipid bilayers. Small molecular ICG is an attractive light sensitizer in liposomes because, unlike large gold nanoparticles, ICG was also compatible with the extrusion protocols even with 30 nm pore membranes.[32,79,80] We manufactured ICG liposomes with a mean diameter of 63 nm using extrusion and even smaller sizes might be possible with high-pressure extrusion or a microfluidizator.[32,81,82] In contrast with a previous report,[58] we did not see ICG-induced aggregation or increased particle size in DLS studies. Most likely, steric stabilization by DSPE-PEG mitigated this problem. Overall, ICG liposomes showed clear benefits compared to the liposomes with gold nanoparticles: small, uniform size, and lack aggregation. In particular, the small size is important in drug delivery because extravasation in many tissues (e.g., tumors, choroid), clearance by the reticuloendothelial system (RES), and endocytosis in many cell types are limited by the

liposome size (typical cutoff values are in the range of 50−200 nm).[83−85]

Interestingly, the molecular dynamics simulations suggest that the location of ICG in the liposomes might be tuned by the preparation method. ICG in the external water solution resulted in the localization of ICG into the PEG sheath (Figure 4A and B). This is understandable because PEG is not completely hydrophilic, as its monomers contain hydrophobic ethylene groups in addition to the polar oxygen atoms. This explains the solubility PEG has in both polar and nonpolar solvents[86] and its interactions with hydrophobic molecules.[87−89] Only a small part of the hydrophobic area of ICG is exposed to the water (Figure 5), thereby stabilizing ICG in the liposomal formulation against water-induced degradation,[51] but thermal degradation of ICG was still present at high temperatures (Figure 2). Importantly, entrapment of ICG among the PEG chains should avoid possible effects of ICG on the lipid bilayer. This hypothesis was supported by the lack of thermoresponsive changes in the liposomes at different ICG concentrations (Figure 3F). The distance from PEG-bound ICG to the lipid bilayer is very short and does not prevent the heat transfer to the lipid bilayer, thus enabling photothermal drug release.[90] On the other hand, the simulations showed clustering of ICG and DSPE-PEG that may lead to self-quenching of ICG fluorescence (Figure 3D).

ICG can also be embedded into the bilayer by dissolving it with the phospholipids into an organic solvent before the thin film hydration step. This was shown in the simulation **Set 2** (Figure 4C and D), where ICG remained within the lipid bilayer and did not get wrapped among the PEG chains. In that case, ICG was localized at a depth of 5−9 DPPC carbon chain atoms from the surface. The simulations indicated a slight preference for ICG interactions with Lyso PC compared to that with the other phospholipids. Within the bilayer, ICG caused a significant change in the structure, including also some penetration of PEG chains into the lipid bilayer. This is expected to alter the phase transition and stability of the liposomal bilayers.

The light activation studies at different ICG concentrations showed that the content release was increased with higher amounts of ICG (Figure 6A), confirming that the light to heat transformation process is unrelated to the fluorescence intensity of ICG that showed self-quenching. Only the highest concentration of ICG (1:25) caused passive content leakage from the liposomes without light exposure, whereas the lower ICG concentrations resulted in minimal passive calcein leakage. At a 1:25 ICG to lipid ratio, the molar amount of ICG is higher than the molar amount of DSPE-PEG. It is possible some ICG was not entrapped by the PEG and might have embedded itself into the lipid bilayer, causing passive leakage of calcein. ICG does degrade upon light exposure, and the heating effect shuts down (data not shown, submitted). This may prevent unnecessary heating of the target tissue. Formulation with lipid composition of DPPC/DSPC/Lyso PC/DSPE-PEG (75:15:10:4 molar ratios) and 1:50 ICG-lipid ratio showed efficient light-triggered calcein release, minimal passive leakage, and a still detectable level of ICG fluorescence that might enable in vivo imaging of the ICG liposomes before light-induced release.

Calcein release can be tuned with the light exposure period because the release was dependent on the length of light exposure. Practically all calcein was released in 4 min with a laser power of 1 W, whereas shorter exposure times, such as 15 s, could be used to release part of the contents (Figure 6B). At 3 W of light energy, faster release was seen with shorter light exposure times, informing that short high power pulses of the triggering light are more efficient than longer exposures at lower power even though the total exposed light energy would be the same. The effect of triggering can be targeted to a smaller area with shorter high power light exposures, and they are also safer for tissues than longer exposures of lower power but equal energy.[23,91] No significant difference was seen in the release profiles of different-sized cargos (calcein, FITC-dextrans of 10 or 20 kDa) (Figure 6B and C). However, slower content release was seen with 4 kDa FITC-dextran, possibly caused by differences in FITC labeling or dextran conformation (small dextrans (<10 kDa) are expandable coils and larger dextrans (≥10 kDa) are highly branched structures).

Fast and efficient light-triggered release of small and macromolecular model drugs was observed. To our knowledge, this is the first report of light-triggered fast release of macromolecules from liposomal DDS and one of the few studies on light-triggered release of macromolecules from any nanocarrier.[92−94] Furthermore, our ICG liposomes showed significantly faster content release than that of previously reported systems (15 s vs several minutes).[93,95] The release of macromolecules is a very important aspect for new biomedicines (proteins, RNA, and DNA) that require nanocarriers for efficient intracellular delivery. Many drug compounds, especially biomedicines, degrade quickly if they are trafficked into lysosomes. Also, the residence time of the DDS may be short in various tissues due to rapid clearance. Generally, interactions with the immunological system are undesired for DDS, but macrophages are important drug delivery targets for the treatment of several diseases. Even though uptake by the RES can be easily achieved with liposomes, suitable pharmacokinetics and tissue site specific drug release may not be satisfactory.[96] The need of timely drug release within the cells is pronounced in macrophages, as their main biological function is to traffic the phagocytosed contents quickly to phagosomes and lysosomes for degradation. In these cases, very rapid light-triggered content release may significantly improve the therapeutic efficacy.

Safety and more versatile manufacturing methods, including ICG localization control in the bilayer, are critical benefits over gold nanoparticle-based light-triggered liposomes. Additionally, because of the dual mode of ICG being a photothermal trigger and fluorescent dye, imaging-guided drug delivery is an attractive possibility. The distribution to the target tissue can be confirmed, and the release-triggering light can be applied at the desired time. The high level of control and good tissue penetration of the triggering light makes ICG liposomes an attractive system for several target tissues and therapeutic conditions, such as eye and skin diseases, gastrointestinal problems, and many cancers.

5. CONCLUSIONS

New light-triggered ICG liposomes have been described. The liposomal composition was carefully optimized to provide strong light-triggered release while minimizing passive leakage and changes during storage. The ICG liposomes show more effective light-induced content release than previous technologies, and they are also applicable for delivery macromolecules. The ICG liposomes can be prepared to a controlled small size; ICG has regulatory approval in clinical imaging, and this technology may allow for the combination of targeted drug

release with imaging of the target site. Overall, ICG liposomes are an interesting option for spatial and temporal control of drug release, and in vivo studies will be indispensable to further evaluate the properties of this technology.

■ ASSOCIATED CONTENT

Supporting Information

The Supporting Information is available free of charge on the ACS Publications website at DOI: 10.1021/acs.molpharmaceut.6b00207.

ICG simulation GROMACS structure file (PDB)

Electrostatic potential mapped at the van der Waals surface of the ICG molecule and a profile of the number of molecule contacts along the sn-1 tail of DPPC in the bilayer (PDF)

■ AUTHOR INFORMATION

Corresponding Author

*E-mail: tatu.lajunen@helsinki.fi.

Notes

The authors declare no competing financial interest.

■ ACKNOWLEDGMENTS

The Academy of Finland is acknowledged for funding via the Programmable Materials Program, project "Light Triggered Nanoparticles" (OMA, 263453). T.L. acknowledges funding from the Academy of Finland Grant 258114. T.V. acknowledges the Academy of Finland for academy research fellow funding (Grants 137053 and 263861). A.B. acknowledges funding from the Academy of Finland (Grant 287963). T.R., M.M., and O.C. acknowledge the Academy of Finland (Center of Excellence program) and the European Research Council (Advanced Grant CROWDED-PRO-LIPIDS) for financial support. We also thank the CSC−IT Centre for Science (Espoo, Finland) for computing resources.

■ REFERENCES

(1) Rawat, M.; Singh, D.; Saraf, S.; Saraf, S. Nanocarriers: promising vehicle for bioactive drugs. *Biol. Pharm. Bull.* **2006**, *29*, 1790−1798.

(2) Peer, D.; Karp, J. M.; Hong, S.; Farokhzad, O. C.; Margalit, R.; Langer, R. Nanocarriers as an emerging platform for cancer therapy. *Nat. Nanotechnol.* **2007**, *2*, 751−760.

(3) Torchilin, V. P. Multifunctional nanocarriers. *Adv. Drug Delivery Rev.* **2012**, *64*, 302−315.

(4) Paasonen, L.; Laaksonen, T.; Johans, C.; Yliperttula, M.; Kontturi, K.; Urtti, A. Gold nanoparticles enable selective light-induced contents release from liposomes. *J. Controlled Release* **2007**, *122*, 86−93.

(5) Paasonen, L.; Sipilä, T.; Subrizi, A.; Laurinmäki, P.; Butcher, S. J.; Rappolt, M.; Yaghmur, A.; Urtti, A.; Yliperttula, M. Gold-embedded photosensitive liposomes for drug delivery: triggering mechanism and intracellular release. *J. Controlled Release* **2010**, *147*, 136−143.

(6) Alvarez-Lorenzo, C.; Bromberg, L.; Concheiro, A. Light-sensitive Intelligent Drug Delivery Systems†. *Photochem. Photobiol.* **2009**, *85*, 848−860.

(7) Fomina, N.; Sankaranarayanan, J.; Almutairi, A. Photochemical mechanisms of light-triggered release from nanocarriers. *Adv. Drug Delivery Rev.* **2012**, *64*, 1005−1020.

(8) Lajunen, T.; Viitala, L.; Kontturi, L.; Laaksonen, T.; Liang, H.; Vuorimaa-Laukkanen, E.; Viitala, T.; Le Guével, X.; Yliperttula, M.; Murtomäki, L. Light induced cytosolic drug delivery from liposomes with gold nanoparticles. *J. Controlled Release* **2015**, *203*, 85−98.

(9) Simões, S.; Moreira, J. N.; Fonseca, C.; Düzgüneş, N. Pedroso de Lima, Maria C On the formulation of pH-sensitive liposomes with long circulation times. *Adv. Drug Delivery Rev.* **2004**, *56*, 947−965.

(10) Schroeder, A.; Kost, J.; Barenholz, Y. Ultrasound, liposomes, and drug delivery: principles for using ultrasound to control the release of drugs from liposomes. *Chem. Phys. Lipids* **2009**, *162*, 1−16.

(11) Timko, B. P.; Dvir, T.; Kohane, D. S. Remotely triggerable drug delivery systems. *Adv. Mater.* **2010**, *22*, 4925−4943.

(12) Mura, S.; Nicolas, J.; Couvreur, P. Stimuli-responsive nanocarriers for drug delivery. *Nat. Mater.* **2013**, *12*, 991−1003.

(13) Torchilin, V. P. Recent advances with liposomes as pharmaceutical carriers. *Nat. Rev. Drug Discovery* **2005**, *4*, 145−160.

(14) Pissuwan, D.; Valenzuela, S. M.; Cortie, M. B. Therapeutic possibilities of plasmonically heated gold nanoparticles. *Trends Biotechnol.* **2006**, *24*, 62−67.

(15) Viitala, L.; Lajunen, T.; Urtti, A.; Viitala, T.; Murtomäki, L. Detection of Phase Transition in Photosensitive Liposomes by Advanced QCM. *J. Phys. Chem. C* **2015**, *119*, 21395.

(16) Harris, N.; Ford, M. J.; Cortie, M. B. Optimization of plasmonic heating by gold nanospheres and nanoshells. *J. Phys. Chem. B* **2006**, *110*, 10701−10707.

(17) Link, S.; El-Sayed, M. A. Size and temperature dependence of the plasmon absorption of colloidal gold nanoparticles. *J. Phys. Chem. B* **1999**, *103*, 4212−4217.

(18) Jain, P. K.; Lee, K. S.; El-Sayed, I. H.; El-Sayed, M. A. Calculated absorption and scattering properties of gold nanoparticles of different size, shape, and composition: applications in biological imaging and biomedicine. *J. Phys. Chem. B* **2006**, *110*, 7238−7248.

(19) Hao, F.; Nehl, C. L.; Hafner, J. H.; Nordlander, P. Plasmon resonances of a gold nanostar. *Nano Lett.* **2007**, *7*, 729−732.

(20) Eichler, J.; Knof, J.; Lenz, H. Measurements on the depth of penetration of light (0.35−1.0 μm) in tissue. *Radiat. Environ. Biophys.* **1977**, *14*, 239−242.

(21) Kielbassa, C.; Roza, L.; Epe, B. Wavelength dependence of oxidative DNA damage induced by UV and visible light. *Carcinogenesis* **1997**, *18*, 811−816.

(22) Kuluncsics, Z.; Perdiz, D.; Brulay, E.; Muel, B.; Sage, E. Wavelength dependence of ultraviolet-induced DNA damage distribution: involvement of direct or indirect mechanisms and possible artefacts. *J. Photochem. Photobiol., B* **1999**, *49*, 71−80.

(23) Delori, F. C.; Webb, R. H.; Sliney, D. H. Maximum permissible exposures for ocular safety (ANSI 2000), with emphasis on ophthalmic devices. *J. Opt. Soc. Am. A* **2007**, *24*, 1250−1265.

(24) Wu, G.; Mikhailovsky, A.; Khant, H. A.; Fu, C.; Chiu, W.; Zasadzinski, J. A. Remotely triggered liposome release by near-infrared light absorption via hollow gold nanoshells. *J. Am. Chem. Soc.* **2008**, *130*, 8175−8177.

(25) Jin, Y.; Gao, X. Spectrally tunable leakage-free gold nanocontainers. *J. Am. Chem. Soc.* **2009**, *131*, 17774−17776.

(26) You, J.; Zhang, G.; Li, C. Exceptionally high payload of doxorubicin in hollow gold nanospheres for near-infrared light-triggered drug release. *ACS Nano* **2010**, *4*, 1033−1041.

(27) Liu, J.; Bu, W.; Pan, L.; Shi, J. NIR-Triggered Anticancer Drug Delivery by Upconverting Nanoparticles with Integrated Azobenzene-Modified Mesoporous Silica. *Angew. Chem., Int. Ed.* **2013**, *52*, 4375−4379.

(28) Goodman, C. M.; McCusker, C. D.; Yilmaz, T.; Rotello, V. M. Toxicity of gold nanoparticles functionalized with cationic and anionic side chains. *Bioconjugate Chem.* **2004**, *15*, 897−900.

(29) Pan, Y.; Neuss, S.; Leifert, A.; Fischler, M.; Wen, F.; Simon, U.; Schmid, G.; Brandau, W.; Jahnen-Dechent, W. Size-dependent cytotoxicity of gold nanoparticles. *Small* **2007**, *3*, 1941−1949.

(30) Albanese, A.; Tang, P. S.; Chan, W. C. The effect of nanoparticle size, shape, and surface chemistry on biological systems. *Annu. Rev. Biomed. Eng.* **2012**, *14*, 1−16.

(31) Guymer, R. H.; Bird, A. C.; Hageman, G. S. Cytoarchitecture of choroidal capillary endothelial cells. *Invest. Ophthalmol. Visual Sci.* **2004**, *45*, 1660−1666.

(32) Lajunen, T.; Hisazumi, K.; Kanazawa, T.; Okada, H.; Seta, Y.; Yliperttula, M.; Urtti, A.; Takashima, Y. Topical drug delivery to retinal pigment epithelium with microfluidizer produced small liposomes. *Eur. J. Pharm. Sci.* **2014**, *62*, 23−32.

(33) Hussain, S.; Hess, K.; Gearhart, J.; Geiss, K.; Schlager, J. In vitro toxicity of nanoparticles in BRL 3A rat liver cells. *Toxicol. In Vitro* **2005**, *19*, 975−983.
(34) Buzea, C.; Pacheco, I. I.; Robbie, K. Nanomaterials and nanoparticles: sources and toxicity. *Biointerphases* **2007**, *2*, MR17−MR71.
(35) Medina, C.; Santos-Martinez, M.; Radomski, A.; Corrigan, O.; Radomski, M. Nanoparticles: pharmacological and toxicological significance. *Br. J. Pharmacol.* **2007**, *150*, 552−558.
(36) Venditto, V. J.; Szoka, F. C. Cancer nanomedicines: so many papers and so few drugs! *Adv. Drug Delivery Rev.* **2013**, *65*, 80−88.
(37) EMA Evaluation of the pharmacokinetics of medicinal products in patients with impaired hepatic function. http://www.ema.europa.eu/docs/en_GB/document_library/Scientific_guideline/2009/09/WC500003122.pdf (accessed 10/1/2015).
(38) FDA Product Insert: Indocyanine Green (IC-Green). http://www.accessdata.fda.gov/drugsatfda_docs/label/2006/011525s017lbl.pdf (accessed 10/1/2015).
(39) Landsman, M. L.; Kwant, G.; Mook, G. A.; Zijlstra, W. G. Light-absorbing properties, stability, and spectral stabilization of indocyanine green. *J. Appl. Physiol.* **1976**, *40*, 575−583.
(40) Speich, R.; Saesseli, B.; Hoffmann, U.; Neftel, K. A.; Reichen, J. Anaphylactoid reactions after indocyanine-green administration. *Ann. Intern. Med.* **1988**, *109*, 345−346.
(41) Alford, R.; Simpson, H. M.; Duberman, J.; Hill, G. C.; Ogawa, M.; Regino, C.; Kobayashi, H.; Choyke, P. L. Toxicity of organic fluorophores used in molecular imaging: literature review. *Mol. Imaging* **2009**, *8*, 341.
(42) Desmettre, T.; Devoisselle, J.; Mordon, S. Fluorescence properties and metabolic features of indocyanine green (ICG) as related to angiography. *Surv. Ophthalmol.* **2000**, *45*, 15−27.
(43) Proulx, S. T.; Luciani, P.; Derzsi, S.; Rinderknecht, M.; Mumprecht, V.; Leroux, J. C.; Detmar, M. Quantitative imaging of lymphatic function with liposomal indocyanine green. *Cancer Res.* **2010**, *70*, 7053−7062.
(44) Ghoroghchian, P. P.; Therien, M. J.; Hammer, D. A. In vivo fluorescence imaging: a personal perspective. *Wiley Interdisciplinary Reviews: Nanomedicine and Nanobiotechnology* **2009**, *1*, 156−167.
(45) Hilderbrand, S. A.; Weissleder, R. Near-infrared fluorescence: application to in vivo molecular imaging. *Curr. Opin. Chem. Biol.* **2010**, *14*, 71−79.
(46) Chen, W. R.; Adams, R. L.; Bartels, K. E.; Nordquist, R. E. Chromophore-enhanced in vivo tumor cell destruction using an 808-nm diode laser. *Cancer Lett.* **1995**, *94*, 125−131.
(47) Chen, W. R.; Zhu, W.; Dynlacht, J. R.; Liu, H.; Nordquist, R. E. Long-term tumor resistance induced by laser photo-immunotherapy. *Int. J. Cancer* **1999**, *81*, 808−812.
(48) Sawa, M.; Awazu, K.; Takahashi, T.; Sakaguchi, H.; Horiike, H.; Ohji, M.; Tano, Y. Application of femtosecond ultrashort pulse laser to photodynamic therapy mediated by indocyanine green. *Br. J. Ophthalmol.* **2004**, *88*, 826−831.
(49) Barth, B. M.; Altinoğlu, I.; Shanmugavelandy, E.; Kaiser, S. S.; Crespo-Gonzalez, J. M.; DiVittore, D.; McGovern, N. A.; Goff, C.; Keasey, T. M.; Adair, N. R.; Targeted, J. H. Targeting indocyanine-green-loaded calcium phosphosilicate nanoparticles for in vivo photodynamic therapy of leukemia. *ACS Nano* **2011**, *5*, 5325−5337.
(50) Ma, Y.; Tong, S.; Bao, G.; Gao, C.; Dai, Z. Indocyanine green loaded SPIO nanoparticles with phospholipid-PEG coating for dual-modal imaging and photothermal therapy. *Biomaterials* **2013**, *34*, 7706−7714.
(51) Saxena, V.; Sadoqi, M.; Shao, J. Degradation kinetics of indocyanine green in aqueous solution. *J. Pharm. Sci.* **2003**, *92*, 2090−2097.
(52) Shimizu, S.; Kamiike, W.; Hatanaka, N.; Yoshida, Y.; Tagawa, K.; Miyata, M.; Matsuda, H. New method for measuring ICG Rmax with a clearance meter. *World J. Surg.* **1995**, *19*, 113−118.
(53) Holzer, W.; Mauerer, M.; Penzkofer, A.; Szeimies, R.; Abels, C.; Landthaler, M.; Bäumler, W. Photostability and thermal stability of indocyanine green. *J. Photochem. Photobiol., B* **1998**, *47*, 155−164.
(54) Kirchherr, A.; Briel, A.; Mäder, K. Stabilization of indocyanine green by encapsulation within micellar systems. *Mol. Pharmaceutics* **2009**, *6*, 480−491.
(55) Yaseen, M. A.; Yu, J.; Jung, B.; Wong, M. S.; Anvari, B. Biodistribution of encapsulated indocyanine green in healthy mice. *Mol. Pharmaceutics* **2009**, *6*, 1321−1332.
(56) Zheng, C.; Zheng, M.; Gong, P.; Jia, D.; Zhang, P.; Shi, B.; Sheng, Z.; Ma, Y.; Cai, L. Indocyanine green-loaded biodegradable tumor targeting nanoprobes for in vitro and in vivo imaging. *Biomaterials* **2012**, *33*, 5603−5609.
(57) Hua, J.; Gross, N.; Schulze, B.; Michaelis, U.; Bohnenkamp, H.; Guenzi, E.; Hansen, L. L.; Martin, G.; Agostini, H. T. In vivo imaging of choroidal angiogenesis using fluorescence-labeled cationic liposomes. *Mol. Vis.* **2012**, *18*, 1045−1054.
(58) Kraft, J. C.; Ho, R. J. Interactions of indocyanine green and lipid in enhancing near-infrared fluorescence properties: the basis for near-infrared imaging in vivo. *Biochemistry* **2014**, *53*, 1275−1283.
(59) Devoisselle, J.; Soulie-Begu, S.; Mordon, S. R.; Desmettre, T.; Maillols, H. In *Fluorescence properties of indocyanin green: I. In-vitro study with micelles and liposomes*; BiOS'97, Part of Photonics West; International Society for Optics and Photonics, 1997; pp 453−460.
(60) Jorgensen, W. L.; Maxwell, D. S.; Tirado-Rives, J. Development and testing of the OPLS all-atom force field on conformational energetics and properties of organic liquids. *J. Am. Chem. Soc.* **1996**, *118*, 11225−11236.
(61) Kulig, W.; Pasenkiewicz-Gierula, M.; Róg, T. Topologies, structures and parameter files for lipid simulations in GROMACS with the OPLS-aa force field: DPPC, POPC, DOPC, PEPC, and cholesterol. *Data in brief* **2015**, *5*, 333−336.
(62) Maciejewski, A.; Pasenkiewicz-Gierula, M.; Cramariuc, O.; Vattulainen, I.; Rog, T. Refined OPLS all-atom force field for saturated phosphatidylcholine bilayers at full hydration. *J. Phys. Chem. B* **2014**, *118*, 4571−4581.
(63) Jorgensen, W. L.; Chandrasekhar, J.; Madura, J. D.; Impey, R. W.; Klein, M. L. Comparison of simple potential functions for simulating liquid water. *J. Chem. Phys.* **1983**, *79*, 926−935.
(64) Bayly, C. I.; Cieplak, P.; Cornell, W.; Kollman, P. A. A well-behaved electrostatic potential based method using charge restraints for deriving atomic charges: the RESP model. *J. Phys. Chem.* **1993**, *97*, 10269−10280.
(65) Wang, J.; Wang, W.; Kollman, P. A.; Case, D. A. Automatic atom type and bond type perception in molecular mechanical calculations. *J. Mol. Graphics Modell.* **2006**, *25*, 247−260.
(66) Hess, B.; Kutzner, C.; Van Der Spoel, D.; Lindahl, E. GROMACS 4: algorithms for highly efficient, load-balanced, and scalable molecular simulation. *J. Chem. Theory Comput.* **2008**, *4*, 435−447.
(67) Bussi, G.; Donadio, D.; Parrinello, M. Canonical sampling through velocity rescaling. *J. Chem. Phys.* **2007**, *126*, 014101.
(68) Parrinello, M.; Rahman, A. Polymorphic transitions in single crystals: A new molecular dynamics method. *J. Appl. Phys.* **1981**, *52*, 7182−7190.
(69) Darden, T.; York, D.; Pedersen, L. Particle mesh Ewald: An N·log (N) method for Ewald sums in large systems. *J. Chem. Phys.* **1993**, *98*, 10089−10092.
(70) Hess, B.; Bekker, H.; Berendsen, H. J.; Fraaije, J. G. LINCS: a linear constraint solver for molecular simulations. *J. Comput. Chem.* **1997**, *18*, 1463−1472.
(71) Murzyn, K.; Zhao, W.; Karttunen, M.; Kurdziel, M.; Róg, T. Dynamics of water at membrane surfaces: Effect of headgroup structure. *Biointerphases* **2006**, *1*, 98−105.
(72) Murzyn, K.; Róg, T.; Jezierski, G.; Takaoka, Y.; Pasenkiewicz-Gierula, M. Effects of phospholipid unsaturation on the membrane/water interface: a molecular simulation study. *Biophys. J.* **2001**, *81*, 170−183.
(73) Róg, T.; Pasenkiewicz-Gierula, M. Cholesterol-phospholipid hydrophobic interactions: A molecular simulation study. *Biophys. Chem.* **2004**, *107*, 151−164.

(74) Rappolt, M.; Rapp, G. Structure of the stable and metastable ripple phase of dipalmitoylphosphatidylcholine. *Eur. Biophys. J.* **1996**, *24*, 381−386.
(75) El Maghraby, G.; Williams, A. C.; Barry, B. Interactions of surfactants (edge activators) and skin penetration enhancers with liposomes. *Int. J. Pharm.* **2004**, *276*, 143−161.
(76) Bekersky, I.; Fielding, R. M.; Dressler, D. E.; Lee, J. W.; Buell, D. N.; Walsh, T. J. Pharmacokinetics, excretion, and mass balance of liposomal amphotericin B (AmBisome) and amphotericin B deoxycholate in humans. *Antimicrob. Agents Chemother.* **2002**, *46*, 828−833.
(77) Gupta, S.; Velpandian, T.; Dhingra, N.; Jaiswal, J. Intravitreal pharmacokinetics of plain and liposome-entrapped fluconazole in rabbit eyes. *J. Ocul. Pharmacol. Ther.* **2000**, *16*, 511−518.
(78) Zheng, X.; Zhou, F.; Wu, B.; Chen, W. R.; Xing, D. Enhanced tumor treatment using biofunctional indocyanine green-containing nanostructure by intratumoral or intravenous injection. *Mol. Pharmaceutics* **2012**, *9*, 514−522.
(79) Mui, B.; Chow, L.; Hope, M. J. Extrusion technique to generate liposomes of defined size. *Methods Enzymol.* **2003**, *367*, 3−14.
(80) Jahn, A.; Vreeland, W. N.; DeVoe, D. L.; Locascio, L. E.; Gaitan, M. Microfluidic directed formation of liposomes of controlled size. *Langmuir* **2007**, *23*, 6289−6293.
(81) Berger, N.; Sachse, A.; Bender, J.; Schubert, R.; Brandl, M. Filter extrusion of liposomes using different devices: comparison of liposome size, encapsulation efficiency, and process characteristics. *Int. J. Pharm.* **2001**, *223*, 55−68.
(82) Pupo, E.; Padrón, A.; Santana, E.; Sotolongo, J.; Quintana, D.; Dueñas, S.; Duarte, C.; Maria, C.; Hardy, E. Preparation of plasmid DNA-containing liposomes using a high-pressure homogenization−extrusion technique. *J. Controlled Release* **2005**, *104*, 379−396.
(83) Gabizon, A. A. Liposome circulation time and tumor targeting: implications for cancer chemotherapy. *Adv. Drug Delivery Rev.* **1995**, *16*, 285−294.
(84) Ishida, O.; Maruyama, K.; Sasaki, K.; Iwatsuru, M. Size-dependent extravasation and interstitial localization of polyethyleneglycol liposomes in solid tumor-bearing mice. *Int. J. Pharm.* **1999**, *190*, 49−56.
(85) Awasthi, V.; Garcia, D.; Goins, B.; Phillips, W. Circulation and biodistribution profiles of long-circulating PEG-liposomes of various sizes in rabbits. *Int. J. Pharm.* **2003**, *253*, 121−132.
(86) Dinç, C. Ö; Kibarer, G.; Güner, A. Solubility profiles of poly (ethylene glycol)/solvent systems. II. Comparison of thermodynamic parameters from viscosity measurements. *J. Appl. Polym. Sci.* **2010**, *117*, 1100−1119.
(87) Lehtinen, J.; Magarkar, A.; Stepniewski, M.; Hakola, S.; Bergman, M.; Róg, T.; Yliperttula, M.; Urtti, A.; Bunker, A. Analysis of cause of failure of new targeting peptide in PEGylated liposome: molecular modeling as rational design tool for nanomedicine. *Eur. J. Pharm. Sci.* **2012**, *46*, 121−130.
(88) Li, Y.; Rissanen, S.; Stepniewski, M.; Cramariuc, O.; Róg, T.; Mirza, S.; Xhaard, H.; Wytrwal, M.; Kepczynski, M.; Bunker, A. Study of interaction between PEG carrier and three relevant drug molecules: piroxicam, Paclitaxel, and hematoporphyrin. *J. Phys. Chem. B* **2012**, *116*, 7334−7341.
(89) Stepniewski, M.; Pasenkiewicz-Gierula, M.; Róg, T.; Danne, R.; Orlowski, A.; Karttunen, M.; Urtti, A.; Yliperttula, M.; Vuorimaa, E.; Bunker, A. Study of PEGylated lipid layers as a model for PEGylated liposome surfaces: molecular dynamics simulation and langmuir monolayer studies. *Langmuir* **2011**, *27*, 7788−7798.
(90) Potdar, D.; Sammalkorpi, M. Asymmetric heat transfer from nanoparticles in lipid bilayers. *Chem. Phys.* **2015**, *463*, 22.
(91) Jacques, S. L. Role of tissue optics and pulse duration on tissue effects during high-power laser irradiation. *Appl. Opt.* **1993**, *32*, 2447−2454.
(92) Yavuz, M. S.; Cheng, Y.; Chen, J.; Cobley, C. M.; Zhang, Q.; Rycenga, M.; Xie, J.; Kim, C.; Song, K. H.; Schwartz, A. G. Gold nanocages covered by smart polymers for controlled release with near-infrared light. *Nat. Mater.* **2009**, *8*, 935−939.
(93) Yan, B.; Boyer, J.; Habault, D.; Branda, N. R.; Zhao, Y. Near infrared light triggered release of biomacromolecules from hydrogels loaded with upconversion nanoparticles. *J. Am. Chem. Soc.* **2012**, *134*, 16558−16561.
(94) Carregal-Romero, S.; Ochs, M.; Rivera-Gil, P.; Ganas, C.; Pavlov, A. M.; Sukhorukov, G. B.; Parak, W. J. NIR-light triggered delivery of macromolecules into the cytosol. *J. Controlled Release* **2012**, *159*, 120−127.
(95) Guha, S.; Shaw, S. K.; Spence, G. T.; Roland, F. M.; Smith, B. D. Clean Photothermal Heating and Controlled Release from Near-Infrared Dye Doped Nanoparticles without Oxygen Photosensitization. *Langmuir* **2015**, *31*, 7826−7834.
(96) Pei, Y.; Yeo, Y. Drug delivery to macrophages: Challenges and opportunities. *J. Controlled Release* **2015**, DOI: 10.1016/j.jconrel.2015.12.014.

9. Additional unpublished results

9.1. Toxicity of near-IR laser and ICG-liposomes on ARPE-19 cell line

The safety of any DDS should be verified in toxicological studies. As a preliminary safety experiment, the effects of NIR light exposure and the ICG-liposomes (study IV) on the viability of the retinal pigment epithelium cell line (ARPE-19) was determined. A light source from Modulight (Tampere, Finland) was used at a light power that released the liposome contents efficiently (9.7 W / cm^2). The cells were exposed to the light on heated (37 °C) 24 well plates for different irradiation times. In another test, the cells were incubated with different concentrations of ICG-liposomes in the growth medium for 24 hours (37 °C). In the third experiment, the cells were incubated with ICG-liposomes (0.3 mM) for 3 hours and then exposed to triggering light for 5 minutes. The control cells were incubated on the same well plates without ICG-liposomes or shielded from the triggering light. The condition of the cells was assessed using two fluorescence assays: Alamar Blue test and Annexin V apoptosis assay. The former evaluates the aerobic respiration of the cells and the latter test determines the stages of programmed cell death with Annexin V-FITC binding at early apoptosis and propidium iodide binding to the necrotic cells.

The triggering light did not show any toxic effects in the cells up to 20 minutes of irradiation at 37 °C (Figure 9A and 9B). The Alamar Blue viability remained unchanged compared to the control. Likewise, the Annexin V experiment did not indicate onset of apoptosis. The negative control cells with 10 minute incubation in 35% EtOH on the other hand showed clear apoptosis. Different concentrations of the ICG-liposomes as well as light activated ICG-liposomes did not reduce the viability of the ARPE-19 cells (Figure 9C, 9D and 9E).

As a conclusion, the DDS and the triggering method appear to be safe for the retinal pigment epithelium cell line. Further cell studies and eventual *in vivo* experiments are needed to determine the toxicity of this method in other tissues.

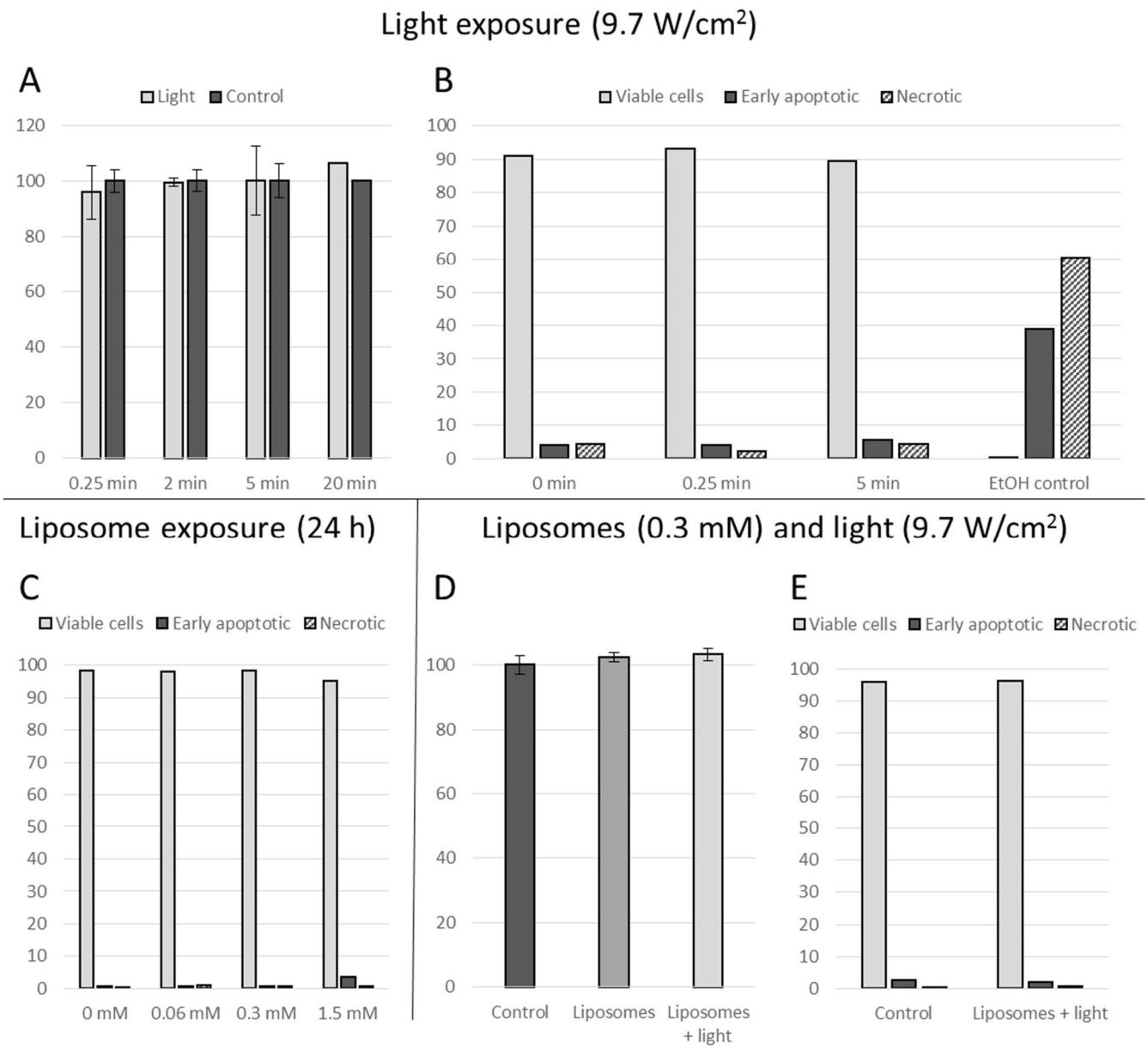

Figure 9. Toxicological measurements with ARPE-19 cells. The viability (% of the control cells) of ARPE-19 cells measured with Alamar Blue after light exposure (A), and liposomes and light exposure (D). Apoptosis of the cells (cell number %) measured with Annexin V kit after light exposure (B), liposome exposure (C) and liposomes with light exposure (E). The error bar represent standard deviations (n = 3).

9.2. Uptake of ICG-liposomes and calcein release upon light activation in ARPE-19 cells

Uptake of ICG-liposomes into ARPE-19 cells was analyzed by measuring encapsulated fluorescent calcein using flow cytometry. The cells were incubated with 1.5 mM of ICG-liposomes for 3 hours and then exposed to the triggering light (9.7 W / cm^2) for 2 minutes at 37 °C. Samples without light exposure and control samples without ICG-liposomes were also prepared.

The ICG-liposomes were efficiently taken up by ARPE-19 cells with almost 100% of the cells internalizing the DDS (Figure 10 left panel). Calcein is a self-quenching molecule that shows reduced fluorescence at high concentrations within the liposomes, but the signal is increased when it is released and diluted to a larger water volume. The calcein fluorescence inside the cells was significantly higher when the cells were exposed to the triggering light indicating that calcein is released from the liposomes (Figure 10 right panel).

Retinal pigment epithelial line (ARPE-19) efficiently internalized the ICG-liposomes and NIR light exposure to the cells caused rapid contents release within the cells. This preliminary study gave promising results on the applicability of ICG-liposomes for intracellular drug delivery.

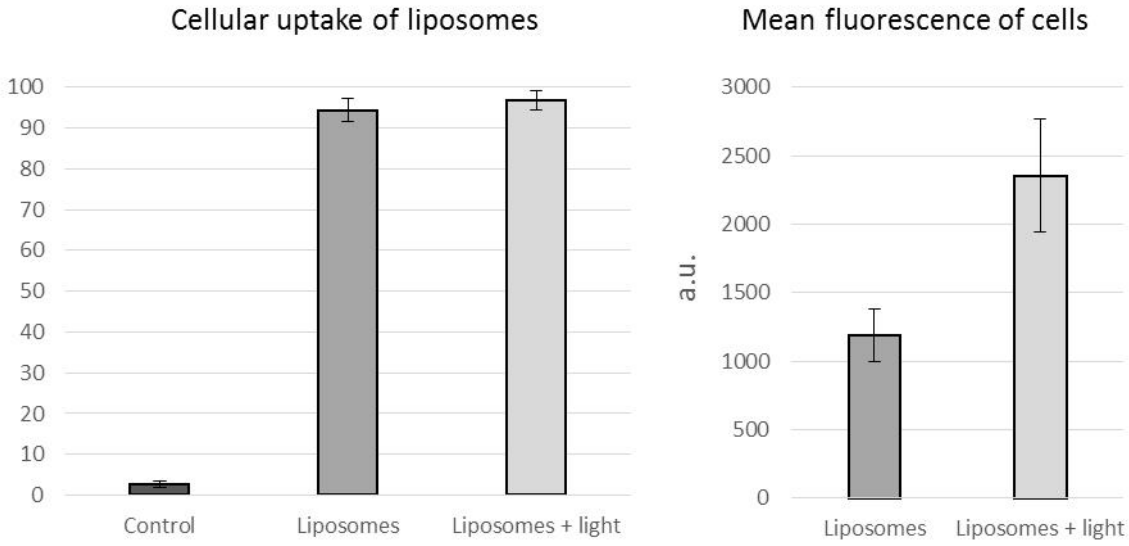

Figure 10. Left panel: Cellular uptake of liposomes (% of cell that have internalized liposomes) measured with flow cytometry. Right panel: Mean fluorescence intensity of the cells. a.u. = arbitrary units. The error bar represent standard deviations (n = 3).

9.3. Production and characterization of small sized ICG-liposomes

In this study, our goal was to produce as small ICG-liposomes as possible with the equipment available in our laboratory. The phospholipid composition was kept unchanged, but additional steps were included to control the liposome size after the thin film hydration. Briefly, the hydrated liposome sample was ultrasonicated in a heated bath sonicator (65 °C) for 15 minutes. After that, the sample was extruded first through a 100 nm pore sized membrane and then through a 30 nm pore sized membrane (11 times). With this process, ICG-liposomes with a diameter around 40 nm were produced (Figure 11A).

Calcein release upon light triggering from the small ICG-liposomes was slightly slower than from the normal ICG-liposomes that released nearly all calcein in 15 seconds. The small ICG-liposomes released around 50% of calcein in 15 seconds and almost complete cargo release was reached in 1-2 minutes (Figure 11B). The phase transition temperatures of the lipid bilayers of two liposome formulations with different sizes were compared. Differential scanning calorimetry results showed that the small ICG-liposomes have higher onset temperature (43.5 °C) for phase transition than the normal sized ICG-liposomes (42 °C) (Figure 11C). The increased curvature of the bilayer may cause different ordering of the phospholipids in the bilayer thus affecting the phase transition (Parthasarathy, et al. 2006). Hence, a more detailed optimization of the phospholipid composition is needed to improve the contents release from the small sized ICG-liposomes.

The small ICG-liposomes were physically stable up to one month at the temperature range 4 – 37 °C (Figure 11D). The stability at the body temperature is due to the higher transition temperature compared to the normal sized ICG-liposomes. The stability of the small ICG-liposomes with modified phospholipid composition for optimal light activation remains to be studied.

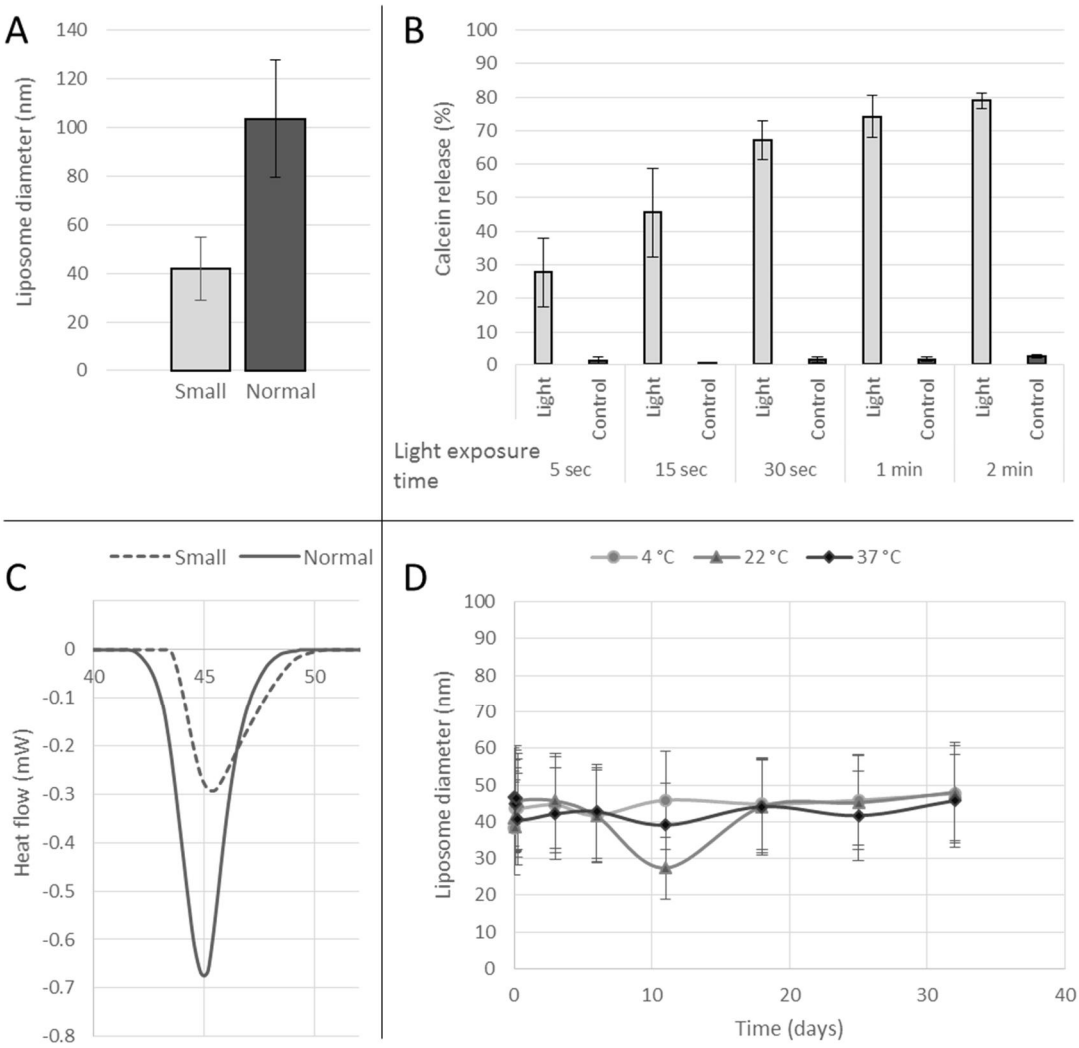

Figure 11. The diameter of small and normal sized ICG-liposomes (A). Contents release from small ICG-liposomes at 37 °C with light exposure times ranging from 5 seconds to 2 minutes (B) (n = 3). Differential scanning calorimetry at temperatures 40 – 55 °C (horizontal axis) of small and normal sized ICG-liposomes (C). Size stability of small ICG-liposomes in various storage temperatures (D). The error bar represent standard deviations.

10. Synopsis of the main results

The main results of the publications and unpublished results are summarized in table 4.

Table 4. Summary of the main results in the publications I-IV and unpublished results.

SMALL MICROFLUIDIZER PRODUCED LIPOSOMES FOR TOPICAL DELIVERY TO RPE (PUBLICATION I)	
PROCESS PARAMETERS FOR SMALL LIPOSOMAL SIZE	Liposomes with 50 nm in diameter were produced by 15 passages through the microfluidizer at 20,000 psi.
ENHANCED DNA ENCAPSULATION	About 80% of DNA was encapsulated in DMPC / DMTAP liposomes of 60 nm in size with double emulsion microfluidizer method.
***IN VIVO* LIPOSOME DISTRIBUTION TO THE RPE**	70 nm transferrin conjugated liposomes distributed to rat RPE after topical instillation. 100 nm transferrin conjugated liposomes distributed to the choroid.
THE MICROFLUIDIZER OFFERS AN ATTRACTIVE OPTION FOR THE SIZE CONTROL OF LIPOSOMES. SMALL LIPOSOMES WITH ACTIVE TARGETING MAY BE A SUITABLE DRUG DELIVERY METHOD FOR THE TREATMENT OF RPE USING TOPICAL APPLICATION.	

LIGHT TRIGGERED GOLD NANOPARTICLE ENCAPSULATING LIPOSOMES (PUBLICATION II)	
TRIGGERED RELEASE	Liposomal contents were released after light triggering of the gold nanoparticle containing liposomes. The release profiles depend on the temperature, pH and NIR light activation. Synergistic release effect of low pH and NIR light activation was demonstrated with pH- and thermosensitive liposomes with gold nanoparticles.
CELLULAR DRUG RELEASE	The optimized formulations released their calcein contents into the cytosol of ARPE-19 and HUVEC cell lines upon light activation. Endosomal escape was not seen in control samples without light triggering.
TOXICOLOGY	Liposome formulations and the light exposure did not affect ARPE-19 and HUVEC cell viability.
THE CONTENT RELEASE FROM THE LIPOSOMES WAS HIGHLY DEPENDENT ON TEMPERATURE, PH AND LIGHT ACTIVATION AT NEAR INFRARED REGION. THE TRIGGERED RELEASE WAS IMPROVED COMPARED TO PREVIOUS FORMULATIONS. THIS TECHNOLOGY MAY BE AN ATTRACTIVE OPTION FOR THE TREATMENT OF PATHOLOGICAL CONDITIONS THAT BENEFIT FROM SPECIFIC CONTROL OF LOCATION AND TIMING OF THE DRUG RELEASE.	

LIGHT-TO-HEAT ENERGY CONVERSION OF GOLD NANOPARTICLES AND INDOCYANINE GREEN IN LIPOSOMES (PUBLICATION III)	
HEAT PRODUCTION UPON LIGHT ACTIVATION	Both thermoprobes, laurdan and CdSe QDs, showed an increase in temperature when gold nanoparticles or ICG were illuminated with NIR light.
LIPID PHASE TRANSITION CAUSED BY LIGHT ACTIVATION	Light triggering of gold nanoparticles or ICG caused a bilayer phase transition to more fluidic form in the liposomes, as indicated by a change in the laurdan polarization.
LIPOSOMAL CONTENTS RELEASE	A fluorescent model compound, calcein, was efficiently released upon light triggering of either gold nanoparticles or ICG. Slightly increased contents release was seen with ICG compared to gold nanoparticles.
CONTENTS RELEASE FROM THE LIPOSOMES IS CAUSED BY THE PHASE TRANSITION IN THE BILAYER UPON HEATING VIA THE PHOTOTRIGGERING AGENTS, GOLD NANOPARTICLES OR ICG. THE RESULTS SHOW THE IMPORTANCE OF FINE TUNING THE BILAYER PHASE TRANSITION AND CHOICE OF TRIGGERING MATERIALS FOR OPTIMAL DRUG RELEASE.	

OPTIMIZED ICG-LIPOSOME FORMULATION FOR NIR LIGHT TRIGGERED DRUG RELEASE (PUBLICATION IV)	
PHOSPOLIPID COMPOSITION OPTIMIZATION	Liposomes consisting of DPPC / DSPC / Lyso PC / DSPE-PEG (molar ratios of 75 : 15 : 10 : 4) had suitable T_m for contents release (slightly above 37 °C) and good stability during storage and body temperatures (4 – 37 °C).
EFFECT OF ICG CONCENTRATION	ICG concentrations (at molar ratio of 1:200 – 1:25 relative to the lipids) did not affect the liposome size. Passive leakage of calcein was observed with 1:25 molar ratio, while other formulations were stable without light induction.
MOLECULAR DYNAMICS	ICG is stabilized and protected from aqueous degradation by the PEG when ICG is mixed into the hydrolyzing solution. Conversely, ICG is located within the lipid bilayer when it is mixed with the phospholipids.
LIPOSOMAL CONTENTS RELEASE	Small molecular calcein and FITC-dextran macromolecules were almost completely released from the liposomes in 15 seconds of NIR light illumination. Significant release of both model compounds was seen with light activation periods as short as 5 seconds.
THE ICG-LIPOSOMES CAN BE PREPARED WITH A CONTROLLED SMALL SIZE. EFFICIENT NIR LIGHT TRIGGERED CONTENTS RELEASE WAS ACHIEVED USING MATERIALS WITH REGULATORY APPROVAL. OVERALL, ICG-LIPOSOMES ARE AN INTERESTING OPTION FOR SPATIAL AND TEMPORAL CONTROL OF DRUG RELEASE.	

CELL STUDIES WITH ICG-LIPOSOMES AND SMALL SIZED ICG-LIPOSOME CHARACTERIZATION (UNPUBLISHED RESULTS)	
TOXICOLOGY	ICG-liposomes and the triggering NIR light did not reduce the viability and did not cause apoptosis of ARPE-19 cells.
LIPOSOME UPTAKE AND CONTENTS RELEASE IN CELLS	ICG-liposomes were efficiently taken up into the cells (over 90% of cells internalized liposomes). Light triggering caused contents release within the cells that was detected based on the increase in fluorescence.
CHARACTERIZATION OF 40 NM SIZED ICG-LIPOSOMES	Combination of ultrasonication and extrusion through 100 nm and 30 nm polycarbonate membranes produced ICG-liposomes with a diameter of 40 nm. These liposomes were physically stable at least for 1 month. Calcein release upon light triggering was slower in 40 nm liposomes than in the 100 nm ICG-liposomes. The lipid phase transition of 40 nm sized liposomes was at higher temperature compared to 100 nm ICG-liposomes.
ICG-LIPOSOMES AND TRIGGERING LIGHT WERE FOUND TO BE SAFE FOR ARPE-19 CELL LINE AND INTRACELLULAR CONTENTS RELEASE WAS OBSERVED UPON LIGHT ILLUMINATION. ICG-LIPOSOMES CAN BE PREPARED AT VERY SMALL SIZE WHILE RETAINING THEIR FUNCTIONALITY. THIS IS IMPORTANT FOR DRUG DELIVERY TO MANY TISSUES. SIZE REDUCTION AFFECTS THE LIPID PHASE TRANSITION, SO OPTIMIZATION OF LIPID COMPOSITION FOR SMALL ICG-LIPOSOMES IS NEEDED.	

11. Discussion and future prospects

As the focus of new therapeutic compounds continues to transfer from traditional small molecular drugs to biologicals, the need for efficient drug delivery methods increases. Liposomes have for a long time been used for drug delivery and still new aspects of liposomes are widely studied (Figure 12). Despite their good properties, the unmodified liposomes lack the spatial and temporal control of drug release. Light activation is one of the most promising approaches to solve this problem. After the pioneering work in the 1980's to 2000, light activated drug delivery has gained interest of the scientific community as indicated by the sharp increase in the number of publications (Figure 12). The field is still relatively young, thus offering several new possibilities for discovery and innovations. This thesis focuses on combining light activated release with the liposome technology. The main therapeutic focus is the challenging drug delivery to the posterior segment of the eye.

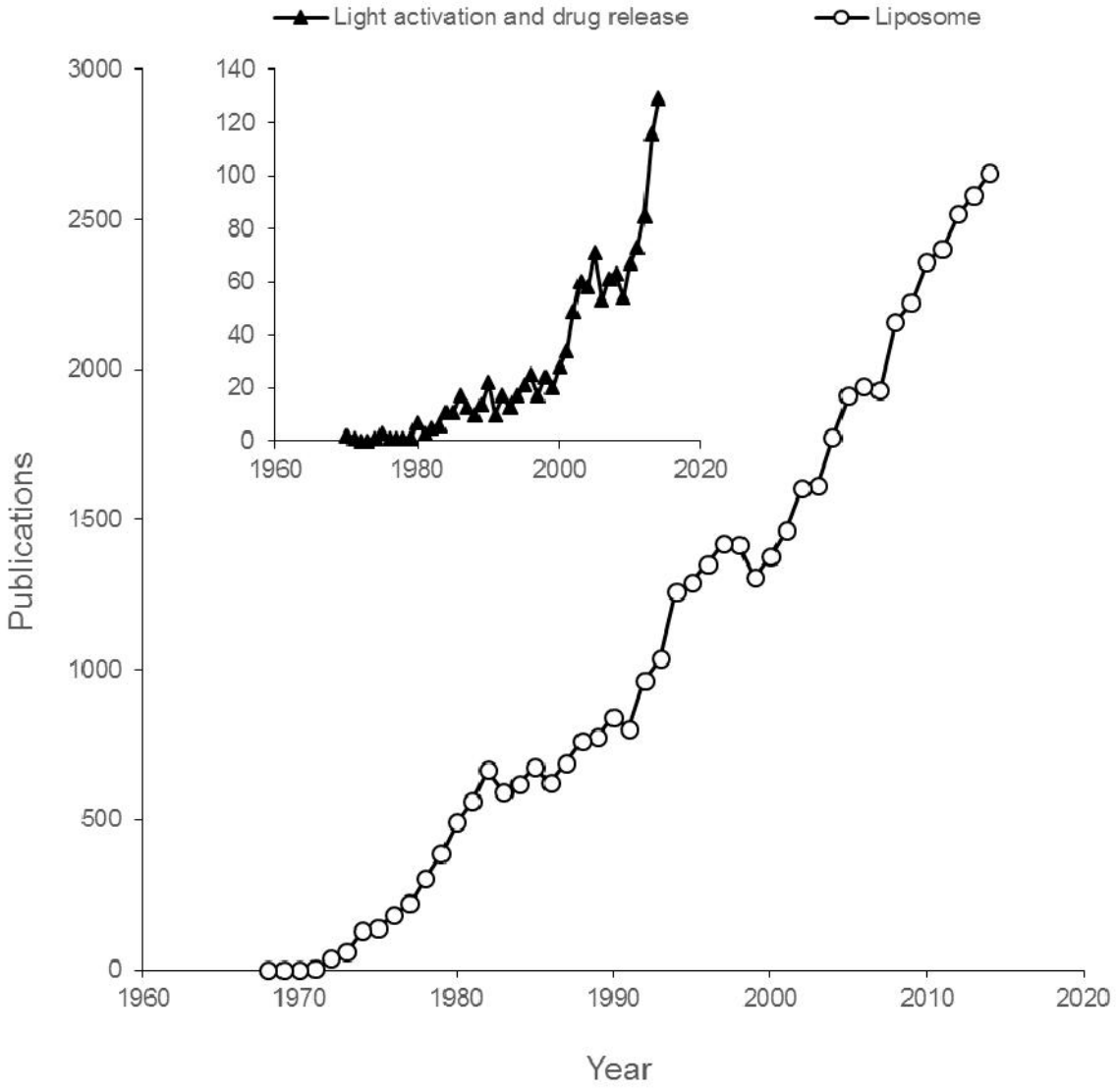

Figure 12. Yearly number of publications (research articles and review articles) indexed in Scopus database on 19th of April 2016 with search terms "liposome" (open circles) and "light activation AND drug release" (solid triangles). Timescale from 1960 to 2014 is presented.

11.1. Microfluidizer for liposome production

Liposome size has traditionally been controlled by sonication or extrusion through a polycarbonate membrane (Ulrich 2002). These methods are useful, but have some caveats, e.g. high polydispersity in case of the sonication, and somewhat limited scale-up potential of the extrusion. Microfluidizer on the other hand produces monodisperse liposomes and this method is scalable from the laboratory scale to commercial production volumes. The technology has already been adopted by food industry (Augustin and Sanguansri 2009) and should also be applicable in pharmaceutical production (Sorgi and Huang 1996; Wagner and Vorauer-Uhl 2011).

In study I, the microfluidizer process parameters for liposome preparation were elucidated and optimized. We used M-110P Microfluidizer that is designed for processing of large volumes of liquids. The minimum sample volume is 50 mL and the upper limit is basically only limited by the size of the product inlet reservoir. The microfluidizer enabled the production of different liposome sizes by changing the operating settings: the size reduction of liposomes was proportional to the increase in pressure. The effect has also been verified in other microfluidizer models (Barnadas-Rodríguez and Sabés 2001). The benefit of the device is the ability to produce liposome lots with various sizes without changing the equipment. The M-110P microfluidizer was also compared to a laboratory scale LV-1 model that can process samples as small as 1 mL. Unfortunately, a similar Y-type interaction chamber used in the M-110P model was not available for the LV-1 model and, therefore, less efficient Z-type chamber was used. Thus, even with the same process parameters (pressure and passage numbers), the LV-1 produced larger liposomes than M-110P. Nevertheless, the LV-1 should achieve similar results with a similar Y-type interaction chamber.

Often, encapsulation efficiency of hydrophilic drugs into liposomes is low with traditional preparation methods (e.g. thin film hydration and extrusion). This is also true in case of the microfluidizer because the drug concentration in the liposomes' inner aqueous space would be equal with the external concentration, unless active encapsulation methods are used (e.g. remote loading by ammonium sulfate gradient) (Bolotin, et al. 1994). Unfortunately, these methods are not widely applicable, since they have specific requirements related to the encapsulated drug. In study I, a more robust method for high encapsulation efficiency was developed. The basis of the method is a water / organic / water double emulsion, where the internal water phase is isolated from the outer bulk aqueous solution. This method has achieved high encapsulation efficiencies by high speed mixing of the double emulsion (Nii, et al. 2003). The method in study I utilized the microfluidizer for smaller liposomal size and polydispersity. It was shown to provide encapsulation efficiencies of about 80% for liposomes with significantly reduced size compared to Nii et al. (i.e. 60 nm vs. 400 nm and larger). A smaller liposome size is vital for drug delivery to many target sites, such as the RPE (Guymer, et al. 2004). In the case of the microfluidized double emulsion liposomes, the hydrocarbon chain lengths of the phospholipids were found to be an important property for determining the final particle size with shorter chains resulting in smaller liposomes.

The importance of liposomal size in drug delivery to the posterior segment of the eye was studied by topical instillation on the rat eyes. The tissue samples were collected 5 and 15 minutes after eye drop application. Liposomes were seen to deposit to the posterior tissues in a few minutes. Such a fast distribution indicated a blood circulation path instead of passive permeation through the layers of the eye. Smaller 70 nm liposomes with active targeting ligands distributed to the RPE, but larger 100 nm liposomes remained in choroidal endothelium even with similar active targeting properties. However, previous reports have shown distribution of larger liposomes to neural retina and ganglion cells after topical instillation (Davis, et al. 2014; Masuda, et al. 1996). Overall, the study showed feasibility of the microfluidizer as a versatile method for liposome preparation. Also, the importance of active targeting and correct carrier size was qualitatively

demonstrated. This may enable the treatment of RPE with drug compounds that normally are not distributed to the target tissue in therapeutically effective concentrations.

11.2. Time and location control of drug release: Light activated liposomes with gold nanoparticles

Distribution of drug carrier to the correct tissue may not be adequate for an effective therapy. The target sites of several compounds are located intracellularly and among these drugs are many biologicals like siRNA, DNA and some proteins. However, in order to exert the therapeutic effects intracellularly, the drugs need to reach the cytosol and other organelles depending on the site of action (e.g. nucleus, mitochondria or endoplasmic reticulum). Large molecules do not permeate across the plasma membrane and, hence, they need to be trafficked and released into the cells with a suitable carrier. Nanoparticles enter the cells usually via endocytosis, but the material is usually transferred to the lysosomes for degradation (Ulrich 2002). The low endosomal pH has been utilized for enhancement of endosomal escape (Han, et al. 2012; Kim, et al. 2009; Simões, et al. 2004; Slepushkin, et al. 1997), but this method lacks the specificity of drug release location at the diseased area of the tissue. Also, the time point of drug release cannot be externally controlled.

Study II focused on light activation as a means to achieve better control over drug release from the liposomes. The proof-of-principle of light activated liposomes with gold nanoparticles has been reported previously (Paasonen, et al. 2007; Paasonen, et al. 2010). Early research in the field utilized UV light for release activation, but the NIR light shows advantages, such as better tissue penetration and safety (Delori, et al. 2007; Standard 1993). In principle, light offers a spatially and temporally focused signal and a lot of possibilities for optimization (e.g. pulse length and shape, intensity, wavelength). Modern fiber optics and good tissue penetration may enable treatment of deeper tissues with minimal invasiveness.

In study II, gold nanorods and gold nanostars were encapsulated into thermosensitive liposomes. Irradiation of these gold nanoparticles with light produces heat via the surface plasmon resonance phenomenon (Jain, et al. 2006). The nanorods absorb light energy at visual wavelength and nanostars at NIR wavelengths, respectively. Furthermore, a novel liposome formulation that combined thermosensitivity with pH-sensitivity was developed. This would, in theory, enable even more focused drug release only in the acidic intracellular compartments. Stabilizing domains consisting of 1,2-dioleoyl-sn-glycero-3-phosphoethanolamine (DOPE) and cholesteryl hemisuccinate (CHEMS) destabilized at endosomal ph 5. This sensitized the formulation for light induced drug release. On the other hand, the liposomes outside cells in neutral conditions (pH 7.4) would not be sensitive to the triggering light signal.

The results showed efficient calcein release after liposome exposure to the triggering signals. Small molecular fluorescent calcein was released *in vitro* and in two cell lines upon light triggering. The triggering light and formulation were safe to the tested cell lines. The pH- and thermosensitive liposomes showed interesting results lipid layer characterization studies. The Langmuir film – BAM data indicated a formation of domains or lipid rafts in the layer at low pH conditions, instead of homogenous mixing of the different phospholipids. This phenomena was supported by the calorimetric measurements that showed multiple transition peaks instead of the typical single peak. The increased fluidity of liposomal bilayer may enhance fusion of the liposomes with the endosomal wall, thus enabling contents escape to the cytosol.

Due to the highly localized heating by light activation, true temperature in the liposomal bilayer is impossible to measure by traditional thermometers. Previously SAXS has been used to measure the phase changes in light activated liposomes with gold nanoparticles and the results indicated that light activation and increased temperature induce similar changes in the lipid bilayers (Paasonen, et al. 2010). However, SAXS did not allow direct determination of temperature in the bilayers. In study III, two nanosized thermometers, laurdan and

CdSe QDs, were utilized to measure the local temperature change in the liposomes and to study the bilayer fluidity. Macroscale methods for the lipid film studies, such as Langmuir film – BAM measurements, could not be used in the experiments on light triggering of the liposomes. Therefore, the nanosized thermometers provided a dual temperature readouts: laurdan in the lipid bilayer and the QDs in the aqueous bulk solution. A change in laurdan polarity also provides information about the bilayer phase transition during the temperature increase. Both, laurdan in the lipid bilayer and CdSe QDs in the bulk solution, showed higher temperatures when gold nanorod concentration was increased. 0.4 nM and 2.0 nM of gold nanorods showed 20.5 °C and 21.5 °C increases in temperature, respectively. The effect was not linear due to pronounced heating at the sample surface compared to deeper portions of the sample, which has also been shown in a previous report (Jang, et al. 2011). The two nanothermometers showed similar temperature changes indicating a rapid distribution of heat in the samples. This heat production was found to effectively release calcein from simple DPPC liposomes with encapsulated gold nanorods.

A few critical problems remain even though the gold nanoparticles are functional in the light triggered drug release from the liposomes. Firstly, the absorbance of the gold nanoparticles is related to their shape and size, with larger particles absorbing at longer wavelengths. Obviously, the carrier must be larger than the gold nanoparticles. Thus, the liposomes were formulated to a size range around 150 – 200 nm, but this size is too large for carrier permeation from choroidal blood vessels to the retinal pigment epithelium. They may be still suitable for intravitreal injections, since they probably diffuse well in the vitreous (Xu, et al. 2013). However, their ability to pass through the inner limiting membrane in the retina is uncertain (Pitkänen, et al. 2004). Smaller liposomes would be advantageous also in terms of distribution to the tumors (Nagayasu, et al. 1999). Secondly, the long-term safety of gold nanoparticles is not known. The inert gold nanoparticles generally do not elicit acute toxicity in the cells and *in vivo*, but only short term studies of toxicology of gold nanoparticles have been reported so far (Alkilany and Murphy 2010). FDA guidelines instruct that pharmaceuticals should be eliminated from the body in order to avoid accumulation, thus reducing the possible toxicity. Gold nanoparticles with diameters larger than 5.5 nm are not filtered through the kidneys into urine (Choi, et al. 2007), and their high chemical stability causes them to accumulate in the spleen and liver (De Jong, et al. 2008). This may have serious long term adverse effects. Also, their distribution and elimination in the eye are unknown.

11.3. ICG-liposomes as light triggered DDS

In study III, the heat production of indocyanine green (ICG) was compared with gold nanorods as triggering material. Like the nanorods, ICG absorbs NIR light at around 800 nm and converts the light energy to heat. In theory, liposomes with ICG do not have the similar limits as the liposomes with larger gold nanoparticles. Furthermore, FDA has already approved ICG for human imaging use and thus it should be safe. Study III showed that ICG decomposed during the light triggering and, therefore, the heating effect and induction of drug release will stop when all ICG has decomposed. Unfortunately, the detection equipment had a maximum time resolution of 1 min, and it did not allow determination of faster changes in temperature. ICG produced comparable heating with the gold nanoparticles. The heat conversion time could be extended with the addition of a single-oxygen quencher, sodium ascorbate, but this may not be necessary for the functionality of the DDS if the drug release is faster than the decomposition of the ICG. Calcein release from DPPC liposomes was also achieved with light triggering of ICG with slightly higher efficiency compared to the gold nanoparticles. The drug release data should not be directly compared, because the concentrations of the light converting materials were not optimized. However, as a proof-of-concept, the nanothermometer studies showed that both triggering materials, gold nanorods and ICG, increase the temperature of the liposomes over the phase transition temperature. The light signal alone did not have the same effect. The temperature dissipates quickly and the heating effect is significantly reduced in relation to the distance from

the triggering agent (Potdar and Sammalkorpi 2015), and thus the heating of the surrounding tissue is should not be significant. The nanothermometer method may be useful in evaluating the heating capabilities and thermal safety profile of various triggering materials.

Study IV describes the development of a new light triggering formulation based on the idea of thermosensitive liposomes with ICG. The phospholipid composition was optimized for sensitive photo-thermal drug release and adequate stability. Molecular dynamics study suggests that the location of ICG in lipid bilayers depends on the preparation method of the liposomes. Previous studies have speculated that amphiphilic ICG would embed itself into the lipid bilayer (Kraft and Ho 2014) and this is indeed the case when ICG is mixed directly with the lipids. However, if PEG is present in the liposome formulation, then ICG is wrapped by the PEG chains when added to the aqueous solution and does not enter the lipid bilayer. This simulation data was supported by the phase analysis of ICG-liposomes: no effects on the phase transition were seen with increasing ICG concentrations. According to our ongoing experiments, when ICG is mixed into an organic phase with lipids including PEG during manufacturing, it partitions between the lipid bilayer and PEG coating (data not shown). The ratio of partitioning is currently being studied. Importantly, the molecular size of ICG enabled the preparation of very small liposomes (around 60 nm) solving the size problem of the gold containing liposomes. Smaller ICG-liposomes should be able distribute efficiently within the vitreous, retinal layers and choroid (including the passage thought fenestrations in the vessels) (Guymer, et al. 2004; Xu, et al. 2013).

The ICG-liposomes released their contents in 15 seconds upon light activation. The fast rate of drug release indicates that the decomposition of ICG shown in study III does not hamper its light activated functionality. In contrast, the decomposition of the light triggering material may be beneficial for the safety of the DDS. As the heat production ends with the decomposition of the ICG, the tissues and cells are not unnecessarily heated even if light irradiation is continued. This is in contrast with photodynamic therapy, where the objective is photothermal destruction of the cells (Dolmans, et al. 2003). Generally, the extended heating might cause localized damage in the target cells in case of stable light triggering materials, like gold nanoparticles. The singlet oxygen decomposition products of ICG have been shown to reduce the viability of cells, but the concentrations were higher than in our DDS (Engel, et al. 2008), and RPE cells are particularly efficient in dealing with oxidative stress (Cai, et al. 2000). In addition to calcein, larger macromolecular model compounds up to a size of 20 kDa were efficiently released from the ICG-liposomes upon light triggering. This is a vital quality in controlled release of biologics. This may offer a potential solution for the important intracellular delivery of DNA and oligonucleotides.

The preliminary toxicity experiments, described in the unpublished results section, showed that the ICG-liposomes and the triggering NIR light did not reduce the viability of retinal pigment epithelial cells (ARPE-19). This conclusion was confirmed with three different markers of cell death. However, toxicological evaluation in one cell line is only the first step in understanding the toxicity profile of the DDS. The results showed that at the triggering light is well tolerated even during long exposures in pigment epithelia, even though the exposed light power was higher than the current limits of light irradiation to eyes (Delori, et al. 2007). The posterior segment of the eye has many cellular layers that are sensitive to the light, especially the light sensing rods and cones of neural retina. Nevertheless, the power and duration of the triggering light may be reduced by optimizing the drug release sensitivity of the DDS. Unfortunately, artificial cultivation of these cells in correct conformation is not a trivial matter, and thus the damage to these cells should be evaluated by *in vivo* experiments (Valjakka, et al. 2007). Furthermore, only acute cellular toxicology has been determined. The long term evaluation of ICG-liposomes is needed to prove their safety.

Cell uptake of ICG-liposomes was excellent in the cultured ARPE-19 cells. This result is comparable to the thermosensitive liposomes with gold nanoparticles in study II. NIR light triggering of ICG-liposomes caused

similar contents release as the gold nanoparticle liposomes in the cells. The experiment with ICG-liposomes showed the release of calcein in the cells, but did not indicate the intracellular location of the release (e.g. endosomes, cytosol). Cytosolic drug release was shown with the gold nanoparticle based liposomes in the study II, and efficiency of cytosolic drug release is currently being researched with ICG-liposomes. One of the most distinctive advantages of ICG as a light triggering material, is the flexibility of controlling the size of the liposomes. The unpublished results showed that it is possible to produce ICG containing liposomes as small as 40 nm with retained light triggering functionality. This quality increases robustness of the DDS enabling drug delivery to a wider selection of target tissues. Size reduction even further is theoretically impossible, as the volume of the internal aqueous space decreases. A phospholipid bilayer is generally 5 nm in thickness (Balgavý, et al. 2001) and thus it is not possible to form very small stable liposomal structures because of the stress induced by the increased curvature and lack of space for the hydrocarbon chains within the bilayer. Manufacturing of ICG-micelles of smaller size (< 20 nm) consisting of single layer lipid spheres may in theory be possible, but then the drug cargo is limited to lipophilic compounds.

The fluorescence of ICG gives an opportunity for imaging and tracking of the DDS *in vivo*. Low laser power should be used for imaging purposes in order to prevent drug release activation before the DDS has reached the target site. The ICG based imaging may enable detection of DDS distribution to different layers in the posterior segment of the eye, for example. When the drug carrier is detected at the target cells, the localized triggering laser signal is applied.

11.4. Considerations for the future

Many aspects of the light triggered liposomes still remain to be studied in the future. So far we have shown the proof-of-principle *in vitro* and optimized the formulation for light activated release. It is still a challenge to translate the technology to therapeutic setting with small molecular drugs or biologics. The safety of the system in systemic or local administration needs to be verified in animal experiments and humans. Additionally, the *in vivo* distribution of the DDS and *in vivo* release with light induction need to be studied. Depending on the target site, different routes of drug administration can be used, e.g. intravenous or intravitreal injections, inhalation and topical delivery methods. Different challenges and requirements apply to each application route and the *in vivo* distribution must be evaluated separately for each case.

In regards to eye medication, light activated liposomes offer many attractive properties. The formulation does not limit the possible administration route, because liposomes can be applied topically, suprachoroidally and intravitreally. The DDS may enable increased bioavailability for challenging drugs including several macromolecules. Furthermore, the light activation pinpoints the drug effect to the diseased tissue, thus drugs with generally poor safety profile may be useful again. Increased treatment efficiency would extend the dosing interval thus reducing the need for uncomfortable and costly procedures to the patient's eyes. Light triggered liposomes might be a so called "enabling technology", which permits treatment with otherwise unusable drugs for the difficult diseases in eyes.

After adequate DDS concentrations at the target site are measured, the actual therapeutic efficacy of the carrier needs to be studied with applicable disease models and finally in patients. Careful selection of the potential pathological conditions is vital. There should be a valid reason and clear advantage for the use of the DDS, such as unsatisfactory efficacy or considerable adverse effects with the current treatment protocols. The new DDS should be able to reach the target and in case of light triggered liposomes, the target site has to be effectively stimulated with NIR-light. Extensive comparisons to current state-of-the-art treatments are required to prove the advantage of the drug administration in light triggered DDS.

The surface of liposomal drug delivery systems can be modified for targeting and prolonged residence time in the compartment of administration (e.g. plasma, vitreous cavity) (Torchilin 2012). In the current form, the ICG-liposomes do not have any active targeting mechanism, but they include PEG moieties for prolonged residence time. PEG coating can be used for the attachment of targeting ligands, as well as for other possible modifications, such as inclusion of cell penetrating peptides for improved cellular uptake. Addition of pH-sensitivity is one of the development possibilities for ICG-liposomes. This requires alterations of the bilayer composition and thus great care should be taken not to hamper the light triggering properties of the DDS. These modifications could result in improved cytosolic drug delivery and higher selectivity of release, i.e. faster drug release in the acidic cellular compartments compared to the neutral extracellular space.

Realistically, there are many hurdles before light activated liposomes could reach the clinical use. For example, attachment of several functions to the DDS imposes problems in the industrial production. Generally, the production cost increases and reproducibility decreases with the number of different compounds in the formulation. The first target for reducing the number of compounds would be the compounds that have similar functions in the system, for example two neutral phospholipids, DPPC and DSPC with different phase transition temperatures. Perhaps, similar properties would be achievable with one bilayer component.

Commercial viability of any system depends on the market situation and pricing of the product. How many people are suffering from a particular disease? Are there already satisfactory lower cost medicines for the condition? Light activated liposomes may be suitable for the treatment of cancer and serious ocular diseases. As described in the introduction, the treatment of these conditions needs improvements in efficiency, safety or patient comfort. Furthermore, as the population in the western world and emerging markets continues to shift towards the elderly demographics, the need for treatments will increase. Likewise, we are on the eve of the new age of biologicals (including gene medicines) and this will further emphasize the need for controlled drug delivery systems.

12. Conclusions

In this thesis, new liposomal drug delivery systems were investigated. The main conclusions of the studies are divided and summarized as follows:

1) The microfluidizer method is capable of producing large sample batches of liposomes with very small uniform particle size (< 80 nm). Small liposomes with transferrin reached the RPE after topical eye drop instillation at detectable quantity. Larger particles do not permeate to the RPE after topical delivery. The microfluidizer method is an attractive option to manufacture small liposomes that may enable treatment of retinal diseases with topical eye drops.

2) Light activated and pH-sensitive liposomes with encapsulated gold nanoparticles were formulated and optimized. After cellular uptake the liposomes released their fluorescent contents to the cytosol upon light activation. The formulations and light activation were safe in two cultured cell lines. These results suggest that a site-specific and light induced drug release in the target cells may be possible with the light activated liposomes, but the size of these liposomes may limit their usefulness in drug delivery.

3) Two triggering materials light induced drug release, gold nanorods and indocyanine green, were evaluated as light-to-heat converters using two nanothermoprobes, laurdan and CdSe QD. Upon NIR light irradiation both materials resulted in liposome heating, phase transition in the lipid bilayers and marker leakage from the liposomes. The method is applicable in mechanistic studies of light inducible nanosystems.

4) ICG-liposomes for light triggered drug release were optimized in terms of lipid composition and quantity of ICG. The ICG-liposomes showed fast contents release in seconds upon NIR light triggering. Almost complete release of small and large encapsulated fluorescence probes was observed. Small functional ICG-liposomes (40 and 100 nm) were formulated at narrow size distribution. These liposomes and activating light signal were safe for retinal pigment epithelial cells in culture. Molecular dynamics simulations informed us about the localization of ICG in the liposomes. Overall, ICG-liposomes have many advantageous properties that warrant further studies on their applicability for light triggered drug release at specific diseases targets, for example in the posterior eye segment.

13. References

Abrahamson, I.A., 1975. Complication of the Use of Ocuserts. Arch. Ophthalmol., 93, 317-317.

Adibkia, K., Shadbad, M.R.S., Nokhodchi, A., Javadzedeh, A., Barzegar-Jalali, M., Barar, J., Mohammadi, G., Omidi, Y., 2007. Piroxicam nanoparticles for ocular delivery: physicochemical characterization and implementation in endotoxin-induced uveitis. J. Drug Target., 15, 407-416.

Agasti, S.S., Chompoosor, A., You, C., Ghosh, P., Kim, C.K., Rotello, V.M., 2009. Photoregulated release of caged anticancer drugs from gold nanoparticles. J. Am. Chem. Soc., 131, 5728-5729.

Ahmed, I., Patton, T., 1985. Importance of the noncorneal absorption route in topical ophthalmic drug delivery. Invest. Ophthalmol. Vis. Sci., 26, 584-587.

Al-Ahmady, Z.S., Al-Jamal, W., Bossche, J.V., Bui, T.T., Drake, A.F., Mason, A.J., Kostarelos, K., 2012. Lipid–peptide vesicle nanoscale hybrids for triggered drug release by mild hyperthermia in vitro and in vivo. ACS nano, 6, 9335-9346.

Alkilany, A.M., Murphy, C.J., 2010. Toxicity and cellular uptake of gold nanoparticles: what we have learned so far? Journal of nanoparticle research, 12, 2313-2333.

Allen, C., Dos Santos, N., Gallagher, R., Chiu, G., Shu, Y., Li, W., Johnstone, S., Janoff, A., Mayer, L., Webb, M., 2002. Controlling the physical behavior and biological performance of liposome formulations through use of surface grafted poly (ethylene glycol). Biosci. Rep., 22, 225-250.

Allen, T.M., Hansen, C.B., de Menezes, Daniel E Lopes, 1995. Pharmacokinetics of long-circulating liposomes. Adv. Drug Deliv. Rev., 16, 267-284.

Alvarez-Lorenzo, C., Bromberg, L., Concheiro, A., 2009. Light-sensitive intelligent drug delivery systems. Photochem. Photobiol., 85, 848-860.

Amir, R.J., Pessah, N., Shamis, M., Shabat, D., 2003. Self-Immolative Dendrimers. Angewandte Chemie, 115, 4632-4637.

Anand, B.S., Mitra, A.K., 2002. Mechanism of corneal permeation of L-valyl ester of acyclovir: targeting the oligopeptide transporter on the rabbit cornea. Pharm. Res., 19, 1194-1202.

Anand, B., Katragadda, S., Nashed, Y., Mitra, A., 2004. Amino acid prodrugs of acyclovir as possible antiviral agents against ocular HSV-1 infections: interactions with the neutral and cationic amino acid transporter on the corneal epithelium. Curr. Eye Res., 29, 153-166.

Andar, A.U., Hood, R.R., Vreeland, W.N., DeVoe, D.L., Swaan, P.W., 2014. Microfluidic preparation of liposomes to determine particle size influence on cellular uptake mechanisms. Pharm. Res., 31, 401-413.

Angelos, S., Choi, E., Vögtle, F., De Cola, L., Zink, J.I., 2007. Photo-driven expulsion of molecules from mesostructured silica nanoparticles. The Journal of Physical Chemistry C, 111, 6589-6592.

Armaly, M.F., Rao, K., 1973. The effect of pilocarpine Ocusert with different release rates on ocular pressure. Invest. Ophthalmol. Vis. Sci., 12, 491-496.

Augustin, M.A., Sanguansri, P., 2009. Nanostructured materials in the food industry. Adv. Food Nutr. Res., 58, 183-213.

Aukunuru, J.V., Sunkara, G., Bandi, N., Thoreson, W.B., Kompella, U.B., 2001. Expression of multidrug resistance-associated protein (MRP) in human retinal pigment epithelial cells and its interaction with BAPSG, a novel aldose reductase inhibitor. Pharm. Res., 18, 565-572.

Balgavý, P., Dubničková, M., Kučerka, N., Kiselev, M.A., Yaradaikin, S.P., Uhríková, D., 2001. Bilayer thickness and lipid interface area in unilamellar extruded 1, 2-diacylphosphatidylcholine liposomes: a small-angle neutron scattering study. Biochimica et Biophysica Acta (BBA)-Biomembranes, 1512, 40-52.

Banerjee, J., Hanson, A.J., Gadam, B., Elegbede, A.I., Tobwala, S., Ganguly, B., Wagh, A.V., Muhonen, W.W., Law, B., Shabb, J.B., 2009. Release of liposomal contents by cell-secreted matrix metalloproteinase-9. Bioconjug. Chem., 20, 1332-1339.

Bangham, A., Standish, M.M., Watkins, J., 1965. Diffusion of univalent ions across the lamellae of swollen phospholipids. J. Mol. Biol., 13, 238-252.

Barenholz, Y.C., 2012. Doxil®—the first FDA-approved nano-drug: lessons learned. J. Controlled Release, 160, 117-134.

Barhoumi, A., Huschka, R., Bardhan, R., Knight, M.W., Halas, N.J., 2009. Light-induced release of DNA from plasmon-resonant nanoparticles: towards light-controlled gene therapy. Chemical Physics Letters, 482, 171-179.

Barnadas-Rodríguez, R., Sabés, M., 2001. Factors involved in the production of liposomes with a high-pressure homogenizer. Int. J. Pharm., 213, 175-186.

Behr, J.P., Demeneix, B., Loeffler, J.P., Perez-Mutul, J., 1989. Efficient gene transfer into mammalian primary endocrine cells with lipopolyamine-coated DNA. Proc. Natl. Acad. Sci. U. S. A., 86, 6982-6986.

Bisby, R.H., Mead, C., Morgan, C.G., 2000. Wavelength-programmed solute release from photosensitive liposomes. Biochem. Biophys. Res. Commun., 276, 169-173.

Bochot, A., Fattal, E., Gulik, A., Couarraze, G., Couvreur, P., 1998. Liposomes dispersed within a thermosensitive gel: a new dosage form for ocular delivery of oligonucleotides. Pharm. Res., 15, 1364-1369.

Bolotin, E.M., Cohen, R., Bar, L.K., Emanuel, N., Ninio, S., Barenholz, Y., Lasic, D.D., 1994. Ammonium sulfate gradients for efficient and stable remote loading of amphipathic weak bases into liposomes and ligandoliposomes. J. Liposome Res., 4, 455-479.

Bondurant, B., Mueller, A., O'Brien, D.F., 2001. Photoinitiated destabilization of sterically stabilized liposomes. Biochimica et Biophysica Acta (BBA)-Biomembranes, 1511, 113-122.

Bourges, J., Bloquel, C., Thomas, A., Froussart, F., Bochot, A., Azan, F., Gurny, R., BenEzra, D., Behar-Cohen, F., 2006. Intraocular implants for extended drug delivery: therapeutic applications. Adv. Drug Deliv. Rev., 58, 1182-1202.

Bourges, J., Gautier, S.E., Delie, F., Bejjani, R.A., Jeanny, J., Gurny, R., BenEzra, D., Behar-Cohen, F.F., 2003. Ocular drug delivery targeting the retina and retinal pigment epithelium using polylactide nanoparticles. Invest. Ophthalmol. Vis. Sci., 44, 3562-3569.

Braun, G.B., Pallaoro, A., Wu, G., Missirlis, D., Zasadzinski, J.A., Tirrell, M., Reich, N.O., 2009. Laser-activated gene silencing via gold nanoshell− siRNA conjugates. Acs Nano, 3, 2007-2015.

Britton, G.L., Kim, H., Kee, P.H., Aronowski, J., Holland, C.K., McPherson, D.D., Huang, S.L., 2010. In vivo therapeutic gas delivery for neuroprotection with echogenic liposomes. Circulation, 122, 1578-1587. doi: 10.1161/CIRCULATIONAHA.109.879338 [doi].

Bungener, L., Huckriede, A., Wilschut, J., Daemen, T., 2002. Delivery of protein antigens to the immune system by fusion-active virosomes: a comparison with liposomes and ISCOMs. Biosci. Rep., 22, 323-338.

Cai, J., Nelson, K.C., Wu, M., Sternberg, P., Jones, D.P., 2000. Oxidative damage and protection of the RPE. Prog. Retin. Eye Res., 19, 205-221.

Calle, D., Negri, V., Ballesteros, P., Cerdán, S., 2015. Magnetoliposomes loaded with poly-unsaturated fatty acids as novel theranostic anti-inflammatory formulations. Theranostics, 5, 489.

Castellarin, A., Pieramici, D.J., 2004. Anterior segment complications following periocular and intraocular injections. Ophthalmol. Clin. North Am., 17, 583-90, vii. doi: S0896-1549(04)00082-3 [pii].

Cavalli, R., Gasco, M.R., Chetoni, P., Burgalassi, S., Saettone, M.F., 2002. Solid lipid nanoparticles (SLN) as ocular delivery system for tobramycin. Int. J. Pharm., 238, 241-245.

Chandra, B., Subramaniam, R., Mallik, S., Srivastava, D., 2006. Formulation of photocleavable liposomes and the mechanism of their content release. Organic & biomolecular chemistry, 4, 1730-1740.

Chen, C., Lin, Y., Wang, C., Tzeng, H., Wu, C., Chen, Y., Chen, C., Chen, L., Wu, Y., 2006. DNA-gold nanorod conjugates for remote control of localized gene expression by near infrared irradiation. J. Am. Chem. Soc., 128, 3709-3715.

Chen, W.R., Adams, R.L., Bartels, K.E., Nordquist, R.E., 1995. Chromophore-enhanced in vivo tumor cell destruction using an 808-nm diode laser. Cancer Lett., 94, 125-131.

Choi, H.S., Liu, W., Misra, P., Tanaka, E., Zimmer, J.P., Ipe, B.I., Bawendi, M.G., Frangioni, J.V., 2007. Renal clearance of quantum dots. Nat. Biotechnol., 25, 1165-1170.

Chonn, A., Cullis, P.R., 1998. Recent advances in liposome technologies and their applications for systemic gene delivery. Adv. Drug Deliv. Rev., 30, 73-83.

Chonn, A., Semple, S.C., Cullis, P.R., 1992. Association of blood proteins with large unilamellar liposomes in vivo. Relation to circulation lifetimes. J. Biol. Chem., 267, 18759-18765.

Chu, C., Dijkstra, J., Lai, M., Hong, K., Szoka, F.C., 1990. Efficiency of cytoplasmic delivery by pH-sensitive liposomes to cells in culture. Pharm. Res., 7, 824-834.

Clejan, S., Bittman, R., Deroo, P.W., Isaacson, Y.A., Rosenthal, A.F., 1979. Permeability properties of sterol-containing liposomes from analogs of phosphatidylcholine lacking acyl groups. Biochemistry (N. Y.), 18, 2118-2125.

Constable, P.A., Lawrenson, J.G., Dolman, D.E., Arden, G.B., Abbott, N.J., 2006. P-Glycoprotein expression in human retinal pigment epithelium cell lines. Exp. Eye Res., 83, 24-30.

Davis, B.M., Normando, E.M., Guo, L., O'Shea, P., Moss, S.E., Somavarapu, S., Cordeiro, M.F., 2014. Topical Delivery of Avastin to the Posterior Segment of the Eye In Vivo Using Annexin A5-associated Liposomes. Small, 10, 1575-1584. doi: 10.1002/smll.201303433.

De Campos, A.M., Sánchez, A., Gref, R., Calvo, P., Alonso, J., 2003. The effect of a PEG versus a chitosan coating on the interaction of drug colloidal carriers with the ocular mucosa. European journal of pharmaceutical sciences, 20, 73-81.

De Jong, W.H., Hagens, W.I., Krystek, P., Burger, M.C., Sips, A.J., Geertsma, R.E., 2008. Particle size-dependent organ distribution of gold nanoparticles after intravenous administration. Biomaterials, 29, 1912-1919.

De Kruijff, B., Cullis, P., Radda, G., 1975. Differential scanning calorimetry and 31 P NMR studies on sonicated and unsonicated phosphatidylcholine liposomes. Biochimica et Biophysica Acta (BBA)-Biomembranes, 406, 6-20.

Del Amo, E.M., Urtti, A., 2008. Current and future ophthalmic drug delivery systems: a shift to the posterior segment. Drug Discov. Today, 13, 135-143.

del Amo, E.M., Vellonen, K., Kidron, H., Urtti, A., 2015. Intravitreal clearance and volume of distribution of compounds in rabbits: In silico prediction and pharmacokinetic simulations for drug development. European Journal of Pharmaceutics and Biopharmaceutics, 95, 215-226.

Delori, F.C., Webb, R.H., Sliney, D.H., 2007. Maximum permissible exposures for ocular safety (ANSI 2000), with emphasis on ophthalmic devices. JOSA A, 24, 1250-1265.

Dey, S., Patel, J., Anand, B.S., Jain-Vakkalagadda, B., Kaliki, P., Pal, D., Ganapathy, V., Mitra, A.K., 2003. Molecular evidence and functional expression of P-glycoprotein (MDR1) in human and rabbit cornea and corneal epithelial cell lines. Invest. Ophthalmol. Vis. Sci., 44, 2909-2918.

Dhillon, B., Kamal, A., Leen, C., 1998. Intravitreal sustained-release ganciclovir implantation to control cytomegalovirus retinitis in AIDS. Int. J. STD AIDS, 9, 227-230.

Dolmans, D.E., Fukumura, D., Jain, R.K., 2003. Photodynamic therapy for cancer. Nature reviews cancer, 3, 380-387.

du Plessis, J., Ramachandran, C., Weiner, N., Müller, D., 1994. The influence of particle size of liposomes on the deposition of drug into skin. Int. J. Pharm., 103, 277-282.

El Halabieh, R.H., Mermut, O., Barrett, C.J., 2004. Using light to control physical properties of polymers and surfaces with azobenzene chromophores. Pure and applied chemistry, 76, 1445-1465.

Engel, E., Schraml, R., Maisch, T., Kobuch, K., König, B., Szeimies, R., Hillenkamp, J., Bäumler, W., Vasold, R., 2008. Light-induced decomposition of indocyanine green. Invest. Ophthalmol. Vis. Sci., 49, 1777-1783.

Essa, E.A., Bonner, M.C., Barry, B.W., 2002. Iontophoretic estradiol skin delivery and tritium exchange in ultradeformable liposomes. Int. J. Pharm., 240, 55-66.

Felgner, P.L., Gadek, T.R., Holm, M., Roman, R., Chan, H.W., Wenz, M., Northrop, J.P., Ringold, G.M., Danielsen, M., 1987. Lipofection: a highly efficient, lipid-mediated DNA-transfection procedure. Proc. Natl. Acad. Sci. U. S. A., 84, 7413-7417.

Felt, O., Furrer, P., Mayer, J., Plazonnet, B., Buri, P., Gurny, R., 1999. Topical use of chitosan in ophthalmology: tolerance assessment and evaluation of precorneal retention. Int. J. Pharm., 180, 185-193.

Flaten, G.E., Dhanikula, A.B., Luthman, K., Brandl, M., 2006. Drug permeability across a phospholipid vesicle based barrier: a novel approach for studying passive diffusion. European journal of pharmaceutical sciences, 27, 80-90.

Fomina, N., Sankaranarayanan, J., Almutairi, A., 2012. Photochemical mechanisms of light-triggered release from nanocarriers. Adv. Drug Deliv. Rev., 64, 1005-1020.

Ganapathy, M., Ganapathy, V., 2005. Amino acid transporter ATB0, as a delivery system for drugs and prodrugs. Current Drug Targets-Immune, Endocrine & Metabolic Disorders, 5, 357-364.

Garty, N., Lusky, M., Zalish, M., Rachmiel, R., Greenbaum, A., Desatnik, H., Neumann, R., Howes, J., Melamed, S., 1994. Investigative Ophthalmology & Visual Science, pp. 2175-2175.

Gaudana, R., Jwala, J., Boddu, S.H., Mitra, A.K., 2009. Recent perspectives in ocular drug delivery. Pharm. Res., 26, 1197-1216.

Gerasimov, O.V., Boomer, J.A., Qualls, M.M., Thompson, D.H., 1999. Cytosolic drug delivery using pH-and light-sensitive liposomes. Adv. Drug Deliv. Rev., 38, 317-338.

Gerasimov, O.V., Schwan, A., Thompson, D.H., 1997. Acid-catalyzed plasmenylcholine hydrolysis and its effect on bilayer permeability: a quantitative study. Biochimica et Biophysica Acta (BBA)-Biomembranes, 1324, 200-214.

Gill, S., Löbenberg, R., Ku, T., Azarmi, S., Roa, W., Prenner, E.J., 2007. Nanoparticles: characteristics, mechanisms of action, and toxicity in pulmonary drug delivery—a review. Journal of Biomedical Nanotechnology, 3, 107-119.

Goldson, A.L., 2012. Cancer Management in Man: Detection, Diagnosis, Surgery, Radiology, Chronobiology, Endocrine Therapy, Springer Science & Business Media.

Gorelikov, I., Field, L.M., Kumacheva, E., 2004. Hybrid microgels photoresponsive in the near-infrared spectral range. J. Am. Chem. Soc., 126, 15938-15939.

Gulsen, D., Chauhan, A., 2004. Ophthalmic drug delivery through contact lenses. Invest. Ophthalmol. Vis. Sci., 45, 2342-2347.

Guymer, R.H., Bird, A.C., Hageman, G.S., 2004. Cytoarchitecture of choroidal capillary endothelial cells. Invest. Ophthalmol. Vis. Sci., 45, 1660-1666.

Han, S., Liu, Y., Nie, X., Xu, Q., Jiao, F., Li, W., Zhao, Y., Wu, Y., Chen, C., 2012. Efficient Delivery of Antitumor Drug to the Nuclei of Tumor Cells by Amphiphilic Biodegradable Poly (L-Aspartic Acid-co-Lactic Acid)/DPPE Co-Polymer Nanoparticles. Small, 8, 1596-1606.

Harashima, H., Sakata, K., Funato, K., Kiwada, H., 1994. Enhanced hepatic uptake of liposomes through complement activation depending on the size of liposomes. Pharm. Res., 11, 402-406.

Hirsch, L.R., Stafford, R.J., Bankson, J.A., Sershen, S.R., Rivera, B., Price, R.E., Hazle, J.D., Halas, N.J., West, J.L., 2003. Nanoshell-mediated near-infrared thermal therapy of tumors under magnetic resonance guidance. Proc. Natl. Acad. Sci. U. S. A., 100, 13549-13554. doi: 10.1073/pnas.2232479100 [doi].

Huang, S., 2008. Liposomes in ultrasonic drug and gene delivery. Adv. Drug Deliv. Rev., 60, 1167-1176.

Huang, X., El-Sayed, I.H., Qian, W., El-Sayed, M.A., 2006. Cancer cell imaging and photothermal therapy in the near-infrared region by using gold nanorods. J. Am. Chem. Soc., 128, 2115-2120.

Huang, S.K., Stauffer, P.R., Hong, K., Guo, J.W., Phillips, T.L., Huang, A., Papahadjopoulos, D., 1994. Liposomes and hyperthermia in mice: increased tumor uptake and therapeutic efficacy of doxorubicin in sterically stabilized liposomes. Cancer Res., 54, 2186-2191.

Immordino, M.L., Dosio, F., Cattel, L., 2006. Stealth liposomes: review of the basic science, rationale, and clinical applications, existing and potential. International journal of nanomedicine, 1, 297.

Jaffe, G.J., Martin, D., Callanan, D., Pearson, P.A., Levy, B., Comstock, T., Fluocinolone Acetonide Uveitis Study Group, 2006. Fluocinolone acetonide implant (Retisert) for noninfectious posterior uveitis: thirty-four–week results of a multicenter randomized clinical study. Ophthalmology, 113, 1020-1027.

Jahn, A., Reiner, J.E., Vreeland, W.N., DeVoe, D.L., Locascio, L.E., Gaitan, M., 2008. Preparation of nanoparticles by continuous-flow microfluidics. Journal of Nanoparticle Research, 10, 925-934.

Jahn, A., Vreeland, W.N., DeVoe, D.L., Locascio, L.E., Gaitan, M., 2007. Microfluidic directed formation of liposomes of controlled size. Langmuir, 23, 6289-6293.

Jain, P.K., Lee, K.S., El-Sayed, I.H., El-Sayed, M.A., 2006. Calculated absorption and scattering properties of gold nanoparticles of different size, shape, and composition: applications in biological imaging and biomedicine. The Journal of Physical Chemistry B, 110, 7238-7248.

Jana, N.R., Gearheart, L., Murphy, C.J., 2001. Wet chemical synthesis of high aspect ratio cylindrical gold nanorods. The Journal of Physical Chemistry B, 105, 4065-4067.

Jang, B., Kim, Y.S., Choi, Y., 2011. Effects of Gold Nanorod Concentration on the Depth-Related Temperature Increase During Hyperthermic Ablation. Small, 7, 265-270.

Jiang, J., Gill, H.S., Ghate, D., McCarey, B.E., Patel, S.R., Edelhauser, H.F., Prausnitz, M.R., 2007. Coated microneedles for drug delivery to the eye. Invest. Ophthalmol. Vis. Sci., 48, 4038-4043.

Jiang, J., Tong, X., Morris, D., Zhao, Y., 2006. Toward photocontrolled release using light-dissociable block copolymer micelles. Macromolecules, 39, 4633-4640.

Jin, Y., Gao, X., 2009. Spectrally tunable leakage-free gold nanocontainers. J. Am. Chem. Soc., 131, 17774-17776.

Jonas, J., Spandau, U., Schlichtenbrede, F., 2008. Short-term complications of intravitreal injections of triamcinolone and bevacizumab. Eye, 22, 590-591.

Kano, K., Tanaka, Y., Ogawa, T., Shimomura, M., Okahata, Y., Kunitake, T., 1980. Photoresponsive membranes. Regulation of membrane properties by photoreversible cis-trans isomerization of azobenzenes. Chem. Lett., 421-424.

Katagiri, K., Imai, Y., Koumoto, K., Kaiden, T., Kono, K., Aoshima, S., 2011. Magnetoresponsive On-Demand Release of Hybrid Liposomes Formed from Fe3O4 Nanoparticles and Thermosensitive Block Copolymers. Small, 7, 1683-1689.

Kayser, O., Lemke, A., Hernandez-Trejo, N., 2005. The impact of nanobiotechnology on the development of new drug delivery systems. Curr. Pharm. Biotechnol., 6, 3-5.

Kidron, H., Vellonen, K., Del Amo, E.M., Tissari, A., Urtti, A., 2010. Prediction of the corneal permeability of drug-like compounds. Pharm. Res., 27, 1398-1407.

Kim, I., Kang, Y., Lee, D.S., Park, H., Choi, E., Oh, Y., Son, H., Kim, J., 2009. Antitumor activity of EGFR targeted pH-sensitive immunoliposomes encapsulating gemcitabine in A549 xenograft nude mice. J. Controlled Release, 140, 55-60.

Kim, S., Kim, J.W., Cho, J., Weitz, D.A., 2011. Double-emulsion drops with ultra-thin shells for capsule templates. Lab on a Chip, 11, 3162-3166.

Kirby, C., Clarke, J., Gregoriadis, G., 1980. Effect of the cholesterol content of small unilamellar liposomes on their stability in vivo and in vitro. Biochem. J., 186, 591-598.

Kirjavainen, M., Urtti, A., Jääskeläinen, I., Marjukka Suhonen, T., Paronen, P., Valjakka-Koskela, R., Kiesvaara, J., Mönkkönen, J., 1996. Interaction of liposomes with human skin in vitro--the influence of lipid composition and structure. Biochimica et Biophysica Acta (BBA)-Lipids and Lipid Metabolism, 1304, 179-189.

Kono, K., Ozawa, T., Yoshida, T., Ozaki, F., Ishizaka, Y., Maruyama, K., Kojima, C., Harada, A., Aoshima, S., 2010. Highly temperature-sensitive liposomes based on a thermosensitive block copolymer for tumor-specific chemotherapy. Biomaterials, 31, 7096-7105.

Kontturi, L., Collin, E.C., Murtomäki, L., Pandit, A.S., Yliperttula, M., Urtti, A., 2015. Encapsulated cells for long-term secretion of soluble VEGF receptor 1: material optimization and simulation of ocular drug response. European Journal of Pharmaceutics and Biopharmaceutics, 95, 387-397.

Kontturi, L., Yliperttula, M., Toivanen, P., Määttä, A., Määttä, A., Urtti, A., 2011. A laboratory-scale device for the straightforward production of uniform, small sized cell microcapsules with long-term cell viability. J. Controlled Release, 152, 376-381.

Koo, O.M., Rubinstein, I., Onyuksel, H., 2005. Role of nanotechnology in targeted drug delivery and imaging: a concise review. Nanomedicine: Nanotechnology, Biology and Medicine, 1, 193-212.

Koren, E., Apte, A., Jani, A., Torchilin, V.P., 2012. Multifunctional PEGylated 2C5-immunoliposomes containing pH-sensitive bonds and TAT peptide for enhanced tumor cell internalization and cytotoxicity. J. Controlled Release, 160, 264-273.

Kostarelos, K., Emfietzoglou, D., Tadros, T.F., 2005. Light-sensitive fusion between polymer-coated liposomes following physical anchoring of polymerisable polymers onto lipid bilayers by self-assembly. Faraday Discuss., 128, 379-388.

Kraft, J.C., Ho, R.J., 2014. Interactions of indocyanine green and lipid in enhancing near-infrared fluorescence properties: the basis for near-infrared imaging in vivo. Biochemistry (N. Y.), 53, 1275-1283.

Kunou, N., Ogura, Y., Yasukawa, T., Kimura, H., Miyamoto, H., Honda, Y., Ikada, Y., 2000. Long-term sustained release of ganciclovir from biodegradable scleral implant for the treatment of cytomegalovirus retinitis. J. Controlled Release, 68, 263-271.

Kuppermann, B.D., Blumenkranz, M.S., Haller, J.A., Williams, G.A., Weinberg, D.V., Chou, C., Whitcup, S.M., 2007. Randomized controlled study of an intravitreous dexamethasone drug delivery system in patients with persistent macular edema. Arch. Ophthalmol., 125, 309-317.

Laitinen, A., Laatikainen, L., Härkänen, T., Koskinen, S., Reunanen, A., Aromaa, A., 2010. Prevalence of major eye diseases and causes of visual impairment in the adult Finnish population: a nationwide population-based survey. Acta Ophthalmol., 88, 463-471.

Lajavardi, L., Bochot, A., Camelo, S., Goldenberg, B., Naud, M., Behar-Cohen, F., Fattal, E., De Kozak, Y., 2007. Downregulation of endotoxin-induced uveitis by intravitreal injection of vasoactive intestinal peptide encapsulated in liposomes. Invest. Ophthalmol. Vis. Sci., 48, 3230-3238.

Lednev, I., Ye, T., Matousek, P., Towrie, M., Foggi, P., Neuwahl, F., Umapathy, S., Hester, R., Moore, J.N., 1998. Femtosecond time-resolved UV-visible absorption spectroscopy of trans-azobenzene: dependence on excitation wavelength. Chemical physics letters, 290, 68-74.

Lee, S.S., Hughes, P., Ross, A.D., Robinson, M.R., 2010. Biodegradable implants for sustained drug release in the eye. Pharm. Res., 27, 2043-2053.

Lee, T.W., Robinson, J.R., 2001. Drug delivery to the posterior segment of the eye: some insights on the penetration pathways after subconjunctival injection. Journal of ocular pharmacology and therapeutics, 17, 565-572.

Lee, R.J., Huang, L., 1996. Folate-targeted, anionic liposome-entrapped polylysine-condensed DNA for tumor cell-specific gene transfer. J. Biol. Chem., 271, 8481-8487.

Lehtinen, J., Magarkar, A., Stepniewski, M., Hakola, S., Bergman, M., Róg, T., Yliperttula, M., Urtti, A., Bunker, A., 2012. Analysis of cause of failure of new targeting peptide in PEGylated liposome: molecular modeling as rational design tool for nanomedicine. European Journal of Pharmaceutical Sciences, 46, 121-130.

Litzinger, D.C., Buiting, A.M., van Rooijen, N., Huang, L., 1994. Effect of liposome size on the circulation time and intraorgan distribution of amphipathic poly (ethylene glycol)-containing liposomes. Biochimica et Biophysica Acta (BBA)-Biomembranes, 1190, 99-107.

Liu, N., Dunphy, D.R., Atanassov, P., Bunge, S.D., Chen, Z., López, G.P., Boyle, T.J., Brinker, C.J., 2004. Photoregulation of mass transport through a photoresponsive azobenzene-modified nanoporous membrane. Nano letters, 4, 551-554.

Lu, J., Choi, E., Tamanoi, F., Zink, J.I., 2008. Light-Activated Nanoimpeller-Controlled Drug Release in Cancer Cells. Small, 4, 421-426.

Ma, Y., Tong, S., Bao, G., Gao, C., Dai, Z., 2013. Indocyanine green loaded SPIO nanoparticles with phospholipid-PEG coating for dual-modal imaging and photothermal therapy. Biomaterials, 34, 7706-7714.

Mannermaa, E., Vellonen, K., Urtti, A., 2006. Drug transport in corneal epithelium and blood–retina barrier: emerging role of transporters in ocular pharmacokinetics. Adv. Drug Deliv. Rev., 58, 1136-1163.

Mansour, H.M., Rhee, Y.S., Wu, X., 2009. Nanomedicine in pulmonary delivery. Int. J. Nanomedicine, 4, 299-319.

Marmor, M.F., Negi, A., Maurice, D.M., 1985. Kinetics of macromolecules injected into the subretinal space. Exp. Eye Res., 40, 687-696.

Maruyama, K., Takizawa, T., Takahashi, N., Tagawa, T., Nagaike, K., Iwatsuru, M., 1997. Targeting efficiency of PEG-immunoliposome-conjugated antibodies at PEG terminals. Adv. Drug Deliv. Rev., 24, 235-242.

Masuda, I., Matsuo, T., Yasuda, T., Matsuo, N., 1996. Gene transfer with liposomes to the intraocular tissues by different routes of administration. Invest. Ophthalmol. Vis. Sci., 37, 1914-1920.

Maurice, D., Mishima, S., 1984. Ocular pharmacokineticsIn: Anonymous Pharmacology of the Eye, Springer, pp. 19-116.

Menon, I., Trope, G., Basu, P., Wakeham, D., Persad, S., 1989. Binding of timolol to iris-ciliary body and melanin: an in vitro model for assessing the kinetics and efficacy of long-acting antiglaucoma drugs. Journal of Ocular Pharmacology and Therapeutics, 5, 313-324.

Miller, C.R., Clapp, P.J., O'Brien, D.F., 2000. Visible light-induced destabilization of endocytosed liposomes. FEBS Lett., 467, 52-56.

Miura, M., Makita, S., Iwasaki, T., Yasuno, Y., 2012. An Approach to Measure Blood Flow in Single Choroidal Vessel Using Doppler Optical Coherence TomographyChoroidal Blood Flow Measurement with Doppler OCT. Invest. Ophthalmol. Vis. Sci., 53, 7137-7141.

Mochizuki-Oda, N., Kataoka, Y., Cui, Y., Yamada, H., Heya, M., Awazu, K., 2002. Effects of near-infra-red laser irradiation on adenosine triphosphate and adenosine diphosphate contents of rat brain tissue. Neurosci. Lett., 323, 207-210.

Moghimi, S.M., Patel, H.M., 1989. Serum opsonins and phagocytosis of saturated and unsaturated phospholipid liposomes. Biochimica et Biophysica Acta (BBA)-Biomembranes, 984, 384-387.

Moghimi, S.M., Szebeni, J., 2003. Stealth liposomes and long circulating nanoparticles: critical issues in pharmacokinetics, opsonization and protein-binding properties. Prog. Lipid Res., 42, 463-478.

Moshfeghi, A.A., Peyman, G.A., 2005. Micro-and nanoparticulates. Adv. Drug Deliv. Rev., 57, 2047-2052.

Mura, S., Nicolas, J., Couvreur, P., 2013. Stimuli-responsive nanocarriers for drug delivery. Nature materials, 12, 991-1003.

Nagarsenker, M., Londhe, V.Y., Nadkarni, G., 1999. Preparation and evaluation of liposomal formulations of tropicamide for ocular delivery. Int. J. Pharm., 190, 63-71.

Nagasaki, T., Shinkai, S., 2007. The concept of molecular machinery is useful for design of stimuli-responsive gene delivery systems in the mammalian cell. Journal of Inclusion Phenomena and Macrocyclic Chemistry, 58, 205-219.

Nagayasu, A., Uchiyama, K., Kiwada, H., 1999. The size of liposomes: a factor which affects their targeting efficiency to tumors and therapeutic activity of liposomal antitumor drugs. Adv. Drug Deliv. Rev., 40, 75-87.

Naveh, N., Muchtar, S., Benita, S., 1994. Pilocarpine incorporated into a submicron emulsion vehicle causes an unexpectedly prolonged ocular hypotensive effect in rabbits. Journal of Ocular Pharmacology and Therapeutics, 10, 509-520.

Negishi, Y., Endo-Takahashi, Y., Matsuki, Y., Kato, Y., Takagi, N., Suzuki, R., Maruyama, K., Aramaki, Y., 2012. Systemic delivery systems of angiogenic gene by novel bubble liposomes containing cationic lipid and ultrasound exposure. Molecular pharmaceutics, 9, 1834-1840.

Nii, T., Takamura, A., Mohri, K., Ishii, F., 2003. Factors affecting physicochemical properties of liposomes prepared with hydrogenated purified egg yolk lecithins by the microencapsulation vesicle method. Colloids and Surfaces B: Biointerfaces, 27, 323-332.

Nikoobakht, B., El-Sayed, M.A., 2003. Preparation and growth mechanism of gold nanorods (NRs) using seed-mediated growth method. Chemistry of Materials, 15, 1957-1962.

Noble, G.T., Stefanick, J.F., Ashley, J.D., Kiziltepe, T., Bilgicer, B., 2014. Ligand-targeted liposome design: challenges and fundamental considerations. Trends Biotechnol., 32, 32-45.

Nomoto, H., Shiraga, F., Kuno, N., Kimura, E., Fujii, S., Shinomiya, K., Nugent, A.K., Hirooka, K., Baba, T., 2009. Pharmacokinetics of bevacizumab after topical, subconjunctival, and intravitreal administration in rabbits. Invest. Ophthalmol. Vis. Sci., 50, 4807-4813.

Olson, F., Hunt, C., Szoka, F., Vail, W., Papahadjopoulos, D., 1979. Preparation of liposomes of defined size distribution by extrusion through polycarbonate membranes. Biochimica et Biophysica Acta (BBA)-Biomembranes, 557, 9-23.

Omata, D., Negishi, Y., Hagiwara, S., Yamamura, S., Endo-Takahashi, Y., Suzuki, R., Maruyama, K., Nomizu, M., Aramaki, Y., 2011. Bubble liposomes and ultrasound promoted endosomal escape of TAT-PEG liposomes as gene delivery carriers. Molecular pharmaceutics, 8, 2416-2423.

Oussoren, C., Zuidema, J., Crommelin, D., Storm, G., 1997. Lymphatic uptake and biodistribution of liposomes after subcutaneous injection.: II. Influence of liposomal size, lipid composition and lipid dose. Biochimica et Biophysica Acta (BBA)-Biomembranes, 1328, 261-272.

Paasonen, L., Laaksonen, T., Johans, C., Yliperttula, M., Kontturi, K., Urtti, A., 2007. Gold nanoparticles enable selective light-induced contents release from liposomes. J. Controlled Release, 122, 86-93.

Paasonen, L., Sipilä, T., Subrizi, A., Laurinmäki, P., Butcher, S.J., Rappolt, M., Yaghmur, A., Urtti, A., Yliperttula, M., 2010. Gold-embedded photosensitive liposomes for drug delivery: triggering mechanism and intracellular release. J. Controlled Release, 147, 136-143.

Park, Y.S., 2002. Tumor-directed targeting of liposomes. Biosci. Rep., 22, 267-281.

Parkinson, T.M., Ferguson, E., Febbraro, S., Bakhtyari, A., King, M., Mundasad, M., 2003. Tolerance of ocular iontophoresis in healthy volunteers. Journal of ocular pharmacology and therapeutics, 19, 145-151.

Parthasarathy, R., Yu, C., Groves, J.T., 2006. Curvature-modulated phase separation in lipid bilayer membranes. Langmuir, 22, 5095-5099.

Pascolini, D., Mariotti, S.P., 2012. Global estimates of visual impairment: 2010. Br. J. Ophthalmol., 96, 614-618. doi: 10.1136/bjophthalmol-2011-300539 [doi].

Patel, S.R., Lin, A.S., Edelhauser, H.F., Prausnitz, M.R., 2011. Suprachoroidal drug delivery to the back of the eye using hollow microneedles. Pharm. Res., 28, 166-176.

Patil, S.D., Rhodes, D.G., Burgess, D.J., 2004. Anionic liposomal delivery system for DNA transfection. The AAPS journal, 6, 13-22.

Pignatello, R., Ricupero, N., Bucolo, C., Maugeri, F., Maltese, A., Puglisi, G., 2006. Preparation and characterization of eudragit retard nanosuspensions for the ocular delivery of cloricromene. Aaps Pharmscitech, 7, E192-E198.

Pitkänen, L., Pelkonen, J., Ruponen, M., Rönkkö, S., Urtti, A., 2004. Neural retina limits the nonviral gene transfer to retinal pigment epithelium in an in vitro bovine eye model. The AAPS journal, 6, 72-80.

Pitkänen, L., Ranta, V., Moilanen, H., Urtti, A., 2005. Permeability of retinal pigment epithelium: effects of permeant molecular weight and lipophilicity. Invest. Ophthalmol. Vis. Sci., 46, 641-646.

Plassat, V., Wilhelm, C., Marsaud, V., Ménager, C., Gazeau, F., Renoir, J., Lesieur, S., 2011. Anti-Estrogen-Loaded Superparamagnetic Liposomes for Intracellular Magnetic Targeting and Treatment of Breast Cancer Tumors. Advanced Functional Materials, 21, 83-92.

Potdar, D., Sammalkorpi, M., 2015. Asymmetric heat transfer from nanoparticles in lipid bilayers. Chem. Phys.

Pouliquen, G., Tribet, C., 2006. Light-triggered association of bovine serum albumin and azobenzene-modified poly (acrylic acid) in dilute and semidilute solutions. Macromolecules, 39, 373-383.

Prausnitz, M.R., Noonan, J.S., 1998. Permeability of cornea, sclera, and conjunctiva: a literature analysis for drug delivery to the eye. J. Pharm. Sci., 87, 1479-1488.

Raghava, S., Hammond, M., Kompella, U.B., 2004. Periocular routes for retinal drug delivery. Expert opinion on drug delivery, 1, 99-114.

Ranta, V., Mannermaa, E., Lummepuro, K., Subrizi, A., Laukkanen, A., Antopolsky, M., Murtomäki, L., Hornof, M., Urtti, A., 2010. Barrier analysis of periocular drug delivery to the posterior segment. J. Controlled Release, 148, 42-48.

Ranta, V., Urtti, A., 2006. Transscleral drug delivery to the posterior eye: Prospects of pharmacokinetic modeling. Adv. Drug Deliv. Rev., 58, 1164-1181. doi: http://dx.doi.org/10.1016/j.addr.2006.07.025.

Regen, S.L., Singh, A., Oehme, G., Singh, M., 1981. Polymerized phosphatidyl choline vesicles. Stabilized and controllable time-release carriers. Biochem. Biophys. Res. Commun., 101, 131-136.

Saeva, F.D., 1990. Photoinduced electron transfer (PET) bond cleavage reactionsIn: Anonymous Photoinduced Electron Transfer I, Springer, pp. 59-92.

Sahoo, S.K., Dilnawaz, F., Krishnakumar, S., 2008. Nanotechnology in ocular drug delivery. Drug Discov. Today, 13, 144-151.

Salminen, L., Urtti, A., Periviita, L., 1984. Effect of ocular pigmentation on pilocarpine pharmacology in the rabbit eye. I. Drag distribution and metabolism. Int. J. Pharm., 18, 17-24.

Sawa, M., Awazu, K., Takahashi, T., Sakaguchi, H., Horiike, H., Ohji, M., Tano, Y., 2004. Application of femtosecond ultrashort pulse laser to photodynamic therapy mediated by indocyanine green. Br. J. Ophthalmol., 88, 826-831.

Sawant, R.R., Sriraman, S.K., Navarro, G., Biswas, S., Dalvi, R.A., Torchilin, V.P., 2012. Polyethyleneimine-lipid conjugate-based pH-sensitive micellar carrier for gene delivery. Biomaterials, 33, 3942-3951.

Schroeder, A., Honen, R., Turjeman, K., Gabizon, A., Kost, J., Barenholz, Y., 2009. Ultrasound triggered release of cisplatin from liposomes in murine tumors. J. Controlled Release, 137, 63-68.

Senior, J., Gregoriadis, G., 1982. Is half-life of circulating liposomes determined by changes in their permeability? FEBS Lett., 145, 109-114.

Sershen, S., Westcott, S., Halas, N., West, J., 2000. Temperature-sensitive polymer–nanoshell composites for photothermally modulated drug delivery. J. Biomed. Mater. Res., 51, 293-298.

Sharma, A., Sharma, U.S., 1997. Liposomes in drug delivery: progress and limitations. Int. J. Pharm., 154, 123-140.

Shedden, A., Laurence, J., Tipping, R., Timoptic-XE® 0.5% Study Group, 2001. Efficacy and tolerability of timolol maleate ophthalmic gel-forming solution versus timolol ophthalmic solution in adults with open-angle glaucoma or ocular hypertension: a six-month, double-masked, multicenter study. Clin. Ther., 23, 440-450.

Shen, Y., Tu, J., 2007. Preparation and ocular pharmacokinetics of ganciclovir liposomes. The AAPS journal, 9, E371-E377.

Shi, D., Matsusaki, M., Kaneko, T., Akashi, M., 2008. Photo-cross-linking and cleavage induced reversible size change of bio-based nanoparticles. Macromolecules, 41, 8167-8172.

Shirasaki, Y., 2008. Molecular design for enhancement of ocular penetration. J. Pharm. Sci., 97, 2462-2496.

Shum, P., Kim, J., Thompson, D.H., 2001. Phototriggering of liposomal drug delivery systems. Adv. Drug Deliv. Rev., 53, 273-284.

Sieving, P.A., Caruso, R.C., Tao, W., Coleman, H.R., Thompson, D.J., Fullmer, K.R., Bush, R.A., 2006. Ciliary neurotrophic factor (CNTF) for human retinal degeneration: phase I trial of CNTF delivered by encapsulated cell intraocular implants. Proc. Natl. Acad. Sci. U. S. A., 103, 3896-3901. doi: 0600236103 [pii].

Simões, S., Moreira, J.N., Fonseca, C., Düzgüneş, N., Pedroso de Lima, Maria C, 2004. On the formulation of pH-sensitive liposomes with long circulation times. Adv. Drug Deliv. Rev., 56, 947-965.

Skrabalak, S.E., Chen, J., Sun, Y., Lu, X., Au, L., Cobley, C.M., Xia, Y., 2008. Gold nanocages: synthesis, properties, and applications. Acc. Chem. Res., 41, 1587-1595.

Slepushkin, V.A., Simoes, S., Dazin, P., Newman, M.S., Guo, L.S., Pedroso de Lima, M.C., Duzgunes, N., 1997. Sterically stabilized pH-sensitive liposomes. Intracellular delivery of aqueous contents and prolonged circulation in vivo. J. Biol. Chem., 272, 2382-2388.

Sorgi, F.L., Huang, L., 1996. Large scale production of DC-Chol cationic liposomes by microfluidization. Int. J. Pharm., 144, 131-139.

Spratt, T., Bondurant, B., O'Brien, D.F., 2003. Rapid release of liposomal contents upon photoinitiated destabilization with UV exposure. Biochimica et Biophysica Acta (BBA)-Biomembranes, 1611, 35-43.

Standard, A., 1993. Z136. 1. American national standard for the safe use of lasers. American National Standards Institute. Inc., New York.

Subrizi, A., Tuominen, E., Bunker, A., Róg, T., Antopolsky, M., Urtti, A., 2012. Tat (48-60) peptide amino acid sequence is not unique in its cell penetrating properties and cell-surface glycosaminoglycans inhibit its cellular uptake. J. Controlled Release, 158, 277-285.

Suzuki, T., Shinkai, S., Sada, K., 2006. Supramolecular crosslinked linear poly (trimethylene iminium trifluorosulfonimide) polymer gels sensitive to light and thermal stimuli. Adv Mater, 18, 1043-1046.

Szoka Jr, F., Papahadjopoulos, D., 1980. Comparative properties and methods of preparation of lipid vesicles (liposomes). Annu. Rev. Biophys. Bioeng., 9, 467-508.

Szoka, F.,Jr, Papahadjopoulos, D., 1978. Procedure for preparation of liposomes with large internal aqueous space and high capture by reverse-phase evaporation. Proc. Natl. Acad. Sci. U. S. A., 75, 4194-4198.

Tagami, T., Foltz, W.D., Ernsting, M.J., Lee, C.M., Tannock, I.F., May, J.P., Li, S., 2011. MRI monitoring of intratumoral drug delivery and prediction of the therapeutic effect with a multifunctional thermosensitive liposome. Biomaterials, 32, 6570-6578.

Tai, L., Tsai, P., Wang, Y., Wang, Y., Lo, L., Yang, C., 2009. Thermosensitive liposomes entrapping iron oxide nanoparticles for controllable drug release. Nanotechnology, 20, 135101.

Takeuchi, H., Matsui, Y., Sugihara, H., Yamamoto, H., Kawashima, Y., 2005a. Effectiveness of submicron-sized, chitosan-coated liposomes in oral administration of peptide drugs. Int. J. Pharm., 303, 160-170.

Takeuchi, H., Thongborisute, J., Matsui, Y., Sugihara, H., Yamamoto, H., Kawashima, Y., 2005b. Novel mucoadhesion tests for polymers and polymer-coated particles to design optimal mucoadhesive drug delivery systems. Adv. Drug Deliv. Rev., 57, 1583-1594.

Talsma, H., Özer, A., Bloois, L.v., Crommelin, D., 1989. The Size Reduction of Liposomes with a High Pressure Homogenizer (Microfluidizer™). Characterization of Prepared Dispersions and Comparison with Conventional Methods. Drug Dev. Ind. Pharm., 15, 197-207.

ter Haar, G., 2007. Therapeutic applications of ultrasound. Prog. Biophys. Mol. Biol., 93, 111-129.

Thanos, C.G., Bell, W.J., O'Rourke, P., Kauper, K., Sherman, S., Stabila, P., Tao, W., 2004. Sustained secretion of ciliary neurotrophic factor to the vitreous, using the encapsulated cell therapy-based NT-501 intraocular device. Tissue Eng., 10, 1617-1622.

Thompson, D.H., Gerasimov, O.V., Wheeler, J.J., Rui, Y., Anderson, V.C., 1996. Triggerable plasmalogen liposomes: improvement of system efficiency. Biochimica et Biophysica Acta (BBA)-Biomembranes, 1279, 25-34.

Thrimawithana, T.R., Young, S., Bunt, C.R., Green, C., Alany, R.G., 2011. Drug delivery to the posterior segment of the eye. Drug Discov. Today, 16, 270-277.

Timko, B.P., Dvir, T., Kohane, D.S., 2010. Remotely triggerable drug delivery systems. Adv Mater, 22, 4925-4943.

Tong, R., Hemmati, H.D., Langer, R., Kohane, D.S., 2012. Photoswitchable nanoparticles for triggered tissue penetration and drug delivery. J. Am. Chem. Soc., 134, 8848-8855.

Torchilin, V., 2012. Liposomes in drug deliveryIn: Anonymous Fundamentals and Applications of Controlled Release Drug Delivery, Springer, pp. 289-328.

Torchilin, V.P., 2005. Recent advances with liposomes as pharmaceutical carriers. Nature reviews Drug discovery, 4, 145-160.

Tsuda, K., Dol, G.C., Gensch, T., Hofkens, J., Latterini, L., Weener, J., Meijer, E., Schryver, D., 2000. Fluorescence from azobenzene functionalized poly (propylene imine) dendrimers in self-assembled supramolecular structures. J. Am. Chem. Soc., 122, 3445-3452.

Ulrich, A.S., 2002. Biophysical aspects of using liposomes as delivery vehicles. Biosci. Rep., 22, 129-150.

Un, K., Kawakami, S., Suzuki, R., Maruyama, K., Yamashita, F., Hashida, M., 2011. Suppression of melanoma growth and metastasis by DNA vaccination using an ultrasound-responsive and mannose-modified gene carrier. Molecular pharmaceutics, 8, 543-554.

Urtti, A., 2006. Challenges and obstacles of ocular pharmacokinetics and drug delivery. Adv. Drug Deliv. Rev., 58, 1131-1135.

Urtti, A., Pipkin, J.D., Rork, G., Sendo, T., Finne, U., Repta, A., 1990. Controlled drug delivery devices for experimental ocular studies with timolol 2. Ocular and systemic absorption in rabbits. Int. J. Pharm., 61, 241-249.

Urtti, A., Salminen, L., 1993. Minimizing systemic absorption of topically administered ophthalmic drugs. Surv. Ophthalmol., 37, 435-456.

Urtti, A., Salminen, L., Miinalainen, O., 1985. Systemic absorption of ocular pilocarpine is modified by polymer matrices. Int. J. Pharm., 23, 147-161.

Uteza, Y., Rouillot, J.S., Kobetz, A., Marchant, D., Pecqueur, S., Arnaud, E., Prats, H., Honiger, J., Dufier, J.L., Abitbol, M., Neuner-Jehle, M., 1999. Intravitreous transplantation of encapsulated fibroblasts secreting the human fibroblast growth factor 2 delays photoreceptor cell degeneration in Royal College of Surgeons rats. Proc. Natl. Acad. Sci. U. S. A., 96, 3126-3131.

Valjakka, A., Ahonen, J., Itkonen, M., Pitkänen, L., Urtti, A., 2007. Comparison of ERG Records From Anaesthetized versus Freely Behaving Rats. Invest. Ophthalmol. Vis. Sci., 48, 1286-1286.

Vellonen, K., Soini, E., del Amo, E.M., Urtti, A., 2015. Prediction of ocular drug distribution from systemic blood circulation. Molecular pharmaceutics.

Vollmer, D.L., Szlek, M.A., Kolb, K., Lloyd, L.B., Parkinson, T.M., 2002. In vivo transscleral iontophoresis of amikacin to rabbit eyes. Journal of ocular pharmacology and therapeutics, 18, 549-558.

Wagner, A., Vorauer-Uhl, K., 2011. Liposome technology for industrial purposes. J. Drug Deliv., 2011, 591325. doi: 10.1155/2011/591325 [doi].

Weissleder, R., 2001. A clearer vision for in vivo imaging. Nat. Biotechnol., 19, 316-317.

Weissleder, R., Ntziachristos, V., 2003. Shedding light onto live molecular targets. Nat. Med., 9, 123-128.

WHO, 2014. **The top 10 causes of death**. , 2016.

Wikström, J., Elomaa, M., Syväjärvi, H., Kuokkanen, J., Yliperttula, M., Honkakoski, P., Urtti, A., 2008. Alginate-based microencapsulation of retinal pigment epithelial cell line for cell therapy. Biomaterials, 29, 869-876.

Willner, I., Pardo-Yissar, V., Katz, E., Ranjit, K.T., 2001. A photoactivated 'molecular train'for optoelectronic applications: light-stimulated translocation of a β-cyclodextrin receptor within a stoppered azobenzene-alkyl chain supramolecular monolayer assembly on a Au-electrode. J Electroanal Chem, 497, 172-177.

Wilson, B.C., Patterson, M.S., 2008. The physics, biophysics and technology of photodynamic therapy. Phys. Med. Biol., 53, R61.

Winkler, B.S., 1981. Glycolytic and oxidative metabolism in relation to retinal function. J. Gen. Physiol., 77, 667-692.

Wu, C., Chen, C., Lai, J., Chen, J., Mu, X., Zheng, J., Zhao, Y., 2008a. Molecule-scale controlled-release system based on light-responsive silica nanoparticles. Chem.Commun., 2662-2664.

Wu, L., Martínez-Castellanos, M.A., Quiroz-Mercado, H., Arevalo, J.F., Berrocal, M.H., Farah, M.E., Maia, M., Roca, J.A., Rodriguez, F.J., Pan American Collaborative Retina Group (PACORES, 2008b. Twelve-month safety of intravitreal injections of bevacizumab (Avastin®): results of the Pan-American Collaborative Retina Study Group (PACORES). Graefe's Archive for Clinical and Experimental Ophthalmology, 246, 81-87.

Xiao, Z., Ji, C., Shi, J., Pridgen, E.M., Frieder, J., Wu, J., Farokhzad, O.C., 2012. DNA Self-Assembly of Targeted Near-Infrared-Responsive Gold Nanoparticles for Cancer Thermo-Chemotherapy. Angewandte Chemie, 124, 12023-12027.

Xu, Q., Boylan, N.J., Suk, J.S., Wang, Y., Nance, E.A., Yang, J., McDonnell, P.J., Cone, R.A., Duh, E.J., Hanes, J., 2013. Nanoparticle diffusion in, and microrheology of, the bovine vitreous ex vivo. J. Controlled Release, 167, 76-84.

Yagai, S., Karatsu, T., Kitamura, A., 2005. Photocontrollable Self-Assembly. Chemistry–A European Journal, 11, 4054-4063.

Yasukawa, T., Ogura, Y., Sakurai, E., Tabata, Y., Kimura, H., 2005. Intraocular sustained drug delivery using implantable polymeric devices. Adv. Drug Deliv. Rev., 57, 2033-2046.

Yatvin, M.B., Kreutz, W., Horwitz, B.A., Shinitzky, M., 1980. pH-sensitive liposomes: possible clinical implications. Science, 210, 1253-1255.

Yatvin, M.B., Weinstein, J.N., Dennis, W.H., Blumenthal, R., 1978. Design of liposomes for enhanced local release of drugs by hyperthermia. Science, 202, 1290-1293.

Yavuz, M.S., Cheng, Y., Chen, J., Cobley, C.M., Zhang, Q., Rycenga, M., Xie, J., Kim, C., Song, K.H., Schwartz, A.G., 2009. Gold nanocages covered by smart polymers for controlled release with near-infrared light. Nature materials, 8, 935-939.

You, J., Zhang, R., Xiong, C., Zhong, M., Melancon, M., Gupta, S., Nick, A.M., Sood, A.K., Li, C., 2012. Effective photothermal chemotherapy using doxorubicin-loaded gold nanospheres that target EphB4 receptors in tumors. Cancer Res., 72, 4777-4786. doi: 10.1158/0008-5472.CAN-12-1003 [doi].

Zhang, Z., Shum, P., Yates, M., Messersmith, P.B., Thompson, D.H., 2002. Formation of fibrinogen-based hydrogels using phototriggerable diplasmalogen liposomes. Bioconjug. Chem., 13, 640-646.

Zhang, Z., Smith, B.D., 1999. Synthesis and characterization of NVOC-DOPE, a caged photoactivatable derivative of dioleoylphosphatidylethanolamine. Bioconjug. Chem., 10, 1150-1152.

Zhang, T., Xiang, C.D., Gale, D., Carreiro, S., Wu, E.Y., Zhang, E.Y., 2008. Drug transporter and cytochrome P450 mRNA expression in human ocular barriers: implications for ocular drug disposition. Drug Metab. Dispos., 36, 1300-1307. doi: 10.1124/dmd.108.021121 [doi].

Zhao, Y., 2007. Rational design of light-controllable polymer micelles. The Chemical Record, 7, 286-294.

Zhu, J., Munn, R.J., Nantz, M.H., 2000. Self-cleaving ortho ester lipids: a new class of pH-vulnerable amphiphiles. J. Am. Chem. Soc., 122, 2645-2646.